Magnetic domains in terbium

Harry Bareham

MAGNETIC DOMAINS IN TERBIUM

by

Harry Bareham B.Sc., M.Inst.P.

A thesis submitted to the University of Durham in candidature for the Degree of Master of Science.

October, 1982.

TO MY WIFE BARBARA AND DAUGHTER ALEXANDRA

ABSTRACT

This thesis discusses the various forms of magnetic ordering and the associated fundamental theory. The phenomena of magnetocrystalline anisotropy and magnetostriction are also discussed. The thesis is especially concerned with the rare earth element terbium which exhibits ferromagnetism at temperatures below $\sim$ 222K. The exchange interaction associated with ferromagnetic ordering is discussed in CHAPTER TWO, while CHAPTER THREE, which deals specifically with the rare earth elements, includes a section on the RKKY exchange interaction and its relevance to the magnetic properties of some of the rare earth metals. The magnetic properties of terbium are also included.

In particular, the thesis deals with magnetic domains and their observation. The energy minimizing process of domain formation is discussed in detail and various types of domain configurations are shown for cubic and hexagonal symmetry. CHAPTER FIVE represents a review of some of the methods of domain observation.

Ferromagnetic domains have been observed in a single crystal of 99.99% pure terbium. These domains have been observed at various temperatures and an attempt has been made to fit the observations to a slab-domain model for 180° Bloch walls. The apparatus used to make the observations is one based upon the magnetic colloid technique and is discussed in detail in CHAPTER SIX. Iron wire is evaporated onto the sample surface in order to outline the surface domain configurations. Photographs of these patterns have been analyzed and domain widths

have been deduced for various temperatures. Domain widths/temperature curves have been included based upon the slab-domain model and it has been found that the experimental data is in excellent agreement with this model.

ACKNOWLEDGEMENTS

I have pleasure in taking this opportunity to acknowledge the help and encouragement given to me by the following people during the course of this work.

Firstly, I would like to thank Professors A. W. Wolfendale and B. H. Bransden for allowing me to make use of the facilities of the Physics Department of the University of Durham.

I would like to offer my sincere and grateful thanks to Dr. B. K. Tanner for his excellent supervision and help for the whole duration of my studies in the department. His advice and encouragement undoubtedly assisted me in the completion of the work.

Also, my thanks are due to Dr. W. D. Corner for his encouragement and help.

I wish to extend sincere thanks to Dr. G. F. Clark for his advice, help and friendship. His assistance at the start of the work was invaluable.

My thanks are also due to Mr. K. G. Moulson for his valuable technical help and advice and to Mr. W. Leslie and his staff for constructing various pieces of apparatus which I have required during the course of the work. Thanks also go to Mr. J. Scott, the departmental glass blower, for providing the glass cryostat and for his general help and assistance with apparatus.

I would like to express my sincere thanks to Mr. R. Collinson for his help in constructing the brass sample holder and to Mr. J. H. Patterson for his expert help with the engineering drawing.

Finally, I would like to thank Mrs. V. Sharp for typing this thesis.

CONTENTS

CONTENTS

CONTENTS

CONTENTS

LIST OF FIGURES

LIST OF FIGURES

LIST OF FIGURES

LIST OF FIGURES

LIST OF FIGURES

LIST OF FIGURES

LIST OF FIGURES

LIST OF FIGURES

LIST OF TABLES

CHAPTER ONE

INTRODUCTION TO MAGNETISM

1.1 MAGNETISM

1.2 THE MAGNETIC FIELD VECTOR H

1.3 THE MAGNETIZATION VECTOR M

1.4 DIPOLE IN A MAGNETIC FIELD

1.5 ORIGINS OF MAGNETISM

1.6 THE BOHR MAGNETON

1.7 DIAMAGNETISM

1.8 PARAMAGNETISM

1.9 FERROMAGNETISM

1.10 MAGNETO CRYSTALLINE ANISOTROPY

1.10.1 Shape Anisotropy

1.10.2 Stress Anisotropy (Magnetostrictive)

1.10.3 Anisotropy introduced by

(a) magnetic annealing

(b) plastic deformation

(c) irradiation

1.10.4 Exchange Anisotropy

1.11 MAGNETOSTRICTION AND MAGNETOELASTIC ENERGY

1.11.1 Volume Magnetostriction

1.11.2 Linear Magnetostriction

1.11.3 Temperature Dependence of the Magnetostriction Constants

1.11.4 The effect of Stress on Magnetization

1.12 ANTIFERROMAGNETISM

1.13 FERRIMAGNETISM

CHAPTER 1

INTRODUCTION TO MAGNETISM

1.1 MAGNETISM

It is thought that it was probably the Greeks who first considered the properties of lodestone over 30 centuries ago. Certainly the Greeks and Chinese were among the first to consider this aspect of solid state physics even if their only interest was the construction and use of the compass. Indeed a significant piece of evidence to suggest that the ancients did not actively engage in the study of the magnetic properties of matter is the fact that, even though it has been used for some 3,000 years, it was not until the latter part of the 16th century that Dr. Gilbert considered the earth to be a large magnet thus providing the means to explain how the compass worked.

The magnetic field concept is a very convenient concept to adopt in order to explain and estimate the magnitude of those quantum mechanical effects which result in the manifestation of the various forms of magnetism. The magnetic field is regarded as a region in space where a magnetic pole would feel a force. The magnetic pole itself is an invention which is denied physical existence by the equations of James Clerk Maxwell.

Two basic principles can be considered to be involved in the manifestation of a magnetic field.

a) the cause.

b) the effect.

The cause can be regarded as the magnetic field intensity (given the symbol $\underline{H}$) and is measured in Amperes per metre. (Am^{-1})

The effect can be regarded as the magnetic field itself, which is measured in terms of the number of field lines per metre squared of material through which the field is permeating. This quantity, given the symbol $\underline{B}$ is known as the magnetic flux density ormagnetic induction and its SI unit of measurement is the Tesla (T) where 1 Tesla = 1 line per square metre or 1 Weber (Wb) m^{-2}.

The induction $\underline{B}$ is related to its cause $\underline{H}$ by a factor which is a property of the medium through which the field is permeating. This property is known as the permeability of the material and is given the symbol μ. μ_o is the permeability of free space (and approximately air). Hence for a magnetizing force $\underline{H}$ giving rise to an induction $\underline{B}$ in free space.

$$\underline{B} = \mu_o \underline{H} \qquad (1.1)$$

1.2 THE MAGNETIC FIELD VECTOR H

Although isolated poles have not been observed in nature, they can be considered to exist in pairs in terms of regions where the resultant forces due to the magnetisation appears to act.

The force between two such poles, either repulsive or attractive depending on the sign of the poles, is given by (in vaccuo).

$$F = \frac{m_1 m_2}{4\pi\mu_o r^2} \qquad (1.2)$$

where F = force in Newtons

m_1 and m_2 = strengths of respective poles in Webers

r = distance of separation in metres.

μ_o = permeability of vacuum. = 4π x 10 Henries per metre.

This force can be considered as comprising of two factors.

(i) a single pole

(ii) a quantity which includes the other pole and a distance.

The second quantity must represent the field which exerts a force on the first quantity. The second quantity is the magnetic field intensity vector $\underline{H}$.

$$F = m\underline{H} \qquad (1.3)$$

A force can also be exerted on a magnetic pole by an electric current. A solenoid of length l having N turns carrying a current I produces a magnetic field of intensity $\underline{H}$ where

$$\underline{H} = \frac{NI}{l} \quad \text{Amperes per metre}$$

$$\underline{H} = nI \quad \text{where } n = N/l = \text{turns per metre} \qquad (1.4)$$

Again the force on the magnetic pole (strength m) is

$$F = m\underline{H}$$

The magnetic flux density $\underline{B}$ inside such a solenoid having an air or vacuum core is

$$\underline{B} = \mu_o n I$$

again

$$\underline{B} = \mu_o \underline{H}$$

1.3 THE MAGNETIZATION VECTOR $\underline{M}$

$\underline{M}$ is the magnetic moment per unit volume and it is used to quantify magnetic substances. The source of magnetism could be either uncompensated poles or Ampérian currents. The quantity $\underline{M}$ can therefore be defined to be consistent with either.

The magnetic moment μ of a dipole is given by

$$\mu = ml \qquad (1.5)$$

where m = pole strength

l = distance of separation.

The magnetic moment per unit volume = $ml/l^3 = \underline{M}$

$\underline{M}$ thus has the same units as $\underline{B}$.

The total flux density of this magnetic material is

$$B = \mu_o \underline{H} + \underline{M} \qquad (1.6)$$

$\underline{M}$ can also have the units of $\underline{H}$ by using the equation

$$B = \mu_o (\underline{H} + \underline{M}) \qquad (1.7)$$

which is consistent with Ampérian currents giving rise to a magnetisation density $\underline{M}$ of the material.

1.7 will be adopted in this thesis.

A solenoid which is long (e.g. a toroid) and carries a current I_s produces a magnetic field intensity $\underline{H}_s$ which gives rise to $\mu_o H$ field lines per unit area through the solenoid. A magnetic material placed inside the solenoid is considered to consist of circular currents which cancel everywhere in the material but which form a series of circles on the surface having the effect of adding a component of current (apparent) Im to that of the solenoid. (Fig.1.1)

From equation (1.4)

$$\underline{H}_s = nI_s$$

$$\underline{B}_s = \mu_o H_s$$

The apparent current due to the magnetic material gives rise to a flux density due to the material.

$$\underline{Bm} = \mu o n \underline{Im}$$

$$\underline{Bm} = \mu o \underline{M} \qquad (1.8)$$

where $\underline{M}$ = the magnetic moment per unit volume using this convention (Sommerfeld) $\underline{M}$ has the same units as $\underline{H}$.

Total flux density due to the solenoid and magnetic material =

$$\underline{B} = \mu o \underline{H_s} + \mu o \underline{M}$$

$$\underline{B} = \mu o(\underline{Hs} + \underline{M})$$

In general $\underline{B} = \mu o(\underline{H} + \underline{M})$ which is equation (1.7)

$$\mu H = \mu o(\underline{H} + \underline{M})$$

$$\frac{\mu}{\mu o} = (1 + \frac{\underline{M}}{\underline{H}}) \qquad (1.9)$$

Where $\frac{\mu}{\mu o}$ is known as the relative permeability

$$\mu r = \frac{\mu}{\mu o} \qquad (1.10)$$

and $\frac{\underline{M}}{\underline{H}}$ is known as the magnetic susceptibility.

$$K = \frac{\underline{M}}{\underline{H}} \qquad (1.11)$$

K varies with temperature and magnetic field strength and its magnitude is useful in distinguishing the various types of magnetic behaviour.

$$\mu r = 1 + K \qquad (1.12)$$

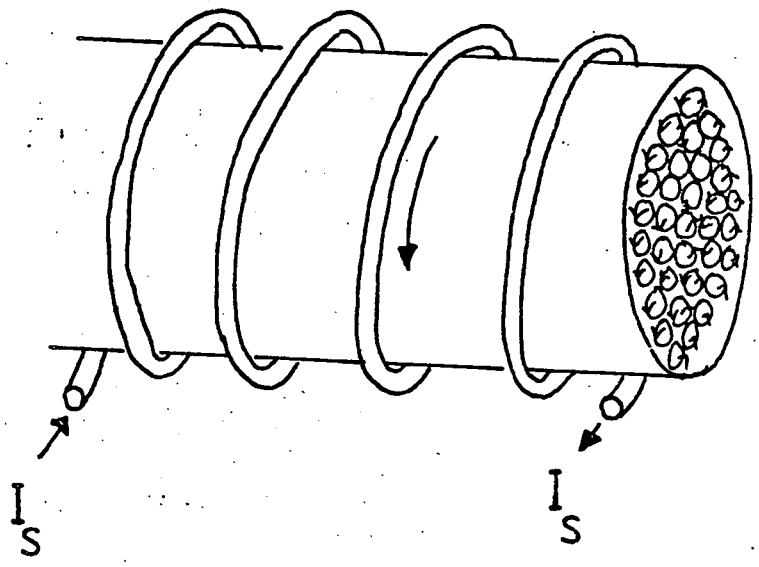

$$\underline{H} = n(I_s + I_m)$$

$$\underline{B} = \mu_o n(I_s + I_m)$$

$$\underline{B} = \mu_o(\underline{H} + \underline{M})$$

Fig I.I Flux due to magnetic material inside a long solenoid.

A substance placed in a magnetic field acquires a magnetic moment, the susceptibility of the material being a measure of this magnetic moment. Hence K is useful in classification of magnetic materials as it may or may not vary with applied field strength and it may be positive or negative.

1.4 DIPOLE IN A MAGNETIC FIELD.

The force on a magnetic pole of strength m in a magnetic field strength $\underline{H}$ is given by equation (1.3)

$$F = m\underline{H}$$

Each pole of the dipole in the field would feel a force, the direction of the force depending on the sign of the pole. A dipole at an angle θ to a uniform magnetic field strength $\underline{H}$ would experience a couple L (fig.1.2)

$$L = Fl \sin\theta$$

where l = length of dipole

$$L = -m\underline{H}l \sin\theta$$

But from equation (1.5) ml = magnetic moment μ

$$L = -\mu\underline{H} \sin\theta \qquad (1.13)$$

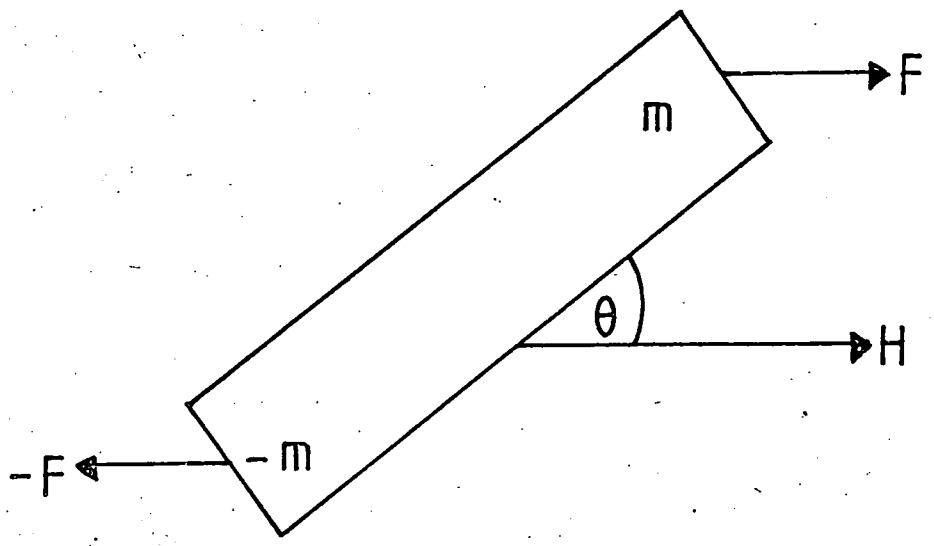

Figure I.2 Dipole in a uniform field.

The action of the uniform field is to rotate the dipole until it is parallel with the field.

Only a non uniform field of gradient $\frac{\partial H}{\partial x}$ would have the effect of producing a translational force.

1.5 ORIGINS OF MAGNETISM

In general, magnetic fields are generated by charge on the move and a fundamental source of moving charge is the electron system of individual atoms. Whether the electrons are regarded as individual particles orbiting the nucleus or as a shell or cloud of charge is immaterial. An electron can be considered as the possessor of two types of movement.

a) an orbital motion with associated quantised angular momentum.

b) a spin motion about its own axis.

These two motions are, then, sources of magnetization.

It is obvious from this that the electronic configuration of a particular atom will have some bearing on its ability to produce a magnetic field. Paired electrons in the same system which would otherwise have the same quantum co-ordinates are compelled by the Pauli Exclusion principle to differ in spin. The spin vectors of paired electrons are antiparallel and hence have no associated magnetic vector.

Materials with filled electron shells will, therefore, have a total spin of zero and will also produce no magnetic resultant due to orbital motion. Yet such materials can exhibit a magnetic moment. They do so under the action of an applied magnetic field.

Nearly all substances can be classified into two general groups in terms of their magnetic properties. The first group contains materials which are said to be diamagnetic or paramagnetic. These materials exhibit very weak magnetism and $\underline{M}$, $\underline{H}$ and $\underline{B}$ are all proportional. The second group consists of substances which are strongly, spontaneously magnetically ordered and non linear. Ferro and Ferrimagnetic substances have spontaneous magnetisation in zero applied field. Some exceptions are stronly paramagnetic salts and substances exhibiting antiferromagnetism.

1.6 THE BOHR MAGNETON

An electron orbiting an atom constitutes a current loop of cross-sectional area A. The magnetic moment m associated with this current loop is IA.

$$I = dq/dt$$

$$Ids = dq\, ds/dt = vdq$$

$$Ids = -ev$$

where e = electronic charge and v is velocity

ds = $2\pi r$ for a circular orbit of radius r

$$I = -ev/2\pi r = -e\omega/2\pi$$

$$m = IA = -e\omega A/2\pi = -e\omega\pi r^2/2\pi$$

$$m = -e\omega r^2/2 \qquad (1.14)$$

Angular momentum = $\underline{L}$ = a vector normal to the plane of the orbit.

$$\underline{L} = m_e \omega r^2$$

where m_e = electronic mass.

$$\underline{M} = -e\underline{L}/2m_e$$

Angular momentum is quantised giving $\underline{L}$ values as multiples of $h/2\pi$

$$L = nh/2\pi = n\hbar \quad \text{where } \hbar = h/2\pi$$

$$\underline{m} = -ne\hbar/2m_e \tag{1.15}$$

∴ the magnetic moment due to orbital motion can only assume values which are an integral multiple of $e\hbar/2m_e$

Hence $e\hbar/2m_e$ is the smallest theoretically possible magnetic moment and is known as the Bohr magneton μ_B

$$\mu_B = e\hbar/2m_e \tag{1.16}$$

SPIN.

Spin is a classical description of a quantum mechanical concept.

$$\underline{m} = \frac{-e}{m_e}\underline{S} \tag{1.17}$$

where $\underline{m}$ = spin magnetic moment

$\underline{S}$ = spin angular momentum

1.7 DIAMAGNETISM

Diamagnetism is an extremely weak form of magnetism which is exhibited by all materials and is the only form of magnetism common to all atoms. Its origin lies in the orbital motion of the atomic electrons and it is the result of perturbations of this orbital motion due to the electrons moving in an applied magnetic field. The orbiting electrons correspond to a current loop and this current loop will respond to an applied magnetic field. According to Lenzs Law a change in the flux linking the electron current loops induces a flow to oppose the charge in flux linkage. A magnetic moment is therefore induced which is opposite in direction to the applied external magnetic field and since no resistance is associated with an electron orbit the diamagnetic moment persists until the external magnetic field is removed. Because the diamagnetic moment opposes $\underline{H}$ then the susceptibility K_{dia} is negative. It is also very small.($\sim 10^{-5}$)

The diamagnetic moment can be calculated either classically or by using quantum mechanics both producing the same result. The result obtained by considering the effect of the force experienced by an electron in a classical orbit situated in an applied field is essentially the same as that provided by the (more correct) quantum mechanical approach. The Larmor precession theorem shows that the orbit precesses around the field direction.

A field $\underline{H}$ established in a direction perpendicular to the plane of a circular orbit produces a force whose direction is towards or away from the centre of the orbit depending on the orbital direction of the electron. This produces a change in the orbital radius which is of second order in $\underline{H}$ and is negligible compared with the change in angular

velocity (induced by the field) for a tightly bound electron.

From equation (1.14) the moment of the electron = $m = \frac{ea}{T}$

and the torque induced by the field = $\frac{Hea}{T}$

$$= ea\omega H/2\pi$$

The reactionary torque of precession $I\omega\omega'$ must equal this torque

I = moment of inertia of precessing electron

ω' = angular velocity of precession

$$ea\omega H/2\pi = I\omega\omega'$$

$$\omega' = eH/2m \qquad (1.18)$$

The electron orbit will, therefore, be one of periodically varying area when viewed along the field axis. The magnetic moment will vary continually.

The change in the orbital magnetic moment = $\Delta m = m_{dia}$

$$m_{dia} = \frac{-e^2HZ\overline{p^2}}{4m} \qquad (1.19)$$

where Z = atomic number

$\overline{p^2}$ is the mean square radius of the electrons orbit projected on a plane perpendicular to H.

$$\overline{p^2} = \overline{x^2} + \overline{y^2}$$

$$K = M/H$$

$$\therefore K = \frac{-e^2Z\overline{p^2}}{4m}$$

For N atoms

$$K = -Ne^2 Z \overline{\overline{\sum p^2}} \qquad (1.20)$$

The double bar indicates a statistical average for a large number of atoms.

In the general case the complete Larmor analysis yields an angular velocity of a precessing orbit the same as that given by equation (1.18).

Equation (1.20) must be extended as the orbit was originally assumed to be perpendicular to $\underline{H}$. For many atoms of random orientation then the statistical mean $\overline{p^2}$ $(=\overline{x^2} + \overline{y^2})$ is $\frac{2}{3}\overline{r^2}$

where $\overline{r^2} = \overline{x^2} + \overline{y^2} + \overline{z^2}$ and is the mean square distance from the nucleus. On average the distribution is spherically symmetrical $\therefore \overline{x^2} = \overline{y^2} = \overline{z^2}$.

For the N atoms all alike in size there is no difference between the statistical mean $\overline{\overline{\sum r^2}}$ for a large number of atoms and the time average $\overline{\sum r^2}$ for a single atom. Hence the atomic susceptibility is found by summing over Z electrons and the volume susceptibility is obtained by multiplying by the number of atoms per unit volume N.

$$\therefore \quad K_{dia} = -NZe^2 \overline{\overline{\sum r^2}}/6m \qquad (1.21)$$

N may be replaced by Avogadro's number L to give K_{molar}.

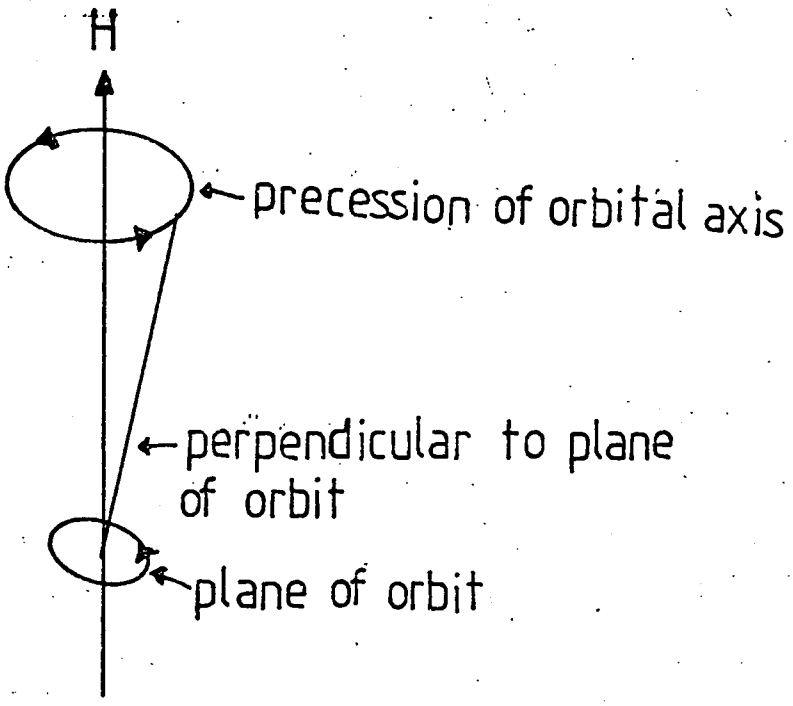

Fig. 1.3 The motion of a bcund classical electron in an applied field $\underline{H}$

Equation (1.21) is Langevins formula and its form suggests that the phenomenon is common to all atoms and that the susceptibility is always negative because $\overline{\sum r^2}$ is always greater than zero. The equation also suggests that the molecular diamagnetism is independent of temperature provided that the molecules retain the same sizes and further that the amount of diamagnetism is proportional to $\sum r^2$ or approximately to the combined areas of the various orbits. Curie preceeded Langevin in experimentally examining the invariance of K_{dia} with T and found that many substances, notably sulphur and phosphorus, had K_{dia} approximately constant with temperature. However, work since then has shown that others, notably bismuth, are not. Small fluctuations in K_{dia} with T may be interpreted in terms of the variation of orbit size with T but the large variation in K_{dia} of bismuth is not explained in this way. The simple Langevin formula is most appropriate to gases rather than being exactly applicable to the liquid or solid state.

To obtain K_{dia} values $\overline{\sum r^2}$ needs to be estimated. Also, for many electron atoms a screening factor σ must be used in order to allow for the effects of the other electrons. More exactly Hartree-Fock wave functions may be used in order to find the mean charge distributions.

Diamagnetic materials will be repelled from the applied $\underline{H}$ and in general if any other type of magnetism is present Dia is masked.

In a crystal each atom is in ananisotropic environment and the application of theLarmor precession theorem is not vigorous. Further, if electrons can undergo transitions to other discrete quantum states there will be an associated magnetic moment which will result in diamagnetism being dominated by paramagnetism.

1.8 PARAMAGNETISM

As a result of having unpaired electrons, or outer electrons not completely arranged in equal and opposite pairs, the atoms or molecules of paramagnetic materials have a permanent magnetic moment. Also some materials have even numbers of electrons but the ground state is such that a non-zero magnetic moment results. The effect also occurs for conductors since the spins of conduction electrons can be rotated by an external field. In conductors the paramagnetism is temperature independent.

Whereas a diamagnetic substance has a very small negative susceptibility and will tend to be attracted toward the weakest part of an applied inhomogeneous magnetic field, a paramagnetic material has a small ($\sim 10^{-3}$) positive susceptibility and will be attracted towards the strongest part of the field. Further, the diamagnetic substance will set itself with its axis across the applied field while the paramagnetic material will align itself with its axis along the field direction. In an applied $\underline{H}$ field there will be a tendency for the atomic dipoles to turn in such a direction as to minimise their potential energy in the field. The orientation is not directly caused by the field because the torque exerted only gives rise to a precessional motion about the field. The potential energy of each dipole in such a field is

$$U = -\underline{M}\underline{H}\cos\theta \qquad (1.22)$$

Where θ = the angle enclosed by the dipole axis and the field $\underline{H}$. Hence the atoms acquire different energies according to their axis direction. A uniform distribution will no longer be compatible with thermal equilibrium and there will be more dipoles with maximum potential energy, (i.e. lying along the field direction). The simplest theory of paramagnetism assumes that the process of dipole movement is one involving energy exchange under thermal agitation resulting in quantum jumps towards the field direction. The susceptibility (for $\mu_B \ll kT$) is independent of the applied magnetic field but has a simple temperature dependence as the process of dipole alignment is the result of the ordering effect of the applied field and the disordering effect of the thermal agitation. The temperature dependence can be expressed in terms of either the Curie Law

$$k = \frac{C}{T} \tag{1.23}$$

or the Curie-Weiss Law

$$k = \frac{C'}{T-\theta p} \tag{1.24}$$

where C and C' are constants

θp is the paramagnetic Curie temperature.

Substances which obey the Curie Law given by equation (1.23) (at least to a first approximation) are called normal paramagnetics.

Langevin provided a theory of paramagnetism using Boltzmann statistics on an ideal gas in a magnetic field.

He regarded the number of atomic moments per unit volume having an angle between θ and $d\theta$, in a system of N atomic moments per unit volume, as $n\theta d\theta$. He considered that this must be proportional to the solid angle $2\pi\sin\theta d\theta$ and also to the Boltzmann factor $\exp(\underline{M}H\cos\theta/kT)$ (which is the relative probability of an atomic moment to make an angle θ with $\underline{H}$). He arrived at an expression:

$$\bar{\mu}/\mu = \coth\alpha - 1/\alpha \equiv L(\alpha) \qquad (1.25)$$

where $\bar{\mu}$ = the mean effective molecular magnetic moment.

$$= \frac{M}{m}$$

where M = the resultant magnetic moment in the field direction and m = number of molecules

$$\alpha = \mu M/kT \qquad \text{where } k = \text{Boltzmanns constant.}$$

$L(\alpha)$ = the Langevin function and a plot of $L(\alpha)$ versus α (Fig 1.4) shows that $\alpha \rightarrow \infty$ L approaches unity. As $\underline{H}$ approaches ∞ the magnetisation in the material becomes a maximum and the dipoles become perfectly aligned with the field.

Brillouin adopted a more vigorous approach observing the restrictions imposed by quantum mechanics. Spatial quantization of angular momentum restricts the spin to discrete orientations. Brillouin considered each atom or ion to have an angular momentum quantum number J and a permanent magnetic moment $Jg\mu_B$ where g = the Landé splitting factor.

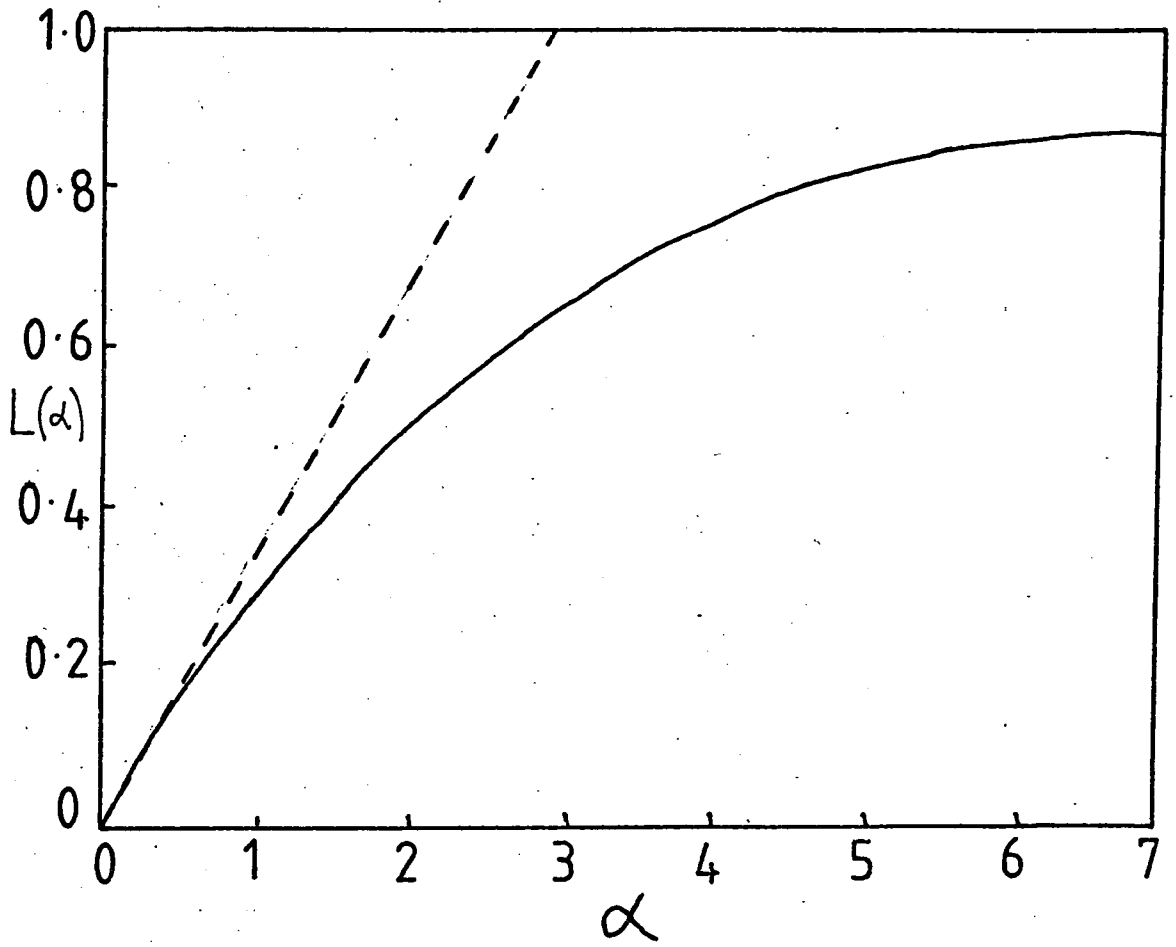

Fig. 1.4 The Langevin Function

$$g = \frac{1 + J(J + 1) + s(s + 1) - L(L + 1)}{2J(J + 1)} \qquad (1.26)$$

in terms of the spectroscopic quantum numbers L s and J.

The number of atoms with a particular orientation will be determined, according to statistical mechanics, by the Boltzmann factor.

$$\exp(M_J g \mu_B H/kT)$$

where M_J = J, (J - 1) ... -(J - 1), J.

= the resolved values of J along the field.

Using this to calculate the population of the levels and summing over the levels equation (1.27) is obtained.

$$\bar{\mu}/\mu = \frac{2J + 1}{2J} \coth \left(\frac{2J + 1}{2J}\right)\alpha - \frac{1}{2J} \coth \left(\frac{\alpha}{2J}\right) = B_J(\alpha) \qquad (1.27)$$

$B_J(\alpha)$ is the Brillouin function of the variable

$\alpha = Jg\mu_B H/kT$

In the absence of quantised orientations the moments can assume any orientation and $J \rightarrow \infty$

$$\therefore \frac{2J + 1}{2J} \sim 1$$

Hence $B(\alpha)$ approaches $L(\alpha)$

The susceptibility is given by (for details see Morrish (1965)) or Martin (1966)).

$$k = \frac{Ng^2 J(J + 1)\mu B^2}{3kT} = \frac{N\mu^2}{3kT} \qquad (1.28)$$

The quantity $g(J(J+1))^{\frac{1}{2}}$ is the effective number of Bohr magnetons

$$\therefore K = N p_{eff}^2 \mu_B^2 / 3kT$$

Hence this gives the Curie Law

$$K = C/T$$

where $C = N\mu^2/3k \quad \therefore K = Ng^2J(J+1)\mu_B^2/3kT$

The treatment above is that of an ideal paramagnetic gas in which the mutual effect of the elementary magnets would be negligible. The treatment was extended by Weiss to include paramagnetics in general and also ferromagnetics. Weiss imagined an internal molecular field which was proportional to the magnetization intensity acquired. Hence the total effective field $\underline{H}$ eff is given by

$$\underline{H}eff = \underline{H}app + N_w \underline{M} \qquad (1.29)$$

where the quantity Nw is the Weiss mean field constant. This quantity is the constant of proportionality relating the internal field with the intensity of magnetization.

Now $K = \underline{M}/\underline{H}$

$$\therefore \underline{M} = \underline{H}K = \frac{\underline{H}\, Ng^2J(J+1)\,\mu_B^2}{T \qquad 3K}$$

$$= \frac{\underline{H}\, C'}{T}$$

$\underline{H}$ must be replaced by $\underline{H}$ eff from equation (1.29)

which gives

$$\underline{M} = \underline{H}_{eff} C'/T = (H_{app} + N_w \underline{M})\, C'/T$$

Now $$K_{Curie\text{-}Weiss} = \underline{M}/\underline{H}_{app}$$

$$\therefore K = (1 + N_w K)\frac{C'}{T}$$

giving $$K = \frac{C'}{T - CN_w}$$

$$= \frac{C'}{(T-\theta_p)}$$

This formula expresses the Curie-Weiss Law and positive θ_p values give ferromagnetic or ferrimagnetic behaviour and negative θ_p values gives antiferromagnetism.

Paramagnetism in metals is due to electrons in the conduction band aligning their spins with the applied field. Using Fermi-Dirac statistics a density of states function can be defined which is a measure of the permissible states available (not necessarily occupied) to conduction electrons. If a magnetic field is applied these free electrons have a spin moment which is spatially quantised, having two possible orientations (corresponding to the spin quantum number $=+\frac{1}{2}$ and $-\frac{1}{2}$ respectively). The magnetic moment parallel or antiparallel with the field will be $g_s m_s \mu_B$ where g_s = spin only g factor = 2 and $m_s = \pm\frac{1}{2}$. $\therefore$ magnitude of the magnetic moment will be $\pm \mu_B$. At T = 0K electrons fill energy levels up to the Fermi level and at temperatures above this only those electrons

at or near this level will obtain enough energy to change quantum numbers. Hence the spin or Pauli paramagnetism is small.

In paramagnetism the total moment will be $M_{para} - M_{dia}$.

1.9 FERROMAGNETISM

Some elements viz. iron, nickel, cobalt, and rare earth elements gadolinium, terbium, dysprosium, holmium, erbium and thulium, while being paramagnetic materials, have magnetic properties which differ vastly from normal paramagnetic behaviour. Taken as a group they are labelled ferromagnetic elements. Whereas the susceptibilities per gram atom of paramagnetics and diamagnetics are about 10^{-1} and 10^{-5}, those of ferromagnetic transition elements are about 10^{3} to 10^{5} bigger. Also, the large positive susceptibilities of ferromagnetics are field and temperature dependent. Most importantly ferromagnetics spontaneously retain their magnetism in the absence of an applied field and this magnetism is retained so long as the material is below a temperature θ_c known as the material's Curie temperature. Above this temperature the material becomes a normal paramagnetic obeying approximately the Curie-Weiss Law.

A theoretical account of the properties of ferromagnetics is not easy. Ferromagnetism can be explained in terms of the quantum theory and the following aspects of the quantum theory are important to the existence of ferromagnetism.

1. In a given system the electron motions will tend to be those allowed motions representing the lowest energies.

2. In complete electron shells the electrons are compelled by the Pauli exclusion principle to pair off, each pair having no net spin or orbital magnetic moment.

3. A pair of electrons which can undergo interaction will do so with their spins either parallel or antiparallel. These interactions are a function of their wave nature rather than being dipole - dipole interactions.

Pairs of electrons forming covalent bonds can have a quantum mechanical motion which involves each electron having its motion associated with one ion in the bond, or both electrons moving around only one of the ions, or both moving around both ions. Further, their spins may be parallel or antiparallel. The electrons in the penultimate shell of the transition elements are allowed a motion of lowest energy with spins parallel and this gives rise to paramagnetism. Certain of the conduction and penultimate shell electrons in ferromagnetic materials can have collective motions involving spins all parallel to one given direction. The motions are a combination of normal electrical conduction type or ones where electrons spend time moving around a pair of adjacent atoms. The consideration which needs to be made is under which circumstances do motions involving parallel spins represent a lower energy than those involving antiparallel spins?

It would appear that a piece of iron should become spontaneously magnetized to saturation and then become very difficult to demagnetize.

The reversibility of the sign of the magnetic moment indicated an internal atomic origin and Weiss postulated the concept of magnetic domains. These domains, he suggested, were regions in the crystal in which the direction of magnetization was constant. These directions are likely to have special relations to the crystal axes and are called directions of easy magnetization. Because each domain may have several easy directions then a demagnetized specimen can be considered to consist of many domains randomly orientated throughout the bulk of the material. The boundaries between domains may be a region of strain or fracture on the edges of a small crystalite or, in a single crystal, a region where the spin orientation changes from that of one domain to that of the other. Good evidence for domains is the Barkhausen effect where the graph of the $\underline{B}$ field of a ferromagnetic material versus $\underline{H}$ is not continuous but consists of a series of jumps. Other evidence is, of course, provided by the various techniques (to be discussed later) of domain observation.

Below the Curie temperature (TC) a Weiss field is postulated and equation (1.29) in the absence of an applied field Happ becomes

$$\underline{H}eff = Nw\underline{M}_s \qquad (1.30)$$

where $\underline{H}eff$ and $\underline{M}_s$ are a function of the temperature T for $T < TC$.

Weiss postulated the existence of magnetic domains in order to explain the large values of magnetization obtained when a ferromagnetic material is subjected to even small applied fields. The domains where magnetization lies in the direction of the applied field grow at the expense of the others. In iron, for example, the force required to

overcome the thermal disordering effect and align neighbouring dipoles is equivalent to a magnetic field strength of about $5.5 \times 10^6 A\,cm^{-1}$ This force is the Weiss molecular field.

The state of magnetization of a ferromagnetic is determined by the equation (1.27).

$$\bar{\mu}/\mu = \frac{2J+1}{2J}\coth\left(\frac{2J+1}{2J}\right)\alpha - 1/2J \coth(1/2J)\alpha$$
$$= B_J(\alpha)$$

The magnetization $M_s(T) = NJg\mu_B B_J\ (Jg\mu_B H/kT)$ (1.31)

where $(Jg\mu_B H/kT) = \alpha$

The saturation predicted by equation (1.30) occurs when $B_J(\alpha) \to 1$ as $\alpha \to \infty$ i.e. as $T \to 0$

(When J becomes great (with μ_B becoming small to keep $J\mu_B$ finite) B_J passes asymptotically into the classical Langevin function $L(\alpha)$).

$$M_s(0) = NJg\mu_B \quad (1.32)$$

The ratio of equation (1.31) to (1.32) gives

$$Ms(T)/Ms(0) = B_J(\alpha) \quad (1.33)$$

Now for ferromagnetics the total field H = Happ + H spontaneous where H spontaneous is given by equation (1.30) as

$$N_w Ms$$

Where $\underline{Ms}$ = $\underline{Ms}(T)$ the spontaneous magnetization which is a function of temperature.

$$\alpha \text{ becomes } \frac{Jg\mu_B(Happ + NwMs(T))}{KT}$$

and for zero applied field

$$\alpha = \frac{Jg\mu_B\, NwMs(T)}{KT} \qquad (1.34)$$

Hence equation (1.33) gives

$$\frac{Ms(T)}{Ms(0)} = \frac{B_J Jg\mu_B NwMs(T)}{KT} \qquad (1.35)$$

Ms(T) appears on both sides of the equation and hence the equation cannot be rearranged to give a simple relationship between Ms(T) and T.

Rearranging equation (1.35) gives

$$Ms(T) = \frac{\alpha\, KT}{Jg\mu_B Nw}$$

and the ratio Ms(T)/Ms(0) becomes

$$\frac{Ms(T)}{Ms(0)} = \frac{KT\,\alpha}{NNwg^2\mu_B{}^2J^2}$$

$$\frac{Ms(T)}{Ms(0)} = \left(\frac{KT}{N_w gJU_B Ms(0)}\right).\alpha \qquad (1.36)$$

(1.36) is linear with a slope proportional to T.

The value of Ms(T) for a given temperature can be obtained by plotting the graphs representing equations (1.33) and (1.36) and looking for the point of intersection of the two curves. Fig. 1.5 shows the method. Plot (a) represents $T > TC$ and no intersection of the curves occur. Spontaneous magnetization = zero. Plot (c) shows an intersection with (d) for $T < TC$. Plot (b) is for $T = TC$ and the line (b) intersects (d) at the origin and is also a tangent to (d) at this point. TC therefore represents a critical temperature below which the straight line intersects curve (d) at two points (one of which is the origin). This occurs for large Nw (or small T).

The slope of the brillouin function at $\lambda \to 0$ is $(J + 1)/3J$ and this can therefore be equated at TC to the slope of the line (C) which is $kT/NNwJ^2g^2\mu_B^2$

$$\text{where } T = TC$$

$$\therefore \frac{J + 1}{3J} = kTC/NNwJ^2g^2\mu_B^2$$

$$\therefore TC = \frac{Ng^2\mu_B^2J(J + 1)\,NW}{3k} \qquad (1.37)$$

This gives (by substituting for Nw in (1.36))

$$M_s(T)/M_s(0) = \frac{J + 1}{3J}\left(\frac{T}{TC}\right)\alpha \qquad (1.38)$$

and M(T)/M(0) as a function of T/TC can be found either algebraically or graphically.

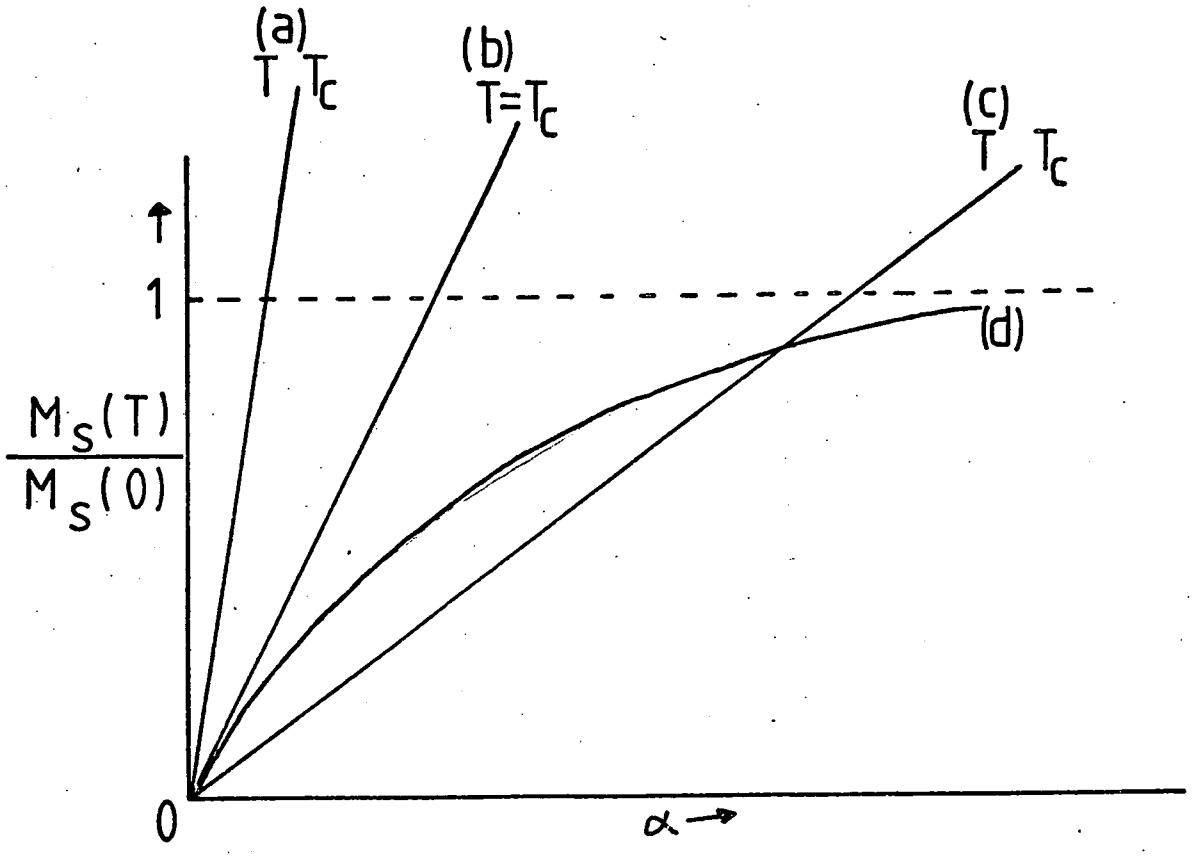

Fig. 1.5 Graphical method to determine spontaneous magnetization at a temperature T.

Curves (a), (b) and (c) represent the equation

$$M_s(T)/M_s(0) = \frac{kT}{g^2J^2U_B{}^2Nw}\alpha$$

Curve (d) represents the equation

$$M_s(T) = M_s(0)B_J(\alpha)$$

Equation 1.38 can also be arranged to give

$$\frac{M_s(T)}{M_s(0)} = B_J\left(\frac{3J}{J+1}\,\frac{Tc}{T}\,\frac{M_s(T)}{M_s(0)}\right) \qquad (1.39)$$

and it is apparent that the variation of $M_s(T)/M_s(0)$ with T/Tc does not depend on parameters which vary from one material to another and should yield a universal curve (according to the Weiss theory) obeyed by all ferromagnetics (for a given J value). Figure 1.6 shows plots of $M_s(T)/M_s(0)$ vs T/Tc.

The value of the molecular field ($\sim 10^{3}$T) is too large to be explained in terms of dipole-dipole interactions. Iron, for example, is characterized by 8 electrons. 2 x 4s electrons which are compensated and 6 x 3p electrons, four of which are uncompensated. Why these electrons should align spontaneously in a given direction in a given state without forming pairs is thought to be a result of an exchange interaction. Orbits of the magnetic electrons can interpenetrate one another and in this way an exchange interaction is set up. This is, in a sense, a quantum electron resonance which is a purely quantum mechanical concept having no classical counterpart. This produces the Weiss field.

Although exchange reaction is electrostatic, the form is equivalent to the magnetic interaction $\underline{S_i S_j}$. (See Chapter Two).
The use of an exchange integral J is convenient and it can be shown that the exchange (interactional) energy W_{ij} between the ith and jth electron spin in a given solid is given by:

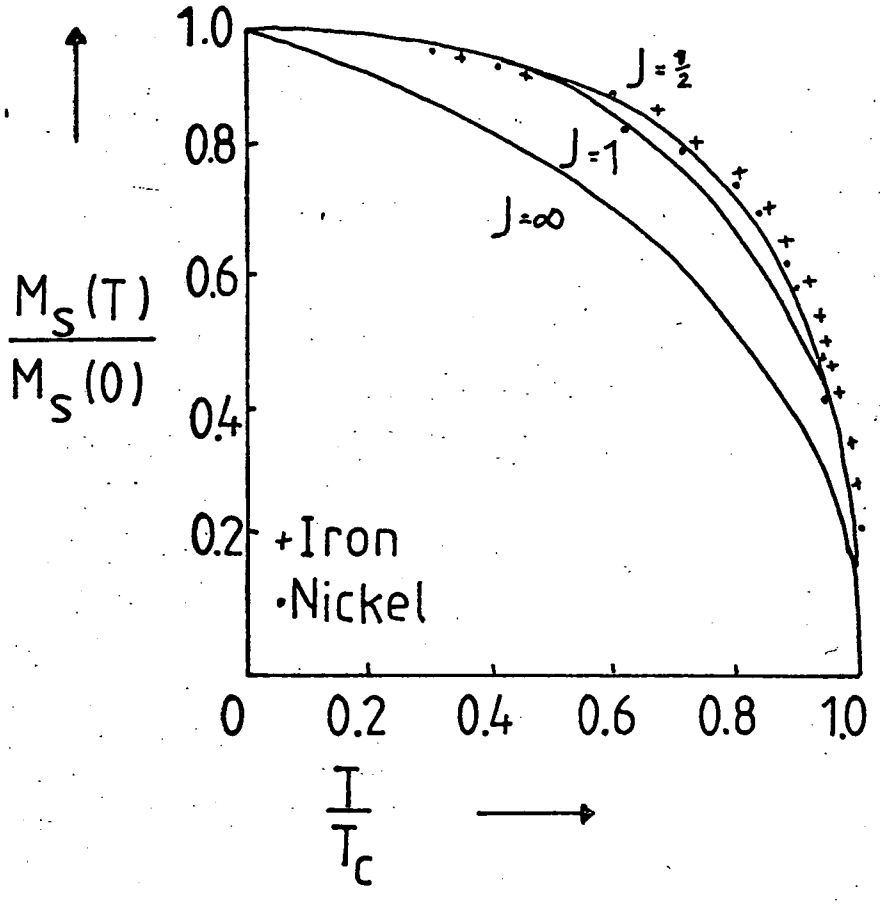

Fig. 1.6 The curves represent the theory.

The points represent experimental data.

(F. Tyler. Phil Mag. 11 596 (1931))

$$W_{ij} = -2JSi.Sj \sum \cos \phi ij \qquad (1.40)$$

where ϕij is the angle between the magnetic moments of the two spins. (Figure 1.8)(a).

The formula represents a general phenomenon but only in ferromagnetics do the spins align in the same direction. Thus exchange integral can be determined as a function of a/r

where a = interatomic spacing

r = shell radius

J can take positive or negative values (Figure 1.7).

Some compounds of Manganese (MnAs, MnB) have a/r ratios greater than 1.5 and are ferromagnetic.

Many ferromagnetics have very large J values and have Curie temperatures above room temperature. Gd has a low J value and has a Curie temperature of 289K.

As can be seen from equation (1.30) the interaction energy is a minimum for $\phi ij = 0^{o}$. If J is negative then Wij is only a minimum for $\phi ij = 180^{o}$, i.e. two antiparallel spins. This state is antiferromagnetism.

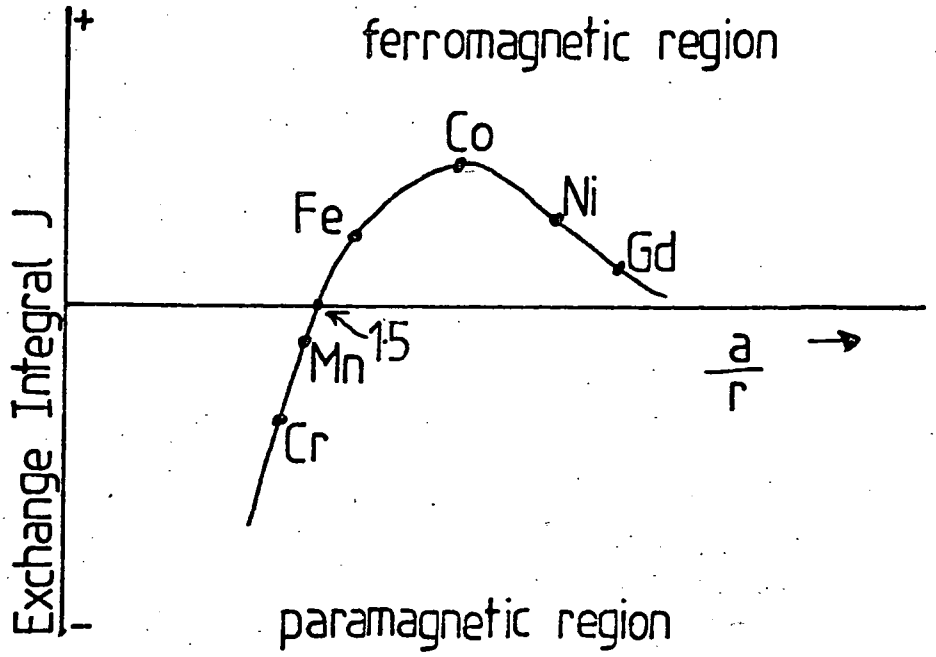

Fig. 1.7 Exchange integral J versus a/r. (Bethes curve)

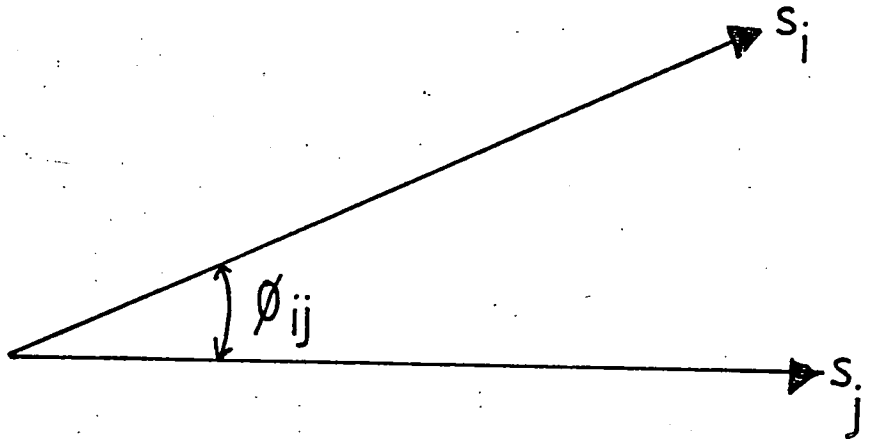

Fig. 1.8(a) The angle between magnetic moments of the spins Si and Sj.

1.10 MAGNETOCRYSTALLINE ANISOTROPY

As previously explained, Weiss postulated a demagnetized ferromagnetic material as consisting of domains of all orientations and that a magnetized ferromagnetic material consisted of domains which may or may not lie all in the same direction but most lying in the direction of magnetization. (A saturated ferromagnetic material being one large domain.) The process of magnetization is, therefore, one of domain alignment. Domains in the applied field direction grow at the expense of domains with other alignments. If a ferromagnetic single crystal is taken to saturation by the application of a gradually increasing field, then the approach to saturation differs according to the orientation of the applied field with respect to the crystal axes. Saturation in one direction will occur for smaller values of $\underline{H}$ than in another direction. Some directions are termed easy, while others are termed hard. In hexagonal cobalt the preffered or easy direction is parallel with the c axis. In iron (body centred cubic lattice) the easy directions lie along the six $\langle 100 \rangle$ directions. (Figure 1.8)(b). Hence saturation with the applied field in this direction occurs for lower values of $\underline{H}$.

The excess energy W_k which is required to magnetize a crystal in a given direction over that required for an easy direction is expressed as a power series of the direction cosines of the magnetization vector with respect to the crystal axes. The phenomenon is called Anisotropy. The expression is constrained by the symmetry of crystal lattice to which it applies.

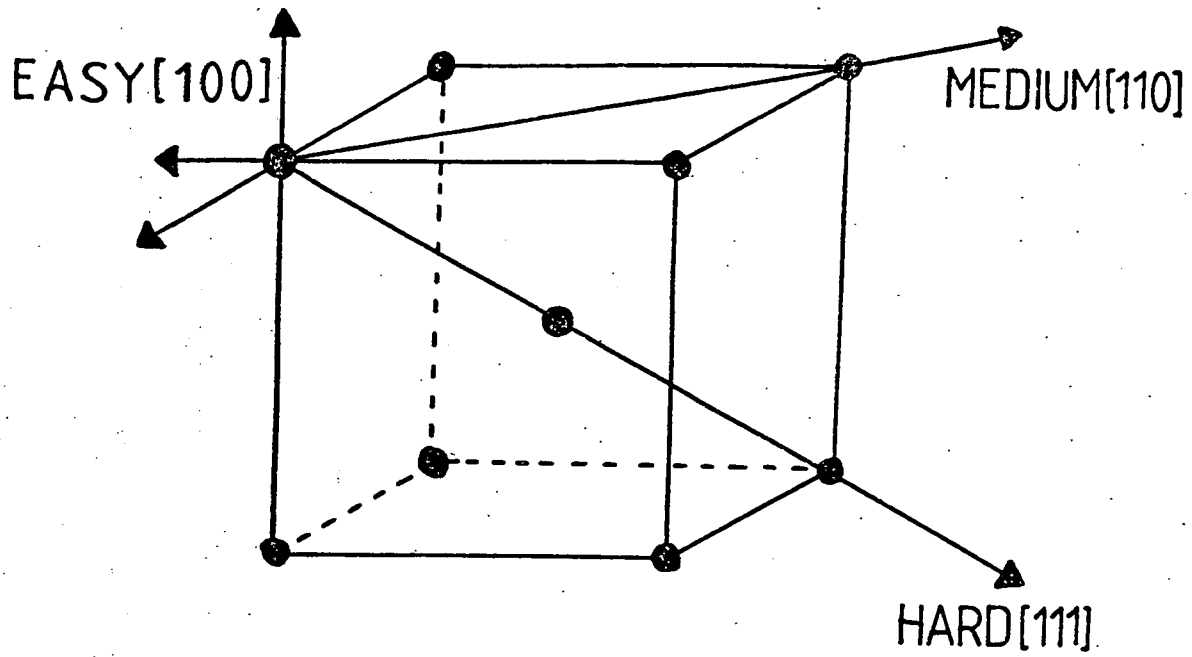

(Iron).

Fig. (1.8)(b.) (See Carey and Isaac (1966))

For a cubic crystal

$$W_k = K_1(\alpha_1^2\alpha_2^2 + \alpha_2^2\alpha_3^2 + \alpha_3^2\alpha_1^2) + K_2\alpha_1^2\alpha_2^2\alpha_3^2 + \ldots \quad (1.41)$$

K_1 and K_2 are constants of the material (the α values represent the direction cosines). Magnetocrystalline anisotropy is important in determining the thickness, energy and mobility of domain walls and is discussed in detail in Chapter Two).

There are other anisotropies which cause the magnetic properties of a material to depend upon applied field direction.

1.10.1 Shape Anisotropy

If the crystal has different demagnetizing factors along its three directions a, b and c, then there is what is termed a shape anisotropy as the demagnetizing factors depend upon the shape of the body to be magnetized.

1.10.2 Stress Anisotropy (Magnetostrictive)

This is introduced by applying mechanical stress to the body and is induced by such things as heat-treating or strain introduced in the crystal growth.

1.10.3 Anisotropy introduced by

(a) magnetic annealing

(b) plastic deformation

(c) irradiation

1.10.4 Exchange anisotropy

Only magnetocrystaline anisotropy is intrinsic to the material, all of the other being extrinsic. 1.10.3 (c) 1.10.4 are uncommon.

1.11 MAGNETOSTRICTION AND MAGNETOELASTIC ENERGY

When the magnetization of a magnetic material is varied there occurs an associated change in its dimensions. This phenomenon is called magnetostriction and it was first observed by Joule in 1842. The dimensional distortion arises because of the interdependence of elastic and magnetic energies and this implies that an applied stress will affect the magnetization of a specimen. (Villari Effect). Stress affects the preferred directions of domain magnetization, hence anisotropy is closely linked with magnetostriction. In iron, for example, the affect of tension is to create a preferred direction of magnetization parallel to the direction of stress. Two kinds of magnetostriction can be distinguished. Linear magnetostriction is an anisotropic magnetostriction as the sample is taken from the ideal demagnetized state up to saturation. The second is a volume magnetostriction occurring as the magnetization is changed with temperature which, in the case of hexagonal crystals, may also be accompanied by a change of shape.

1.11.1 Volume Magnetostriction

The magnitude of volume magnetostriction is small compared with that of linear magnetostriction, and is associated with the forces of interaction (exchange energy) between electron spins in the crystal.

The effect is a volume difference between the state in which there is ordering of the atomic moments (ferromagnetic or antiferromagnetic) and the state in which they are disordered (paramagnetic) and, as such, can be considered as an anomalous thermal expansion which occurs when the sample is heated or cooled through the respective transition temperature. Figure 1.9 shows the volume magnetostriction (defined as the volume change per unit volume) as a function of temperature. The exchange interaction (Chapter Two) causes parallel alignment in ferromagnetics and antiparallel alignment in antiferromagnetics according to the sign of the exchange integral J. The Bethe-Slater curve (Figures 1.11 (a) 1.7 and 2.2) shows how the magnitude and sign of J is a function of the ratio of interatomic distance to diameter of sub-shell of the atoms responsible for the atomic magnetic moments. Figure 1.11(b) shows the Curie temperature θ_c and the Neel temperature θ_N as a function of this ratio. Figure 1.12 shows what happens to the length of an iron specimen as it is cooled to temperatures below its Curie temperature. The continuous curve shows what should happen to the length as a result of thermal cooling. At point B on the curve however (corresponding to the length at the Curie temperature) ordering begins to take place thereby introducing an exchange energy term W_E. The crystal expands slightly resulting in elastic energy being stored and exchange energy W_E being reduced. In order to minimise the total energy due to these two components the crystal dimensions are adjusted resulting in the broken line of figure 1.12. Hence, without the phenomenon of magnetic domain formation and the associated exchange energy, the interatomic spacing of iron at room temperature would be a_1.

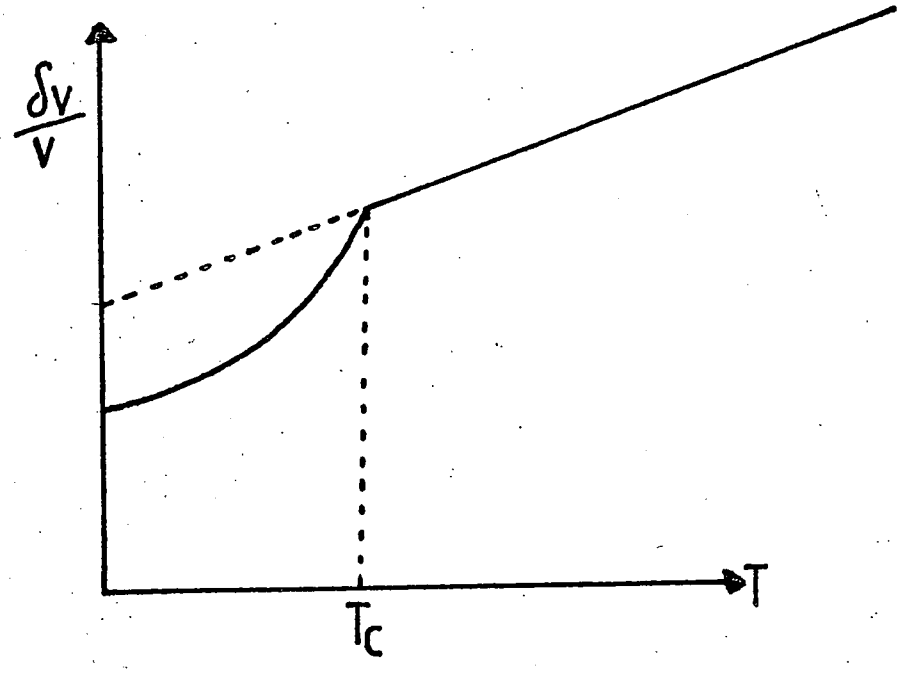

Fig. 1.9 Volume magnetostriction versus temperature. The broken line shows the hypothetical paramagnetic state. The relative volume difference (between the curves) is $\sim 10^{-3}$.

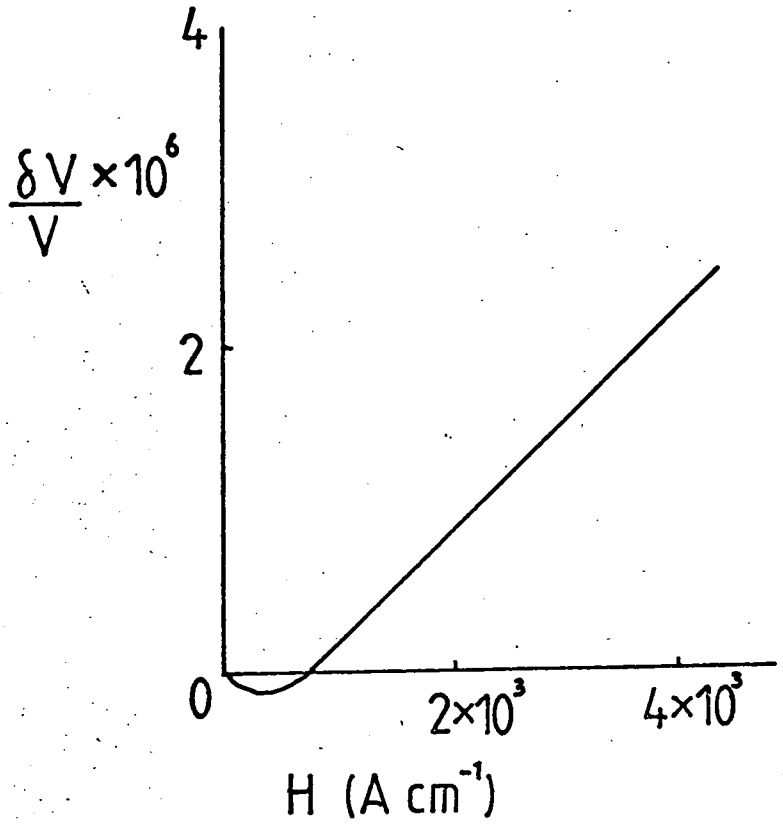

Fig. 1.10 Volume magnetostriction of iron for high applied fields (in the direction of the applied field).

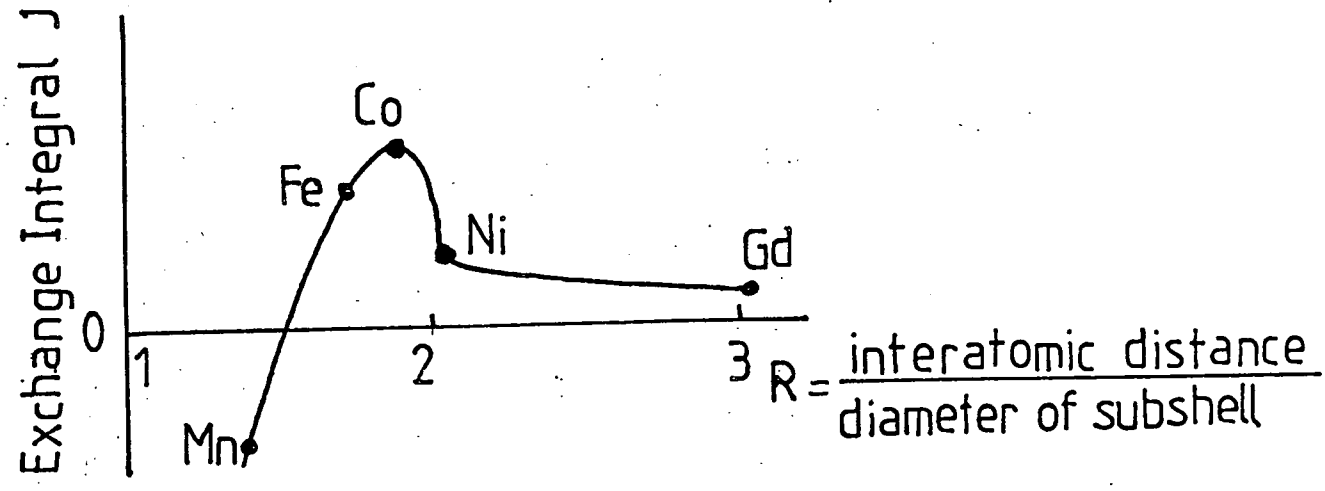

(a)

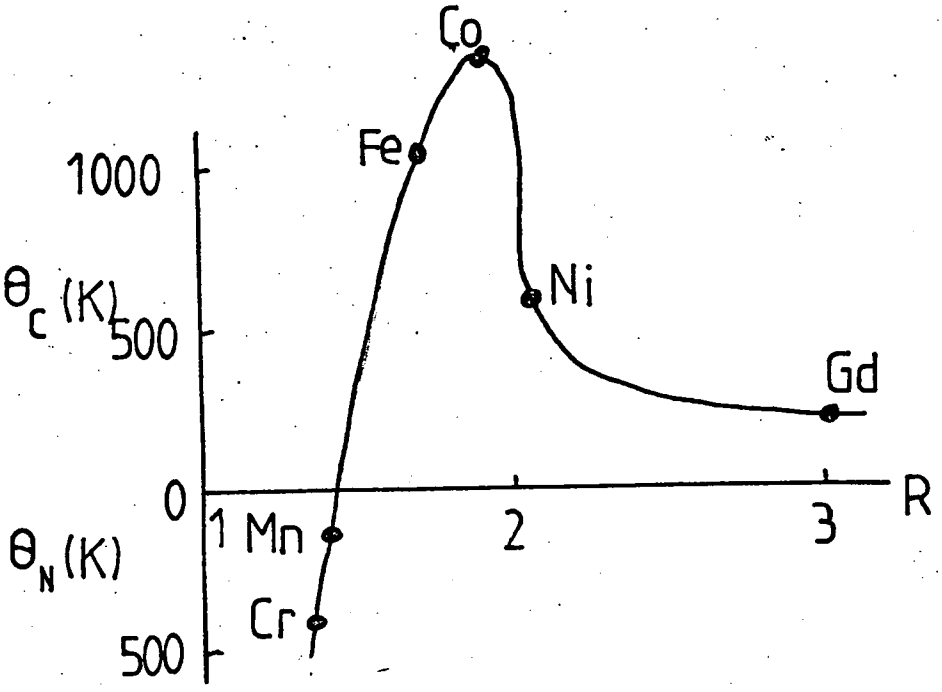

(b)

Fig. 1.11 (a) Bethe-Slater curve.

(b) Curie temperature θ_c, Néel temperature θ_N versus ratio.

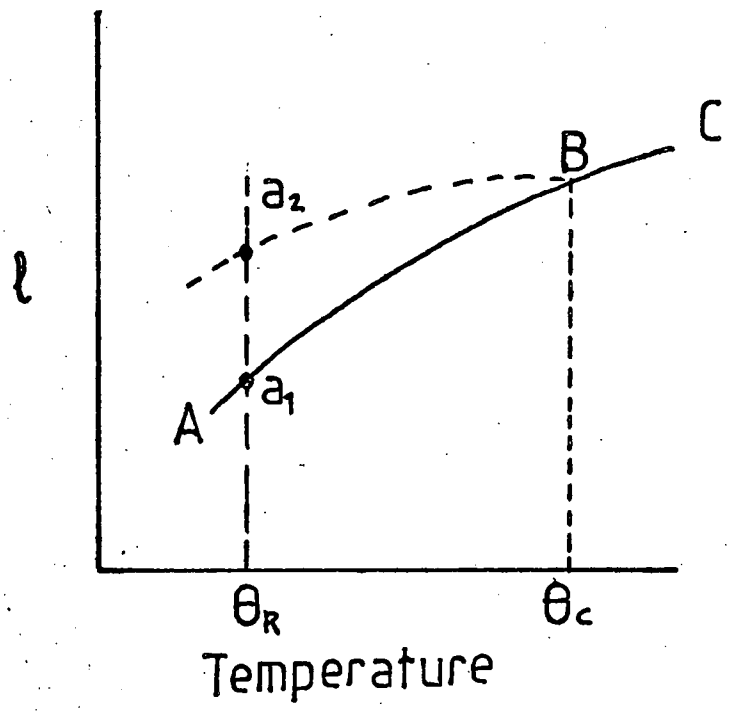

θ_R = room temperature

Fig. 1.12 Variation of length of iron sample as it is cooled below θc. Broken line indicates the actual contraction due to volume magnetostriction effects. The continuous curve from B to A is a hypothetical curve ignoring the effects of domain formation and exchange energy.

Because the lattice adjusts to minimise the combination energy of exchange and elastic energies, the actual room temperature interatomic spacing is a_2.

1.11.2 Linear Magnetostriction

The magnetostriction is defined as the fractional change in length associated with a change in magnetization from zero to saturation.

$$\lambda = \delta l / l$$

The value of the magnetostriction depends upon direction. Simple expressions describing the magnetostriction of cubic crystals were derived by Akulov (1928) and Becker and Doring (1939). An expression commonly accepted utilizes five constants.

$$\begin{aligned}\delta l/l = {} & h_1(\alpha_1^2\beta_1^2 + \alpha_2^2\beta_2^2 + \alpha_3^2\beta_3^2 - \tfrac{1}{3}) \\ & + 2h_2(\alpha_1\alpha_2\beta_1\beta_2 + \alpha_2\alpha_3\beta_2\beta_3 + \alpha_3\alpha_1\beta_3\beta_1) \\ & + h_3 s \ [\text{for iron}] \qquad [\text{or } h_3(s-\tfrac{1}{3}) \text{ for nickel}] \\ & + h_4(\alpha_1^4\beta_1^2 + \alpha_2^4\beta_2^2 + \alpha_3^4\beta_3^2 + \tfrac{2}{3}s - \tfrac{1}{3}) \\ & + 2h_5(\alpha_1\alpha_2\alpha_3^2\beta_1\beta_2 + \alpha_2\alpha_3\alpha_1^2\beta_1\beta_3 + \alpha_3\alpha_1\alpha_2^2\beta_3\beta_1)\end{aligned} \qquad (1.42)$$

where $s = \alpha_1^2\alpha_2^2 + \alpha_2^2\alpha_3^2 + \alpha_3^2\alpha_1^2$

the α's denote the direction cosines of the magnetization with respect to the crystal axes.

The β's denote the direction cosines of the measurement direction with respect to the crystal axes.

Because of the dependence of magnetostriction upon direction λ is conveniently defined in terms of the major cubic crystal axes.

λ_{100} is the change in length along [100] when the magnetization is also in that direction.

λ_{111} is the change in length along [111] when the magnetization is also along that direction.

Very often equation 1.42 can be reduced (by considering only dipole-dipole interaction terms) to

$$\delta\ell/\ell = \tfrac{3}{2}\lambda_{100}(\alpha_1^2\beta_1^2 + \alpha_2^2\beta_2^2 + \alpha_3^2\beta_3^2 - \tfrac{1}{3}) + 3\lambda_{111}(\alpha_1\alpha_2\beta_1\beta_2 + \alpha_2\alpha_1\beta_2\beta_1 + \alpha_3\alpha_1\beta_3\beta_1) \qquad (1.43)$$

Hence the magnetostriction in a cubic crystal can be expressed in terms of λ_{100} and λ_{111}.

Also λ_{110} is related to λ_{100} and λ_{111} according to

$$\lambda_{110} = \tfrac{1}{4}\lambda_{100} + \tfrac{3}{4}\lambda_{111} \qquad (1.44)$$

By putting $\lambda_{100} = \lambda_{111} = \lambda$ equation 1.33 becomes

$$\delta\ell/\ell = \tfrac{3}{2}\lambda[(\alpha_1\beta_1 + \alpha_2\beta_2 + \alpha_3\beta_3)^2 - \tfrac{1}{3}]$$

$$\delta\ell/\ell = \tfrac{2}{3}\lambda(\cos^2\theta - \tfrac{1}{3}) \qquad (1.45)$$

where θ is the angle between the magnetization and the measurement direction.

For a polycrystalline material with crystallites orientated at random the saturation longitudinal magnetostriction coefficient λ_s is calculated by averaging equation 1.44 giving

$$\lambda_s = \tfrac{2}{5}\lambda_{100} + \tfrac{3}{5}\lambda_{111} \qquad (1.46)$$

Clark (1980A) determines an expression for $\delta l/l$ (cubic) using the definition

$$\delta l/l = \sum_{i \geq j} \epsilon_{ij}^{eq} \beta_i \beta_j \quad \text{(Kittel (1949))} \qquad (1.47)$$

where ϵ_{ij}^{eq} are the equilibrium strains.

The expression arrived at contains three constants

$$\delta l/l\,(\text{cubic}) = \lambda^{\alpha} + \tfrac{3}{2}\lambda_{100}(\alpha_1^2\beta_1^2 + \alpha_2^2\beta_2^2 + \alpha_3^2\beta_3^2 - \tfrac{1}{3}) + 3\lambda_{111}(\alpha_1\alpha_2\beta_1\beta_2 + \alpha_2\alpha_3\beta_2\beta_3 + \alpha_3\alpha_1\beta_2\beta_1) \qquad (1.48)$$

The symmetry modes are illustrated in Figure 1.13 (See Wohlfarth 1980).

For hexagonal crystals a typical expression (to second order in the direction cosines) for the magnetostriction is:

$$\begin{aligned}\delta l/l = {} & (\lambda_1^{\alpha,0} + \lambda_1^{\alpha,2}(\alpha_3^2 - \tfrac{1}{3}))(\beta_1^2 + \beta_2^2) \\ & + (\lambda_2^{\alpha,0} + \lambda_2^{\alpha,2}(\alpha_3^2 - \tfrac{1}{3}))\beta_3^2 \\ & + \tfrac{1}{2}\lambda^{\gamma,2}((\alpha_1\beta_1 + \alpha_2\beta_2)^2 - (\alpha_1\beta_2 - \alpha_2\beta_1)^2) \\ & + 2\lambda^{\epsilon,2}(\alpha_1\beta_1 + \alpha_2\beta_2)\alpha_3\beta_3\end{aligned} \qquad (1.49)$$

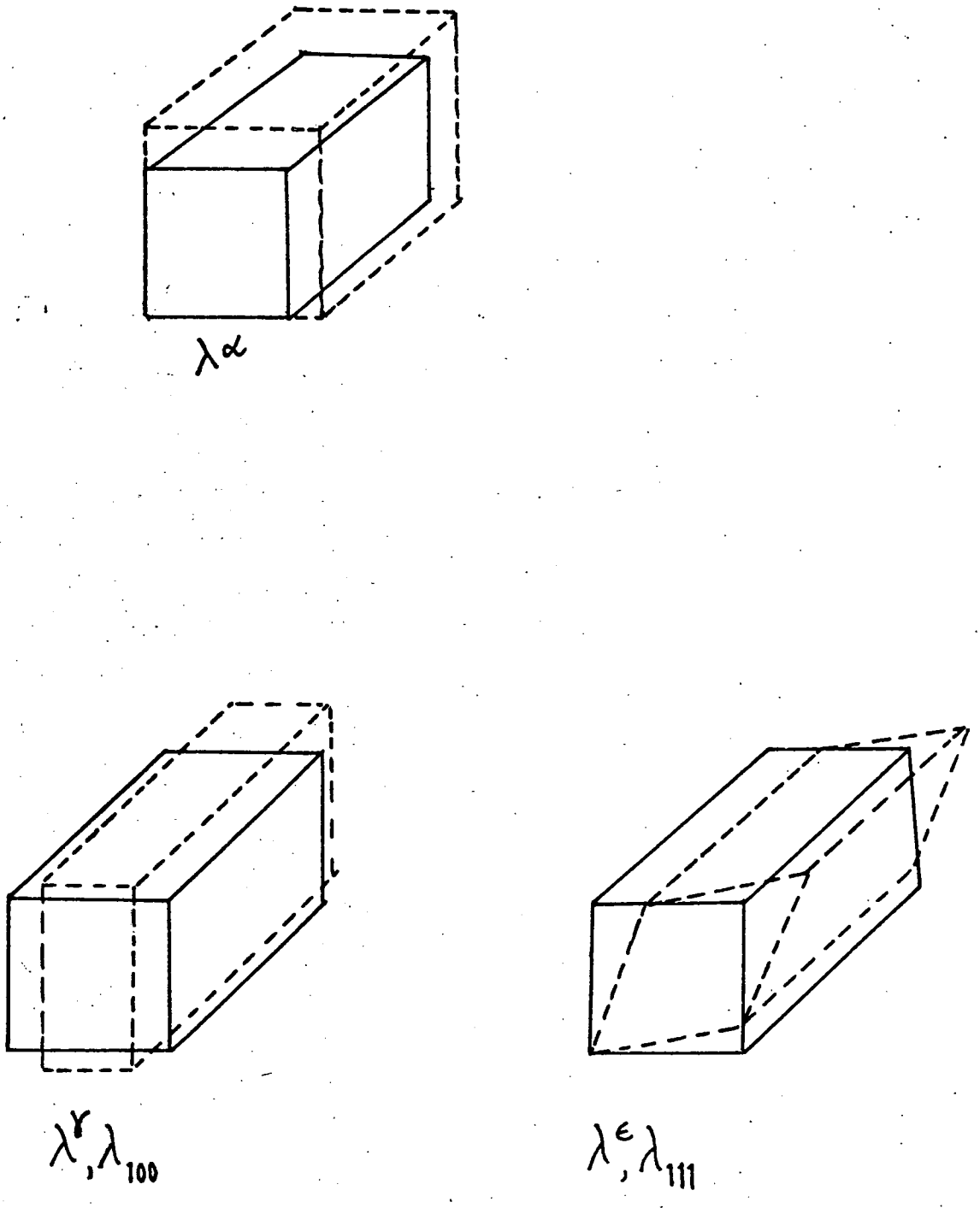

Fig. 1.13 Magnetostriction modes for cubic crystals.

The constants $\lambda_1^{\alpha,0}$, $\lambda_1^{\alpha,2}$, $\lambda_2^{\alpha,0}$, $\lambda_2^{\alpha,2}$, $\lambda^{\gamma,2}$, $\lambda^{\epsilon,2}$ are experimentally determined quantities.

$\lambda_1^{\alpha,0}$ and $\lambda_2^{\alpha,0}$ are related to the anomalous thermal expansion resulting from exchange processes. The strain mode is described by the subscripts α, ϵ and γ.

Figure 1.14 illustrates these modes.

Those modes subscripted with α have symmetry preserved.

$\lambda_2^{\alpha,2}$ denotes a symmetry preserving dilation along the c axes, while $\lambda_1^{\alpha,1}$ denotes a similar process along the basal plane.

As can be seen from Figure 1.14 γ denotes a distortion of the hexagonal symmetry into orthorhombic

In the case 1 = 2 the distortion is a circle to an ellipse.

The ϵ mode is a c axis shear.

In some cases it is necessary to consider terms which are of the fourth order in spin operators or in α_i

The expression below (1.50) was derived by MASON (1954) and can be written following DARNELL (1963) and RHYNE and LEGVOLD (1965) to represent the hcp structure.

$$\begin{aligned}\delta l/l = {} & A(2\alpha_1\alpha_2\alpha_3 + (\alpha_1^2-\alpha_2^2)\beta_1)^2 \\ & + B\alpha_3^2((\alpha_1^2-\alpha_2^2)(\beta_1^2-\beta_2^2) + 4\alpha_1\alpha_2\beta_1\beta_2) \\ & + C((\alpha_1^2-\alpha_2^2)(\beta_1^2-\beta_2^2) + 4\alpha_1\alpha_2\beta_1\beta_2) \\ & + D(1-\alpha_3^2)(1-\beta_3^2) + E\alpha_3^2\beta_3^2(1-\alpha_3^2) \\ & + F\alpha_3^2(1-\alpha_3^2) + G\beta_3^2(1-\alpha_3^2) + H\alpha_3\beta_3(\alpha_1\beta_1+\alpha_2\beta_2) \\ & + I\alpha_3^3\beta_3(\alpha_1\beta_1+\alpha_2\beta_2) + J\alpha_3^2(1-\beta_3^2) + K\alpha_3^2\beta_3^2\end{aligned} \qquad (1.50)$$

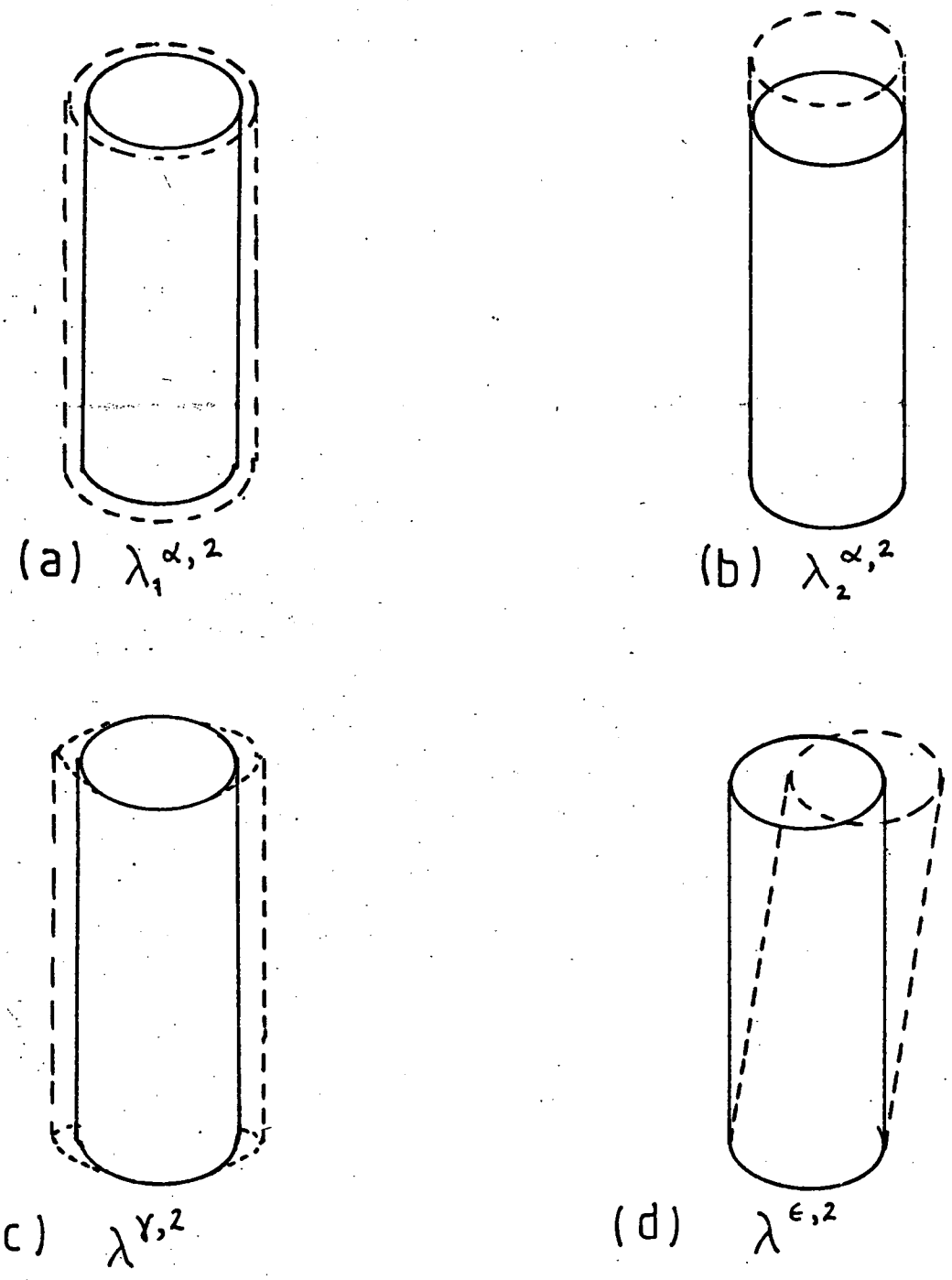

Fig. 1.14. MAGNETOSTRICTION strain modes in l = 2 for hexagonal symmetry.
(After Clark, De Savage and Bozorth (1965))
(Also Taylor and Darby (1972))

The constants A, B, E, F and I are the fourth order magnetostriction constants. C, D, G, H, J and K are linear combinations of the magnetostriction constants due to CALLEN and CALLEN (1965) and those of CLARK etal (1965). (See Coqblin 1977 for a review on the relationships between these coefficients.)

For a material, e.g. Cobalt, where cylindrical symmetry can be assumed such that the magnetostriction in the basal plane is isotropic, then the magnetostriction is given by:

$$\begin{aligned}\delta l/l &= K_1(\alpha_1^2-1)\beta_1^2 + K_2(\alpha_2^2\beta_2^2+\alpha_3^2\beta_3^2)\\ &+ K_3(\alpha_3^2\beta_2^2+\alpha_2^2\beta_3^2) + 2(K_2-K_3)\alpha_2\alpha_3\beta_1\beta_3\\ &+2K_4\alpha_1\beta_1(\alpha_3\beta_3+\alpha_2\beta_2)\end{aligned} \qquad (1.51)$$

For values of K_N see BOZORTH (1954)

In some of the rare earths the easy direction of magnetization is in the basal plane. This means that the anisotropy is so high that there is no significant rotation out of the basal plane in fields of normal magnitude. This is so with Terbium (Chapter Four). The magnetostriction in this case with $\alpha_3 = 0$ can be written

$$\begin{aligned}\delta l/l &= A(2\alpha_1\alpha_2\beta_1 + (\alpha_1^2-\alpha_2^2)\beta_2)^2\\ &+C((\alpha_1^2-\alpha_2^2)(\beta_1^2-\beta_2^2)+4\alpha_1\alpha_2\beta_1\beta_2)\\ &+D(1-\beta_3^2)+G\beta_3^2\end{aligned} \qquad (1.52)$$

1.11.3 Temperature dependence of the magnetostriction constants

Callen and Callen (1965) obtained expressions to relate the variation of the constants to temperature (for single ion case)

$$\lambda(T) = \lambda(T=0)\,\hat{I}_{1+1/2}\left(\mathcal{L}^{-1}(m(T))\right) \qquad (1.53)$$

where $I_{1+1/2}$ is a reduced hyperbolic Bressel function of order $1 + \frac{1}{2}$ and $\mathcal{L}^{-1}(m(T))$ is the inverse Langevin function of the reduced magnetization.

1.11.4 The effect of stress on magnetization (Inverse magnetostriction effects)

If a uniform tension σ is applied to a cubic crystal (for example) such that $\gamma_1\gamma_2\gamma_3$ are the direction cosines then the following terms are added to the crystal free energy.

$$E_\sigma = -\tfrac{3}{2}\lambda_{100}\sigma\left(\alpha_1^2\gamma_1^2 + \alpha_2^2\gamma_2^2 + \alpha_3^2\gamma_3^2\right) - 3\lambda_{111}\sigma\left(\alpha_1\alpha_2\gamma_1\gamma_2 + \alpha_2\alpha_3\gamma_1\gamma_3 + \alpha_3\alpha_1\gamma_3\gamma_1\right) \qquad (1.54)$$

The expression can be simplified by assuming that $\lambda_{100} = \lambda_{111} = \lambda$ or by letting λ = a weight of mean of λ_{100} and λ_{111}

$$E_\sigma = -\tfrac{3}{2}\lambda\sigma\cos^2\theta \qquad (1.55)$$

where $E\sigma$ = magnetoelastic energy

θ = angle between stress direction and magnetization

1.12 ANTIFERROMAGNETISM

If the exchange integral J takes a negative value then energy minimization occurs when the spins are antiparallel. Antiferromagnetism is similar to ferromagnetism in that antiferromagnetic materials show hysterisis effects but have much lower susceptibilities than ferromagnetics. Antiferromagnetic materials are characterized by containing two interlocking sets of atoms or atomic groupings and the crystal structure is such that atoms occupy two separate interpenetrating sublattices, A and B. within a structure as a whole. (Figure 1.15). The negative exchange interaction between nearest neighbours means that the spins of nearest neighbours are always antiparallel. However, parallel alignment can take place within the sublattices.

At low temperatures there are strong interactions between spins resulting in antiparallel spin alignment and the residual magnetization in an applied $\underline{H}$ field is low. K is small($\sim 10 - 4$). At absolute zero none of the spins have a resultant in the applied field direction. As the temperature is increased thermal agitation results in the spins no longer mutually cancelling. The susceptibility rises and a very weak magnetization results. Such a system has a critical temperature called the Néel temperature T_N below which the atomic moments are arranged alternately parallel and antiparallel. Above T_N the moments are paramagnetically disordered. Also some antiferromagnets show ferromagnetic behaviour below T_N or above a critical applied field value. This is known as metamagnetism. Antiferromagnets also show domain effects. (See B.K.Tanner Contemp. Phys. 20 (1979)).

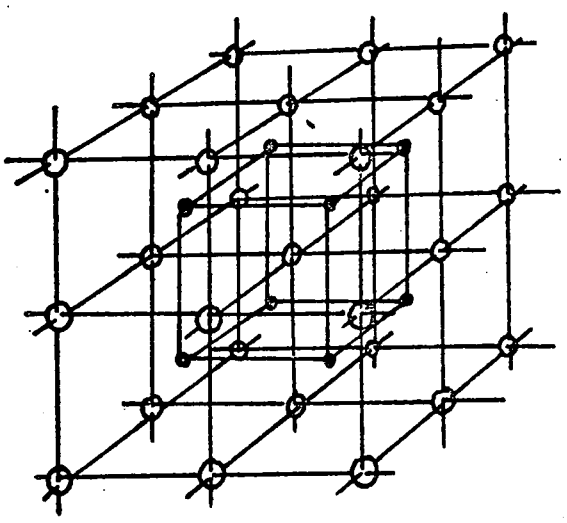

○ A sublattice + spin ↑

● B sublattice − spin ↓

Fig. 1.15 Two sublattice model of an antiferromagnet.

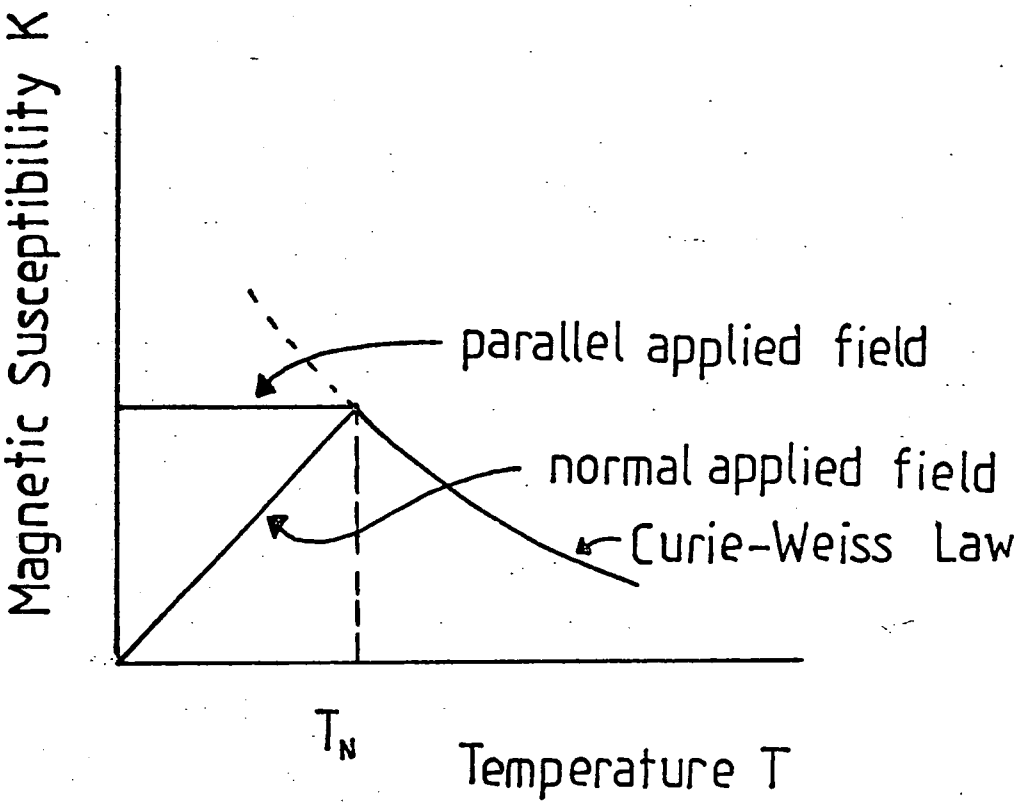

Fig. 1.16 Relative susceptibility as a function of temperature for a ferrimagnetic material.

1.13 FERRIMAGNETISM

In a ferrimagnetic material the magnetic moments of the atoms on different sublattices oppose as in antiferromagnetism. However, the opposing moments are unequal and a spontaneous magnetization remains.

The term ferrospinel, or ferrite, is applied to an iron oxide group having the general formula XOY_2O3, X being a divalent cation and Y a trivalent cation.
The crystal structure is a close packed face centre cubic structure of oxygen anions. The cations are distributed interstitial between the oxygen ions. Eight cations on A sites are surrounded tetrahedrally by 4 oxygen ions, the remaining 16 cations occupy B sites and are surrounded octahedrally by 6 oxygen ions.(Figure 1.17).

In the normal spinel arrangement the divalent cations occupy the A sites while the trivalent cations occupy the B sites. In the so-called inverse spinel arrangement the A sites are occupied by one half of the Y cations while the B sites are occupied with random distribution by the other half of the Y cations plus the X cations.

Three types of interaction are possible. The exchange interaction J for ions on similar sites (J_{AA} and J_{BB}) are positive and comparatively weak, while J_{AB} interactions are strong and predominate. In the inverse spinel structure the A and B sites are quite distant from each other and the assumption is made that the oxygen ion transfers the interaction from the A site atom to the B site atom. (Superexchange)

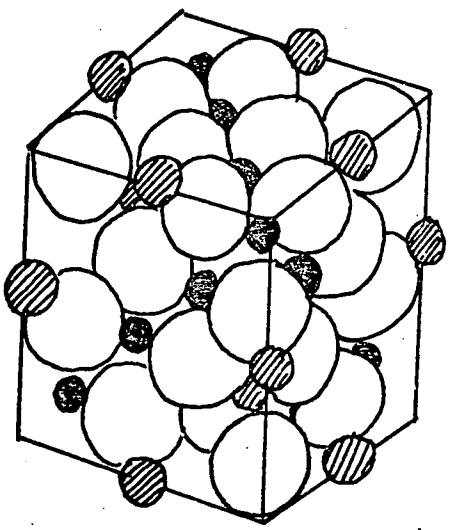

○ O^{2-}

● A sites (tetrahedral)

• B sites (octahedral)

Fig. 1.17 Crystal structure of normal spinel.

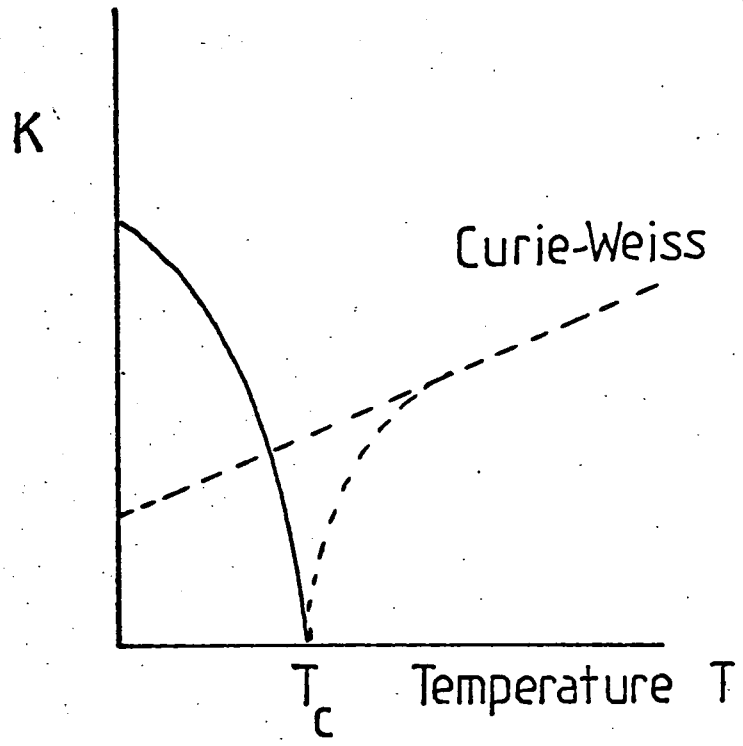

Fig. 1.18 Variation of susceptibility K with T for ferrites.

The J value is negative and antiparallel pairing results. However, A and B site atomic magnetic moments are not equal so a small net magnetic moment results. The oxygen ions lose their two valence electrons in the bonding and these constitute no magnetic moment. The materials have a domain structure which is, in the main, totally randomized and hence do not spontaneously magnetize. Domains however do grow in the direction of an applied field and the material remains magnetized when $\underline{H}_{app}$ is removed. Above Tc the materials are paramagnetic.

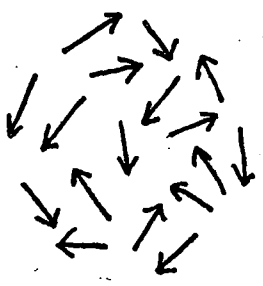

Paramagnetism.

Weak interaction between equal moments. Random spin vectors.

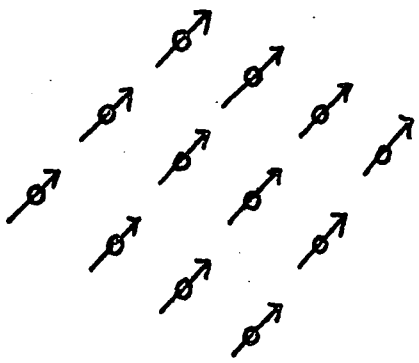

Ferromagnetism.

Positive interactions between equal moments. Parallel spin vectors.

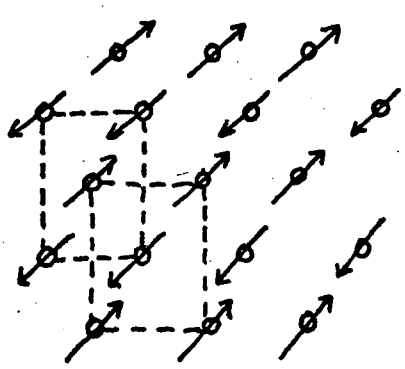

Antiferromagnetism.

Negative interaction between equal moments. Antiparallel spin vectors on two sites.

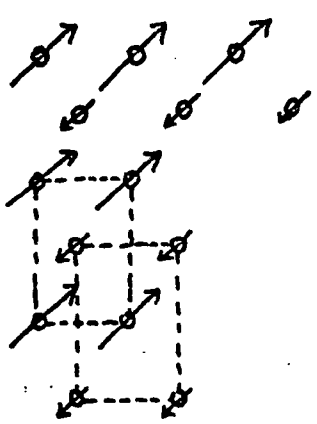

Ferrimagnetism.

Negative interaction between unequal moments. Antiparallel spin vectors on two sites.

(Fig. 1.19)

SUMMARY

DIAMAGNETISM AND PARAMAGNETISM	-	explanation in terms of quantum states and on electron spins of the ion concerned.
FERROMAGNETISM, ANTIFERROMAGNETISM and FERRIMAGNETISM.	-	depends on crystal structures as well as on spin direction.
PARAMAGNETISM, FERROMAGNETISM, ANTIFERROMAGNETISM, FERRIMAGNETISM.	-	all the result of the interaction of electron spin vectors at various lattice sites.
PARAMAGNETISM	-	weak random interactions.
FERROMAGNETISM	-	strongly coupled parallel spin vectors.
ANTIFERROMAGNETISM	-	negative interaction.
FERRIMAGNETISM	-	paired antiparallel but unequal spins

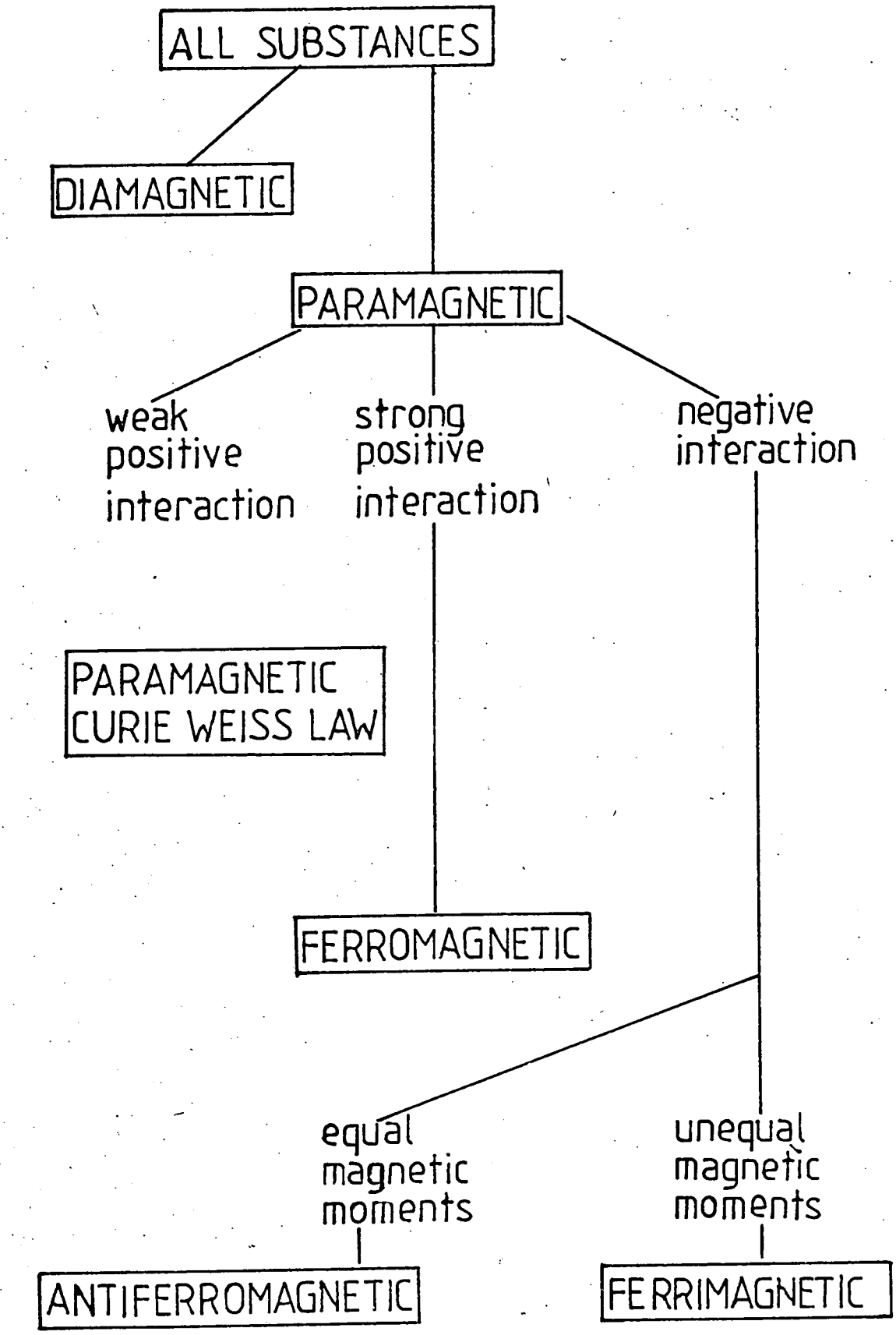
ALL SUBSTANCES
DIAMAGNETIC
PARAMAGNETIC
weak positive interaction
strong positive interaction
negative interaction
PARAMAGNETIC CURIE WEISS LAW
FERROMAGNETIC
equal magnetic moments
unequal magnetic moments
ANTIFERROMAGNETIC
FERRIMAGNETIC

Figure 1.20

CHAPTER TWO

FERROMAGNETISM

CHAPTER 2

FERROMAGNETISM

2.1 THE EXCHANGE INTERACTION

As previously mentioned (Chapter 1.), the Weiss internal field cannot be explained in terms of dipole - dipole interactions. Curie temperatures of hundreds of degrees K mean that thermal energies per atom required to destroy magnetic ordering are $\sim 10^{-7}$J whereas the dipole energy is approximately 10^{-9}J per atom and cannot, therefore, be solely responsible for the internal field. Also, the fact that the internal field is proportional to the existing magnetization suggests that the greater the degree of spin alignment the greater is the force tending to align the spins in that region.

Consider a simple system containing two electrons. As an example, consider the hydrogen molecule. Because this system contains positive and negative charges, then electrostatic coulomb forces would be expected to exist between these charges. The energy of the system contains two terms. The first corresponds to the classical coulomb interaction. The second term has its origins in the Pauli exclusion principle and has, as such, no classical analogue. The energy due to the coulombic forces can easily be calculated using Coulomb's law. For example, if the two electrons are separated by a distance r_{12}, which is great enough to prevent overlapping wave functions, then the electrostatic interaction between them is given by the coulomb formula:

$$E = \iint |\psi_1|^2 d\tau_1 |\psi_2|^2 d\psi_2 / r_{12} \qquad (2.1)$$

where Ψ_1 and Ψ_2 are the charge densities and γ_1 and γ_2 are elementary volumes. As the two atoms approach, however, there is, eventually, an overlapping of wave functions and the Pauli exclusion principle must be applied. This compels the electrons to assume states which are mutually different. The Pauli principle, therefore, tends to keep electrons with parallel spins apart thereby reducing the coulombic repulsion. However, while quantum theory offers no objection to the existence of these Coulomb forces, which are classical in nature, it imposes a constraint on the system by regarding the two electrons as being indistinguishable. In other words, in, for example, the hydrogen molecule the possibility of electron 1, which is moving around nucleus 1, changing places with electron 2, which is moving around nucleus 2, must be allowed for. This constraint adds a term to the system's energy over and above that of equation 2.1. This additional term is known as the exchange energy and the exchange effect is concerned with the degeneracy associated with the possibility of the two electrons changing places. When spin wave functions are symmetrical, orbital wave functions are antisymmetrical and vice versa. Any change in spin symmetry must alter orbital symmetry and thereby redistribute charge. Hence there is a correlation between the two electron spins which, in fact, is proportional to the scalar product of the spin magnetic moments S_1 and S_2. When the Schödinger equation of the system is considered there is a contribution W_{12}, due to this exchange effect, to the total Hamiltonian according to equation 1.30.

$$W_{12} = -2 J_{12} S_1 S_2 \cos \phi 12$$

where J_{12} is the exchange energy between electron 1 and electron 2. Any pair of electrons which can interact can either have parallel or antiparallel spins. The difference in energy between these configurations is the exchange energy.

The idea of exchange was suggested approximately simultaneously and independently by Heisenberg (1926) and Dirac (1926). In 1927 the idea of an exchange interaction was suggested by Heitler and London (1927) in their work on chemical bonding in the hydrogen molecule. Heisenberg's treatment (1928), based on the Heitler London treatment of the hydrogen molecule, showed that, under certain conditions, a positive interaction could have effects similar to those of the Weiss molecular field when electrons having parallel spins have a lower energy than those with an antiparallel spin alignment. Any particular system, wherever possible, will adopt a state of lowest energy and this state, in terms of parallel or antiparallel spins, is determined by the sign of the exchange integral J.

In his treatment, Heisenberg assumed that the magnetic moment was due entirely to the spin of the electron. The roles of spin and orbital motions were examined by Einstein and it was postulated that the process of turning dipoles toward a particular direction during the magnetization process should result in an increase in the total angular momentum about an axis in the field direction. If the angular momentum of the whole specimen is initially zero, then the amount gained by the atomic system must induce an equal and opposite gain by the specimen as a whole in order to conserve angular momentum. The Einstein-de Hass experiment observed this and it was suggested that spin only was involved in ferromagnetism (or at least the spin contribution was about 90%). The Einstein-de Hass effect, therefore, gave foundation to Heisenberg's assumption. Heisenberg showed that the hydrogen molecule J was always negative, thereby making the lower energy state that of antiparallel spins. Figure 2.1 shows a plot of exchange integral J versus internuclear separation.

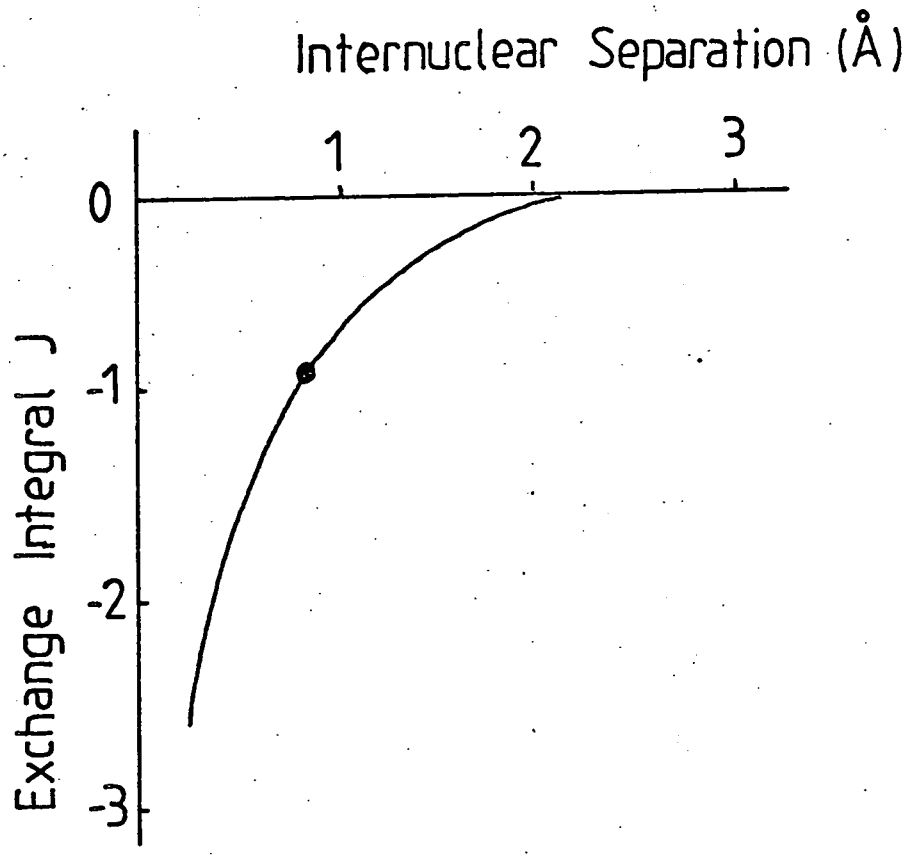

Fig. 2.1 Exchange Integral of hydrogen molecule vs intermolecular separation of atoms. The dot shows the equilibrium separation.

The essentials of exchange in a two electron system are given here. For a fuller treatment see Martin Chapters 5 and 6.

Consider two electrons, say in hydrogen molecule, which are moving in similar potential fields. Assuming that these particles occupy non-degenerate states then the solution of the Schrödinger equation for the system gives rise to a fundamental ambiguity.

Let q_1 and q_2 represent the spatial and spin co-ordinates of electrons 1 and 2 respectively.

i.e. $q_1 = x_1, y_1, z_1, \sigma_1$ where x, y and z are the cartesian co-ordinates fixing the electrons position and σ_1 represents the spin.

A solution of the Schrödinger equation is:

$$\psi(q_1, q_2)$$

However, because the electrons are indistinguishable $\psi(q_2 q_1)$ must also represent a solution of the equation. But, the solution is non-degenerate and therefore only one solution exists.

It follows, therefore, that

$$\psi(q_1 q_2) = K\psi(q_2 q_1) \qquad (2.2)$$

Also

$$\psi(q_2 q_1) = K\psi(q_1 q_2) \qquad (2.3)$$

From this the values of $K = \pm 1$

Hence any interchange of the co-ordinates of the particles will give a value of K = 1 thus leaving the wave function unchanged (symmetrical) or

K = -1 giving an antisymmetrical wave function by changing its sign. Thus for two identical particles the following wave functions are possible.

$$\psi_A = \psi_1(q_1)\psi_2(q_2) - \psi_1(q_2)\psi_2(q_1) \quad (2.4)$$

$$\psi_B = \psi_1(q_1)\psi_2(q_2) + \psi_1(q_2)\psi_2(q_1) \quad (2.5)$$

The wave function of equation 2.4 is antisymmetrical while the wave function of equation 2.5 is symmetrical.

Experiment shows that electrons have wave functions which are always antisymmetrical. A direct consequence of this is the Pauli exclusion principle as the probability that two particles having antisymmetrical wave functions will occupy the same state is zero.

For a two electron system, then, in which the electrons do not interact, the solutions for the Schrödinger equation are:

$$\psi_a(1)\,\psi_b(2) \pm \psi_a(2)\,\psi_b(1)$$

$\psi_a(1)$ is the wave function of electron 1 when it is in atom a etc.

When allowance is made for an interaction taking place between the two electrons then the allowed energies of the system are:

$$E = EO + K_{12} + J_{12} \quad (2.6)$$

where EO is the energy of the unperterbed system

K_{12} is the average coulomb interaction energy.

$$K_{12} = \int \psi_a^*(1)\,\psi_b^*(2)\,V_{12}\,\psi_a(1)\,\psi_b(2)\,d\tau_1\,d\tau_2$$

$$J_{12} = \int \psi_a^*(2)\,\psi_b^*(1)\,V_{12}\,\psi_a(1)\,\psi_b(2)\,d\tau_1\,d\tau_2$$

J_{12} is the exchange integral and represents the probability of electrons 1 and 2 changing places.

$$V_{12} = e^2\left(\frac{1}{r_{ab}} + \frac{1}{r_{12}} - \frac{1}{r_{1b}} - \frac{1}{r_{2a}}\right) \qquad (2.7)$$

where r_{ab} = distance between nuclei

r_{12} = distance between electrons

r_{1b} and r_{2a} are distances between a nucleus and the electron in the other atom.

(See Figure 2.3)

For the condition $E = Eo + K_{12} + J_{12}$ the triplet state has the lower energy and the parallel spin configuration is favoured. For $E = Eo + K_{12} - J_{12}$ the singlet state represents the lower energy and antiparallel spins are favoured. In general J is negative. The reason for this can be seen from equation 2.7.

$\left(\frac{1}{r_{ab}} + \frac{1}{r_{12}}\right)$ represents the repulsion between electrons and the repulsion between the nuclei.

See Figure 2.3.

$\left(\frac{1}{r_{1b}} + \frac{1}{r_{2a}}\right)$ represents the attraction between the nuclei and the electrons.

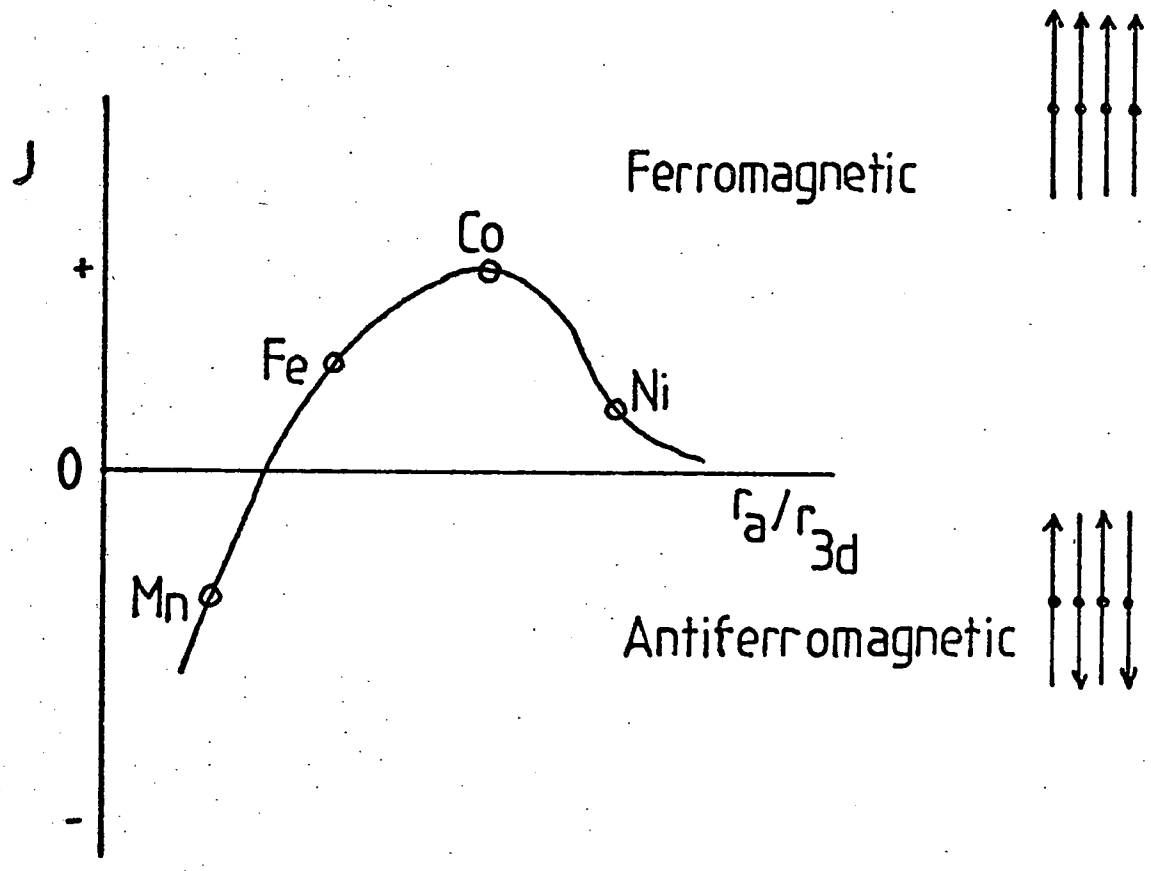

Fig. 2.2 Bethe-Slater curve showing the variation of the exchange integral J with the ratio

$$\frac{\text{ra (radius of atom}}{\text{r3d (radius of 3d orbit)}}$$

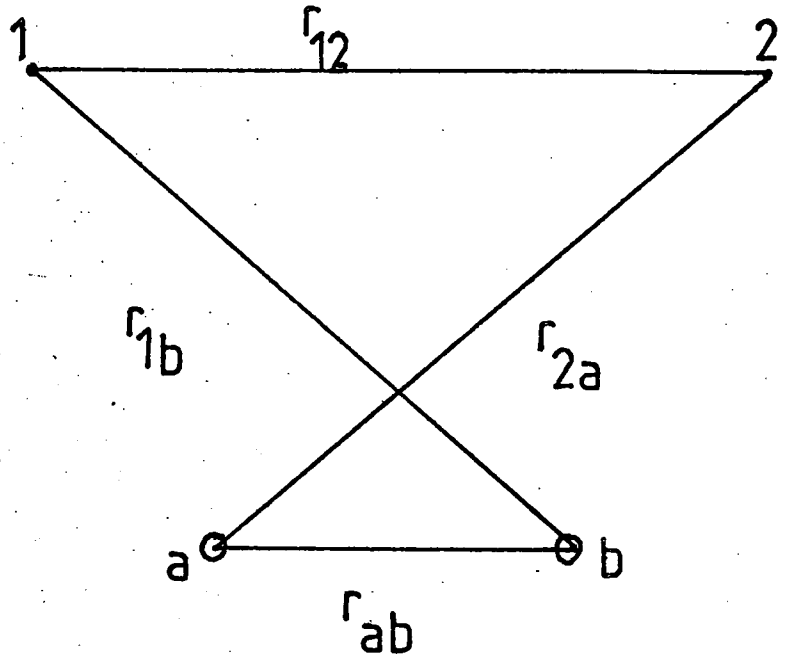

Fig. 2.3 Diagram indicating the distance parameters involved in the exchange Hamiltonian.

Now generally the latter exceeds the former making the quantity V_{12} negative (as can be seen from equation 2.7) J can, however, under certain circumstances, take positive values.

Supposing that, in the region of the overlap, ψ_a and ψ_b have no nodes. $\psi_a^*(1)\psi_b^*(2)\psi_a(2)\psi_b(1)$ is positive.

J_{12} will then be positive if the aforementioned condition is reversed.

i.e. if $(1/r_{ab} + 1/r_{12}) > (1/r_{1b} + 1/r_{2a})$

i.e. the positive term of the Hamiltonian exceeds the negative terms.

This condition is favoured when the wave functions are large midway between the nuclei because it is here where r_{12} is small. The term $-\frac{e^2}{r_{1b}}$ and $-\frac{e^2}{r_{2a}}$ are a minimum for wave functions which are small close to the nuclei. These conditions are favoured for a value of about 1.5 for the ratio r_{ab}/r_{al}. J is positive when the interatomic spacing is large compared with the radii of the orbitals. Hence ferromagnetism is likely to occur in materials with incomplete d or f subshells of a diameter which is less than the internuclear separation. Hence ferromagnetism is likely in some iron and rare earth materials. Manganese is not ferromagnetic at room temperature but some of its compounds are. MnAs and MnSb are ferromagnetic due, probably, to a small change in lattice parameter which favours ferromagnetism by making J positive. The curve of Figure 1.6 is the empirical Bethe-Slater curve and is reproduced as Figure 2.2 for convenience.

Looking at the Eigen values of the S_1 and S_2 gives the result that

$$Vab = K_{12} + J_{12} \text{ when } S_1.S_2 = -\tfrac{3}{4}$$

and

$$Vab = K_{12} - J_{12} \text{ when } S_1.S_2 = \tfrac{1}{4}$$

These can be combined to give

$$E = K_{12} - \tfrac{1}{2}J_{12} - 2J_{12}S_1.S_2 \qquad (2.8)$$

When considering ferromagnetism we need only consider the third term of equation 2.8 as the other two do not depend upon spin. This third term is the two electron Hamiltonian. Now the exchange interaction between two electrons is intimately related to the states of motion. Spin and orbital motion depend upon the environment and in the solid state atoms undergo a perturbation in the presence of their neighbour. Because of the restrictions imposed on the itinerant electrons by the Pauli principle their movements become correlated. Hence applying equation 2.8 (even minus the first two terms) to a multielectron assembly is extremely difficult. An estimation of the energy of such an assembly must include further simplifications. Consider two atoms each with more than one electron with an unpaired spin.

The exchange Hamiltonian is then:

$$W = -2J_{ij}\sum_{ij} Si.Sj$$

$$= -2J_{ij}\sum Si.\sum_j Sj$$

$$W = -2JijSi.Sj \qquad (2.9)$$

According to equation 2.9 the exchange interaction vanishes for closed shells of electrons hence only partly filled shells of atoms or ions need be considered. Exchange forces decrease rapidly with distance hence a further simplification can be made if the interaction is considered only between an atom and its nearest neighbours.

Hence $$W = -2J\sum_{\text{neighbours}} S.S.$$

or $$W = -2JS^2\sum \cos \phi ij \qquad (2.10)$$

where ϕ is the angle between the spins.

reducing, for small values of ϕ to

$$W = JS^2\phi^2 \qquad (2.11)$$

Landau and Lifshitz derived an alternative expression (1935) expressing the exchange energy as

$$E_{EX} = \frac{2JS^2}{a}\int\left[(\nabla\alpha_1)^2 + (\nabla\alpha_2)^2 + (\nabla\alpha_3)^2\right] \qquad (2.12)$$

where a = the lattice parameter and $\alpha_1 \alpha_2$ and α_3 the direction cosines.

$$A = 2JS^2/a = \text{the exchange constant.}$$

For a derivation of equation 2.12 see MORRISH.

2.2 BAND MODEL THEORIES OF FERROMAGNETISM

The Heisenberg model of exchange is based upon the assumption that the electrons are localized at the atoms. Bearing in mind that at temperatures above OK there will be free charge in terms of holes and electrons in metallic solids then any theory which attempts to interpret ferromagnetism must allow for itinerant charge.

Calculations have been made on holes in 3d band and electrons in the 4s band by employing Bloch wave functions. Slater (1936) obtained results for Nickel which gave reasonable agreement in experiment. Stoner (1938) gave the first simple treatment of a model dealing with an electron gas. Stoner named the process collective electron ferromagnetism. The theory is based on three assumptions.

1. The 3d band is parabolic near the Fermi level.
2. Exchange interaction may be represented by a molecular field.
3. Fermi Dirac statistics apply (this is a direct consequence of antisymmetrical wave functions).

The electrons occupy certain energy bands and the internal field is proportional to the magnetization. There is a resulting difference in energy between those spins parallel to the internal field and those antiparallel to the internal field. This can be represented by dividing

the energy band into two halves. Figure 2.4 shows division of an energy band with an applied magnetic field (see Bleaney and Bleaney). Electrons transfer from one half band to the other in proportion to the density of states function resulting, if the density of states is large, in a decrease in energy. Electrons will only transfer if doing so does reduce the energy. The condition is satisfied for d bands but not s bands. However, it is possible that overlapped d and s bands in transition metals may have co-operative magnetic states. The resulting magnetization depends on the net transfer of spins between the two half bands and therefore the net dipole moment need not correspond to an exact integral multiple of Bohr magneton. The assumption in this model is that the d electrons are all itinerant. This gives rise to a second long range exchange which is oscillatory and can be negative. Such an exchange was proposed by Rudderman and Kittel. (See RKKY reaction Chapter 3.)

Whatever the origin of the exchange interaction the form of the coupling is given by equation

$$W_{ij} = -2J_{ij}\underline{S}i.\underline{S}j$$

2.3 MAGNETOSTATIC ENERGY

Work is done in assembling a system of magnetic dipoles and, as such, the system will possess potential energy.

The potential energy of a magnetized body in an applied magnetic field is given by

$$E = -\underline{B}.\underline{M} \qquad (2.13)$$

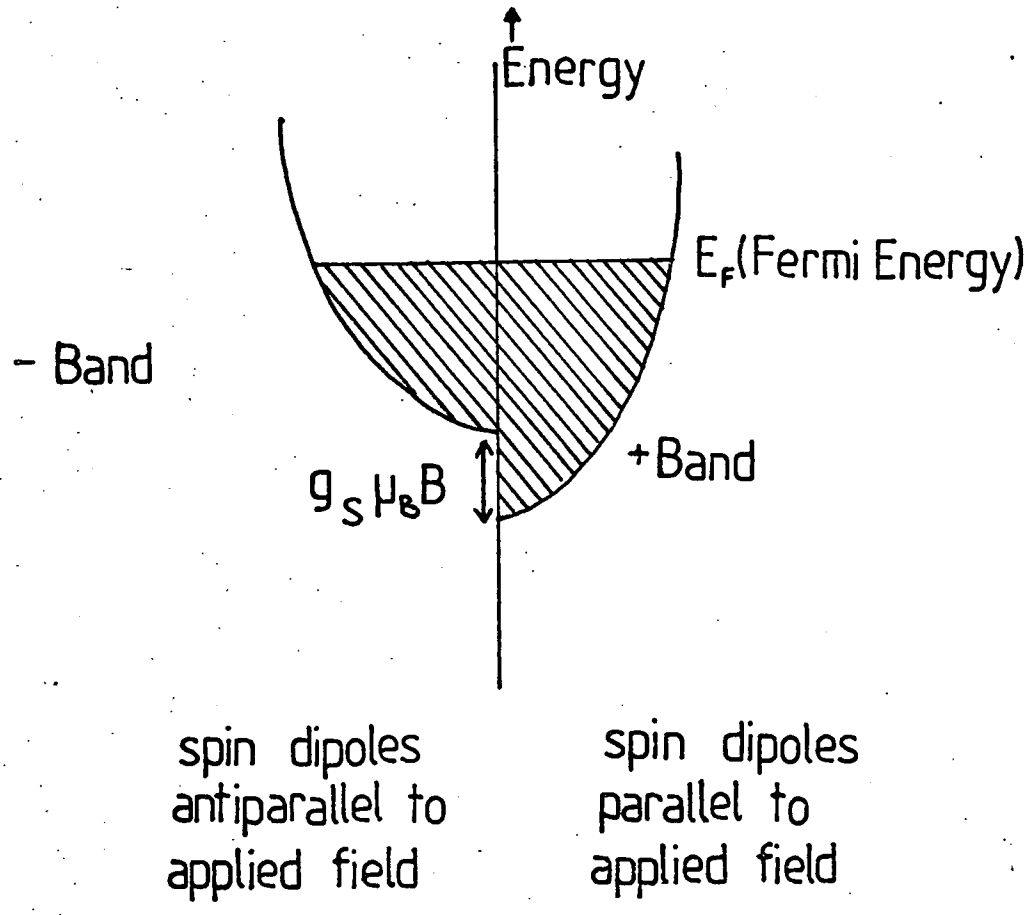

Fig. 2,4 The diagram shows the displacement of + and - bands of conduction electrons by an applied magnetic field. The difference in energy between the two half bands is equal to the difference of energy of a spin dipole parallel and antiparallel to a flux density B.

Now if the magnetized body is situated in a flux density Bo then the field acting in the body = BI where

$$BI = Bo - B_D \tag{2.14}$$

B_D is the demagnetizing field.

From equation 2.14 it can be seen that B_D opposes the applied field. Figure 4.5 shows how this happens. Although B_D varies in magnitude from specimen to specimen, it occurs in all magnetized specimens. Its value depends upon the shape of the specimen and on the magnitude of M.

$$B_D = DM \tag{2.15}$$

where D is known as the demagnetizing factor.

Figure 2.5 shows plots of D versus length/width ratio for ellipsoids and for cylinders.

Now the magnetostatic energy per unit volume of the body when it is situated in an applied magnetic field Bo is given as

$$\begin{aligned} Em &= -\tfrac{1}{2}B_D M - BoM \\ &= -\tfrac{1}{2}DM^2 - BoM \end{aligned} \tag{2.16}$$

With no applied field the terms $-\frac{1}{2}DM^2$ in equation 2.16 becomes positive. The ½ is introduced to avoid mutual interactions in the solid being counted twice. i.e. the mutual energy of two dipoles is the product of the field of one and the dipole moment of the other.

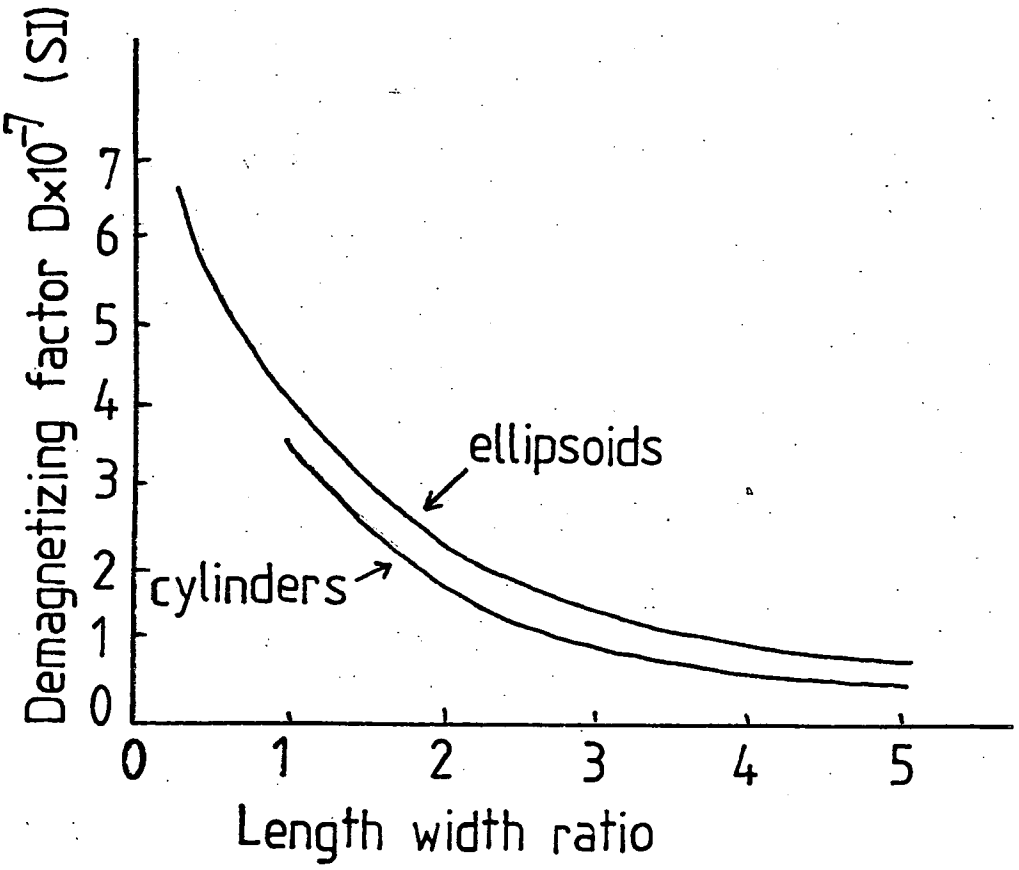

Figure 2.5 Demagnetizing factors for ellipsoids and cylinders

The energy given by the first term in 2.16 can be large and domains are formed as a process by which this energy can be minimized (see Chapter 4.)

For the evaluation of demagnetizing factor for ellipsoids see Stoner (1945) and Osborne (1945).

2.4 MAGNETOCRYSTALLINE ANISOTROPY

2.4.1 Introduction

As mentioned in several places in this thesis, the ease with which a particular specimen can be magnetized depends upon the direction of the applied magnetic field with respect to the crystal axes. This phenomenon is called magnetocrystalline anisotropy and an energy term which depends upon the direction of the spontaneous magnetization is called a magnetic anisotropy energy. In the absence of an applied field the spontaneous magnetization takes up a specific direction with respect to the crystal axes. These preferred directions, or easy directions, are formally expressed in terms of energy functions which go to a minimum in those directions.

2.4.2 Magnetocrystalline energy

The magnetocrystalline energy is defined in terms of the work required to magnetize the specimen in a selected crystallographic direction. If the magnetization is rotated out of an easy direction by the application of an applied field, then this represents an overall increase in energy in the material. This is the anisotropy energy.

Because the total work done depends upon the angle θ through which the magnetization is turned away from an easy direction, the anisotropy energy may be regarded very simply as the energy required to rotate the magnetization through this angle.

The simplest case is that of a uniaxial crystal such as cobalt. Cobalt is a hexagonal crystal with a single easy direction along the c-axis. The basal plane represents a hard direction. Because the anisotropy energy must be the same whether the initial magnetization points up or down along the c-axis then the energy can be expressed as some even function of the angle θ. It is the accepted convention to express the energy as a power series in sin θ containing only even terms. Hence for a uniaxial crystal such as cobalt the anisotropy energy E_K is given by

$$E_K = K_1 \sin^2\theta + K_2 \sin^4\theta + \cdots \Sigma K_n \sin^{2n}\theta \quad (2.17)$$

The third or higher term in equation 2.17 can often be omitted. Indeed it is quite usual to consider only the first term for many practical purposes.

K_n are magnetocrystalline anisotropy constants.

For Cobalt $K_1 = 4.1 \times 10^5$ Jm^{-3}

The anisotropy is also dependent on the azimuthal angle about the c-axis but this term is as small as the third term in equation 2.17 and can often be ignored.

In the general case the direction of magnetization must be related to three crystal axes and the anisotropy energy is usually expressed in terms of the direction cosines α_1 α_2 α_3.

Consider the simple case of a cubic crystal such as iron. Because of the high symmetry involved in a cubic crystal structure, there are many equivalent directions in which the anisotropy energy has the same magnitude (see Figure 2.6). This fact allows the expansion of the anisotropy energy in terms of the direction cosines α_1 α_2 α_3 to yield an expression which can be simplified to a large extent. Because of the crystal symmetry the expression is independent of any change of sign of the direction cosines, i.e. reversal of the direction of magnetization does not change the anisotropy energy. Hence the expression will include only even powers of θ. Also the expression is independent of any interchange of any two α's. For example, when the magnetization makes an angle θ with the x-axis in the x-y plane, this is equivalent to it making an angle θ in the y-axis in the x,y plane. (as shown in Figure 2.6). For any given combination of a, b and c the terms of $\alpha_i^a \alpha_j^b \alpha_k^c$ must have the same coefficient for any interchange of i, j and k. The total energy can be written, meeting the conditions outlined above, up to the sixth term as follows:

$$
\begin{aligned}
EK = \quad & A\left(\alpha_1^2 + \alpha_2^2 + \alpha_3^2\right) && \text{(i)}\\
& + B\left(\alpha_1^2 + \alpha_2^4 + \alpha_3^4\right) && \text{(ii)}\\
& + C\left(\alpha_1^2\alpha_2^2 + \alpha_2^2\alpha_3^2 + \alpha_3^2\alpha_1^2\right) && \text{(iii)}\\
& + D\left(\alpha_1^6 + \alpha_2^6 + \alpha_3^6\right) && \text{(iv)}\\
& + E\left(\alpha_1^4\alpha_2^2 + \alpha_2^4\alpha_3^2 + \alpha_3^4\alpha_1^2 + \alpha_2^4\alpha_1^2 + \alpha_3^4\alpha_2^2 + \alpha_1^4\alpha_3^2\right) && \text{(v)}\\
& + F\left(\alpha_1^2\alpha_2^2\alpha_3^2\right) && \text{(vi)}
\end{aligned}
$$

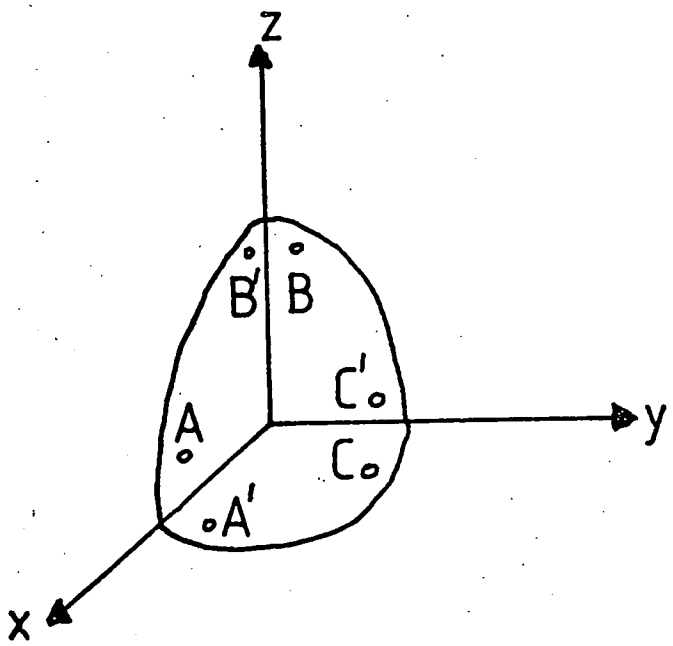

Fig. 2.6 The diagram shows an octant of a unit sphere. Points A and A^j etc are equivalent points along which the anisotropy energy is the same.

Now the anisotropy is dependent on θ. But, using the usual relationship for direction cosines, $\alpha_1^2 + \alpha_2^2 + \alpha_3^2 = 1$

Hence term (i) does not result in any isotropy and is, therefore, redundant.

term (ii) can be expressed as

$$\alpha_1^4 + \alpha_2^4 + \alpha_3^4 = 1 - 2(\alpha_1^2\alpha_2^2 + \alpha_1^2\alpha_3^2 + \alpha_2^2\alpha_3^2)$$

term (iv) can be espressed as

$$1 - 3(\alpha_1^2\alpha_2^2 + \alpha_1^2\alpha_3^2 + \alpha_3^2\alpha_1^2) + 3\alpha_1^2\alpha_2^2\alpha_3^2$$

term (v) can be expressed as $(\alpha_1^2\alpha_2^2 + \alpha_2^2\alpha_3^2 + \alpha_3^2\alpha_1^2) - 3\alpha_1^2\alpha_2^2\alpha_3^2$

The terms (ii), (iii), (iv), (v) and (vi) can, therefore, be grouped together as

$$K_1(\alpha_1^2\alpha_2^2 + \alpha_1^2\alpha_3^2 + \alpha_2^2\alpha_3^2) + K_2\alpha_1^2\alpha_2^2\alpha_3^2$$

Hence the energy can be written as

$$E_k = K_0 + K_1(\alpha_1^2\alpha_2^2 + \alpha_2^2\alpha_3^2 + \alpha_3^2\alpha_1^2) + K_1\alpha_1^2\alpha_2^2\alpha_3^2 + \ldots\ldots (2.18)$$

For iron $K_1 = 4.8 \times 10^4\ Jm^{-3}$

$K_2 = \pm 5 \times 10^3\ Jm^{-3}$

For Nickel $K_1 = -4.5 \times 10^3\ Jm^{-3}$

$K_2 = -2.38 \times 10^3\ Jm^{-3}$

If $K_1 > 0$ then a minimum occurs at the [100] [010] and [001] directions.

If $K_1 < 0$ then a minimum occurs at the [111] direction.

Hence iron has its easy directions along [100] [010] and [001] directions whereas nickel has an easy direction along [111] axes.

For hexagonal crystals it is usual to express the free energy as an expansion in powers of sin θ

$$E_K = K_0 + K_1 \sin^2\theta + K_2 \sin^4\theta + K_3 \sin^6\theta + K_4 \sin^6\theta \cos\phi \quad (2.19)$$

where θ and ϕ are the polar angles of the magnetization relative to the c-axis.

It is often convenient to rewrite equations 2.18 and 2.19 in terms of expansion of sin θ.

Also an alternative representation involves the use of spherical harmonics leading to

$$E_K = K_0 + K_4 g_4 + K_6 g_6 + K_8 g_8 + \cdots\cdots \quad (2.20)$$

(The g's are linear combinations of spherical harmonics reflecting cubic symmetry)

for cubic crystals and

$$E_K = (K_0^0)' + (K_2^0)' Y_2^0(\theta) + (K_4^0)' Y_4^0(\theta) + (K_6^0)' Y_6^0(\theta) + (K_6^6)' Y_6^6(\theta\,\phi) + \cdots\cdots \quad (2.21)$$

for hexagonal crystals

where $Y_l^m(\theta)$ are normalized spherical harmonics.

For a single ion interaction the coefficients K_l^m vary with temperature according to the following equation.

$$K_l^m(T) = K_l^m(0^\circ)\,\hat{I}_{l+\frac{1}{2}}[\mathcal{L}^{-1}(\sigma)]$$

(Callen and Callen (1966))

Spherical harmonics are useful when relating theory to experimental work (See Birss and Keeler (1974)).
For a comprehensive account of anisotropy in rare earth metals and alloys see, for example, Coqblin (1977)).

2.4.3 Origins of Magnetic Anisotropy

The exchange energy depends only on the relative directions of coupled spins. It is essentially isotropic as the expression representing the exchange energy contains no terms which refer to the crystal structure. To account quantitatively for magnetocrystalline anisotropy it is necessary to invoke some mechanism which relates spins with their environment in the crystal structure. Hence, as well as mutual coupling between elementary moments, there must also be a coupling between these moments and the lattice.

The simplest form of coupling is that of dipole - dipole.

$$E_{dipole} = -\frac{1}{4\pi\mu_o r_{12}^3}\left[(\underline{M}_1\underline{M}_2) - \frac{3}{r_{12}^2}(\underline{M}_1\cdot\underline{r}_{12})(\underline{M}_1\underline{r}_{12})\right] \qquad (2.22)$$

where $\underline{M}_1$ and $\underline{M}_2$ are the magnetic moments.

r_{12} is the distance between them.

Workers such as Akulov (1929) and Mahajani (1929) showed that the observed facts could not adequately be explained purely in terms of magnetic interactions. In 1956 Van Vleck introduced the concept of a pseudo dipole and pseudo quadripole coupling using ad-hoc large coupling constants in an equation which had the form of equation 2.22. Spin and orbital motions are associated with magnetic moments of free atoms. In a crystal, however, the orbital motions are strongly coupled to the lattice and even an applied magnetic field has little effect on the situation. In ferromagnetic materials, however, domain formation is linked with strong interaction forces. The spin axes are not tightly bound to the lattice as are the orbital axes. There is a weak coupling between these spin and orbital motions resulting in a weak spin lattice coupling. It is suggested that it is this spin-orbit coupling which gives domains directional magnetic properties and provides the forces of magnetic anisotropy. Also, because the incomplete sub shells in the crystal atoms are not spherically symmetrical, an applied field causes a slight deflection of orbital axes because of the spin orbit torque. Hence a change in crystal dimensions occur. Magnetostriction and magnetocrystalline anisotropy are, therefore, closely linked.

For systems of localised moments, two types of mechanism are considered.

(a) Single ion anisotropy.

(b) Two ion anisotropy.

2.4.3.1 Single-Ion Model

In the single ion model it is assumed that the anisotropy is due to the various quantum states of single ions within the crystalline field. It is thought that the field itself (which reflects the symmetry of the lattice) affects the charge clouds of individual ions. In the absence of an applied field the anisotropic (except for S state ions) charge clouds will minimize their energies by adopting specific orientations with respect to the crystalline field. The easy directions are defined by the spins aligning in a particular direction with respect to the crystal lattice. These preferred directions, therefore, are governed by the lattice symmetry and the spin-orbit coupling. The application of a field will distort the charge clouds giving rise to the anisotropy energy.

The Hamiltonian for an ion in such a system can be written as

$$\mathcal{H} = g\mu_B \underline{B}_m \cdot \underline{S} + V_c(\underline{r}) + \mathcal{H}_{SL} + \mu_B \underline{B}_o(\underline{L} + 2\underline{S}) \qquad (2.23)$$

$\underline{B}_m$ represents an effective isotropic molecular field.

$$V_c(r) = \sum_{l,m} r^l A_l^m Y_l^m(\theta,\phi) \qquad (2.24)$$

and is the crystalline field potential expressed in terms of spherical harmonics.

$\underline{B}o$ = external field.

θ = angle between magnetization and c-axis.

ϕ = angle between the projections of the magnetization vector in the basal plane and an a-axis.

The quantity A_l^m depends upon the distance to neighbouring atoms, the valency and the screening effect of the conduction electrons. Stevens (1952) introduced operator equivalents of the spherical harmonics. These are expressed in equation 2.25 as O_l^m and equation 2.24 can be rewritten thus.

$$V_c(\underline{r}) = \sum_{l,m} B_l^m O_l^m \qquad (2.25)$$

The operator O_l^m are polynomials in $\underline{L}$ or $\underline{J}$. replacing the spherical harmonics.

$$B_l^m = \langle r^l \rangle A_l^m \alpha_l$$

$\langle r^l \rangle$ = average of radial wave function

α_l = l^{th} pole moment of charge distribution

αl are constants known as Stevens factors.

The very large single ion anisotropy of the heavy rare earth ions (with the exception of gadolinium) arises from the interaction betwen the large multipolemoments of the 4f charge cloud and the hexagonal field symmetry. For hexagonal symmetry equation 2.25 is written as:

$$Vc(\underline{r}) = B_2^0 O_2^0(J) + B_4^0 O_4^0(J) + B_6^0 O_6^0(J)$$
$$B_6^6 (O_6^6(J) + O_6^{-6}(J)) + \text{-------} \qquad (2.26)$$

$$O_l^m(\hat{J}) = Y_l^m(\hat{\alpha}) O_l^m(\hat{J}') \qquad (2.27$$

where $\hat{J}$ = spin direction referred to c-axis

$\hat{J}'$ is spin direction referred to magnetization axis.

(Callen and Callen 1966)

Darby and Isaac (1974) have expressed zero temperature anisotropy coefficients in terms of Stevens factors. (which show only small variations for heavy rare earths and, therefore, dominate the anisotropy). and the J values.

$$K_2^0(0) = 2\alpha_2 A_2^0 \langle r^2 \rangle J(J-1/2)$$

$$K_4^0(0) = 8\alpha_4 A_4^0 \langle r^4 \rangle J(J-1/2)(J-1)(J-3/2)$$

$$K_6^0(0) = 16\alpha_6 A_6^0 \langle r^6 \rangle J(J-1/2)(J-1)(J-3/2)(J-2)(J-5/2)$$

$$K_6^6(0) = \alpha_6 A_6^6 \langle r^6 \rangle J(J-1/2)(J-1)(J-3/2)(J-2)(J-5/2) \quad (2.28)$$

This single ion model explains the anisotropy in most of the rare earths. The two ion model is also proposed as an explanation though at present the suggestion is controversial.

2.4.3.2. Two-Ion Model

In an attempt to explain anisotropy, Van Vleck suggested two types of coupling between the spins of neighbouring ions.

(a) pseudodipole - dipole interaction

$$\mathcal{H}_b = \sum_{i<j} b_{ij} [\underline{S}_i \underline{S}_j - 3(\underline{S}_i \underline{R}_{ij})(\underline{S}_j \cdot \underline{R}_{ij}) R_{ij}^{-2})] \quad (2.29)$$

(b) pseudo quadripole-quadripole interaction

$$\mathcal{H}_q = \sum_{i<j} Q_{ij} (\underline{S}_i \cdot \underline{R}_{ij})^2 (\underline{S}_j \cdot R_{ij})^2 \quad (2.30$$

where Q_{ij}, D_{ij} are empirical constants.

The two ion effect has its origins in the interaction between the charge clouds. This interaction depends upon the shape of the charge clouds. The spin orbit coupling links the spin with the charge cloud and hence with the charge cloud of another ion. There are two types of interaction between the charge clouds. The first is a coulomb interaction and the second is an exchange interaction. The anisotropy is a result of high order perturbations on the anisotropic exchange. In the rare earths, however, the exchange itself can be anisotropic.

2.4.4 Temperature dependence of Anisotropy

At zero temperature all spins are aligned in some direction. When the temperature increases the spins spread into a cone about the magnetization direction due to the random thermal motion. The spreading can either be away from or towards an easy direction depending upon the original direction of the magnetization. If the magnetization is originally in an easy direction the spreading obviously will tend to take the spins away from the easy direction thereby increasing the anisotropy energy. If the original magnetization is in a hard direction then thermal spreading of the spins results in a decrease in anisotropy energy. The anisotropy is smaller at higher temperatures. (See Figure 2.7).

The temperature dependence of anisotropy constants is usually written as a power law in terms of the magnetization.

$$\frac{K(T)}{K(0)} \quad \frac{(M(T))^n}{(M(0))} = (M(T))^n \qquad (2.31)$$

M(T) is the reduced magnetization.

An excellent review of the theoretical laws governing the temperature dependence of the inisotropy constants is given by COQBLIN (1977). Only a very brief account will be given here. The original work on the temperature dependence of the anisotropy constants was carried out by various workers, e.g. AKULOV (1936), ZENER (1954), KEFFER (1955), VAN VLECK (1959).
It was suggested that the first cubic anisotropy constant K_1 could be represented by a tenth-power law of the magnetization.

$$\frac{K_1(T)}{K_1(0)} = (M(T))^{10} \quad (T \ll Tc) \tag{2.32}$$

This expression gave reasonably good results for iron at low temperatures but deviations occur at higher temperatures, due to such effects as thermal expansion (CARR (1960)) and magnetoelastic coupling (CALLEN and CALLEN (1963)) Nickel obeys a fiftieth power law.

The treatment proposed by ZENER (1954) was essentially a classical one. He regarded the temperature as causing fluctuations in the spin direction. His result yielded an expression

$$\frac{K_1'(T)}{K_1'(0)} = (M(T)^{1(1+1)/2} \tag{2.33}$$

$$(MT = \frac{M_s(T)}{M_0(0)} = \text{reduced magnetization})$$

where the K_1 coefficients are defined considering surface spherical harmonics.

This gives:

$$\frac{K_1(T)}{K_1(0)} = (M(T)^{10} \approx \frac{K_4(T)}{K_4(0)} \qquad (2.34)$$

which is in accordance with the results of AKULOV (at low temperatures and with those of VAN VLECK.

Sato and Chandrasekar (1956) showed that in order to determine the nature of the temperature of dependence of K_1, an accurate value of the K_2 constant is required. They gave an improved version of the Zener equation for the first cubic constant.

$$K_1(T) = (K_1(0) + 1/11\ K_2(0)\ )\ (M(T))^{10} - 1/11\ K_2(0)\ (M(T))^{21} \qquad (2.35)$$

In their review on the history of the power law, Callen and Callen (1966) obtained an expression.

$$K_1(T) = K_1(0)\ \hat{I}_1 + 1/2\ (X) \qquad (2.36)$$

where, as stated in Chapter one, $\hat{I}_1 + 1/2\ (X)$ is a reduced hyperbolic Bessel function. X is defined by

$$M_T = \hat{I}\ 3/2\ (X) \qquad (2.37)$$

At low temperatures equation 2.36 becomes

$$K_1(T) = K_1(0)\ M_T(1(1 + 1)/2)$$

which is equation 2.33 (The Zener power law)

For the two ion case the result depends upon temperature. The reason for this is that the spins of each ion must be considered. At low temperatures the alignment of the spins will be good and hence the pair can be treated effectively as one giving the Zener power law. As the temperature increases, however, the correlation breaks down and when the thermal spin waves have wavelengths comparable to the order of magnitude of the range of the two ion mechanism the correlation is zero and the equation governing the temperature dependence of the inisotropy becomes:

$$K_1(T) = K_1(0)\, M_T^{1} \tag{2.38}$$

Yang (1971) obtained expressions for the temperature dependence of K_1 and K_2 allowing for both single and two ion correlations. The equations representing the hexagonal close packed crystals were:

$$\frac{K_1(T)}{K_1(0)} = a^{1}\hat{I}_{5/2}(X) + b^{1}\hat{I}_{9/2}(X) + a^{11}(M_T)^2 + b^{11}(\hat{I}_{5/2}(X))^2 \tag{2.39}$$

$$\frac{K_2(T)}{K_2(0)} = c^{1}\hat{I}_{9/2}(X) + c^{11}(\hat{I}_{5/2}(X))^2 \tag{2.40}$$

$$X = \hat{I}^{-1}_{3/2}(M_T)$$

$\hat{I}_{9/2}(X)$ and $\hat{I}_{5/2}(X)$ are single ion contributions.

The two ion contributions are

$$(\hat{I}_{5/2}(X))^2 \text{ and } (\hat{I}_{3/2}(X))^2 = M_T^{2}$$

The coefficients a^1 etc. are constants of unknown value.

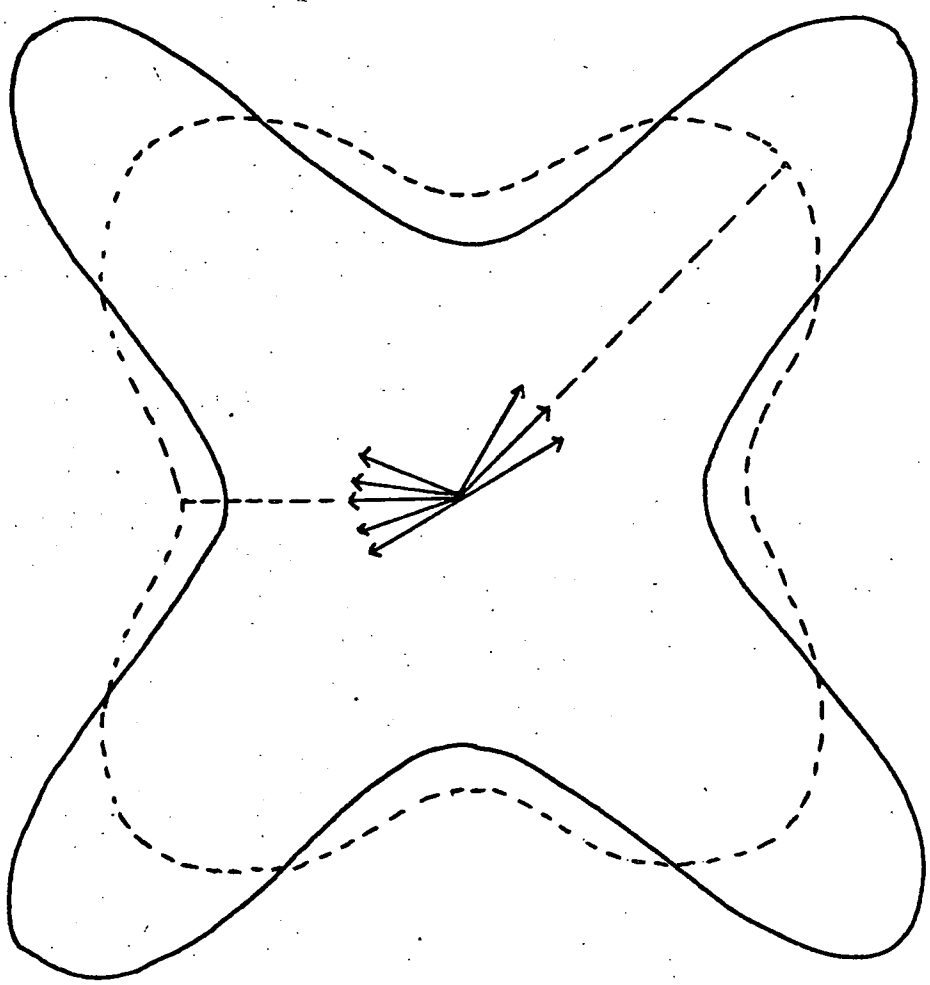

Figure 2.7 – Anisotropy Surface at 0K
--- Anisotropy Surface at T = 0K

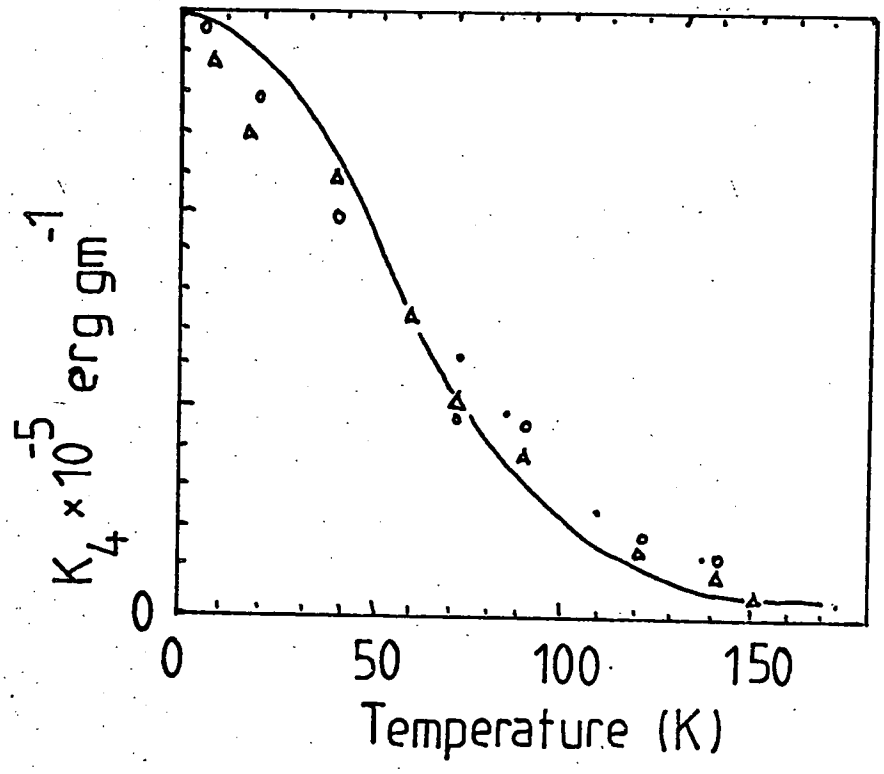

Rhyne and Clark a-axis

Rhyne and Clark b-axis

present measurements (1968)

Fig. 2.8 Variation of K_4 with temperature for Tb compared with the theoretical curve of Callen and Callen.
(After Bly, Corner, Taylor and Darby (1968)).

CHAPTER THREE

THE RARE EARTH ELEMENTS

CHAPTER 3

THE RARE EARTH ELEMENTS

3.1 INTRODUCTION

The rare earth elements (or lanthanides [after the name of the first member of the series]) are the fifteen elements from lanthanum to lutetium inclusive. (Table 3.1) The close similarity of many of their respective chemical properties justifies their sub-group status in the periodic table. It is this similarity of properties which inevitably results in many of them being found together in the various rare earth minerals. Indeed, the separation of these elements was once (before the advent of ion-exchange techniques) a formidable problem in classical inorganic chemistry, so much so that the title rare earth is not really areflection on the scarcity of the elements (which are not rare) but is the result of the degree of difficulty involved in isolating the elements and obtaining them in a pure state. Two other elements, scandium (atomic number 21) and yttrium (atomic number 39) are, because of the great similarity between their chemical properties and those of the lanthanides, usually included in the rare earth group of elements. They occur just before the group III elements in the periodic table and both elements are to be found in rare earth minerals (yttrium in larger proportions than scandium). The problem of isolating the rare earths is partly underlined by the fact that over 100 years separates the isolation and identification of yttrium by Gadolin in 1794 and the discovery of Lutetium in 1907. For a historical review of the discovery of the rare earths see TOPP (1964).

Lanthanum	La	LIGHT EARTHS
Cerium	Ce	
Praseodymium	Pr	
Neodymium	Nd	
Promethium	Pm	
Samarium	Sm	
Europium	Eu	
Gadolinium	Gd	MIDDLE EARTHS
Terbium	Tb	
Dysprosium	Dy	
Holmium	Ho	
Erbium	Er	HEAVY EARTHS
Thulium	Tm	
Ytterbium	Yb	
Lutetium	Lu	

Table 3.1 The Rare Earth Elements

3.2 ELECTRONIC STRUCTURE

Table 3.2 shows the electronic configuration of the inert gas Xenon followed by the electronic configurations of tha lanthanides. It can be seen from the table that each element in the lanthanide group has the Xenon core $1_s^2 2_s^2 2_p^6 3_s^2 3_p^6 3_d^{10} 4_s^2 4_p^6 4_d^{10} 5_s^2 5_p^6$. In the element lanthanum, the 4f state represents a higher energy than the 5d state, hence the 4f state is unoccupied. Cerium has two 4f electrons and the 5d state is unoccupied. Table 3.2 shows the progressive occupation of the 4f shell as the lanthanide group progresses from lanthanum to lutetium. From cerium the population of the 4f state rises from 2 electrons until it becomes the maximum 14 at the element ytterbium. Because there is a tendency to retain the stable half full and full configurations, gadolinium and lutetium retain the 5d electron leaving the 4f state half full and full respectively. In the other lanthanides, once the 4f state is populated, the 5d electron transfers to the 4f shell. In cerium, rather than have one 4f electron thereby retaining the 5d electron, the 5d electron joins the electron in the 4f shell. Also, in europium the $4f^7$ electron represents a stable state and gadolinium maintains this by having an electron in 5d. In terbium the 5d electron transfers to 4f joining the eight electrons there.

This progressive occupation of the 4f state can be represented by the general formula for the lanthanides.

$$Xe\ (1s - 4d)\ 4f^n 5s^2 5p^6 5d^{(1)} 6s^2 \quad \text{where } n = 0 - 14$$

The valency, with a few exceptions, of the lanthanides is 3. This is due to the ease with which the $5d^1$ plus $6s^2$ electrons or one of the 4f electrons plus $6s^2$ electrons become conduction electrons.

Table 3.2 Electronic configurations of the Rare Earth elements showing the Xenon core.

	1s	2s	2p	3s	3p	3d	4s	4p	4d	4f	5s	5p	5d	5f	6s
Xe	2	2	6	2	6	10	2	6	10		2	6			
La	2	2	6	2	6	10	2	6	10		2	6	1		2
Ce	2	2	6	2	6	10	2	6	10	2	2	6			2
Pr	2	2	6	2	6	10	2	6	10	3	2	6			2
Nd	2	2	6	2	6	10	2	6	10	4	2	6			2
Pm	2	2	6	2	6	10	2	6	10	5	2	6			2
Sm	2	2	6	2	6	10	2	6	10	6	2	6			2
Eu	2	2	6	2	6	10	2	6	10	7	2	6			2
Gd	2	2	6	2	6	10	2	6	10	7	2	6	1		2
Tb	2	2	6	2	6	10	2	6	10	9	2	6			2
Dy	2	2	6	2	6	10	2	6	10	10	2	6			2
Ho	2	2	6	2	6	10	2	6	10	11	2	6			2
Er	2	2	6	2	6	10	2	6	10	12	2	6			2
Tm	2	2	6	2	6	10	2	6	10	13	2	6			2
Yb	2	2	6	2	6	10	2	6	10	14	2	6			2
Lu	2	2	6	2	6	10	2	6	10	14	2	6	1		2

Outer Configurations of Rare Earths			
4f	5d	6s	
	1	2	La
2		2	Ce
3		2	Pr
4		2	Nd
5		2	Pm
6		2	Sm
7		2	Eu
7	1	2	Gd
9		2	Tb
10		2	Dy
11		2	Ho
12		2	Er
13		2	Tm
14		2	Yb
14	1	2	Lu

Valency variations occur in elements cerium (which loses two 4f electrons) and ineuropium and ytterbium which are divalent retaining the stable complement of $4f^7$ and $4f^{14}$ respectively.

Scandium and yttrium have, respectively, the argon core + $3d^1 4s^2$ electrons and the krypton core with $4d^1 5s^2$ outer electrons. Hence as terpositive ions, scandium and yttrium have the configurations of krypton and argon respectively. The addition of ten 3d electrons after scandium and ten 4d electrons after yttrium give rise to the first and second transition element series. However, at lanthanum, the 5s and 5p shells have been filled and the deep lying 4f electrons do not, as do the 3d and 4d states in the first and second transition series, have any but the slightest chemical significance. It is this fact which largely accounts for the close similarity of the lanthanides and, indeed, it is the 4f electrons which give rise to the magnetic properties of the ions.

In general, throughout the periodic table, there is a tendency for the atomic radii of elements to decrease with increasing atomic number. This also happens to the lanthanides but, because of the successive addition of 14 electrons not taking part in chemical bonding, the contraction occuring to the ionic radius of the lanthanides occurs nowhere else in the periodic table. (Actually, in the actinide series a similar process occurs with the 5f state but some of these electrons take part in bonding.). In the rare earth series the radii of the 4f wave function varies with increasing atomic number. As the nuclear charge is increased one electron is added to the 4f shell. Owing to the shape of the orbitals the electronic shielding is imperfect thus resulting in an increased effective nuclear charge, resulting in a reduction in the size of the 4f shell.

The addition of the extra positive nuclear charge causes a large electron energy decrease near the nucleus and this results in the 4f shell being drawn in towards the nucleus and the electron distribution in the 4f shell cannot be screened by the extra electron from its corresponding increase in positive charge. Hence, due to electrostatic attraction the outer shell radius is decreased. This is known as the lanthanide contraction. Figures 3.1, 3.2 and 3.3 show the variation of radius of 3^+ ion, radius of atom in metal and atomic volume versus atomic number of lanthanide respectively. (Data from WELFORD (1974)).

Early separation techniques involved fractional crystallisation and basicity separations which used the ionic radius or the ratio of charge/radius. The lanthanide contraction resulted in a similarity between the radii of holmium and yttrium which meant that in early separations yttrium appeared among the heavy earths. (Table 3.1 shows how the lanthanides are split into groups of light, middle and heavy earths.)

3.3 CRYSTAL STRUCTURE OF THE RARE EARTH ELEMENTS

Table 3.3 shows the crystal structures of the rare earth elements and associated allotropes. At room temperature the light rare earths (with the exception of cerium (f.cc), samarium (rhombohedral) and europium (b.c.c) crystallize in the double hexagonal close packed structure. The heavy earths (with the exception of ytterbium (f.c.c) take up the hexagonal close packed structure. Figure 3.4 shows the structure of the rare earths as being represented by three layers A, B and C. The stacking of these layers gives rise to the various crystal structures shown.

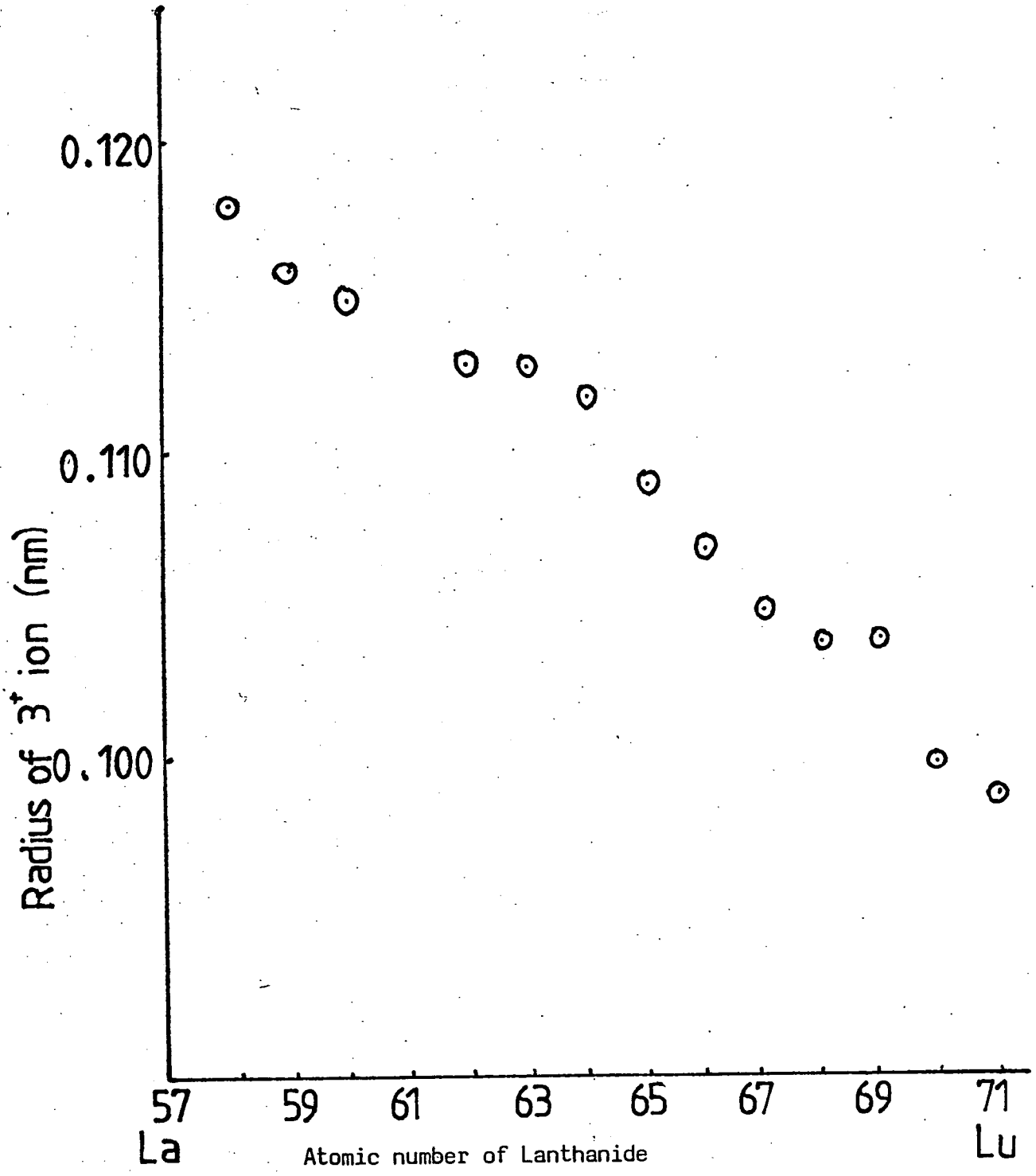

Fig. 3.1 Variation of radius of 3^{+}ion (Rare Earths) vs. atomic number DATA FROM WELFORD (1974)

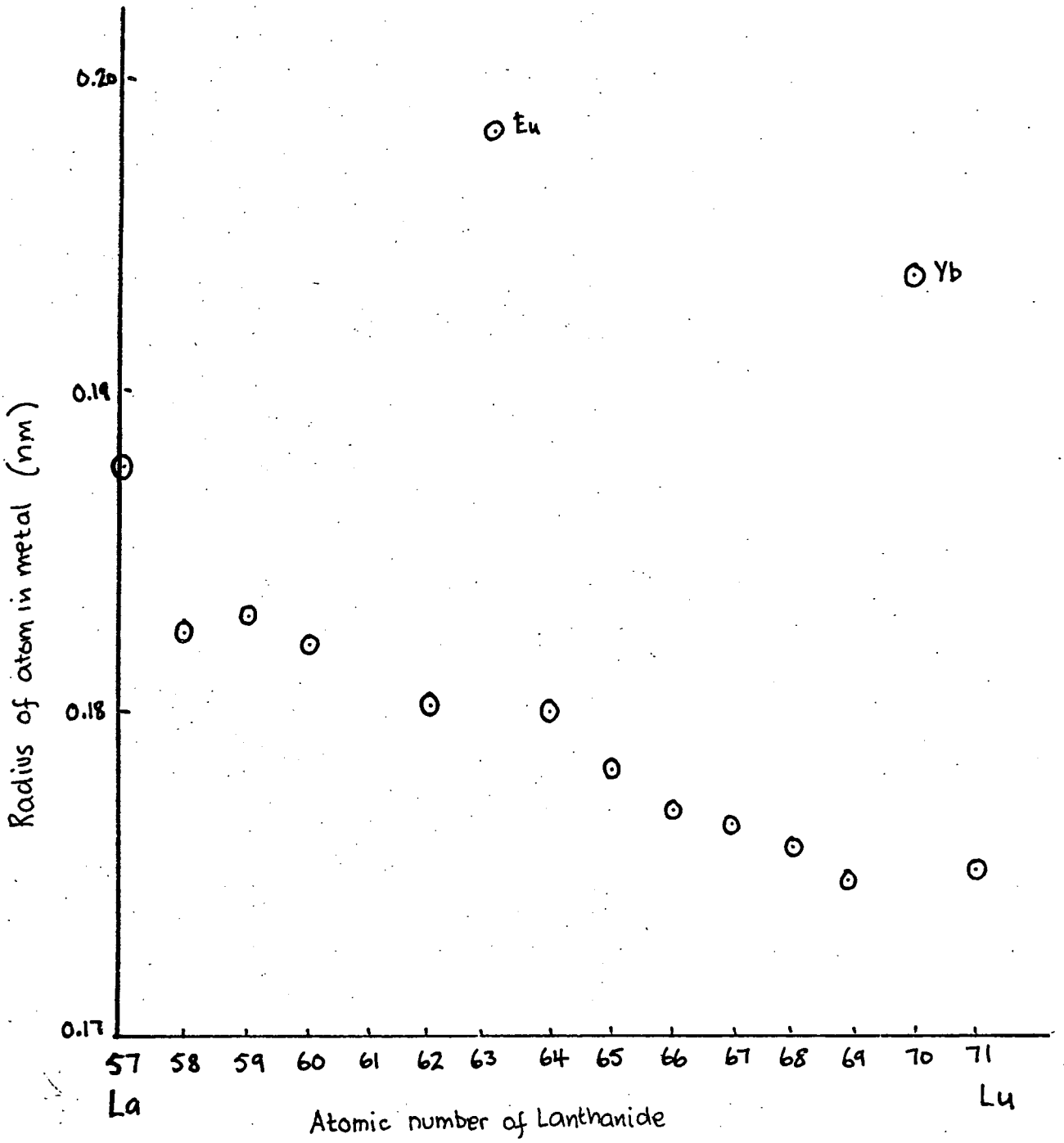

Fig. 3.2 Radius of atom in metal vs. atomic number

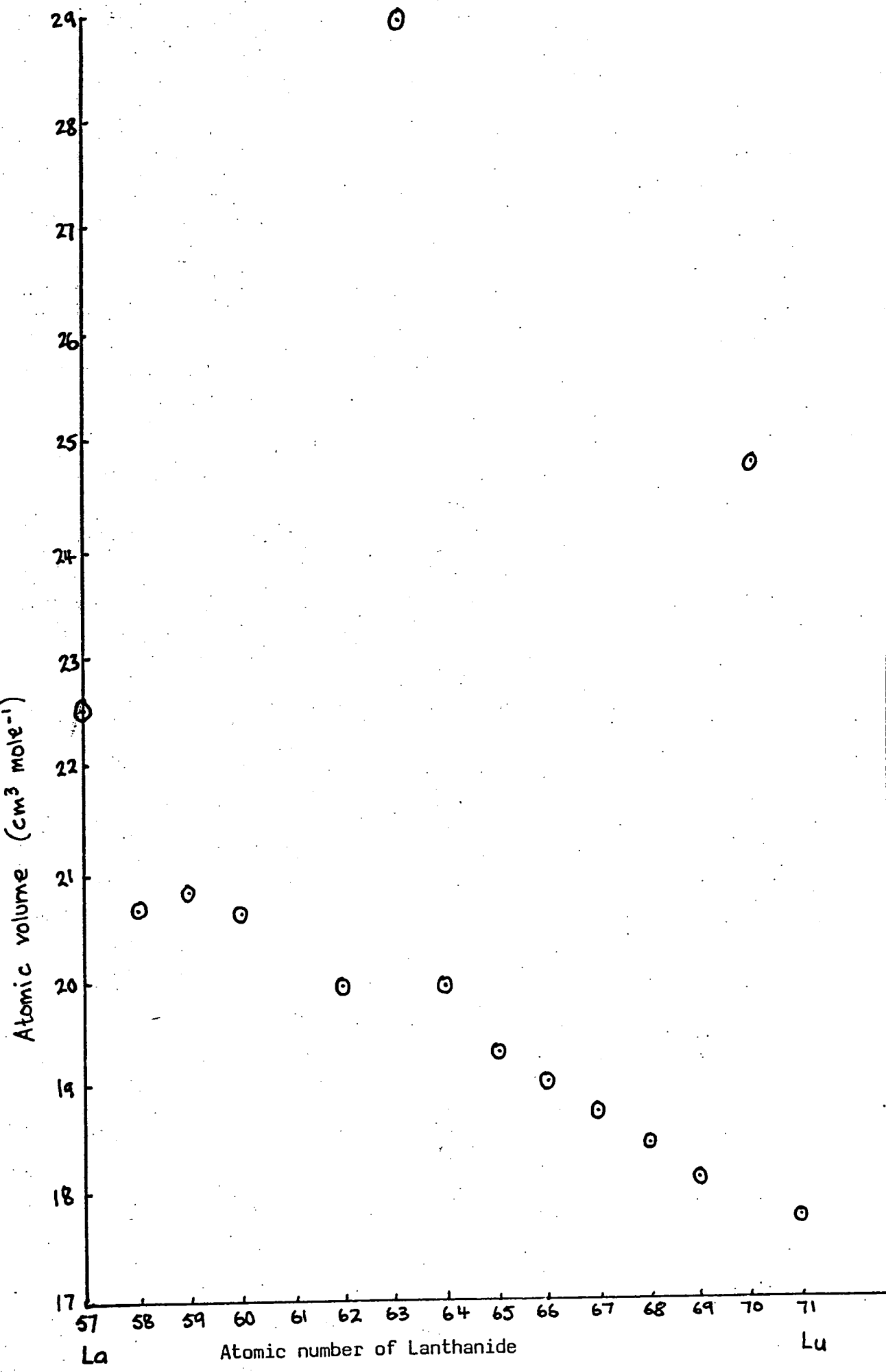

Fig. 3.3 Atomic volume (cm^3/mole) of lanthanides vs. atomic number

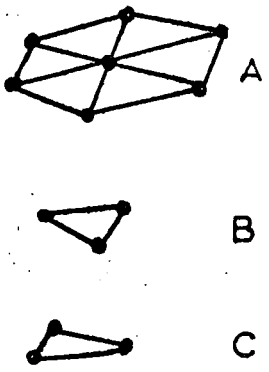

(a) stacking layers

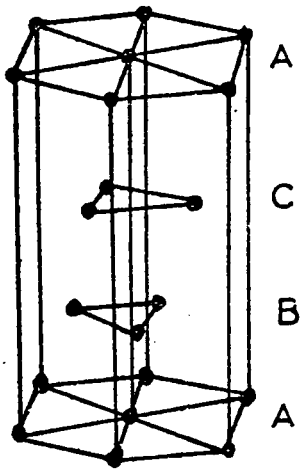

(b) structure of face - centered cubic (f.c.c.)

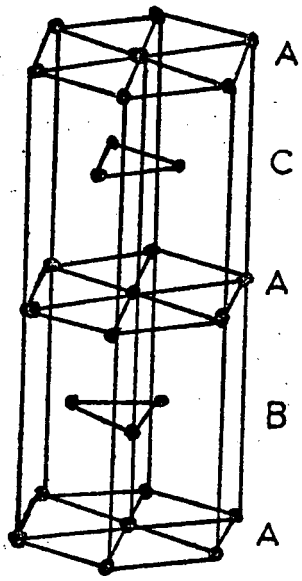

(c) double hexagonal

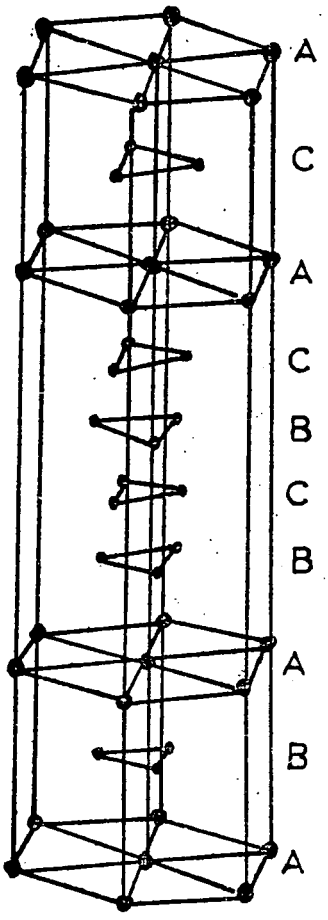

(d) Samarium type

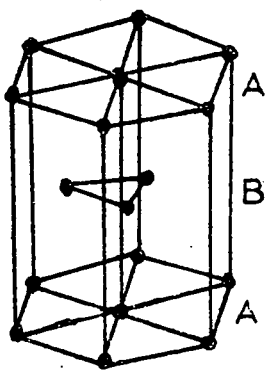

(e) hexagonal close - packed (h.c.p.)

Fig. 3.4 Schematic representation of structures occurring in the rare earth elements (After TAYLOR (1970))

For a discussion on general properties of the rare earth elements see TAYLOR (1970).

3.4.1 Magnetic properties

For aggregates of atoms, large internal forces outweigh those between the magnetic moment of an atom and an external magnetic field. Because the exchange forces between electrons in different atoms are nearly always of opposite sign to those between electrons in the same atom, the general trend is that most bound atoms do not exhibit a permanent magnetic dipole moment. In the solid state most substances consist of ions and are diamagnetic. The notable exceptions are the transition elements and, indeed, it is the incomplete 4f shell of the lanthanides which gives rise to their magnetic properties. The 4f elements bear a close resemblance to an assembly of free ions when the paramagnetic state is considered..

Equations (1.16) and (1.17) show that for pure orbital motion

$\mu_B = \frac{e\hbar}{2m}$ where $\hbar = \frac{h}{2\pi}$ = unit of angular momentum for orbital motion.

and for pure spin motion spin magnetic moment.

$\underline{M} = -\frac{e}{m}\underline{S}$ where s = unit of spin angular momentum.

In general these two equations can be represented by the equation:

$\mu = \gamma J$ where J is the total angular momentum (either orbital or spin)

Metal	Temperature Range (°C)		Structure
Scandium	to 1337		α h.c.p
	> 1337		β b.c.c
Yttrium	to 1478		α h.c.p
	> 1478		β b.c.c
Lanthanum	to 310		α d.h.c.p
	310 - 865		β f.c.c
	> 865		γ b.c.c
Cerium	-150	transformations exhibit hysteresis *	γ f.c.c
	-150 to -10		α f.c.c
	> 730		β d.h.c.p
			δ b.c.c
Praseodymium	to 795		d.h.c.p
	> 795		β b.c.c
Neodymium	to 863		α d.h.c.p
	> 863		β b.c.c
Promethium			α d.h.c.p
Samarium	to 734		α rhombohedral
	734 to 922		β h.c.p
	>922		γ b.c.c
Europium	to 822 (M.Pt.)		b.c.c
Gadolinium	to 1235		α h.c.p
	> 1235		β b.c.c
Terbium	to 1289		α h.c.p
	> 1289		β b.c.c
Dysprosium	to 1381		α h.c.p
	> 1381		β b.c.c
Holmium	to 1474 (M.Pt)		h.c.p
Erbium	to 1529 (M.Pt.)		h.c.p
Thulium	to 1545 (M.Pt.)		h.c.p
Ytterbium	to 795		α f.c.c
	> 795		β b.c.c
Lutetium	to 1656 (M.Pt.)		h.c.p

* KOSMAKI et al (1974)

Table 3.3 Structure of rare earth elements.
(After Jones et al. (1978))

and γ = magnetomechanical ratio

$= \frac{e}{2m}$ for orbital motion

$= -\frac{e}{m}$ for spin

There are several possible electron interactions within an atom and it is the relative magnitudes of these interactions which determine how the atomic electrons combine to form a stable state. (i.e. spin spin, spin orbit, orbit orbit interactions between electrons.)

The spins form a resultant vector $\underline{S}$ which represents the whole atom and the orbital resultant is given by $\underline{L}$. $\underline{S}$ and $\underline{L}$ are combined into a resultant vector $\underline{J}$ where the corresponding J quantum number can take the values $J = |L-S|, |L-S+1|, \ldots\ldots |L+S-1|, |L+S|$

The 4f shell is filled in accordance with Hunds rules which state that the magnitude of moment associated with an incomplete ionic shell is given by

(i) an arrangement of the electron spins such that the maximum total moment ($S = \sum s$), i.e. the maximum number of unpaired electron spins associated with the ion, is consistent with the Pauli Exclusion principle.

(ii) the combination (alignment) of orbital moments to give a maximum angular moment L consistent with (i) above and the Pauli Exclusion principle.

The total angular moment J is then given by

$J = L - S$ for $< \frac{1}{2}$ filled shell

$J = L + S$ for $> \frac{1}{2}$ filled shell

Provided that the lowest 4f energy levels of the ions are well separated and $\mu_B B \ll kT$ the susceptibility of a solid containing these ions will be given by the equation (1.28)

$$\chi = Ng^2\mu B^2(J(J+1))/3KT \qquad \text{(Hund)}$$

Two electrons having opposite spins occupying the same orbital involves large electrostatic repulsions. If such dual occupations are minimized, energy is lowered giving as many like spins as possible. This argument leads to the fact that partially filled d and f electron shells in the transition elements possess relatively large magnetic moments.

The equation above (1.28) can be rewritten as

$$\chi = p_{eff}^2 \, N\mu_B^2 / 3kT$$

where, as described in Chapter One, $P_{eff} = g(J(J+1))^{\frac{1}{2}}$ and is the effective number of Bohr magnetons.

Figure 3.5 (CRANGLE) shows a plot of P_{eff} versus 4f electron number of ion for the rare earths. The line is drawn for the curve obtained by calculation using the simple theory. Fitted on this is experimental data representing measured P_{eff} values for rare earth salts and metals. The generally good agreement would appear to indicate that the deep lying 4f electrons are effectively shielded by the 5s and 5p electrons. Intra-crystalline electric fields have little effect on the 4f electrons responsible for the paramagnetism and it is this insensitivity to the external influences exerted by neighbouring atoms that renders the magnetic moment due to the 4f electrons unquenched. Indeed it also

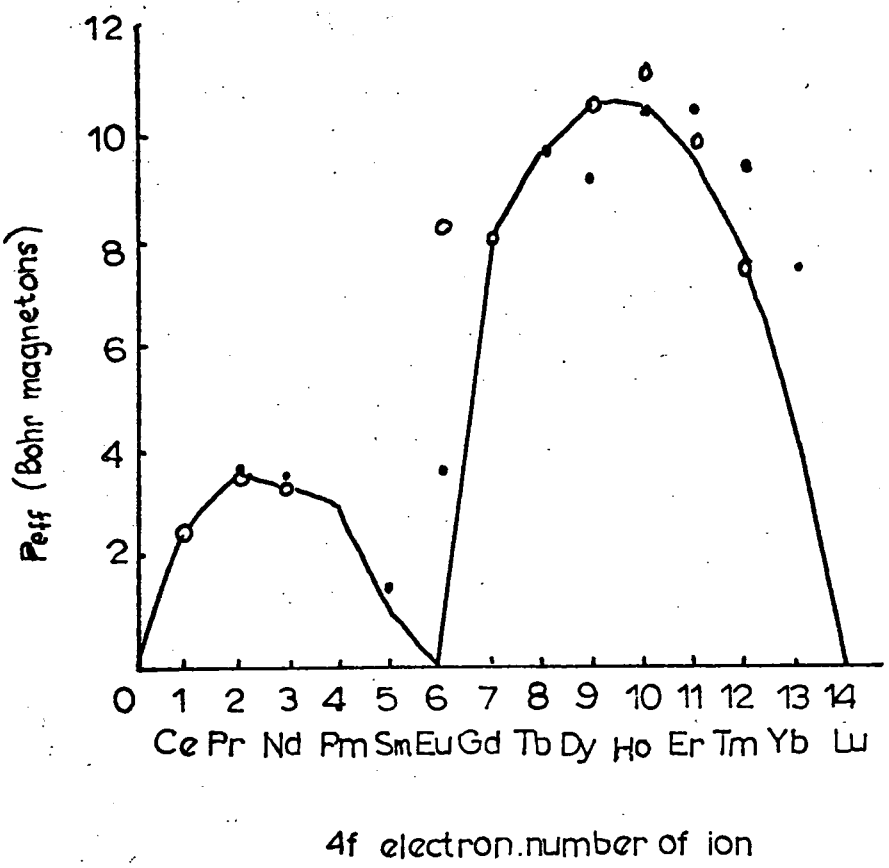

Fig. 3.5 Experimental and calculated values of P_{eff} for rare earths

o Metal

• Sesquioxide R_2O_3

line calculated

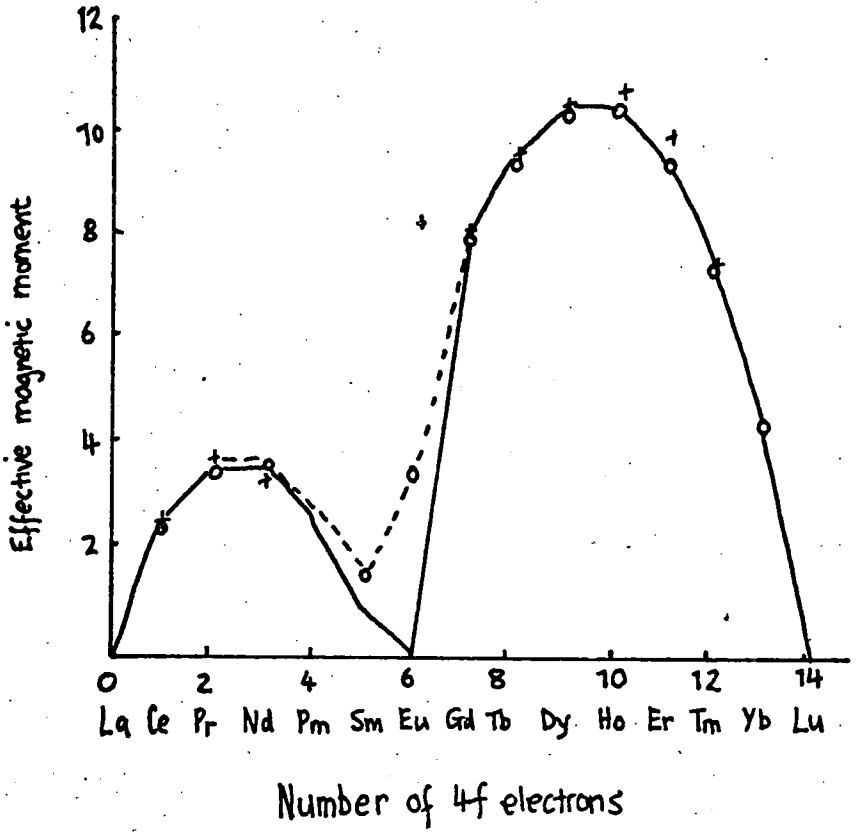

Fig. 3.6 Atomic magnetic moment as a function of the number of 4f electrons measured for trivalent ions in compounds and for rare earth metals. These are compared with Hund and Van Vleck - Franktheories.

——— Hund

- - - - Van Vleck - Frank

o Trivalent ion

\+ Metal

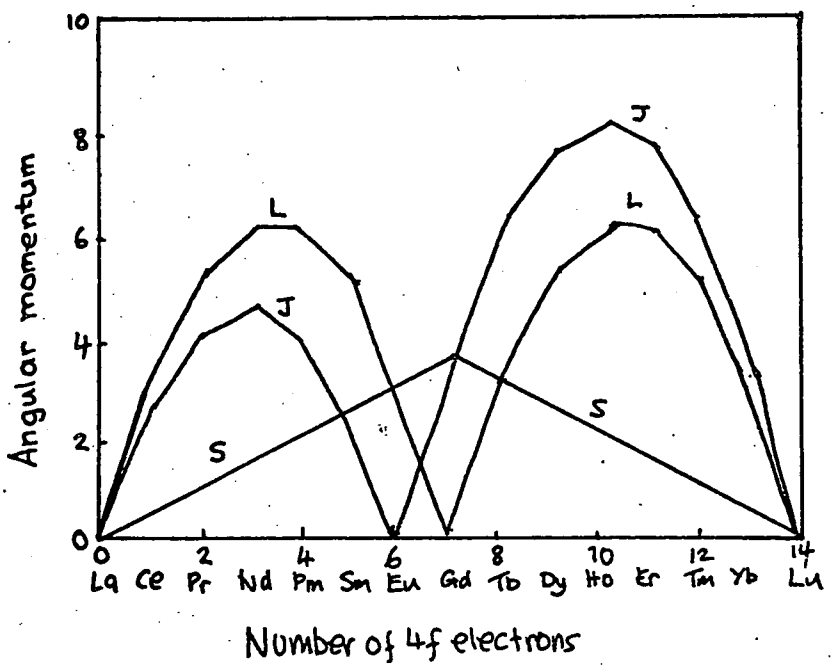

Fig. 3.7 Spin S, orbital L and resultant angular momentum J as functions of the number of 4f electrons of trivalent rare earth ions.

accounts for the similarity of the chemical properties of the rare earths. In most atoms which exhibit a magnetic moment it is the valence electrons which give rise to the moment. If the atoms ionize they lose their magnetic moments. With the rare earths, however, the magnetic moment is retained by the ions and because, as previously stated, the 4f electrons are shielded from the effect of neighbouring atoms, the rare earths approximate to an assembly of free atoms. For most of the rare earths, the magnetic moment is, therefore, very close to the theoretical value for the moment for the trivalent ion. The calculations to obtain the susceptibilities of the rare earths using equation (1.28) are done using the assumption that the multiplets are wide and that there is no electron exitation. If, however, the level splitting does not give rise to wide multiples (i.e. when the multiplet spacing is comparable to KT) then there will be occupation of higher multiplets and second or higher terms need to be considered. Van Vleck (1932) adds a term αJ to the Hund formula for the susceptibility.

$$\chi = p_{eff}^2 N\mu_B / 3kT + \alpha J \qquad (3.1)$$

αJ is normally small but when electron exitation to higher levels occurs αJ (which derives from the high frequency part of the atomic magnetic moment) must be considered. Notably large discrepancies occur for Europium and Samarium. Sm^{3+} and Eu^{3+} have susceptibilities which are greater than that given by the Hund equation. The reason for this is that the multiplet spacing is not large and not all of the atoms are in their ground state. J is small compared to L and S and the αJ term becomes important. Figure 3.8 shows multiplet spacing of Sm^{3+} and Eu^{3+} at 300K. Table 3.4 gives p^2 values both calculated and experimental

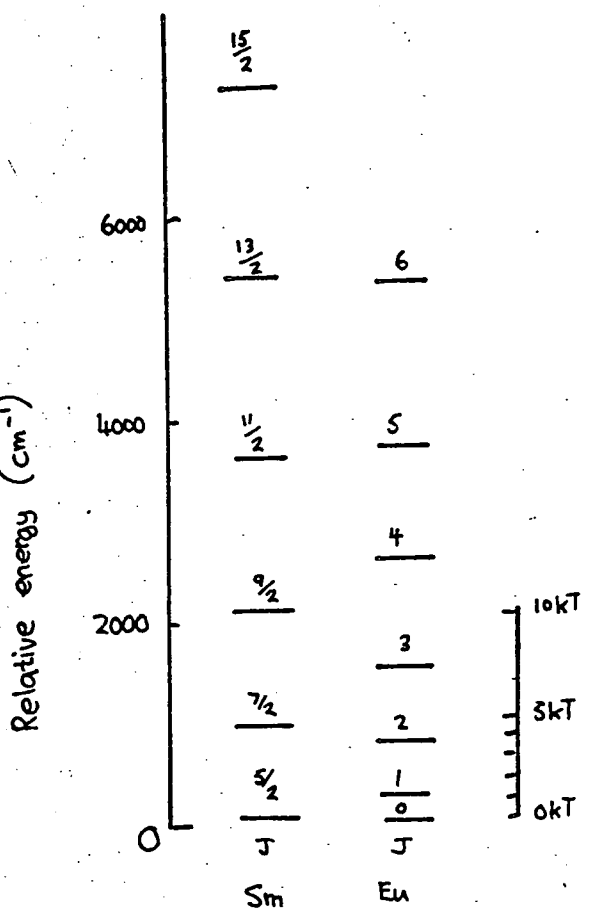

Fig. 3.8 Multiplet spacing of Sm^{3+} and Eu^{3+}. The scale for thermal energy is for temperature = 300K

Number of electrons in 4f shell	Ion	Ground Spectroscopic state	S	L	J	g	$p^2 = g^2 J(J+1)$	Average experimental value of p^2
0	La^{3+}	$^1S_0$	0	0	0	-	0	0
1	Ce^{3+}	$^2F_{5/2}$	1/2	3	5/2	6/7	6.43	6
2	Pr^{3+}	$^3H_4$	1	5	4	4/5	12.8	12
3	Nd^{3+}	$^4I_{9/2}$	3/2	6	9/2	8/11	13.1	12
4	Pm^{3+}	$^5L_4$	2	6	4	3/5	7.2	-
5	Sm^{3+}	$^6H_{5/2}$	5/2	5	5/2	2/7	0.71 (2.5)	2.4
6	Eu^{3+}	$^7F_0$	3	3	0	-	0 (12)	12.6
7	Gd^{3+}	$^8S_{7/2}$	7/2	0	7/2	2	63	63
8	Tb^{3+}	$^7F_6$	3	3	6	3/2	94.5	92
9	Dy^{3+}	$^6H_{15/2}$	5/2	5	15/2	4/3	113	110
10	Ho^{3+}	$^5I_8$	2	6	8	5/4	112	110
11	Er^{3+}	$^4I_{15/2}$	3/2	6	15/2	6/5	92	90
12	Tm^{3+}	$^3H_6$	1	5	6	7/6	57	52
13	Yb^{3+}	$^2F_{7/2}$	1/2	3	7/2	8/7	20.6	19
14	Lu^{3+}	$^1S_0$	0	0	0	-	0	0

(The values for Sm and Eu are those calculated by Van Vleck allowing for population of excited states with higher values of J, at T = 293K)

Table 3.4 Comparison of theoretical and measured values of p^2 for trivalent rare earth ions.

for the rare earths. The values given in parentheses for Sm^{3+} and Eu^{3+} are those calculated by Van Vleck. The susceptibilities of Sm^{3+} and Eu^{3+} do not follow a simple Curie-Weiss law. The susceptibilities of Eu^{3+} and Sm^{3+} are temperature dependent and Figure 3.9 shows Franks calculated curves for $1/\chi$ versus T for Sm^{3+} and Eu^{3+}. The measurement of χ for a range of temperatures are made on magnetically dilute salts. i.e. the paramagnetic ions are so far apart that mutual interaction can be neglected. The flat susceptibility at very low temperatures for Eu^{3+} is due to the αJ term. Since Eu^{3+} has a singlet grc state with J = 0. Eu^{3+} would, therefore, have a paramagnetic susceptibility of 0 but for the αJ term.

Most of the rare earths exhibit reasonably strong magnetic interactions below room temperature. (The exceptions being lanthanum, ytterbium and lutetium). Cerium, praseodymium, neodymium, samarium and europium show antiferromagnetic order, While gadolinium (which does not show an antiferromagnetic phase) terbium, dysprosium, holmium, erbium and thulmium show either ferromagnetism or antiferromagnetism depending on the temperature. One of the most striking features of the magnetic properties of the rare earths is that most of those elements with 4f shells $> \frac{1}{2}$ full show a helical arrangement of spins at temperatures above Tc (which is destroyed at the Néel temperature). Neutron diffraction techniques have played a large part in determining these.

In rare earths with 4f shell less than $\frac{1}{2}$ full no ferromagnetism appears. The heavy lanthanides exhibit large magnetocrystalline anisotropies and this, coupled with interactions between the 4f electrons and the itinerant electrons, leads to complex magnetic ordering. Because of the large

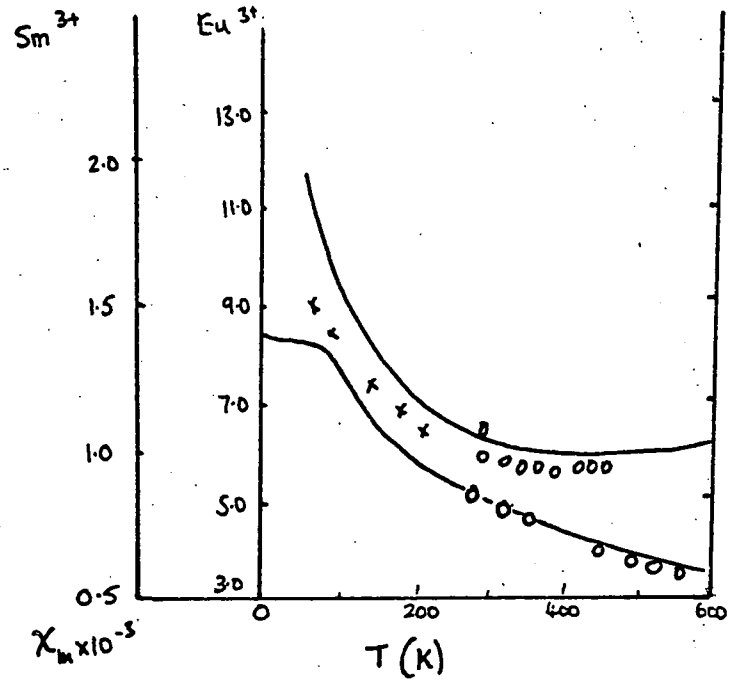

Fig. 3.9

$1/\chi$ versus T for Sm^{3+} and Eu^{3+} ions

(Experimental data: Sm^{3+} oxide, hyd. sulphate

Eu^{3+} Anhyd. sulphate)

From A. Frank, Phys Rev 39, 119 (1932)

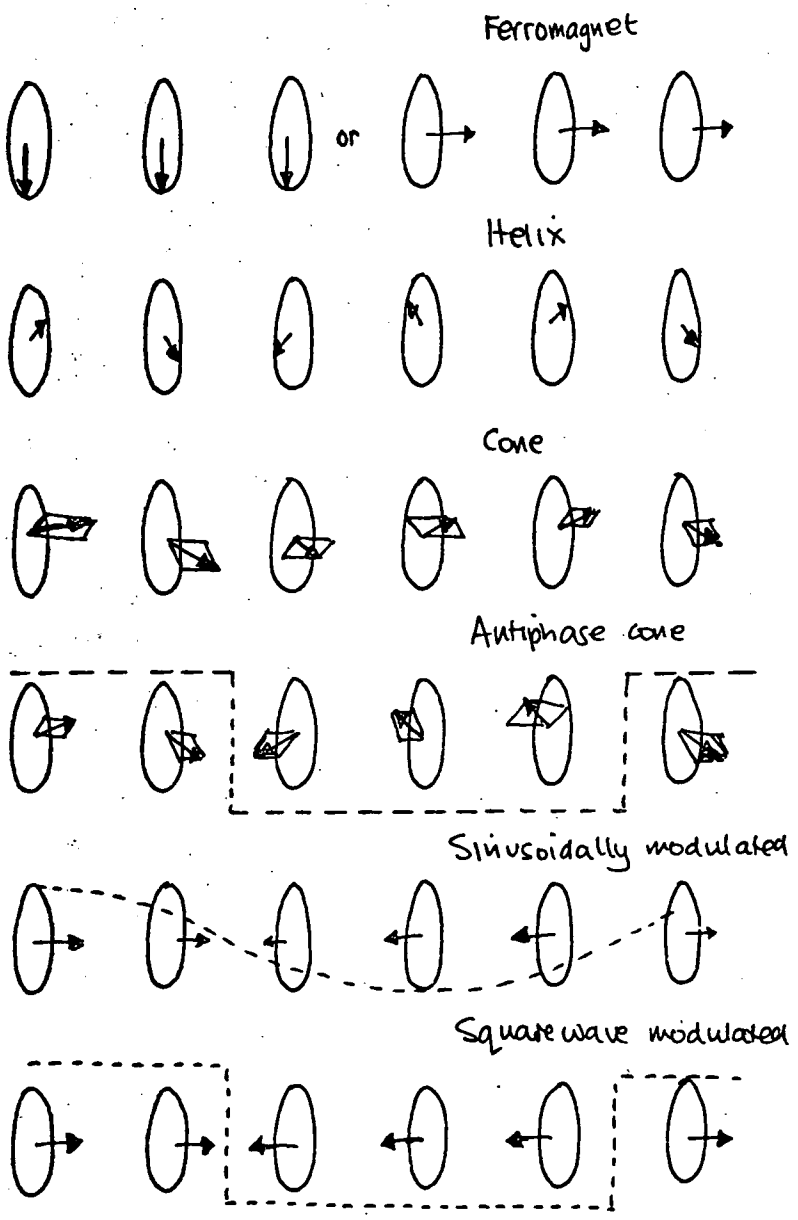

Fig. 3.10 Types of magnetic structures found in the metallic heavy rare earths.

magnetocrystalline anisotropies it is very difficult to achieve saturation of the moments in directions other than the easy direction. It is for this reason that neutron diffraction techniques have proved more appropriate to the study of magnetic moment configurations.

3.4.2 Helical Magnetism

The helical spin system is the most commonly found structure in the antiferromagnetic phase. (e.g. Dy and Tb). The process involves the parallel alignment (as in ferromagnetism) of the magnetic moments in any one plane of the h.c.p structure. A progression through the crystal lattice sees the plane of this alignment changing from one plane to another and the constant angle through which the magnetic moment changes between successive planes is called the turn angle. This angle is temperature dependent and decreases with increasing temperature. An applied field will distort the helix until the spins form a fan structure. This fan structure is destroyed with further increase of field and saturation is approached (Figure 3.11(b). The magnetic moment throughout the crystal (when helical magnetism exists) undergoes an oscillatory variation due to the turn angle.

Because the 4f electrons are effectively shielded by the 5s and 5p electrons, dipole - dipole and simple Heisenberg exchange interactions form only a small part of the total magnetic interaction. The exchange interaction which dominates is an indirect exchange via the conduction electrons. The exchange responsible for the magnetic order previously described must vary in magnitude and decrease with separation. It must also have a long range and its sign must change between nearest and next nearest neighbours. A mechanism proposed to explain the interaction (and to replace the inadequate Heisenberg interaction as applied to the

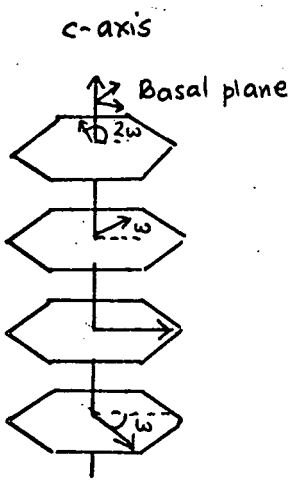

(a) Oblique view of the helical spin structure in which each plane has ferromagnetic ordering. The moment direction changes through an angle ω (turn angle) from plane to plane.

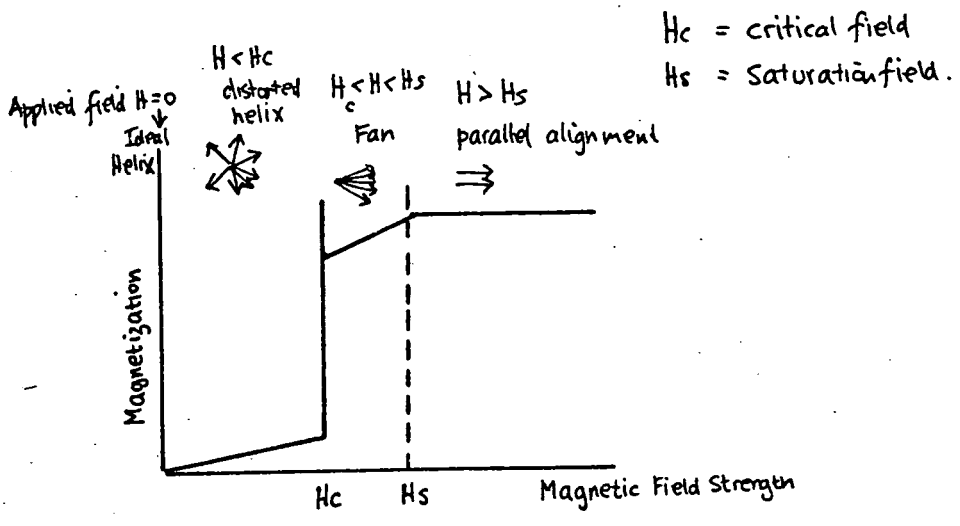

(b) Effect of an applied field on helical magnetism.

Fig. 3.11 Representation of Helical Magnetism

(KNR. TAYLOR. Contemp. Phys. Vol.11 No.5)(1970)

heavy rare earths) was one which involved constructive and destructive interference of wave functions. In their work on nuclear magnetic resonance, Ruderman and Kittel (1954) investigated nuclear magnetic moments surrounded by a distribution of conduction electrons. They proposed a mechanism which showed how conduction electrons could interact with local magnetic moments and could propagate between different magnetic sites. The theory was developed and extended by Kasuya and then Yosida to apply to s - f and s - d electrons, and the mechanism proved more appropriate to the rare earths than did the application of the Heisenberg exchange interaction. The mechanism is known as the Ruderman-Kittel-Kasuya-Yosida (RKKY) interaction and can be explained in terms of an exchange interaction where magnitude oscillates with distance.

The RKKY theory was developed for free electrons having a spherical Fermi surface. In essence, the theory regards local moments residing on lattice sites as regions which distort the wave functions of conduction electrons with spin parallel to the moment (while remaining an unfavourable site to those conduction electrons with spin antiparallel to the moment). This polarisation of the wave function of the conduction electrons means that the wave function is larger in the vicinity of the ion. The wave functions add in the vicinity of the ion such that they are all in phase with each other and constrictively interfere at the position of the ion. The effect is as though only states above the Fermi level are added. Because the wave functions represent a range of wavelengths, as the distance from the ion increases they begin to interfere destructively giving the overall effect of an oscillatory distribution of spins which reduces in magnitude as the distance from the ion increases (See Figure 3.13). The exchange interaction between conduction electron spins S and that of the single

ion Si is represented by the Hamiltonian

$$\mathcal{H} = -\Gamma(S_i.s) \tag{3.1}$$

where Γ is the exchange energy and is a constant whose magnitude depends on the separation of the ion and conduction electron.

The polarisation about the ion is given by

$$P_i(r) = \frac{9\pi Z^2 \Gamma}{4V^2 E_F} S_i F(2\underline{k}_F.\underline{r}) \tag{3.2}$$

where Z = number of conduction electrons per atom.

V = atomic volume

E_F = Fermi energy $= \frac{k^2\hbar^2}{2m}$

K_f = wave vector of electrons at the Fermi surface (Fermi momentum)

r = distance from the magnetic ion.

The assumption of a free electron distribution having a spherical Fermi surface leads to a function

$$F(x) = (\sin x - x\cos x)/x^4 \equiv F(2\underline{k}_F.\underline{r}) \tag{3.4}$$

Those conduction electrons with spin antiparallel with the local moment distort their wave functions to be a minimum at the moment and this produces an oscillatory absence of antiparallel spin. The overall effect is to maintain charge density uniformity and the spin density oscillation is in fact a function of the wavelenths of the wave functions of those conduction electrons at the Fermi level.

As the distance from the first moment increases, the spin density will at some point go negative and reach a maximum negative value at some further point. If a second ion is situated at this point with an interaction energy which is negative, then it will experience positive coupling (ferromagnetic alignment.). If, however, the ion with negative interaction energy is situated in a region where the spin wave amplitude is negative then antiferro.alignment results. In other words an ion situated an arbitrary distance from the original local moment will either interact ferromagnetically or antiferromagnetically depending on whether it is situated in a positive or negative part of the conduction electron polarization wave of the first atom. (See Figure 3.13). This ionic interaction has the same oscillatory form as the conduction electron polarization and is given by

$$\mathcal{H}_{ij} = (-9\pi Z^2 \Gamma^2 / 4V^2 E_F) \sum F(2\underline{k}_F . \underline{r}_{ij}) \underline{S}_i . \underline{S}_j \qquad (3.5)$$

For a description of indirect exchange see KITTEL (1968) de GENNES (1962).

The quantities Si and Sj must be replaced by (g-1) Ji and (g-1)Jj. This is because the rare earths are specified by their total angular momentum J and hence S is replaced by its projection on J. (which is given by (g-1)J). This gives an expression for the Hamiltonian of

$$\mathcal{H}_{ij} = - J(g - 1)^2 J(J + 1) \qquad (3.6)$$

where the quantity $(g - 1)^2 J (J + 1)$ is known as the de Gennes factor and J is the exchange integral.

Element	T_N(K)	Tc(K)	Saturation moment (μ_B)	Ionic moment (μ_B) from neutron diff. data	gJ (μ_B)	Antiferromagnetic spin structure
Ce	12.5			0.63	2.14	Ferromagnetic in planes with moments along c-axis but not antiferromagnetic
Pr	25			0.7-1.0	3.20	Adjacent layers antiparallel.
Nd	19			2.3(hex) 1.8(cubic)	3.27	Sinusoidal modulation in plane
Sm	14.8				0.71	
Eu	90		3	5.9	0	Helix
Gd	-	293	7.55		7	
TD	22a	222	9.34	9	9.0	Helix
Dy	179	85	10.6	9.5	10.0	Helix
Ho	131	20	10.34	10.0	10.0	Helix
Er	84	20	9.0	9.0	9.0	Sinusoidal c-axis 85-53.5K helix + c axis Sinusoidal 53.5-20
Tm	56	25	7.14	6.8	7.0	
Yb	Does not order				4.0	

Table. 3.5 (TAYLOR (1970)

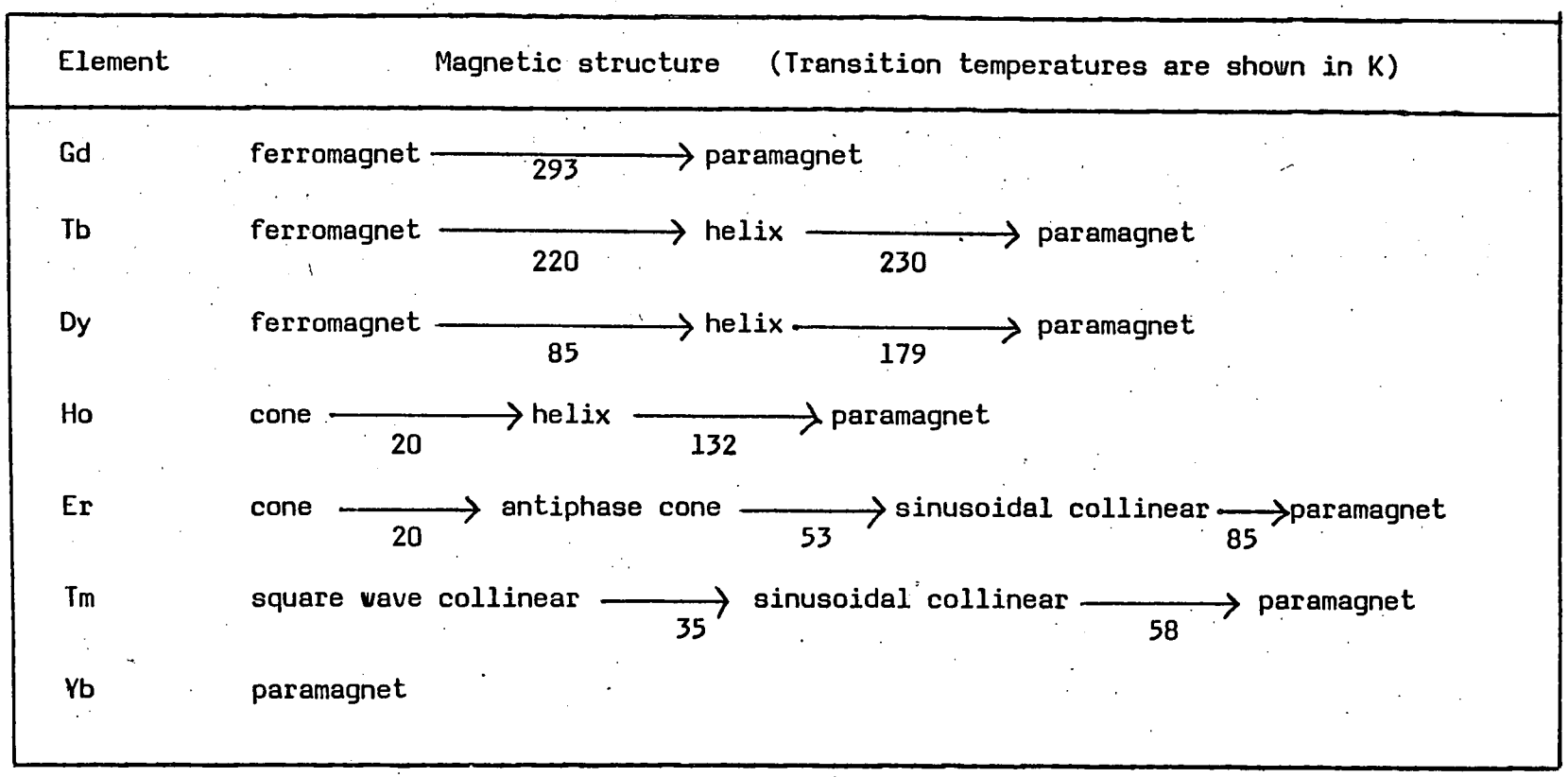

Fig. 3.12 Magnetic structures of the heavy rare-earth metals (CRANGLE)

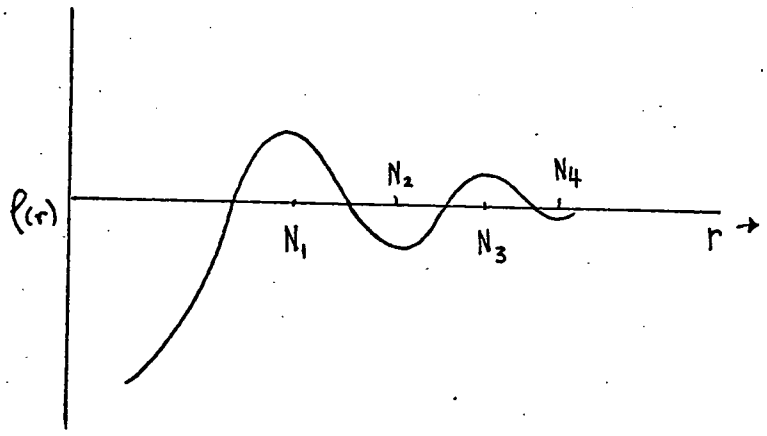

Fig. 3.13 Spin density ρ (r) v. distance from local moment.

Points N_2 and N_4 represent points where a second ion whose exchange energy < 0 will experience ferromagnetic alignment (i.e. spin wave is -ve)

Antiferromagnetic coupling will result if the interionic separation corresponds to the positions N_1 and N_2.

The RKKY mechanism provides results which are close to experimental results and it provides the necessary requirements in that it gives a magnetic interaction which operates over a large range, there is quite a large variation in strength and there is a change of sign. The limitations of the mechanism are firmly based in the nature of the assumption on which the theory is based. It assumes conduction electrons are purely S electrons and also a spherical fermi surface is assumed. It is evident from both theory and experiment that the fermi surfaces of the rare earths do not correspond to that of a free electron system and calculations have been carried out by Temple et al (1977) using a non-spherical fermi surface.

Damping of the oscillation by scattered conduction electrons must also be considered and any results obtained using the RKKY treatment must be interpreted within the context of these limitations. Also, it is often difficult to obtain the value for Z and therefore K_f. Nevertheless, the fact remains that the RKKY mechanism remains the major contribution to the heavy rare earth magnetic ordering. In fact, ferromagnetic and antiferromagnetic coupling between next nearest and nearest neighbours occurs via the RKKY interaction. Figure 3.15 shows helical antiferromagnetic ordering.

3.5 MAGNETIC PROPERTIES OF TERBIUM

The element terbium (atomic number 65) crystallises in the h.c.p. arrangement. It possesses both ferromagnetic and antiferromagnetic phases, the transition between the antiferromagnetic and ferromagnetic phases being due to the competing processes of exchange in the undistorted lattice (which favours the spiral arrangement) and magnetostriction, or hexagonal anisotropy, (which favours ferromagnetic ordering.) Because the effects depend on temperature in a different way, the transition occurs. The antiferromagnetic temperature range is quite narrow and is bounded by the Curie and Néel temperatures Tc and TN). While it has been established (using neutron diffraction techniques)(Koehler etal. (1963) and Koehler (1967)), that the structure in this narrow temperature range is oscillatory, it is not certain that the structure is indeed helical, (though the argument for helical structure is certainly very strong.) The reason for this uncertainty is that the structure undergoes a spontaneous transformation to a planar ferromagnet long before the moments saturate in the "helical" phase. This helical structure phase begins at the Néel temperature, when the paramagnetic structure breaks down. The reported values of the Néel temperature range between 225K and 230K. The helix-planar ferromagnet transition occurs at the Curie temperature, the reported values of which range between 214 to 228K. There occurs at the helix-ferromagnet transition a temperature hysteresis which results in a coexistence of helical and ferromagnetic structures over a small temperature range.

Discrepancies exist between the reported values of Tc and a possible reason for this could be the state of strain in the sample.

Clark (1980) reports the results of Palmer (1980) in which values of 214K and 219K were obtained for Tc using the same technique (ultra-sonic) on two samples. The value of 214K was obtained using a similar sample to that which gave 219K but the former had been extensively used in previous experiments.

Terbium possesses two paramagnetic curie temperatures (θp). This arises because the paramagnetic susceptibility in the basal plane is higher than that along the c-axis. Figure 3.14 shows a plot of $1/\chi$ versus temperature for terbium. One of the lines represents $1/\chi$ versus temperature for the c-axis while the other represents $1/\chi$ versus temperature for the axes in the basal plane. (Hegland et al(1963). The physical basis for this has been suggested by Kasuya (1966) who reasoned that the crystal fields are responsible.

Figure 3.15 shows helical antiferromagnetic order as displayed by terbium in the interlayer region. The turn angle ϕ (the angle between the magnetization in adjacent planes) is about 20^{o} just below the Néel temperature and falls to about $16 - 18^{o}$ before rising again to about 20^{o} at the Curie temperature. Figure 3.16 shows a plot of turn angle versus temperature using the curves of Dietrich (1967) and Koehler (1965). Below the Curie temperature terbium is ferromagnetically ordered with the magnetic moments lying in the basal plane, the $(10\bar{1}0)$ or b-axis being the easy direction of magnetization. Terbium has a massive axial anisotropy and applied fields of up to ten million oersteds would be required to drag the magnetization into the c direction. (This state of affairs exists for other heavy rare earth single crystals.) As the temperature is lowered saturation occurs (as shown

by neutron diffraction data) with a moment of $9.34\mu_B$ as compared with the theoretical value $9.0\ \mu_B$. It has been suggested that the surplus $0.34\ \mu_B$ is due to conduction band polarization. (Roeland et al. (1975)).

Figure 3.18 shows the temperature dependence of the second order anisotropy constant in terbium (for a discussion on anisotropy see Chapter Two). Curve a is the theoretical curve $5.65 \times 10^8 \hat{I}_{5/2}[\mathcal{L}^{-1}(\sigma)]$ and curve b is an experimental curve due to Féron (1969). The value of K_2 on extrapolation of the curve to T = 0K gives a value 5.65×10^8 (erg cm^{-3}). This contrasts with that value due to Rhyne and Clark (1967) of 5.5×10^8 (erg cm^{-3}). Figure 3.19 shows the data of Rhyne and Clark together with the theoretical curve $5.5 \times 10^8 \hat{I}_{5/2}[\mathcal{L}^{-1}(\sigma)]$ Figure 3.20 shows the fourth order anisotropy in terbium versus temperature. Again the experimental data is that of Féron (1969). Figures 3.21 and 3.22 show the variation of the basal plane anisotropy constant K_6^6 with temperature.

3.5.1 Magnetostriction of Terbium

Magnetostriction and magnetoelastic energy is discussed in Chapter One-(1.11). Equation (1.50) gives an expression for the linear magnetostriction for the h.c.p structure as

$$\begin{aligned}
\delta\ell/\ell = {} & A(2\alpha_1\alpha_2\alpha_3 + (\alpha_1^2 - \alpha_2^2)\beta_1)^2 \\
& + B\alpha_3^2((\alpha_1^2 - \alpha_2^2)(\beta_1^2 - \beta_2^2) + 4\alpha_1\alpha_2\beta_1\beta_2) \\
& + C((\alpha_1^2 - \alpha_2^2)(\beta_1^2 - \beta_2^2) + 4\alpha_1\alpha_2\beta_1\beta_2) \\
& + D(1-\alpha_3^2)(1-\beta_3^2) + E\alpha_3^2\beta_3^2(1-\alpha_3^2) \\
& + F\alpha_3^2(1-\alpha_3)^2 + G\beta_3^2(1-\alpha_3^2) + H\alpha_3^2\beta_3(\alpha_1\beta_1 + \alpha_2\beta_2) \\
& + I\alpha_3^3\beta_3(\alpha_1\beta_1 + \alpha_2\beta_2) + J\alpha_3^2(1-\beta_3^2) + K\alpha_3^2\beta_3^2
\end{aligned}$$

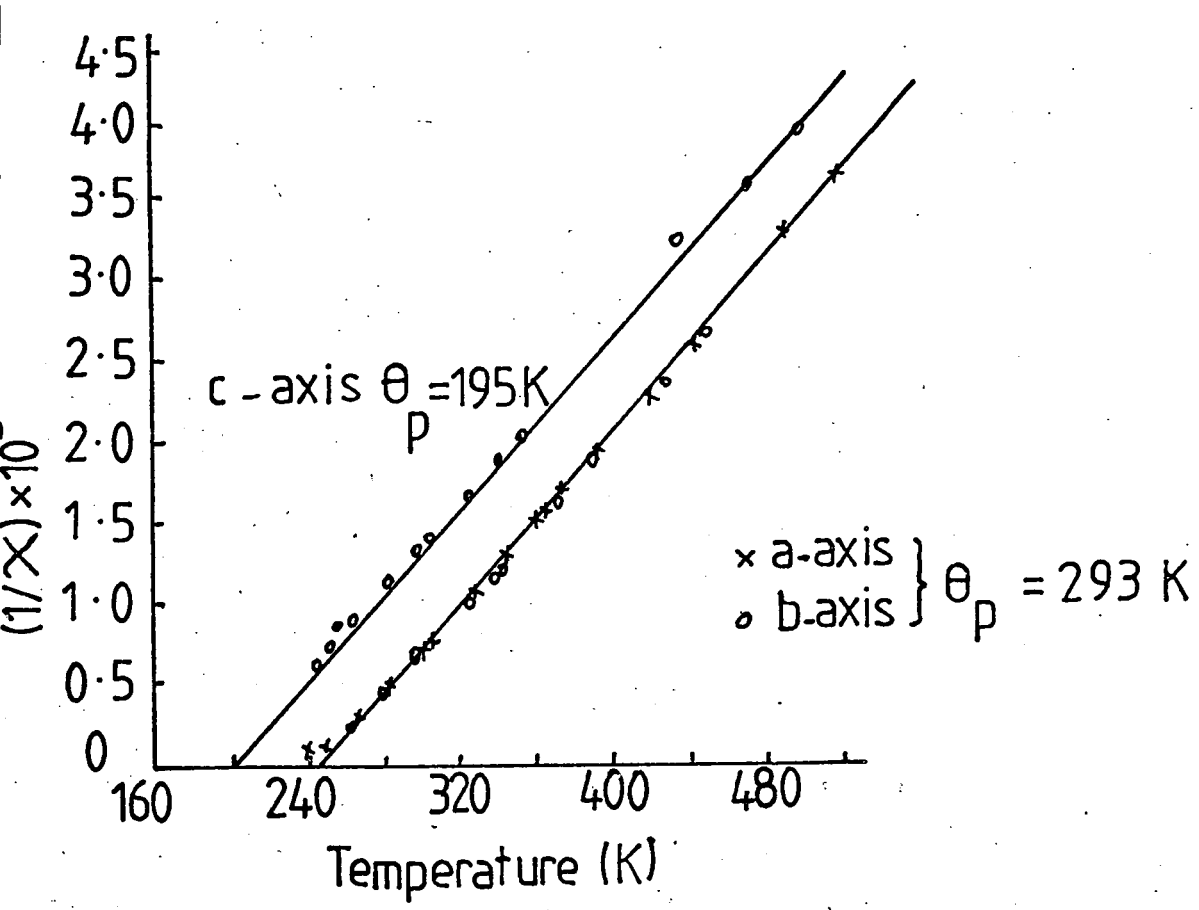

(After Hegland et al. (1963))

Fig. 3.14 The reciprocal of the paramagnetic susceptibility of a, b, c axis samples of terbium versus temperature.

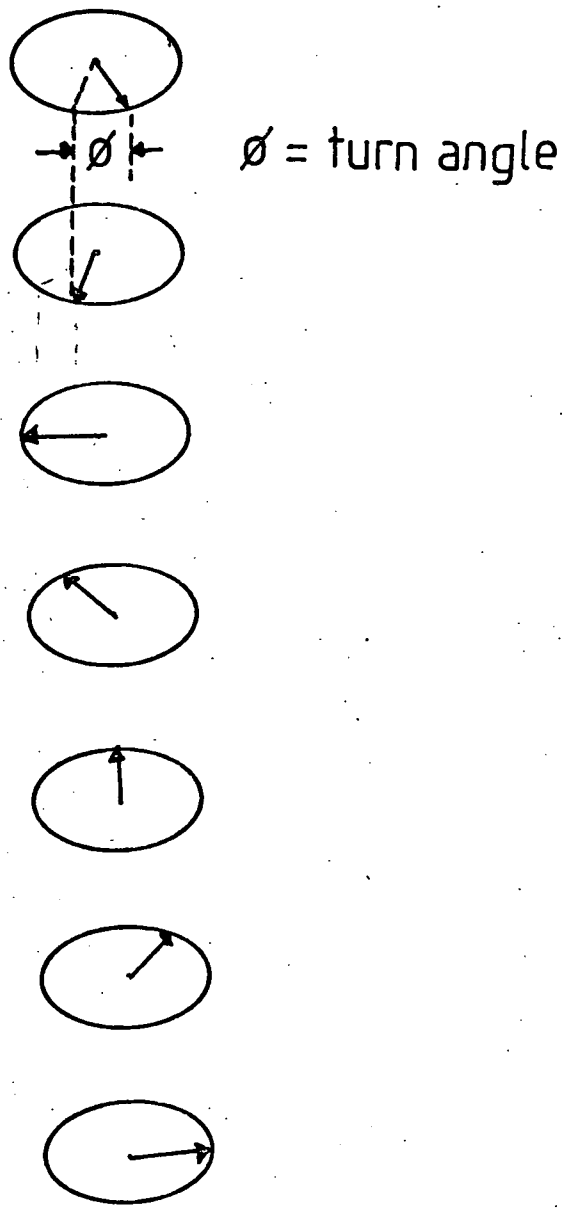

Fig. 3.15 Helical Antiferromagnetic order

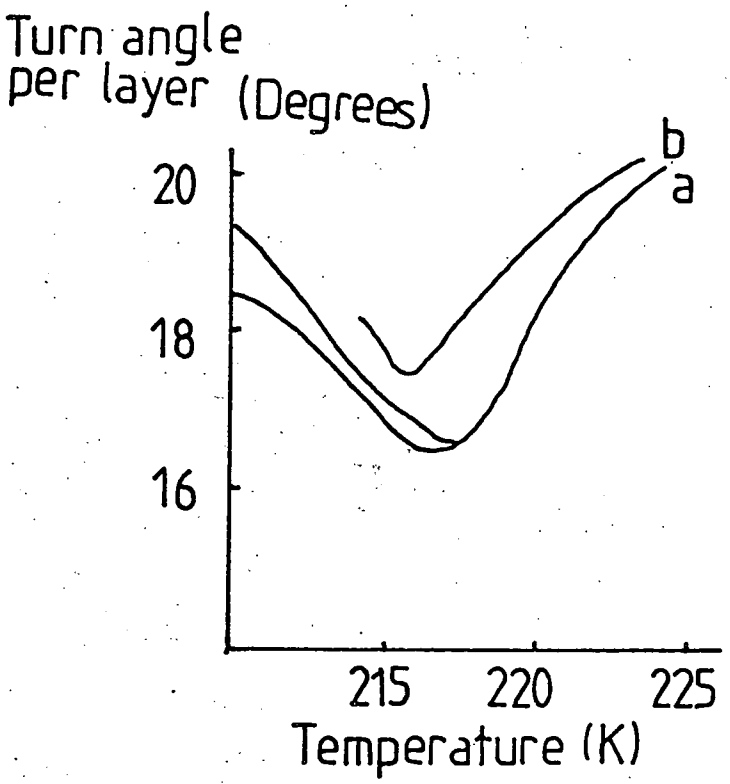

Fig. 3.16 Interplaner turn angles for Terbium as a function of temperature.

(a) Dietrich (1967)

(b) Koehler (1965)

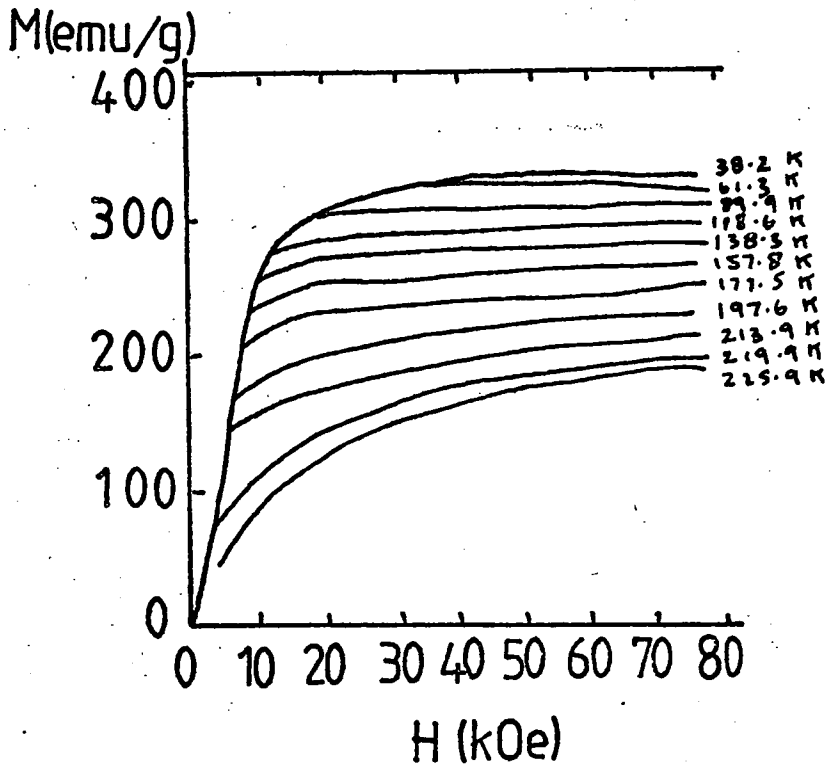

(AFTER FÉRON (1969))

Fig. 3.17 Variation of magnetization M versus magnetic field H applied along the a axis at different temperatures (Terbium)

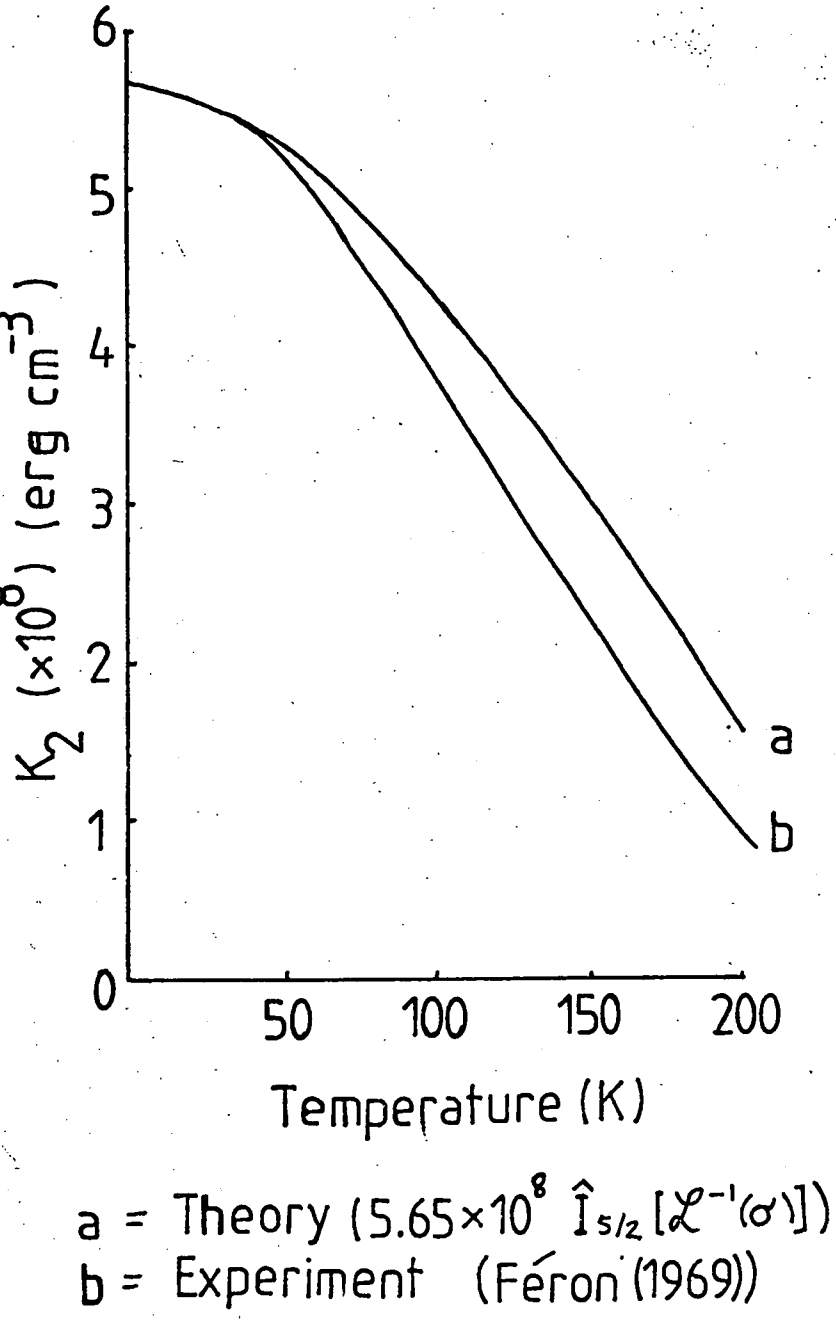

a = Theory (5.65×10^8 $\hat{I}_{5/2}[\mathcal{L}^{-1}(\sigma)]$)
b = Experiment (Féron (1969))

Fig. 3.18 Terbium 2nd order axial anisotropy constant.

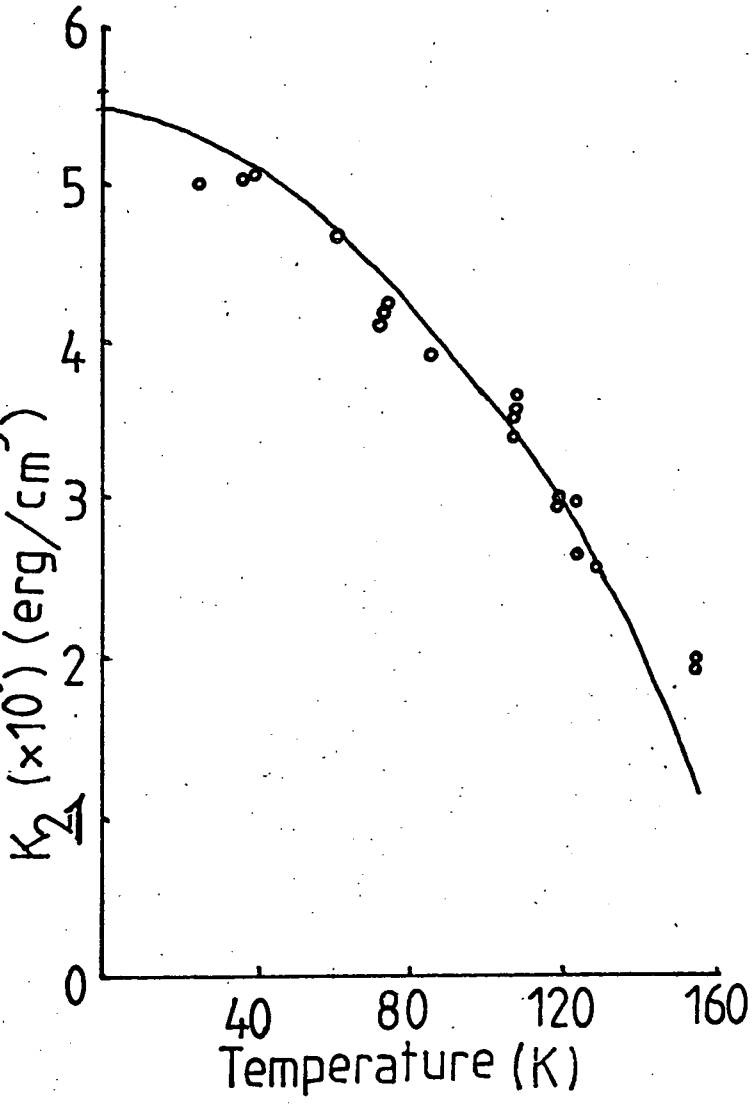

• = data by Rhyne and Clark (1967)
curve = theoretical curve $5.5 \times 10^8 \hat{I}_{5/2}[\mathcal{L}^{-1}(\sigma)]$

Fig. 3.19 Terbium 2nd order anisotropy constant

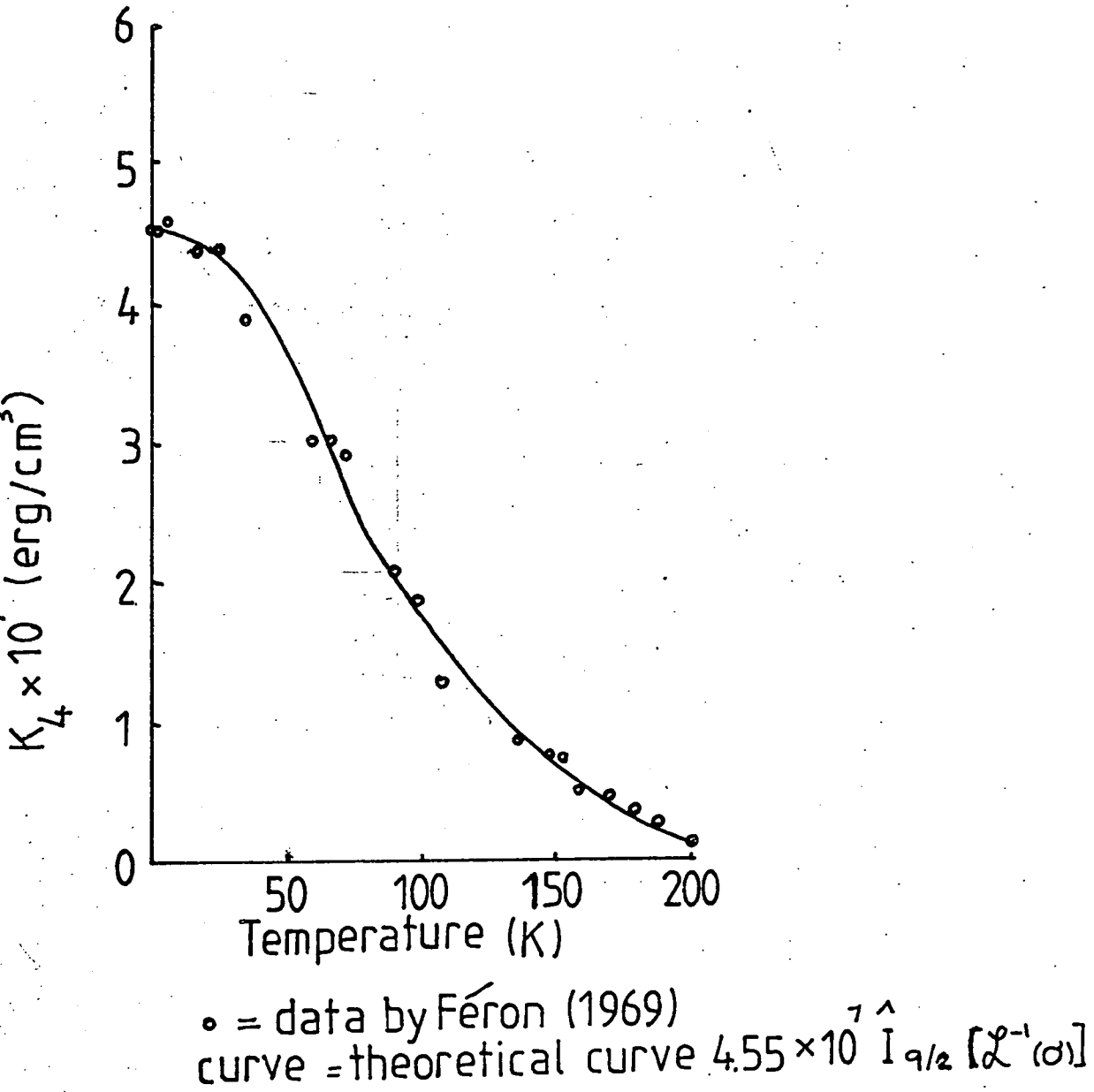

Fig. 3.20 Terbium 4th order anisotropy constant versus temperature.

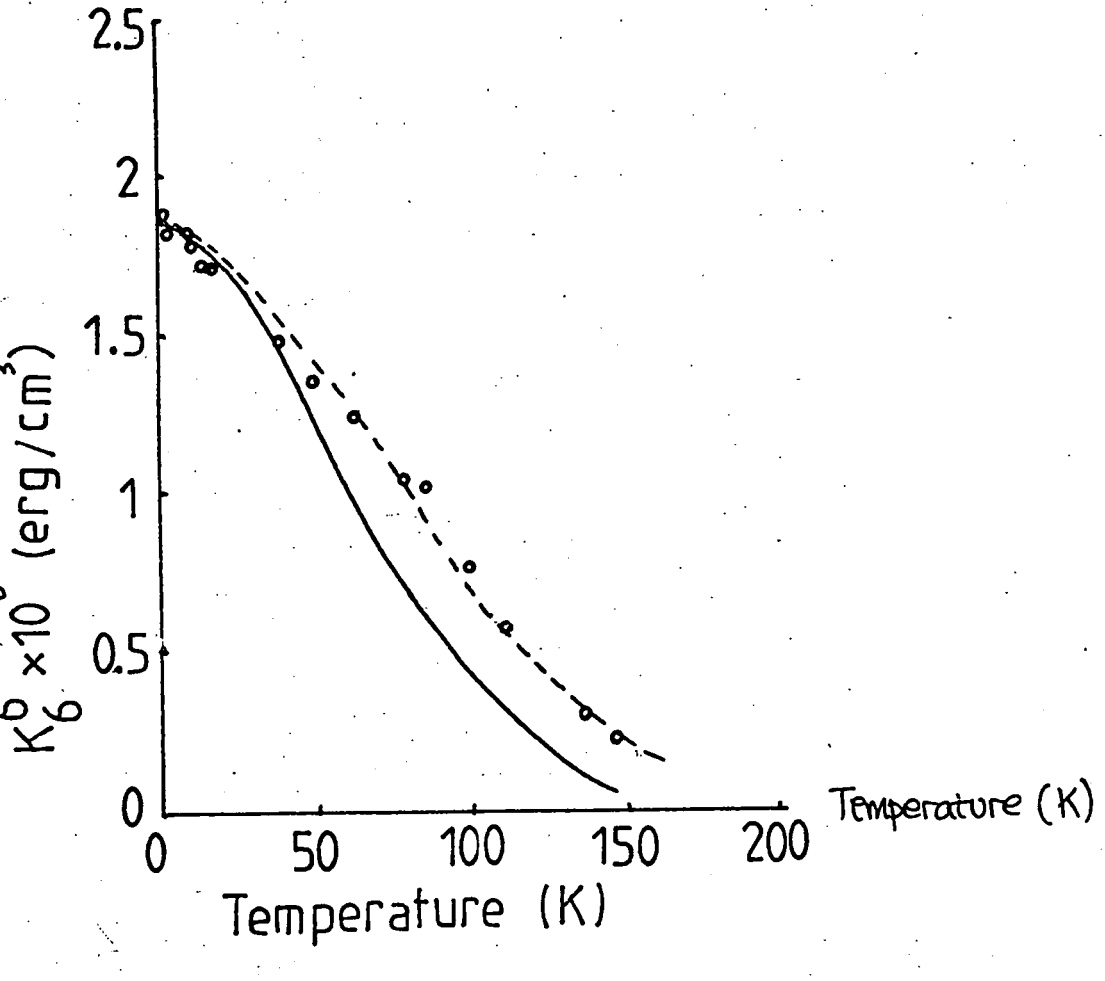

o = data by Féron (1969)
curve = theory

Fig. 3.21 Terbium Basal Plane Anisotropy Constant versus temperature.

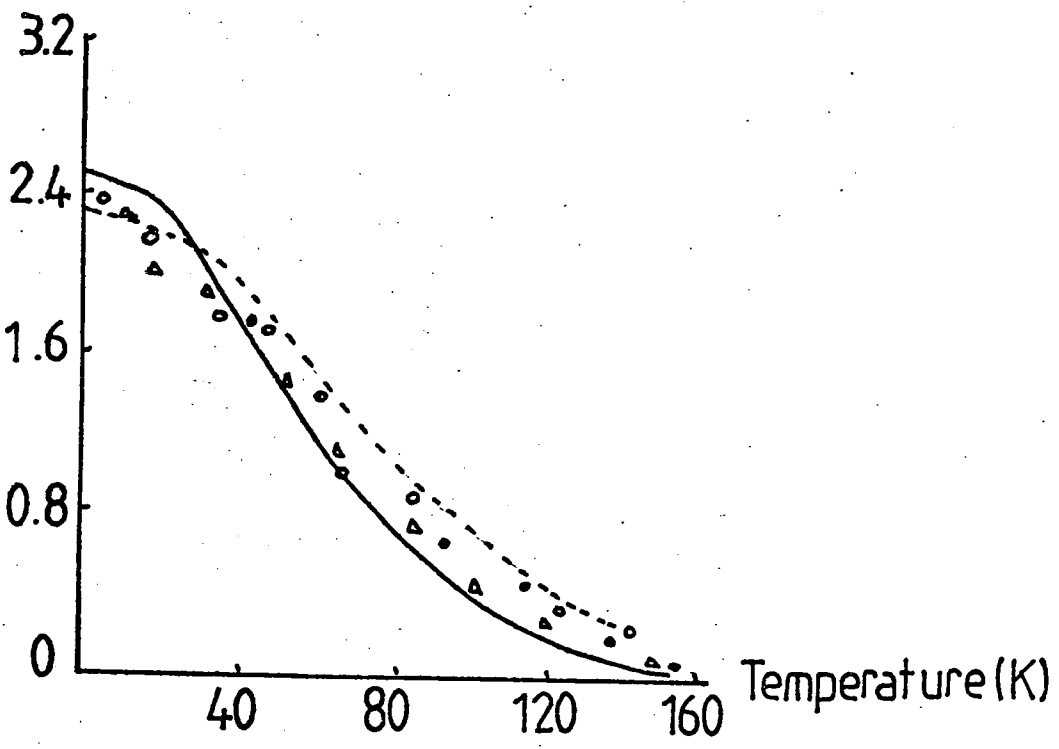

△ = Rhyne and Clark (1967) ($\vec{a}$ - axis) measurement

• = Bly et al (1968)

○ = Rhyne and Clark (1967) ($\vec{b}$ - axis) measurement

dotted = theoretical curve $2.2\,\hat{I}_{5/2}[\mathcal{L}^{-1}(\sigma)]\,\hat{I}_{9/2}[\mathcal{L}^{-1}(\sigma)]$

full = theoretical curve $2.42\times10^{6}\,\hat{I}_{13/2}[\mathcal{L}^{-1}(\sigma)]$

(theoretical curves after Rhyne and McGuire (1972))

Fig. 3.22 Terbium Basal Plane Anisotropy constant K_6^6 versus temperature.

As previously mentioned, terbium has a massive anisotropy which keeps the magnetic moments in the basal plane. Hence the direction cosines representing the c axis (α_3) in the above equation will be zero thereby reducing the equation to equation 1.52.

$$\begin{aligned}\delta l/l &= A(2\alpha_1\alpha_2\beta_1 + (\alpha_1^2 - \alpha_2^2)\beta_2)^2 \\ &+ C((\alpha_1^2 - \alpha_2^2)(\beta_1^2 - \beta_2^2) + 4\alpha_1\alpha_2\beta_1\beta_2) \\ &+ D(1 - \beta_3^2) + G\beta_3^2\end{aligned}$$

Figures 3.23 to 3.26 show magnetostriction in terbium. The magnetostriction for the h.c.p. structure can also be represented by equation 1.49.

$$\begin{aligned}\delta l/l &= (\lambda_1^{\alpha,0} + \lambda_1^{\alpha,2}(\alpha_3^2 - 1/3))(\beta_1^2 + \beta_2^2) \\ &+ (\lambda_2^{\alpha,0} + \lambda_2^{\alpha,2}(\alpha_3^2 - 1/3))\beta_3^2 \\ &+ \tfrac{1}{2}\lambda^{\gamma,2}((\alpha_1\beta_1 + \alpha_2\beta_2)^2 - (\alpha_1\beta_2 - \alpha_2\beta_1)^2) \\ &+ 2\lambda^{\epsilon,2}(\alpha_1\beta_1 + \alpha_2\beta_2)\alpha_3\beta_3\end{aligned}$$

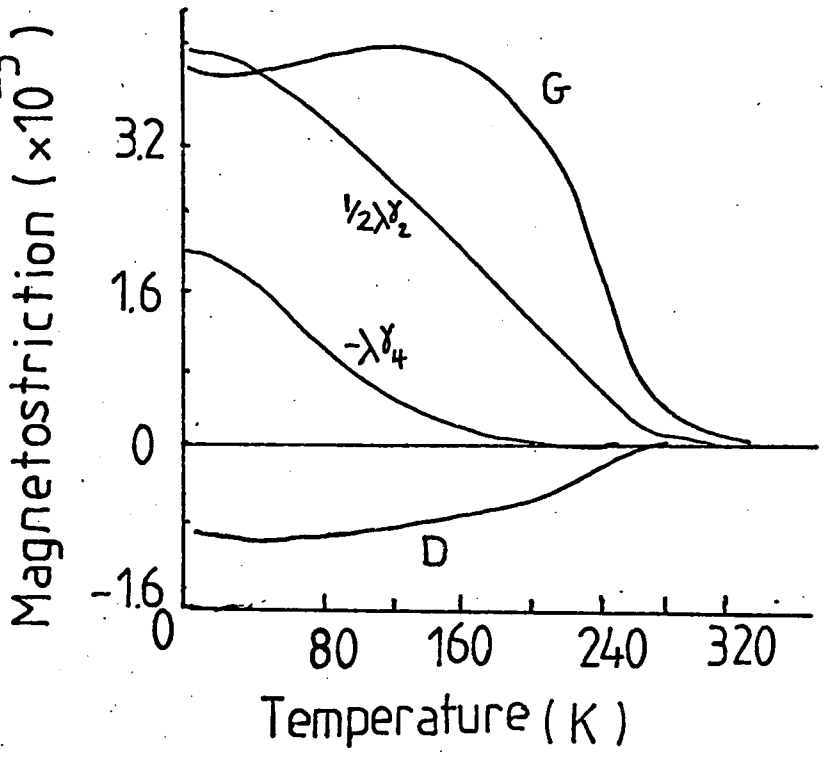

(AFTER RHYNE and LEGVOLD (1965))

Fig. 3.23 Magnetostriction coefficients of Terbium.

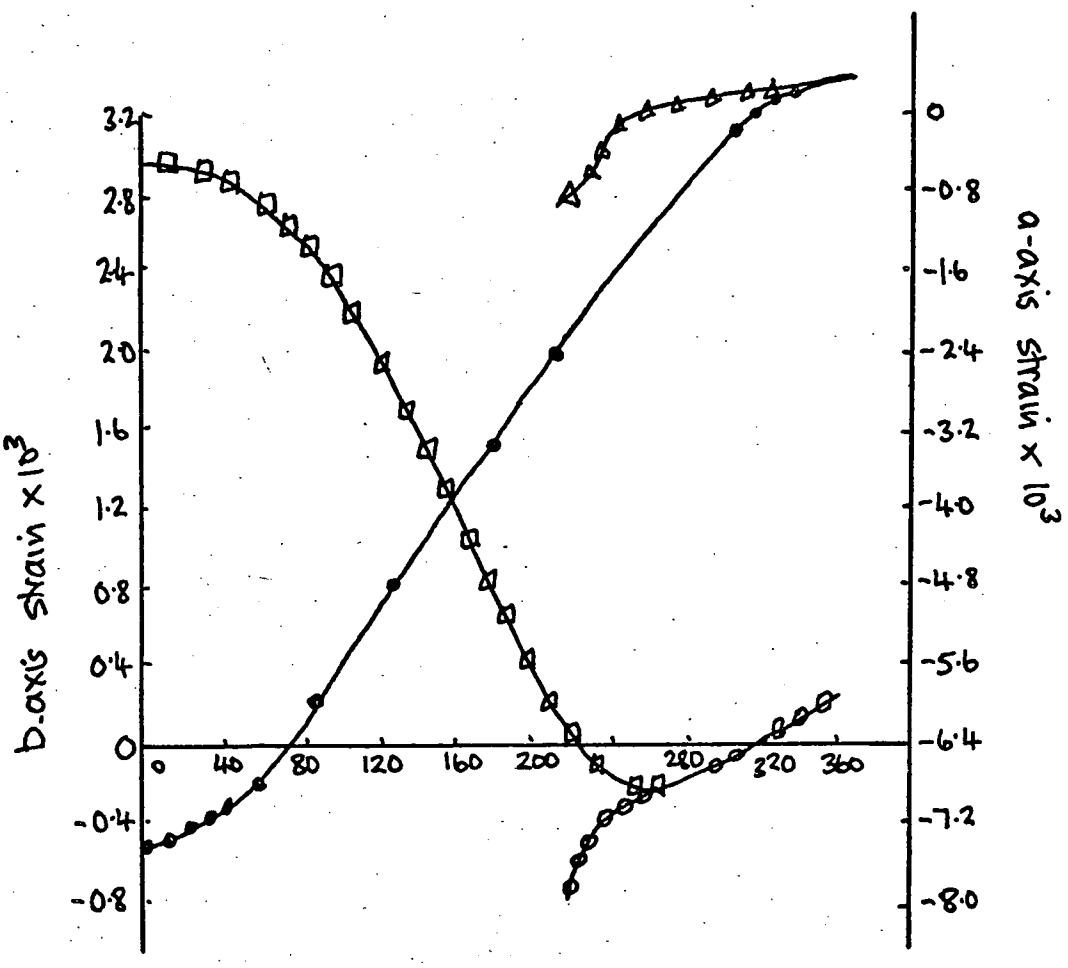

Δ a - axis H = 30 k Oe

• a - axis H = 0

□ b - axis H = 30 kOe

o b - axis H = 0

Fig. 3.24 Magnetostriction of terbium single crystals

(Taken from RHYNE and LEGVOLD 1965)

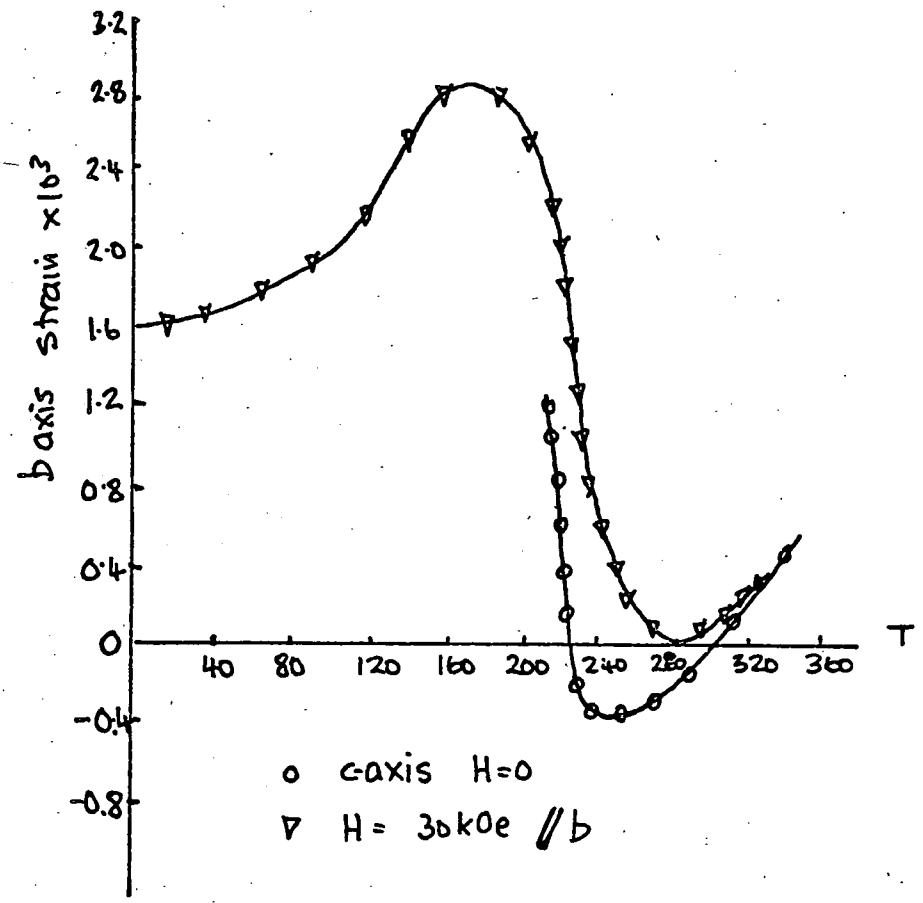

Fig. 3.25 Magnetostriction of terbium single crystals

(From RHYNE and LEGVOLD 1965)

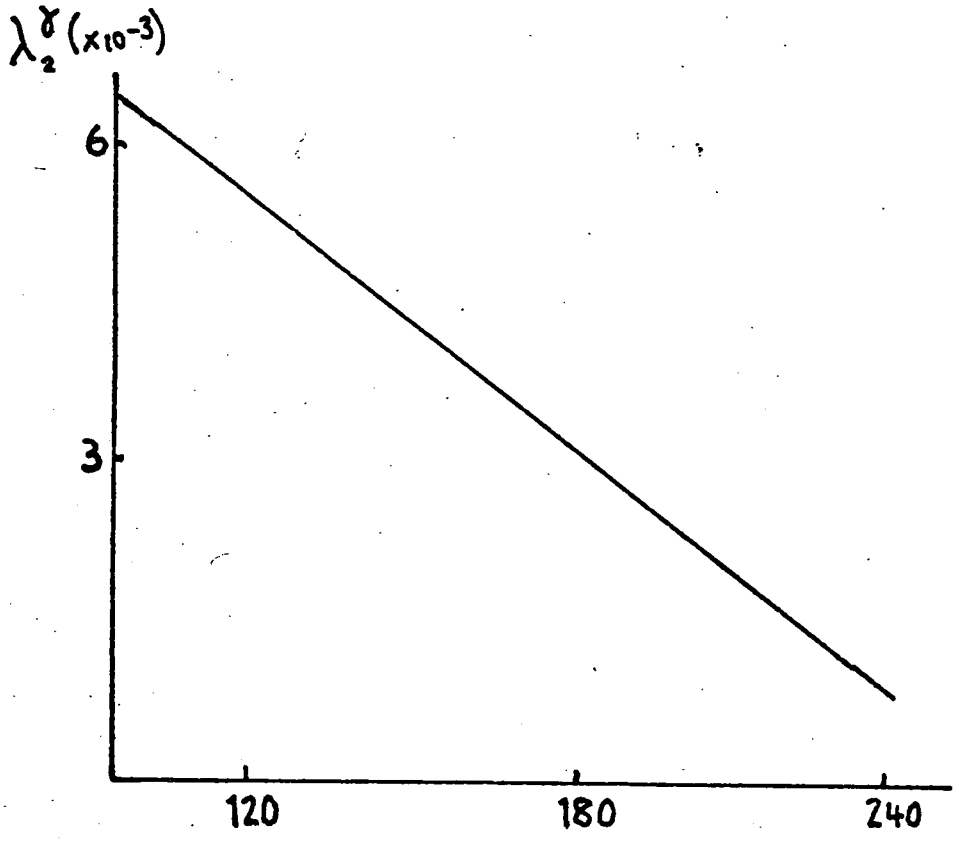

Fig. 3.26 Magnetostriction of Terbium

(BIRSS et al. 1978)

CHAPTER FOUR

MAGNETIC DOMAINS

CHAPTER 4

MAGNETIC DOMAINS

4.1 INTRODUCTION

As mentioned in CHAPTER ONE, the Weiss molecular field theory, together with the contribution made later by Heisenberg, represented a successful and important contribution towards explaining the spontaneous magnetization which takes place in ferromagnetic materials. There is, however, an important aspect of the theory which is incomplete in that it did not explain observations of the magnetization of ferromagnetic materials below a critical temperature (Curie temperature). The theory predicted that below the Curie temperature (above which ferromagnetic materials are paramagnetic) ferromagnetic materials would spontaneously magnetize to saturation in the absence of applied magnetic fields. Figure 4.1 shows the spontaneous magnetization, Is, for nickel as a function of temperature. Figure 4.2 shows the curve of reduced magnetization Is/Io versus T/Tc where Tc is the Curie temperature. Is = spontaneous magnetization and Io is the maximum value of Is. The curve shows that Is = 0 at T = Tc. This would suggest that below the Curie temperature ferromagnetic materials should become permanent magnets. This is clearly not the case as it is quite usual for a piece of iron at room temperature (below it's Curie temperature) to be in an unmagnetized state in the absence of an applied field. In order to explain this, Weiss suggested that a ferromagnetic material could have zero net magnetization below it's Curie temperature if the material was considered to consist of many small regions with moments pointing in different directions to each other. Although the regions are small they contain many atoms whose magnetic moments lie in the same direction. Hence

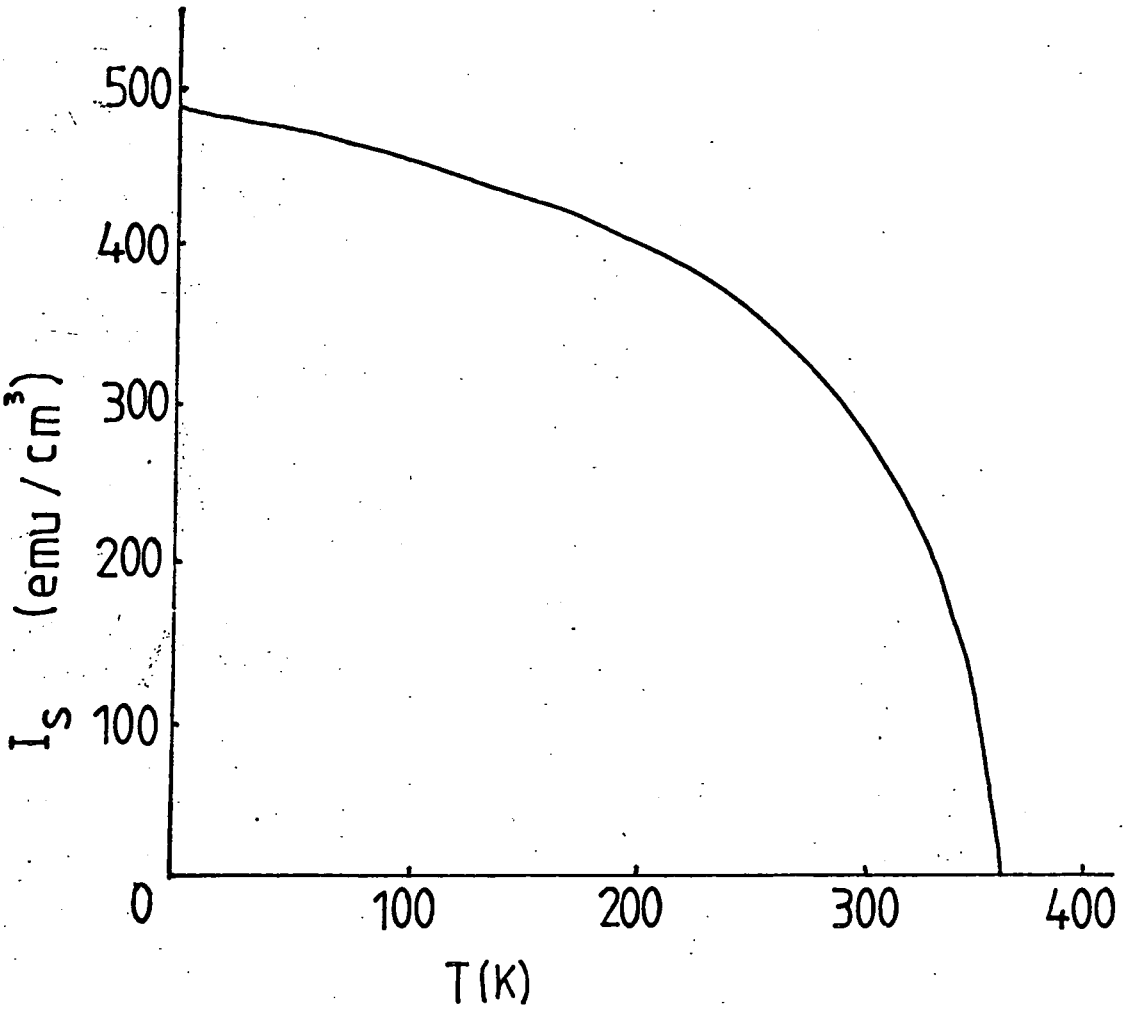

Fig. 4.1 Variation of spontaneous magnetization Is with temperature T For Nickel.

(Carey and Isaac)

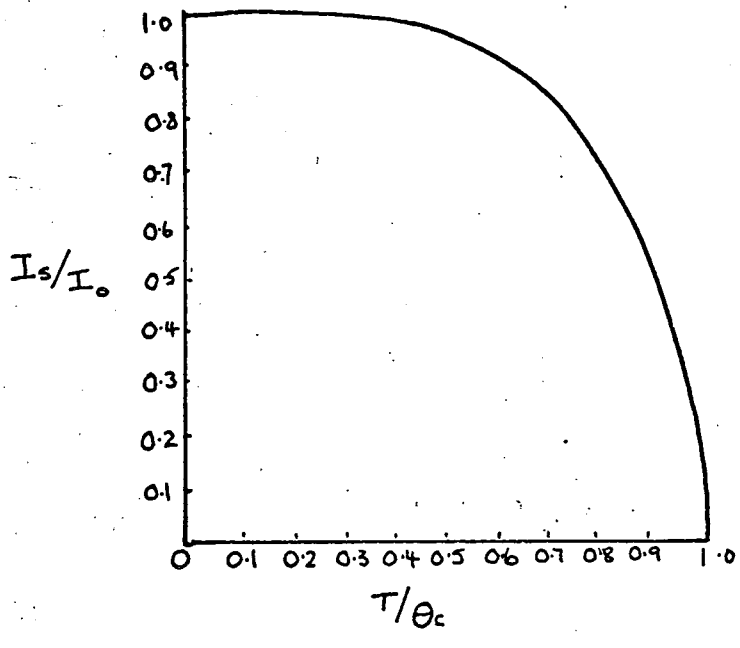

Fig. 4.2 Reduced magnetization Is/Io versus T/θc

Is = saturation magnetization

Io = maximum value of Is

θc = Curie temperature

these regions each approximate to a permanent magnet and, because of the large number of atoms contained in each region, the overall magnetization is virtually independent of thermal agitation effects and the size of the domain, though temperature dependent, is constant at a given temperature.

These regions, postulated by Weiss, in which the magnetization is constant in magnitude and direction, are called domains and it is the variation of the magnetic moment orientation between domains which renders the overall magnetization zero in the absence of an applied field. Within the domains full magnetization occurs as a result of exchange interactions and the overall effect is one of energy minimization. While forming boundaries between neighbouring domains costs energy, the formation of domain structures actually reduces the potential energy of the sample and the resultant overall magnetization, which is the vector sum of the domain moments, can take values between, and including, zero and saturation.

4.1.1 Domain Formation

Figure 4.3(i) shows a magnetization curve for a ferromagnetic material. If, however, a single crystal is used as the specimen, the magnetization curve has a different shape according to the direction in which the specimen is magnetized. As previously mentioned in CHAPTER ONE, the ease with which a specimen can be magnetized varies with crystallographic direction. Figure 4.4 shows magnetization curves for iron in the [100], [110] and [111] directions (See Figure 1.8b which shows these directions) and from the diagram it is evident that the sample is easier to magnetize along the [100] direction. This direction

in iron is an easy axis of magnetization. The area between the magnetization curves gives the anisotropy energy.

Domain formation is best illustrated by taking the very simple case of a rectangular single crystal magnetized (along a single easy direction) to saturation. This specimen is now, in effect, one single domain and in 1935 Landau and Lifshitz proposed an explanation of domain formation for such a specimen. The specimen is a permanent magnet having all magnetic moments aligned. This situation results in an external magnetic field together with an internal field. Figure 4.5 shows that the internal alignment of the dipoles gives rise to an internal field which is counter to the external field. The external field tends to reduce the magnetization of the block and is known as the demagnetizing field. Since the block is situated in its own magnetic field which opposes the blocks magnetization, the potential energy of the system is high. It is possible in this situation to reduce this potential energy. If the specimen consisted of two domains of equal volume and opposite spin orientation then the potential energy would be halved. Further subdivision would reduce the potential energy of the system. Figure 4.6 provides a simple illustration of the reduction of the demagnetizing field by the process of domain formation. The formation of domains, however, cannot proceed indefinitely. The regions separating neighbouring domains are known as domain walls. In these regions the magnetization vector rotates from the orientation of the vector in one domain to the orientation of the vector in the neighbouring domain. See Figure 4.7. The wall width is the length over which this change in spin orientation takes place. These domain boundaries were first studied by Bloch in 1932. Because exchange forces favour parallel alignment of spins everywhere it is more economical in terms of energy to change spin orientation gradually rather than have an abrupt transition between domains.

The domain wall width is influenced by both exchange forces, which favour domain walls as wide as possible, and anisotropy forces, which favour narrow domain walls. Whatever the width of the walls they require energy to form and the energy stored in the domain walls increases as new domains form throughout the crystal. Inevitably, a point is reached where formation of new domains (with the resulting reduction in the demagnetizing field) actually means an increase in the overall energy of the system. At this point, subdivision stops and the energy of the system is minimized. There are many possible configurations for domain formation and the actual configuration for a particular specimen depends upon the magnetic properties of the material such as anisotropy and spontaneous magnetization and also on such variables as shape, stress and purity. Figure 4.6 (ii) shows two possible configurations showing closure domains. The closure domains resemble magnetic keepers and the demagnetizing field is reduced accordingly.

The first evidence of the existence of domains was obtained in 1919 by Barkhausen. Barkhausen wrapped a secondary coil around an unmagnetized ferromagnetic specimen and gradually magnetized the specimen by the application of a magnetizing field. The changes in magnetization in the specimen induced voltages in the coil. These voltages were amplified using triode valve amplifiers and the output from the amplifier was fed into a suitable output transducer such as a cathode ray oscilloscope or headphones. A series of clicks or rustling heard using headphones was interpreted by Barkhausen as being due to discontinuous charges in flux caused by the rotation of domains as they aligned with the applied field.

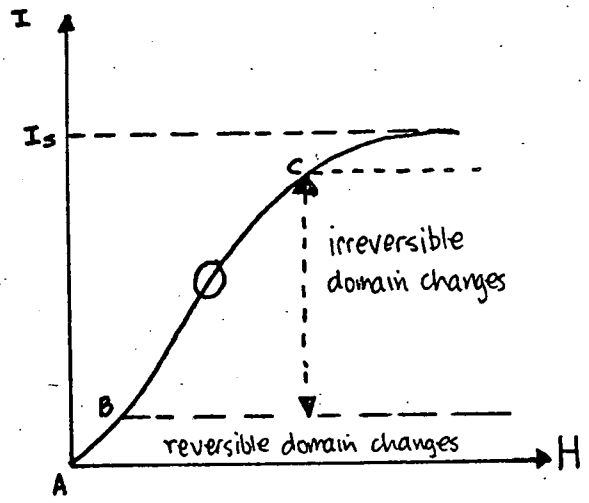

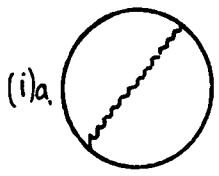

Enlarged section of the I/H curve.

(i) Magnetization curve of ferromagnetic material

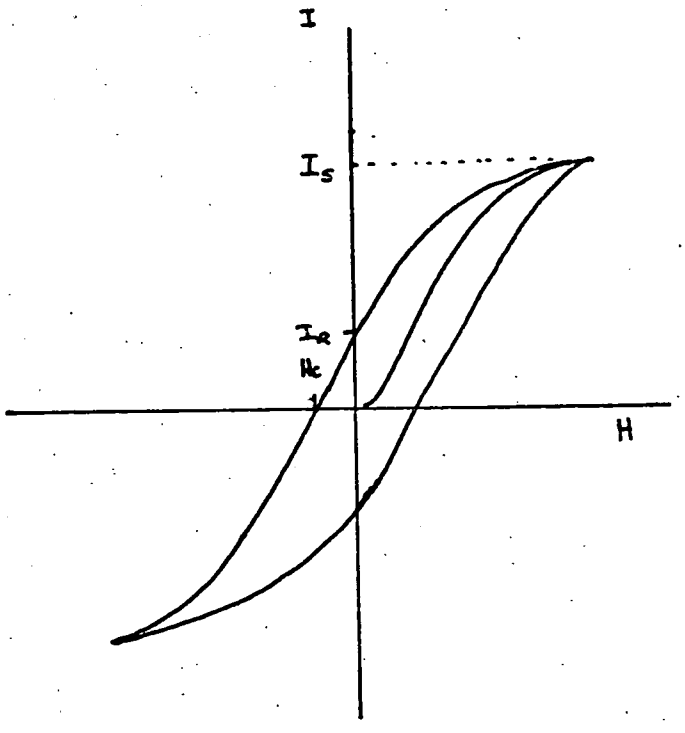

(ii) Hysteresis loop

IR = remanance

Hc = coercivity

Fig. 4.3

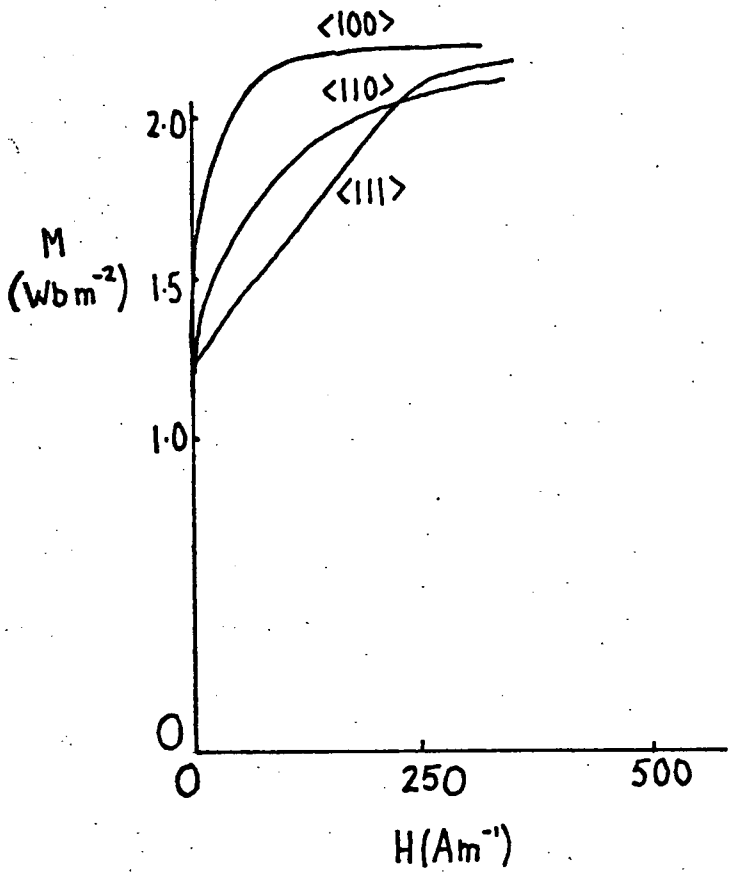

Fig. 4.4 Magnetization curves for the ⟨100⟩, ⟨110⟩ and ⟨111⟩ directions in a single crystal of iron.

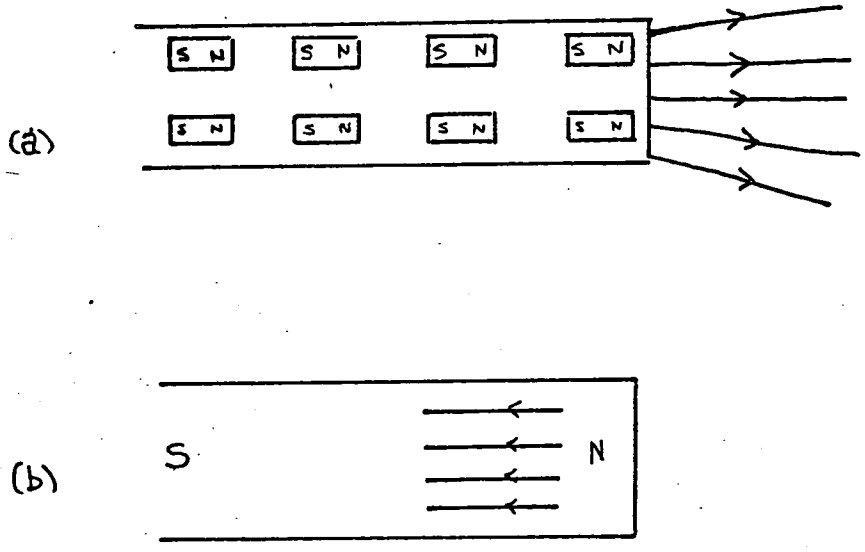

Fig. 4.5 Simple representation of atomic dipoles showing alignment to form permanent magnet.

(a) shows external field due to dipole alignment.

(b) shows internal field which is in opposite direction to the external field and hence tending to reduce the magnetization.

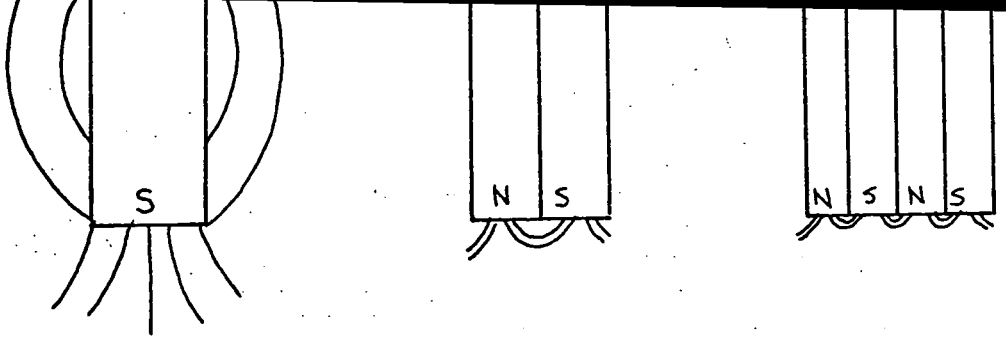

Fig. 4.6 (i) Reduction of demagnetizing field by subdivision into domains.

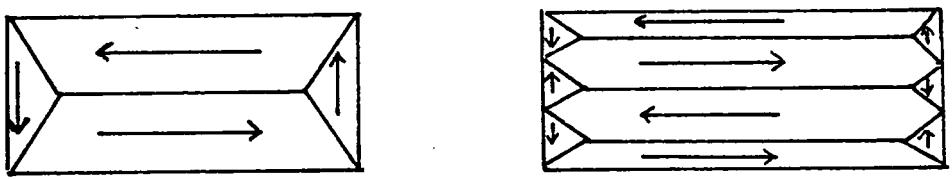

(ii) Possible domain configurations showing closure domains The closure domains resemble magnetic keepers and the demagnetizing field is further reduced.

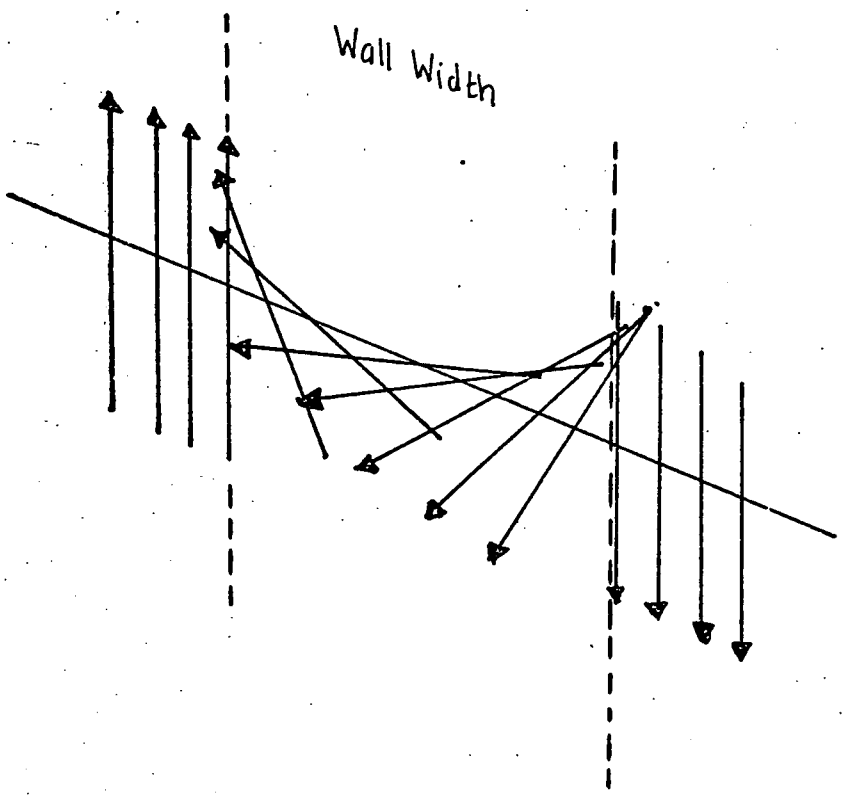

Fig. 4.7 Variation of spin orientation in a domain (Bloch) wall.

4.1.2 Hysteresis and the Magnetization Process

Studies on paramagnets show that the application of weak fields have a very small effect on the magnetization of a system which consists of free discrete elementary magnetic moments. When ferromagnetics below their Curie temperature are subjected to small magnetizing fields, very large changes in the overall magnetization of the specimen occur. This would suggest that the application of the field was not resulting in the induction of magnetism at the atomic level, but was in fact aligning spin vectors either by rotating these vectors or by changing the shape of the domains.

Figure 4.3(i) shows a plot of magnetization I versus applied field H for a ferromagnetic material.

If a field H is applied which is gradually increased from zero, the specimen will eventually be magnetized to saturation. Experiment shows that the process of magnetization of a ferromagnetic material below its Curie temperature involves the growth of those domains with spin vectors in the field direction at the expense of those with spin orientations opposed to the field direction. Also the magnetization within each domain may be rotated so as to align with the field, with the result that the domain walls disappear. Domain wall motion requires the least energy and at small values of the applied field the domain walls move small distances and are able to return to their original position once the field is removed. This motion corresponds to the section AB of the magnetization curve of Figure 4.3 (i). In 1947 Williams and Shockley showed that not only are domain walls mobile but their movement accounts for a large part of the change in magnetization.

Once the specimen is magnetized to saturation it is, effectively, a single domain. On being magnetized to saturation the material goes through the region BC on the curve. In this section of the curve irreversible domain changes take place. If, once saturation has been reached, the applied field H is now reduced slowly to zero, it is found that the specimen retains a certain amount of its magnetization. This residual or remanent magnetization, IR, is known as the remanence. If the magnetizing field is now increased slowly in the other direction then a certain value of field, Hc, will be required to reduce the residual magnetization to zero. This value of the field Hc is known as the coercive field or coercivity. If the field is, again, slowly increased, the specimen saturates once more and a reduction of the field leads to a remanence in the opposite direction to the first when the field becomes zero. Increasing the field in the original direction now leads to the completion of the loop shown in Figure 4.3 (ii). The loop shown in Figure 4.3 (ii) is known as a hysteresis loop (because I lags H). The coercive force is a measure of how difficult it is to move domain walls. The shape of the hysteresis loop depends upon the material. For example if the material is magnetically soft, such as soft iron, then the loop will tend to be narrow with a large remanence and low coercivity. Figure 4.8 shows hysteresis loops for soft iron and steel. The loop for soft iron shows that it is easy to magnetize, i.e. it saturates at low values of H. The coercivity is small indicating that it is relatively easy to move the domains. The loop for steel, however, shows that it saturates at high values of H and that, though the remanence is smaller than that of soft iron, it is more difficult to remove and therefore the coercivity is large, indicating that it is difficult to move the domains. In fact it is the impurities in the steel which help to pin the domain walls.

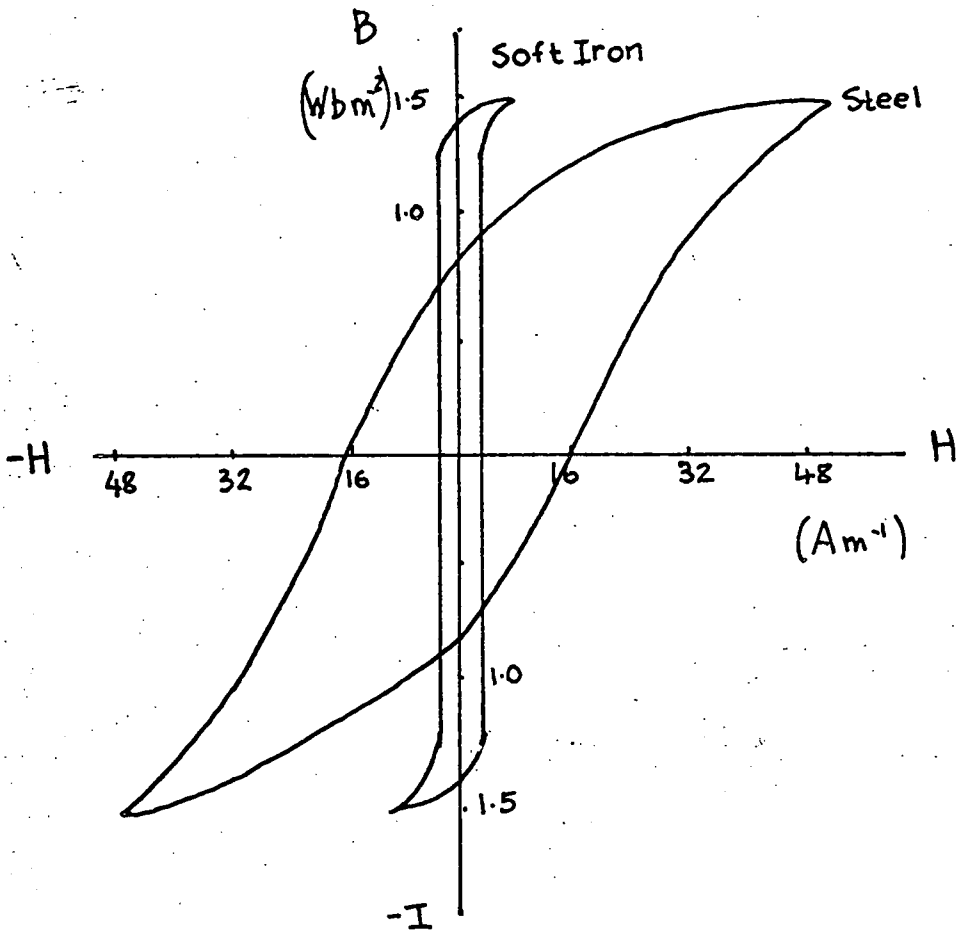

Fig. 4.8 Hysteresis curves for iron and steel.

The area under the loop is given by

$$W = \oint HdI \qquad (4.1)$$

and is the work done per unit volume in taking the specimen around the loop i.e. in moving the domains to alignment in one direction and then in the other.

It is with hysteresis that domain structure is associated and, because of the reversibility of the magnetization, it is evident that domain wall movement is indeed the source of hysteresis.

The ease with which the domains move depends, as previously mentioned, on the direction of the applied field with respect to the crystal orientation. The curves of Figure 4.4 show that whichever direction is chosen, saturation is reached if the applied field is big enough. If the field were applied along the [110] direction then the domains would align along easy axes mutually at right angles. Only when the field value was raised high enough to overcome the anisotropy energy would the magnetization align along the direction of the applied field. The magnetization would be

$$I = Is \cos 45 \qquad (4.2)$$

Likewise, if the applied field were in the [111] direction then the domains would initially align along three easy axes and since, in iron, the [111] axis makes an angle of 54^{o} with a cube edge

$$I = Is \cos 54 \qquad (4.3)$$

Hence if the field is applied in a non easy direction, alignment takes place in these directions first. Only when the field is high enough is the magnetization pulled out of the easy directions to align with the applied field.

Another phenomenon associated with magnetic materials is magnetostriction. When a ferromagnetic material is subjected to a magnetic field it becomes magnetized and its length changes slightly. This change, due to magnetostriction, can be either positive or negative depending on the material. From this it should follow, therefore, that physically stressing a ferromagnetic material should affect the magnetization. This does indeed happen. Dislocations in the crystal lattice tend to stress the material. Also, because of the difference in the size of impurity atoms with respect to the lattice atoms impurities also stress the material. This stress could, for example, affect the 'easiness' of an easy direction. Should this stress increase the 'easiness' of an easy direction then domains lying in this direction will be reluctant to move from it. Hence, in the absence of an applied field, the domains will take up directions which depend upon both anisotropy and internal stresses.

This elastic behaviour associated with domain wall movement is the result of large forces which tend to restrict domain wall movement. Low initial susceptibilities result and if the initial susceptibility is to be higher the local anisotropy effects due to stress must be removed. Impurities also have the effect of pinning the domain walls. When the domains are pinned by non magnetic inclusions or dislocations or impurities a suitably large applied field will have the effect of overcoming the 'elastic' forces and will free the domain wall. The wall will then move until it is pinned again.

Consider Figure 4.9 which shows the variation of wall energy W_γ with position x for a 180° Blochwall. Domain walls are defined in terms of the difference in orientation of the vector it separates, i.e. a 180° wall separates domains where spin orientations are antiparallel like those in Figure 4.6 (i) The left hand diagram 4.6 (ii) contains 1 x 180° wall and 4 x 90° walls. The application of a magnetizing field represents the application of a force which is opposed by those pinning the domain walls. Hence the application of a field H_A will result in the domain wall moving to a position corresponding to position A on the W_γ / x curve. When the wall stops moving the force exerted by the applied field ($2 H_A I_s$) equals the slope of the curve at this point.

$$2 H_A I_s = \left(\frac{dW_\gamma}{dx}\right)_A \qquad (4.4)$$

At point C the wall energy reaches a maximum and the applied force is now able to cause the wall to 'slide' over the barrier to position D. However, if the field is still applied the wall is able to move to a position E on the curve where $\frac{dW_\gamma}{dx}$ is equal to that at a point just before C. Hence there is a large increase in magnetization for no increase in applied field. This is a Barkhausen discontinuity. Again the domain wall experiences strong forces which, if the field is removed, will return the domains to point D on the curve. However, if the domains are to return to point A a force is required (coercive force) to again surmount the barrier pinning them. Hence there is a remanence. The effect is therefore a hysteresis effect. Hence any explanation of hysteresis must include an account of those processes which give rise to a variation of domain wall energy with position.

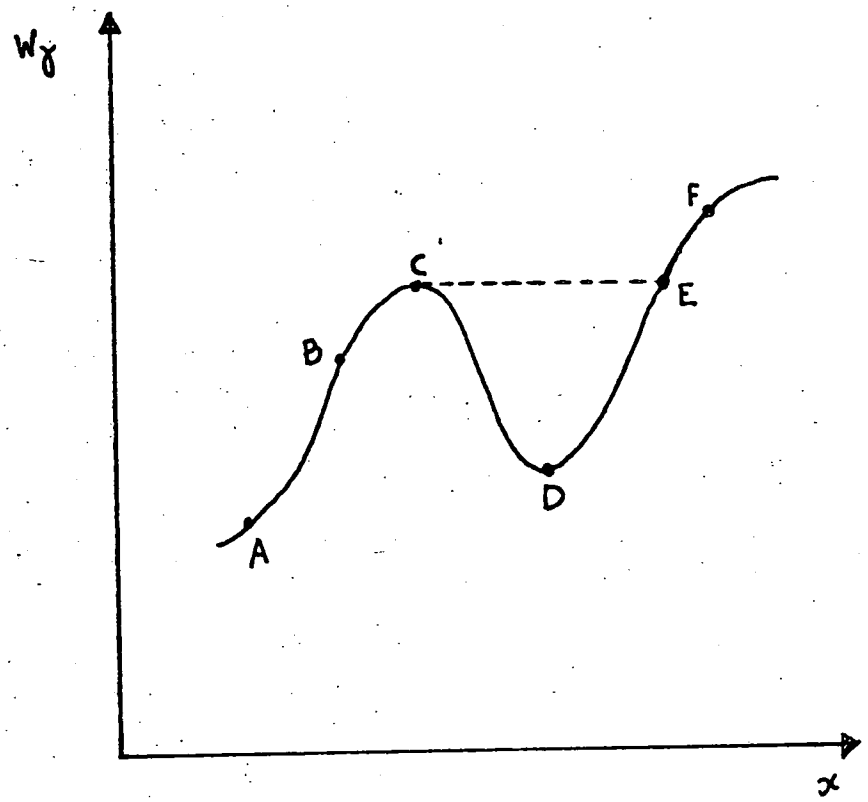

Fig. 4.9 Variation of wall energy W_γ with position for a 180^0 Bloch wall.

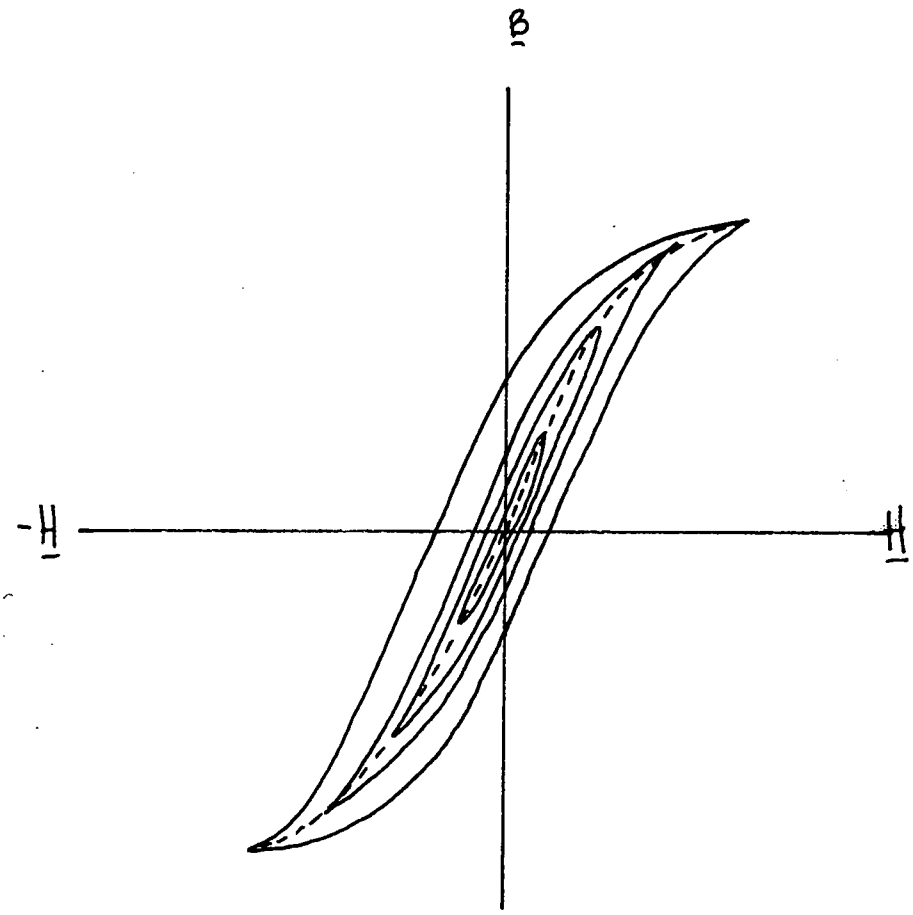

Fig 4.10
Subsidiary hysteresis loops

4.2 DOMAIN WALLS

The structure of domain walls was first investigated by Bloch (1932). As previously mentioned the domain wall has a finite width, the magnitude of which is decided by the conflicting constraints imposed by anisotropy and exchange forces. The wall will not be of an abrupt nature (i.e. one atom thick) as this would involve exchange forces of extremely high values.

Domain formation, while lowering the internal demagnetizing energy and magnetostriction energy, results in an increase in energy due to the fact that energy is stored in the wall. The wall energy is obtained by multiplying the wall energy per unit area γ_W by the wall area.

The total wall energy = exchange energy + anisotropy energy.

Exchange energy is discussed in CHAPTER TWO.

The exchange energy between two neighbouring spins is given by

$$W_{ex} = -2Js^2 \cos\theta$$

θ = angle enclosed by the spins.

Now in a Bloch wall the spin varies only slightly in orientation with distance across the wall and the rotation is in the wall plane. Hence the angle θ enclosed by neighbouring spins can be approximated to give

$$W_{ex} = Js^2\theta^2$$

Now a rough estimation of this energy can be made if an assumption to the effect that the rate of change of θ with distance across the wall is constant. In fact the spatial derivative $\frac{d\theta}{dx}$ of the angle of turn

is not necessarily constant. However, assuming that it is constant

$$\frac{\theta}{N} = \pi$$

$$Wex = \frac{JS^2\pi^2}{N^2}$$

Where N = the number of layers in the wall.

If a = the lattice constant for a simple cubic lattice, then there are, for a(001) surface, $\frac{1}{a^2}$ atoms per unit area.

Hence the exchange energy per unit area is given by

$$\gamma_{ex} = \frac{N}{a^2} W_{ex} = \frac{JS^2\pi^2}{a^2 N} \qquad (4.5)$$

Equation 4.5 shows that γ_{ex} decreases with an increasing number of layers in the wall. Energy minimization therefore favours an increase in domain wall thickness for this component of the wall energy.

Now, any increase in the width of the domain wall must increase the magnetocrystalline anisotropy energy as this process entails moving spins away from an easy direction. The anisotropy energy per unit volume is given approximately by

$$\gamma_a = K_1 N_a \text{ per unit area} \qquad (4.6)$$

Hence anisotropy energy increases with N.

The total wall energy is obtained by combining equations 4.5 and 4.6

$$\gamma = \frac{JS^2\pi^2}{a^2 N} + K_1 N a \qquad (4.7$$

The total energy is a minimum when the first derivative of expression 4.7 is set to zero.

$$\frac{d\chi}{dN} = \frac{-Js^2\pi^2}{aN} + Ka = 0$$

giving

$$N = \left(\frac{Js^2\pi^2}{Ka^3}\right)^{1/2} \qquad (4.8)$$

Now the thickness = Na $\therefore$ from 4.8

$$N_a = \left(\frac{Js^2\pi^2}{Ka}\right)^{1/2} \qquad (4.9)$$

The treatment above is approximate in that it assumes that the turn angle ($\frac{\delta\theta}{\delta x}$) a is invariant across the domain wall. In general this is not the case because the way in which the spins rotate depends upon the equilibrium condition.

A treatment due to Lilley (1950) takes the invariance of the turn angle into consideration.

Consider an unstrained ferromagnetic material with no external applied field. The total exchange energy due to the misalignment of the spins is given by

$$\gamma_E = A \int_{-\infty}^{\infty} \left(\frac{\delta\theta}{\delta x}\right)^2 \sin^2\phi \, dx \qquad (4.10)$$

where A = the exchange constant JS^2/a.

θ = the angle between the moment and the normal to the wall.

ϕ = the angle between the projection of the moment on the wall and some fixed axis.

Figure 4.11 shows θ and ϕ. The fixed axis for ϕ in the diagram is the y axis.

Figure 4.12 illustrates the transition of the spin vector in a 180^{o} wall.

Now there is also a contribution to the wall energy made by the anisotropy energy γ_A

$$\gamma_W = \gamma_A + \gamma_E \tag{4.11}$$

Now θ is constant and the magnetocrystalline anisotropy is a function of ϕ and γ_A is given by

$$\gamma_A = \int_{-\infty}^{\infty} \beta_f \, dx \tag{4.12}$$

for the boundary region

where β_f $(\theta\ \phi)$ is the reduced anisotropy energy (i.e. it's value is zero when the magnetization lies along an easy direction.)

The total increase of energy per unit area of the wall is then given by

$$\gamma_W = \int_{-\infty}^{\infty} \left[J s^2 \sin^2\phi \left(\frac{\delta\theta}{\delta x}\right)^2 + \beta_f \right] dx \tag{4.13}$$

$$\text{or } \gamma_W = \int_{-\infty}^{\infty} \left[A \sin^2\phi \left(\frac{\delta\theta}{\delta x}\right)^2 + \beta_f \right] dx \tag{4.14}$$

(where the values of A depend upon the type of lattice).

Now for a stable spin configuration this integral should be a minimum.

Let the angle θ at $x = x_c$ be changed by $\delta\theta$. The total wall energy will be changed by an amount $\delta\gamma$ given by

$$\delta\gamma = \int_{-\infty}^{\infty} \left(2A \sin^2\phi \left(\frac{\delta\theta}{\delta x}\right) \delta\left(\frac{\delta\theta}{\delta x}\right) + \left(\beta \frac{\delta f}{\delta\theta}(\psi,\theta)\, \delta\theta\right) dx$$

Now such an integral $\int g\,dx$ will be a minimum if the integrand provides a solution to a differential equation of the form

$$\frac{dg}{dy} - \frac{d}{dx}\left(\frac{dg}{dy}.dx\right) = 0$$

Such an equation is a Euler equation and when this condition is applied to 4.14 we obtain

$$\beta f(\phi,\theta) = A\sin^2\phi \left(\frac{\delta\theta}{\delta x}\right)^2 \qquad (4.15)$$

which shows that the exchange and anisotropy energies are equal throughout the wall.

Using this and the fact that the maximum rate of change of angle occurs at x = 0 allows the wall thickness to be expressed as

$$\delta = \pi \left(\frac{A}{K_1}\right)^{1/2} \qquad (4.16)$$

If there is appreciable magnetostriction, as in the heavy rare earths, then βf must be taken as a combination of contributions due to magneto-crystalline anisotropy and magnetoelastic energy.

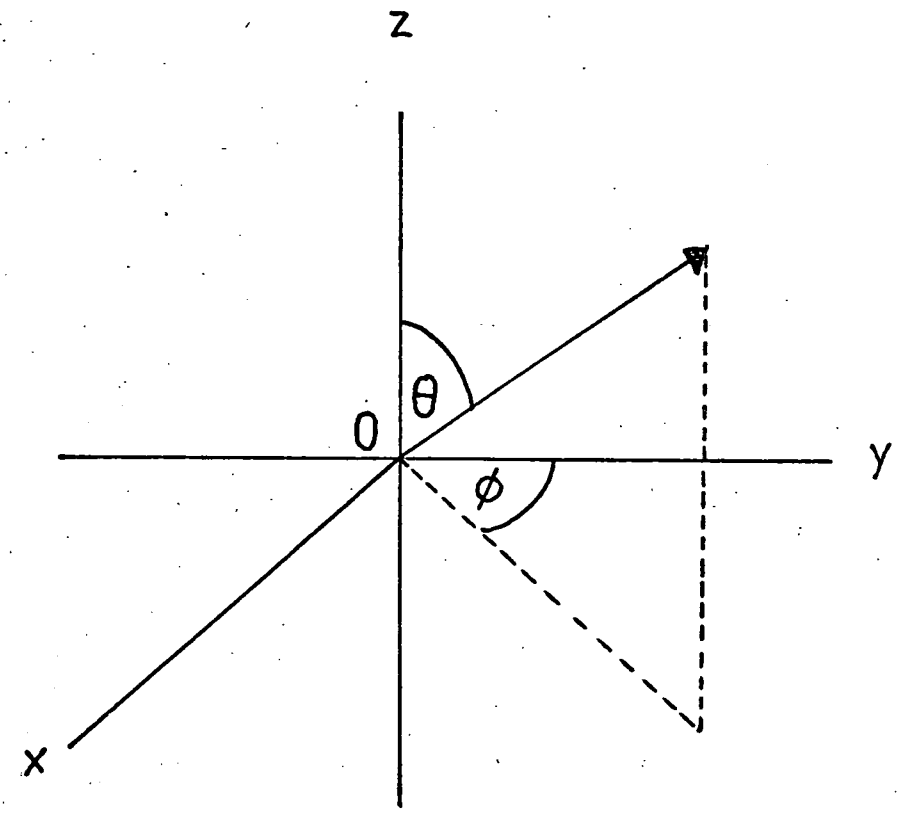

Fig. 4.11 Direction of atomic moment in terms of angular coordinat (θ Ø) The z axis (OZ) lies normal to the plane of the domain wall (OXY plane).

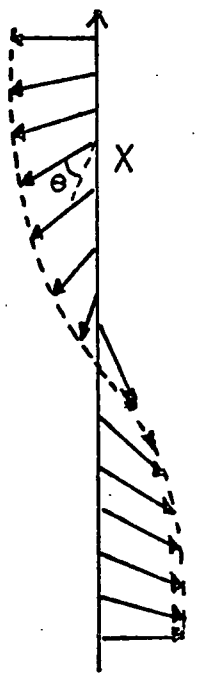

Fig. 4.12 Angle of spin rotation.

4.3 DOMAIN STRUCTURES

In any specimen the shape, size and arrangment of the domains present under conditions of equilibrium depend upon the geometry of the material. The domain configuration also depends upon anisotropy, exchange and the saturation magnetization. The domain arrangement will represent a minimum in terms of the magnetostatic energy. (Landau and Lifshitz (1935)).

4.3.1 Types of domain wall

Several types of domain walls exist. In the bulk material Bloch walls prevail and no consideration is given to the magnetostatic energy associated with the free poles which exist when the walls intersect the surface. When the specimen is thin, however, these effects become important especially in samples where the anisotropy is low and the energy term due to the intersection may dominate. Néel (1935) suggested a spin transition which differed from that of Bloch. Figure 4.13 illustrates the difference between a Bloch wall and a Néel wall. In the Bloch wall the magnetization makes the transition between neighbouring domains while rotating in the plane of the domain wall. In the Néel wall, however, the vector rotates in the plane of the sample. Figure 4.13 shows Bloch and Neel walls (for the simple 180^{o} case).

In 1958 Huber, Smith and Goodenough reported the discovery of a new type of wall. This wall consisted of a main wall cut at right angles at regular intervals by cross-ties. Figure 4.14 shows a diagramatic representation of the cross-tie wall in which the alternating polarity of the wall at the film surface and at the wall surface serves, via short flux closure paths, to reduce the magnetostatic energy. Early attempts

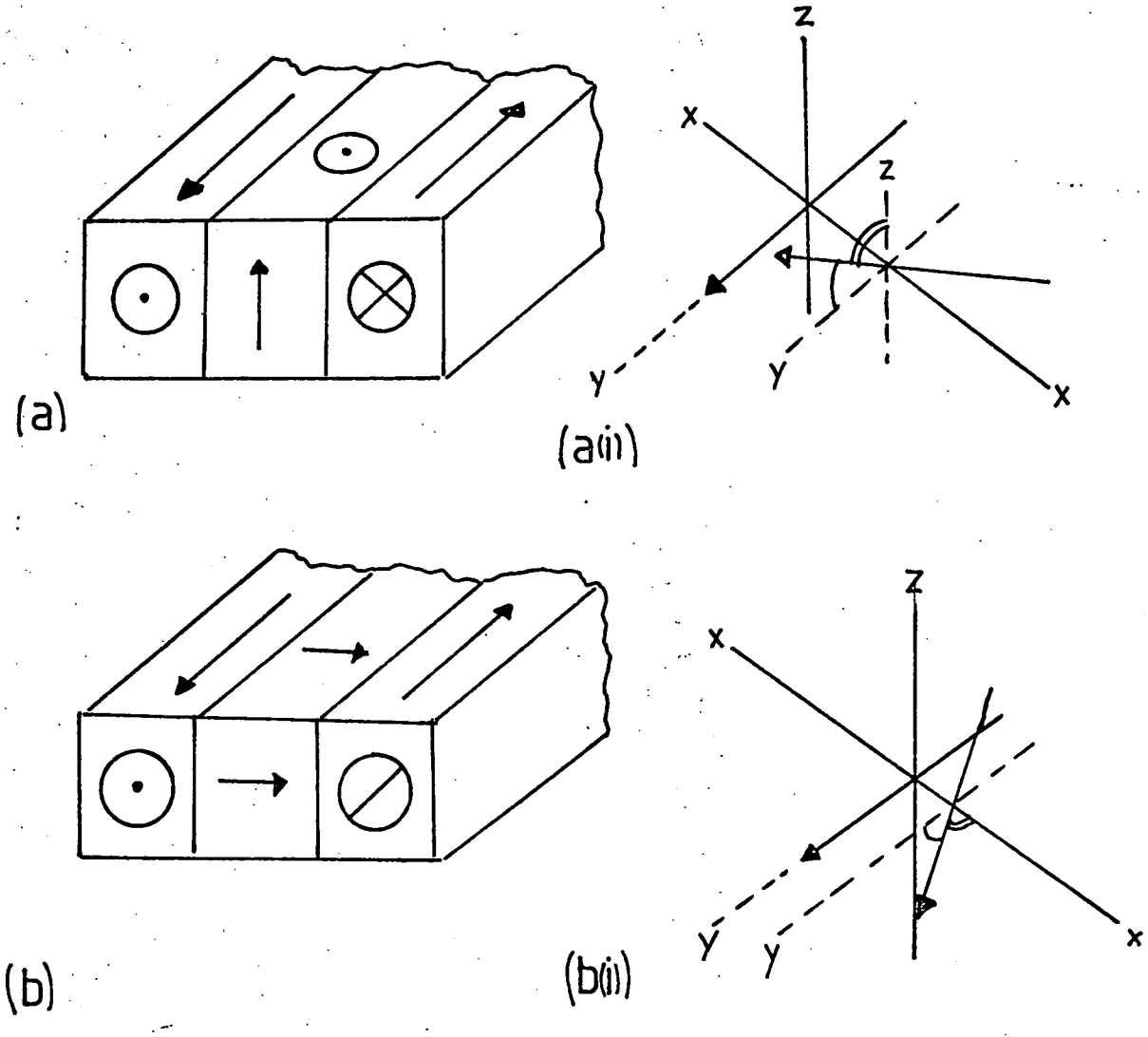

Fig. 4.13 (a) Bloch wall

(a)(i)shows the rotation of the vector is in the ZY plane.

(b) Neel wall

(b)(i)shows the rotation of the vector is in the XY plane.

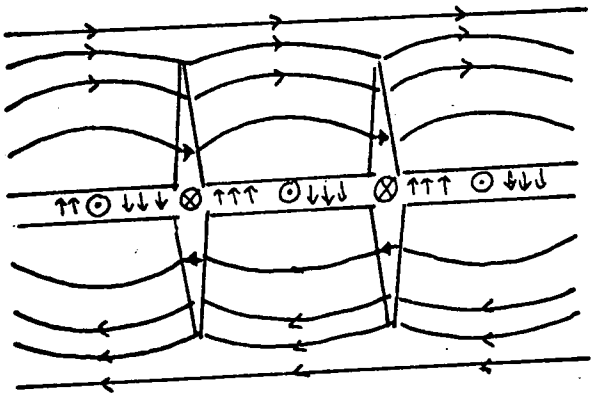

Fig. 4.14 Cross-tie walls in a low anisotropy thin film.

(After Huber, Smith and Goodenough (1958)).

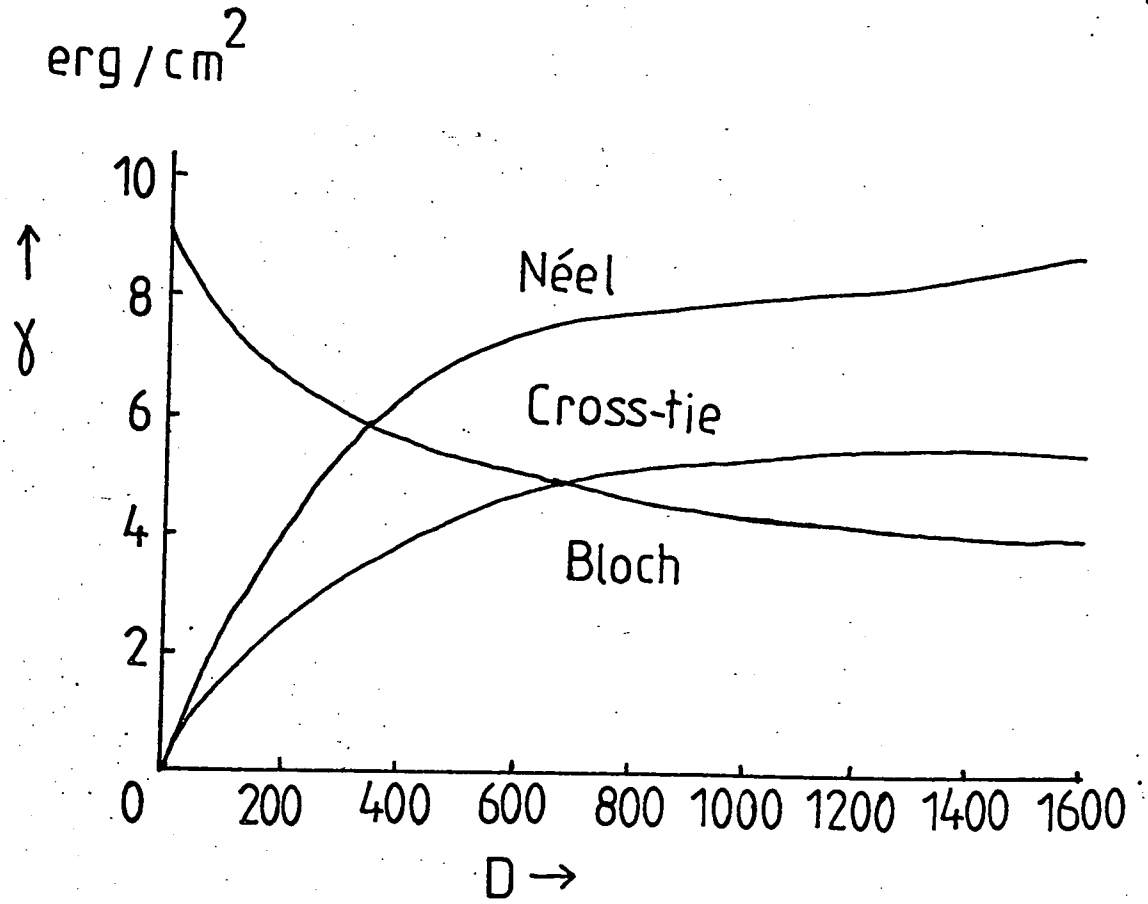

Fig. 4.15 Energy per unit area of a Bloch wall, a Neel wall and a cross-tie wall versus sample thickness D.

(After Middlehoek (1963))

by Middlehoek to calculate the energies of these walls gave values which differed from those obtained experimentally (probably due to the drastic approximations made).

Complex walls have been observed in bulk materials and Williams and Goertz (1952) showed a changing polarity along a wall/surface intersection. This type of wall can be described as a Bloch type transition which alternates with sections where the transition is the Néel type. For a discussion on this type of wall see CAREY and ISAAC (1966).

4.3.2 Uniaxial domain structures

Uniaxial crystals show high anisotropy with respect to the easy direction. As such the magnetization is confined to the easy direction and as a result 180° walls are those expected. Figure 4.16 shows a variety of domain structures proposed for uniaxial materials the simplest of which is 4.16 (a). This simple slab configuration has been shown to exist for thin specimens, the magnetostatic energy of which is given by

$$W_m = 0.8525\, M_s^2 d \quad \text{per unit area} \qquad (4.17)$$

where d = domain spacing

(Kittel 1949)

Now if L = crystal thickness and γ is the wall energy per unit area, total wall energy = $\gamma L/d$

Hence the total wall energy is given by

$$E_T = 2W_m + W_\gamma = 1.705\, M_s^2 + \gamma L/d \qquad (4.18)$$

This is a minimum when

$$d = \left(\frac{\gamma L}{1.705\, M_s^2} \right)^{1/2} \qquad (4.19)$$

Similar expressions are obtainable for the configurations shown in figures 4.16(b) and (d) and the general expression for minimization of the surface energy for these simple domain patterns is

$$d = \left(\frac{\gamma L}{C M_s^2} \right)^{1/2}$$

where C depends upon the geometry of the crystal domains.

When the sample thickness takes larger values ($\sim 10 \mu m$) the domain walls undulate (Figure 4.17). Such patterns were reported by Roberts and Bean (1954). The domain structures shown in Figures 4.16 (a), (b), (d) and (e) do not involve closure domains. These types of domain structure are expected in materials of high anisotropy as closure domains in these materials are energetically unfavourable. The structure shown in Figure 4.16 (e) represents spike domains as proposed by Goodenough (1956). These domains represent a compromise energetically as the magnetostatic energy at the surface is reduced with a minimum increase in the wall energy. Observations of this type of pattern on manganese bismuth alloys and cobalt by various workers (notably Goodenough (1956) and Kozlowski and Zietek (1966) have shown that the patterns can become exceedingly complex. The resulting patterns depend upon the specimen thickness. Goodenough suggested that the Kittel slab domain configuration was more energetically favourable for thick specimens than was an undulatory wall configuration throughout the sample. The amplitude of the undulations therefore decrease with crystal depth. Figure 4.18.

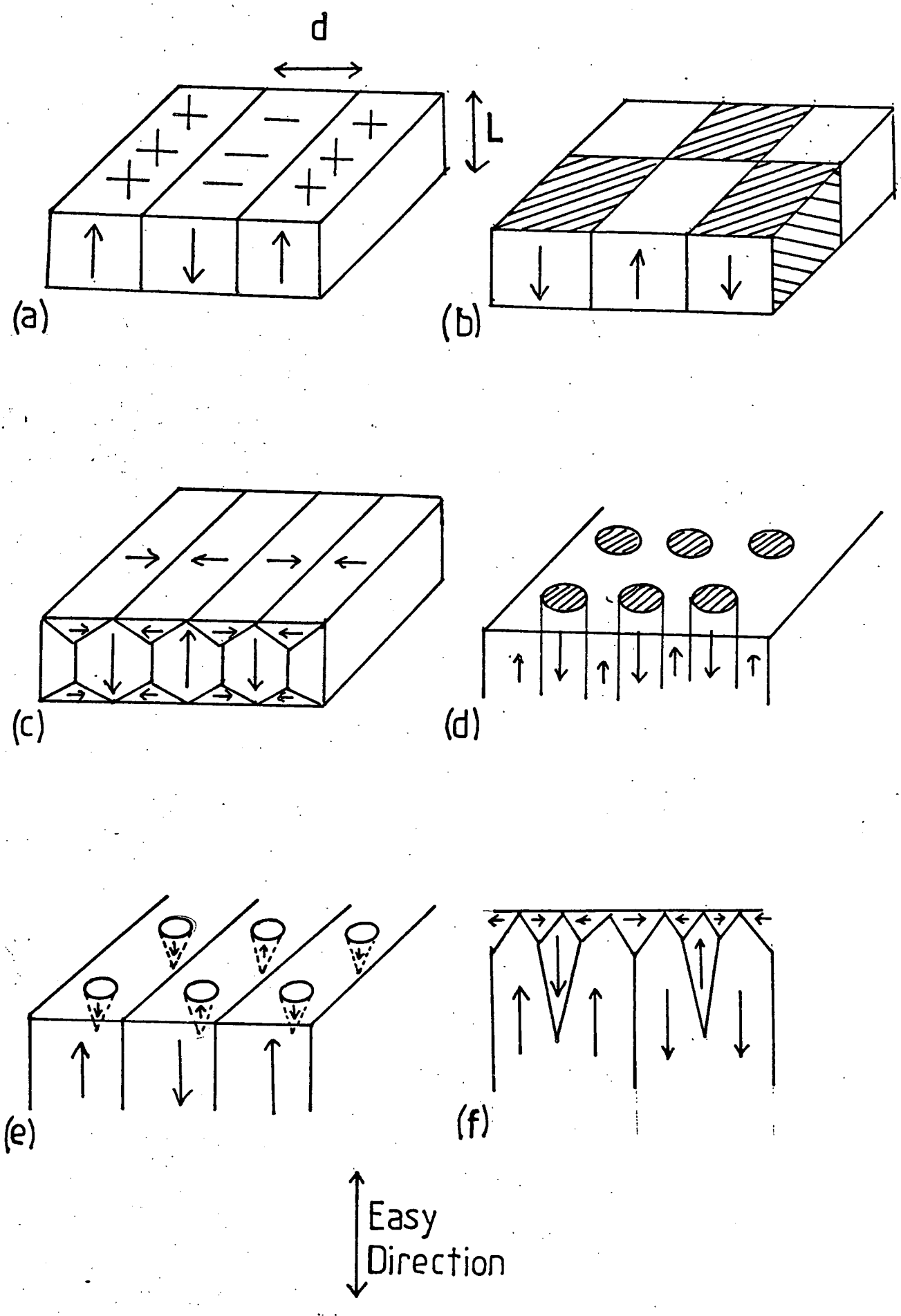

Figure 4.16 Domain structure models for uniaxial crystals.

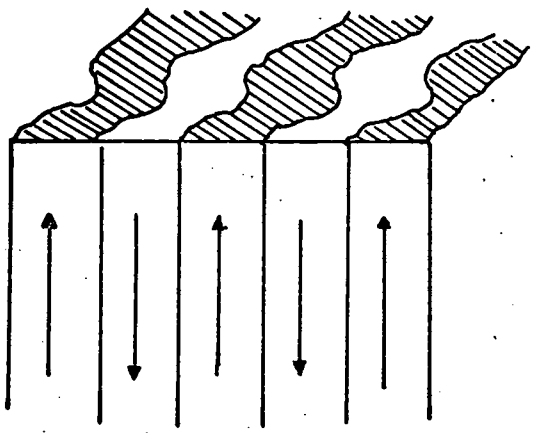

Fig. 4.17 Undulating domain walls

(Roberts and Bean (1954))

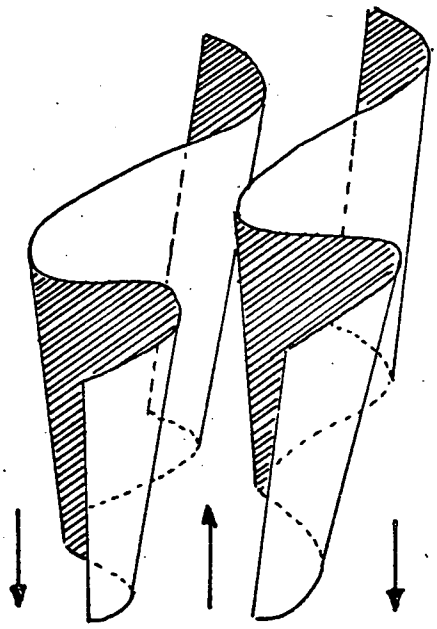

Figure 4.18 Undulatory domain walls with amplitude decreasing with depth. (Goodenough (1956)).

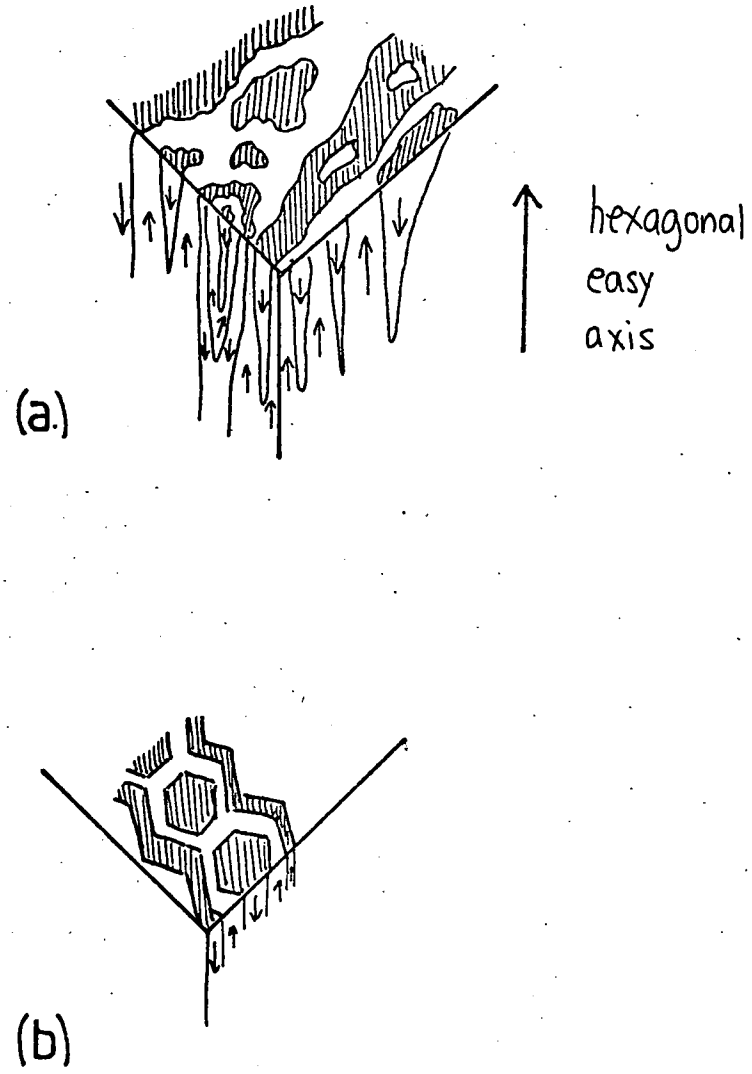

Fig. 4.19 (a) Uniaxial domain structure.
(b) Simple interpretation (after Kozlowski and Zietek (1965)).

Any wall undulations necessarily increase wall area and, therefore, this type of structure is confined to crystals which are not too thick (10 - 100 μm). As the thickness increases spike domains are favoured and these patterns become very complex. Figure 4.19 (a) shows a complex pattern showing undulatory domain walls. The large number of opposing magnetization orientations at the surface greatly reduces the magnetostatic energy while the 'spike' type domains minimize the increase in wall energy due to domain formation. By considering the various geometric factors of their simplified model of the patterns of the type shown in Figure 4.19 Kozlowski and Zietek minimized the surface magnetostatic energy and obtained much simplified symmetric domain configurations to represent those of 4.19 (a) (See 4.19(b)). The domain configuration shown in 4.16(f) is that proposed by Lifshitz (1944) as an improvement on those proposed by Lifshitz and Landau (1935).

For thin samples cylindrical domain structures, as shown in 4.16 (d), c nform. This type of domain structure can represent binary digits in terms of the direction of magnetization. As such they have been used increasingly in memory devices in digital computers. Such memories are known as bubble memories and extensive work has been done on developing various configurations of domains. (See Jones (1976)).

4.3.3 Domain structures in cubic iron-like crystals.

In cubic crystals such as iron, there are six easy directions of magnetization. Hence, for a specimen magnetized with the magnetization along easy directions, both 180° and 90° walls are to be expected. Figure 4.20 shows simple domain structures for a cubic (iron-like) crystal with the x and z axes easy. The domain structures shown in Figure 4.20

are very simple structures and represent those obtained when the crystal is a single crystal whose surface is in the plane of one of the crystallographic planes. Williams, Bozorth and Shockley (1949) showed that the surface domain configuration depends upon the crystal orientation at the surface. When the surface of their samples (silicon-iron) were slightly misorientated with respect to the (100) plane, they obtained domain patterns known as fir tree patterns (Figure 4.21). The internal structure of the crystal is still that of 180^0 domains, The magnetization of the main domains is along the (100) direction hence the surface pole density is M sin θ. The tree patterns are, therefore, partial closure domains minimizing the surface magnetostatic energy. Figure 4.22 (a) shows the formation of fir tree domains (and Figure 4.23). Figure 4.22(b) shows the effect of increasing the angle of orientation (θ) of the crystal surface with respect to the (100) plane. The tree branches increase in size with θ. Figure 4.22 (b) shows the increase in the fir tree branches with θ.

Figure 4.24 shows magnetic domains in a picture frame sample (hollow rectangle). Such samples were studied by Williams and Shockley (1949) using silicon-iron. The edges of the samples were parallel to (100) planes which resulted in the formation of four domains as shown in 4.24 (a). The demagnetizing field of such a specimen is very low and this type of specimen provides a very simple means of making quantitative studies on magnetic domains. Williams and Shockley applied a magnetic field and studied the impedance of domain wall movement by local inhomogeneities and inclusions. Figure 4.24 (a) represents perfect flux closure. When a field is applied patterns like that shown in 4.24 (b) result.

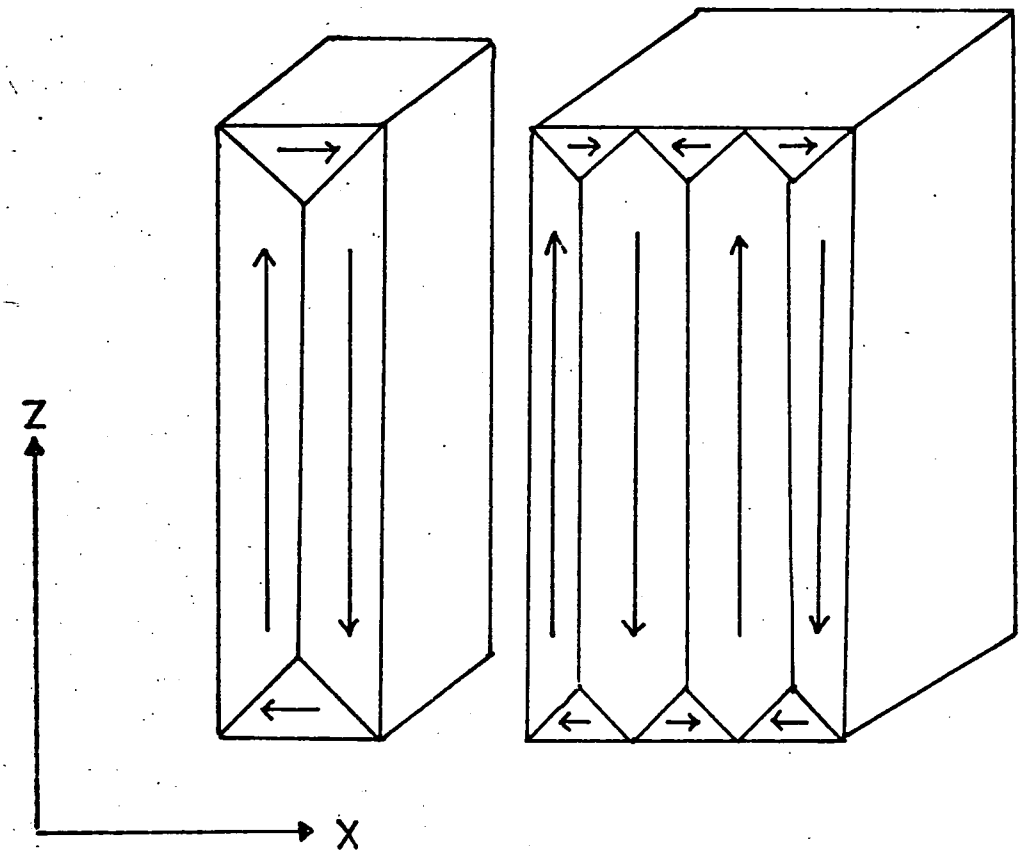

Fig.4.20 Simple domain structures for a cubic material with x and y axes easy.

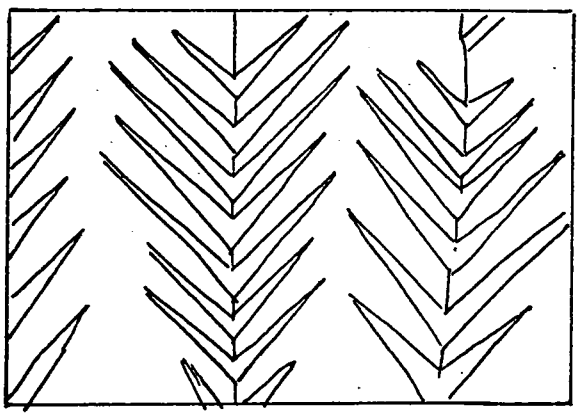

Fig. 4.21 Fir tree domains

(After Williams, Bozorth and Shockley (1949)).

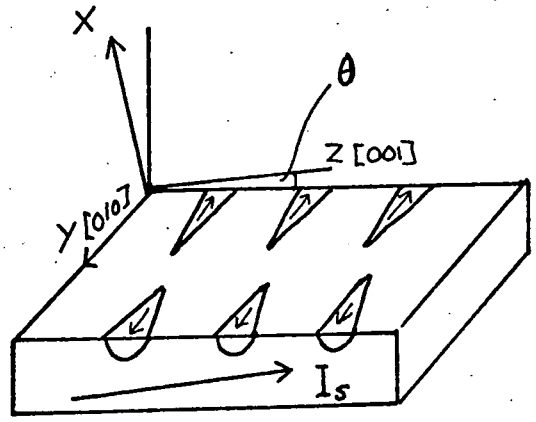

a

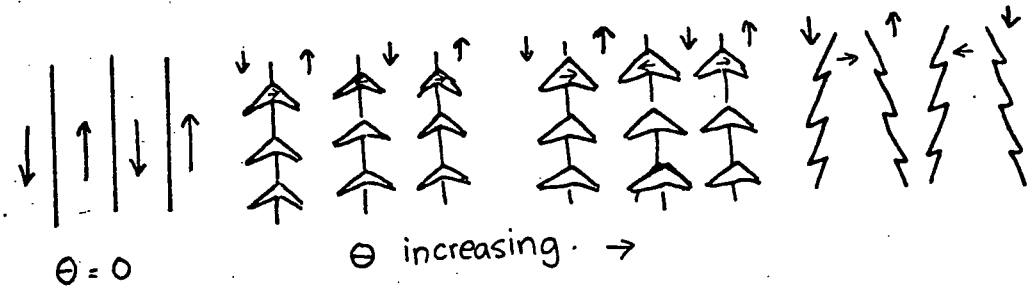

b

Fig. 4.22 Fir tree domains.
(b) Effect of increasing θ

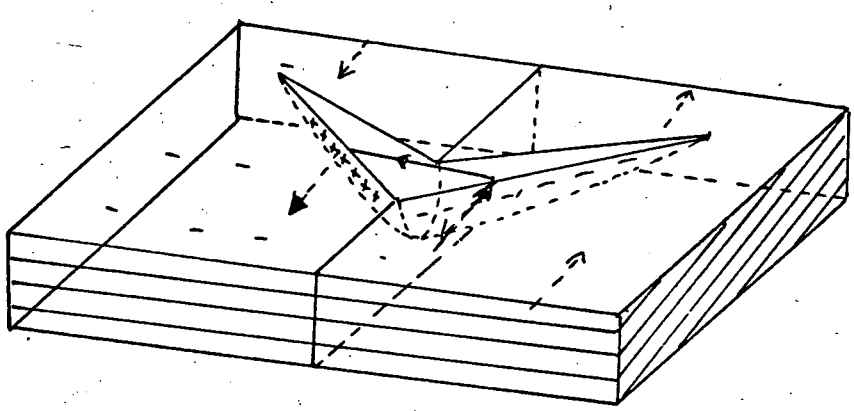

Fig. 4.23 Fir tree patterns

(After Stoner (1950)).

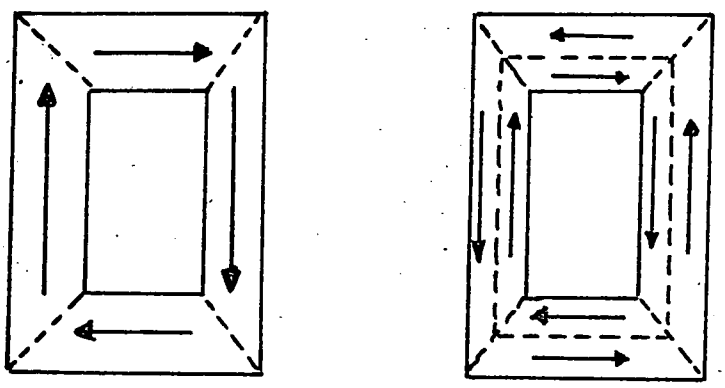

Fig. 424 Picture frame specimens showing domains
(Domain walls = - - - -)

(After Williams and Shockley (1949))

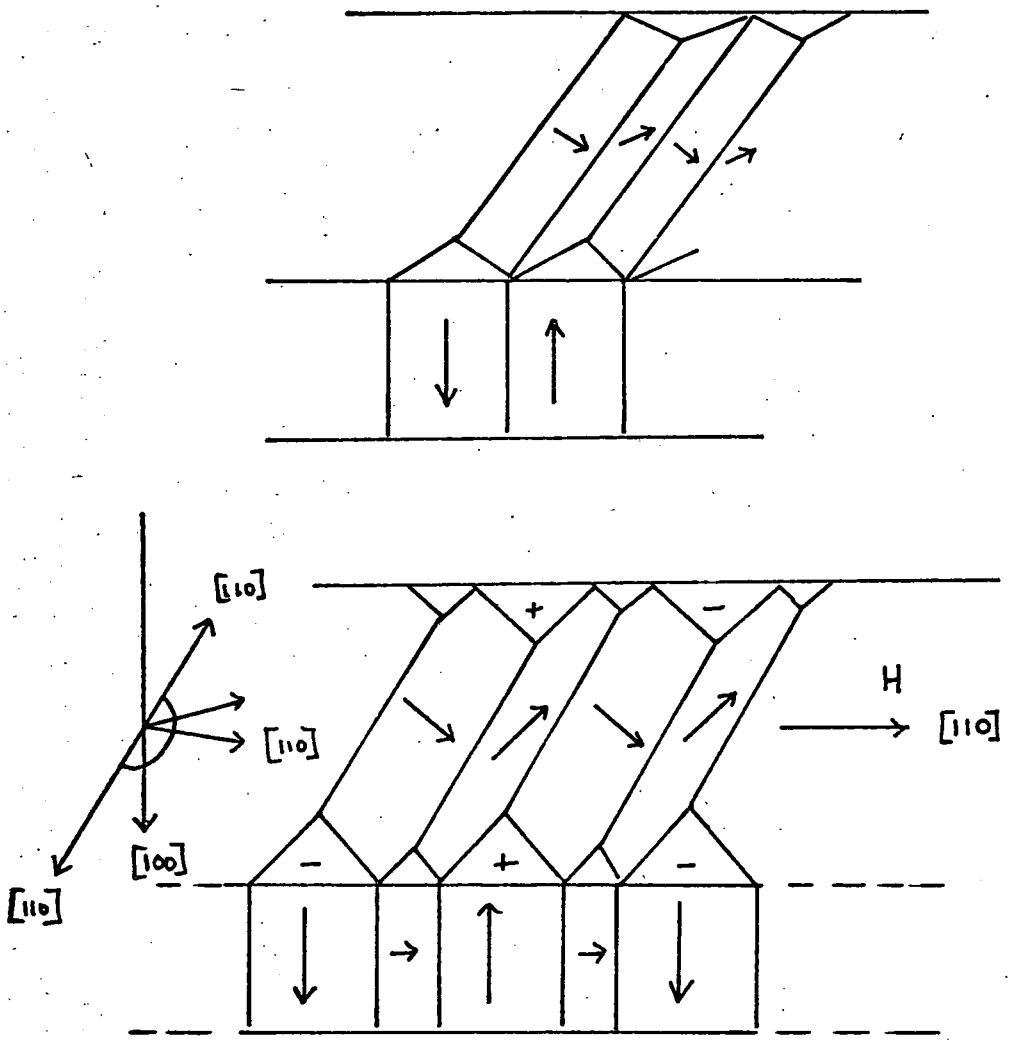

Fig. 4.25 Domain structure of a Néel block (Néel (1944))

(a) zero applied field

(b) applied field in [110] direction

By showing that the specimen magnetization varies linearly with domain wall position, Williams and Shockley demonstrated the correlation between bulk magnetization and the movement of domain walls.

Another type of closure domain structure is shown in Figure 4.25(a) Néel (1944) studied this type of structure theoretically. The crystal is a slab with surfaces parallel to the (100) and (110) planes, and the postulated domain structure is that of 90^{o} walls. Figure 4.25 (b) shows how the structure changes on the application of an applied field in the (110) direction. The structure was confirmed by Bates and Neale (1949).

Apart from the simple picture frame sample, domain structures in bulk samples prove difficult to analyse. Work on iron whiskers has proved to provide useful information by giving very simple domain patterns. For example, a whisker cut with its long axis along $\langle 100 \rangle$ shows two 180^{o} walls and simple closure domains at the ends. Figure 4.26 (a) and (b) show domain structures proposed by Scott and Coleman (1957). In (a) the applied field is zero. In (b) the field is applied perpendicular to the long axis of the crystal. Figures 4.26 (c) and (d) are after Fowler et al. When the specimen is subjected to an increasing field along the $\langle 100 \rangle$ direction it eventually saturates leaving small reverse domains at the extremeties.

4.3.4 Domain structures in nickel-like materials

Nickel has negative anisotropy and this type of crystal structure (face centred cubic) has eight [111] easy directions. Patterns produced on (110) surfaces favoured 71^{o}, 109^{o} and 180^{o} walls (corresponding to

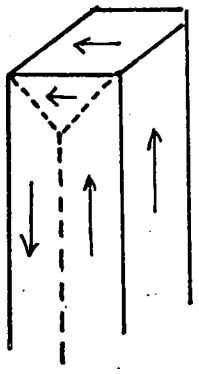

(a) Zero Applied field

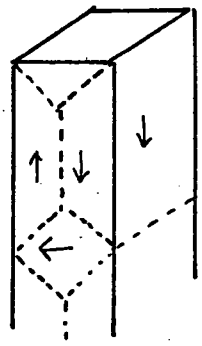

(b) Field applied perpendicular to crystal axis

(c)

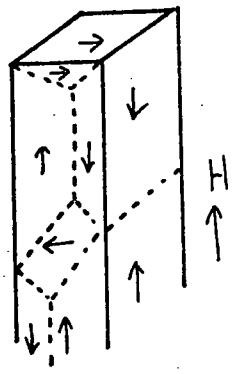

Applied field as shown

(d)

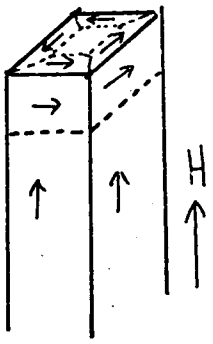

Applied field increased specimen is saturated but small reverse domains persist.

(After Fowler, Fryer and Treves) (1960)

Figure 4.26 Magnetic domains in <100> iron whiskers.

180^{o} and 90^{o} walls on (100) iron surfaces). Figure 4.27 shows a domain pattern on nickel with a (110) surface (Stephan (1955)). Because of the low anisotropy and quite high magnetostriction in nickel, it is extremely sensitive to strain. Mechanical polishing leaves a strained layer which must be removed before observing domain structures. Despite this, various workers, notably Stephan (1955), Bates and Wilson (1951) and Yamamoto and Iwata (1953) have observed domain structures by colloid methods.

As with iron, tree patterns form when the surface is at a slight angle to the (110) plane. While the tree branches in iron are at 45^{o} to the trunk, those in nickel-type structures are at 35^{o} and 55^{o} to the trunk. (180^{o} wall). Other tree patterns occur for "trunks" consisting of the 109^{o} and 71^{o} walls. Figure 4.28 shows a complex parallelogram net pattern on nickel (Yamamoto and Iwata (1953). In fact the sketch omits fir tree patterns which were present during the original experiment due to the curvature of the specimen surface. The parallelogram net is essentially due to magnetostrictive interference between four regions of 180^{o} slab domains. Many other complex patterns are obtainable. A(112) nickel surface gives 180^{o} slab domains with reverse spikes. This is reasonably predictable as there is only one easy axis present for this orientation. Also for those surfaces with no easy axis (i.e. parallel to (100) or (111) planes) then very complex patterns (corresponding to those on (111) iron planes) are found. For a comprehensive discussion of magnetic domain structures see for example, Carey and Isaac (1966) or Craik and Tebble (1965).

The study of domain structure is very complex as patterns can very easily be complicated due to such things as local inhomogeneities or

inclusions. Because domain formation is essentially an energy minimization exercise it is quite reasonable to postulate possible domain structures for crystals of specific geometry and then minimize the expression with respect to the relevant crystal parameters in order to obtain the conditions for domain formation. Of course, several possible domain structures may be postulated for a given specimen but it is reasonable to accept that domain configuration which yields the lowest value for the free energy.

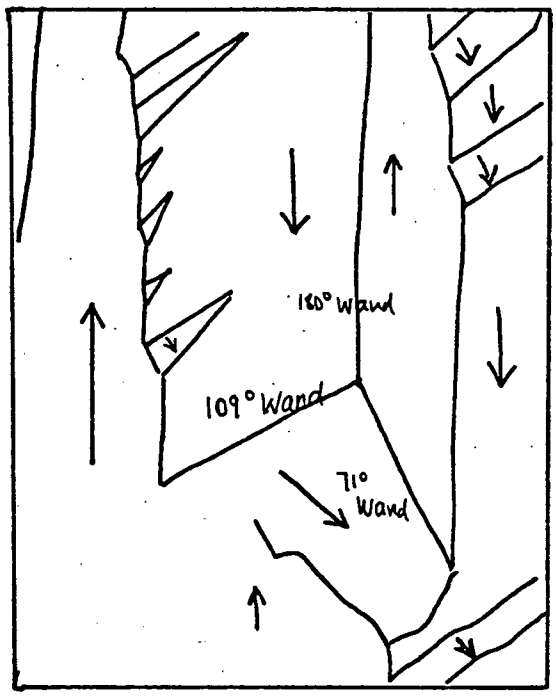

Fig. 4.27 Sketch of Bitter pattern obtained by Stephan (1955) on a (110) Nickel surface.

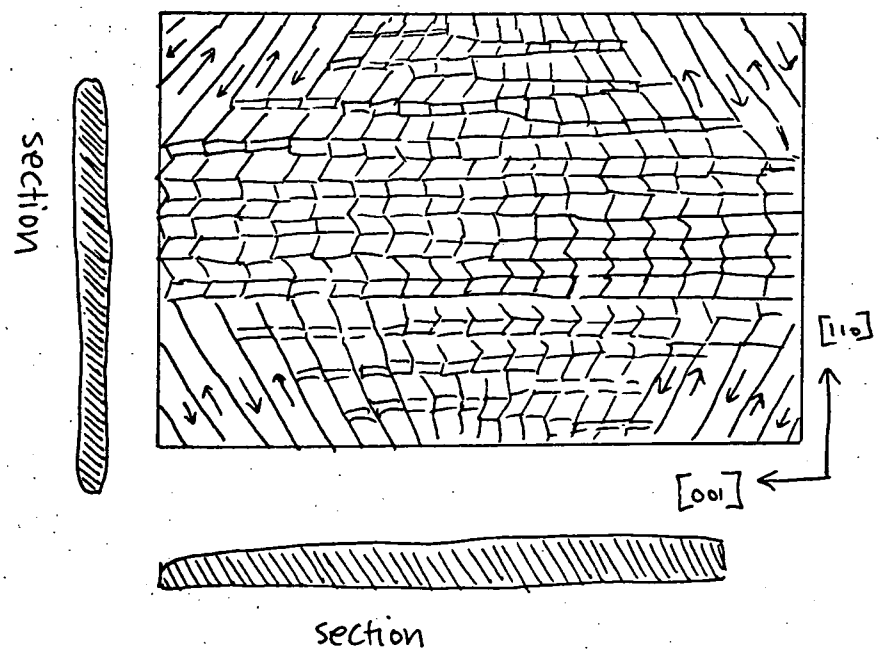

Fig. 4.28 180^{o} and 109^{o} walls in nickel forming a parallelogram net pattern.
The central position collides with a (110) plane.
(After Yamamoto and Iwata (1953)).

CHAPTER FIVE

METHODS OF DOMAIN OBSERVATION

CHAPTER 5

METHODS OF DOMAIN OBSERVATION

5.1 THE COLLOID TECHNIQUE

This technique for observing magnetic domains is discussed in more detail in Chapter Six.

The technique was the first direct method of observing magnetic domains used. Bitter (1931) devised the method which involves covering the surface of the specimen with magnetic particles (either suspended in some liquid such as alcohol (wet colloid) or else evaporated onto the surface by some method (dry colloid)). The magnetic particles, under the right conditions, are attracted to and stick to those regions on the surface where there are stray fields (e.g. due to scratches or intersection of domain walls at the surface). Both methods (wet and dry) have been popular and are still popular. It is for this reason that the technique has been modified and improved by many workers (crystal polishing techniques and modification of apparatus for specific application being just two areas of interest).

5.2 MAGNETOOPTIC TECHNIQUES

5.2.1 Introduction

Magnetooptical effects in a magnetic material can basically be described in terms of the anisotropy induced in the optical parameter by the magnetization. When a beam of radiation is incident on a specimen it is either reflected or transmitted (i.e. the majority of the radiation) Magnetooptical effects are, therefore, classified into two types.

(i) magnetooptical effects where the radiation is transmitted.

(ii) magnetooptical effects where the radiation is reflected.

(i) is termed the Faraday effect.

(ii) is termed the Kerr magnetooptical effect.

As well as this classification, the effect can also be classified in terms of the orientation of the magnetization in the specimen. Figure 5.1 shows the longitudinal, transverse and polar effects and the orientation of the magnetization with respect to the incident (and reflected or transmitted) rays.

5.2.2 The Faraday effect.

The Faraday effect is the rotation of the plane of polarization of plane polarized light as it is transmitted by a ferromagnetic material. The rotation is produced by any component of the magnetization which lies in the direction of propagation. The amount by which the plane of polarization is rotated depends on the magnitude of the magnetization and the direction in which the polarization plane rotates depends upon thedirection of the magnetization.

To examine domain structures using the Faraday effect it is necessary to illuminate the specimen using plane polarized light. This is done by placing a polarizer, such as a Glan Thompson prism, between the light source and the specimen. The light passes through the specimen and then through a microscope/analyser arrangement. Any fluctuations of magnetization in the specimen will result in the light being composed of different polarizations according to which part of the specimen transmitted that part of the beam.

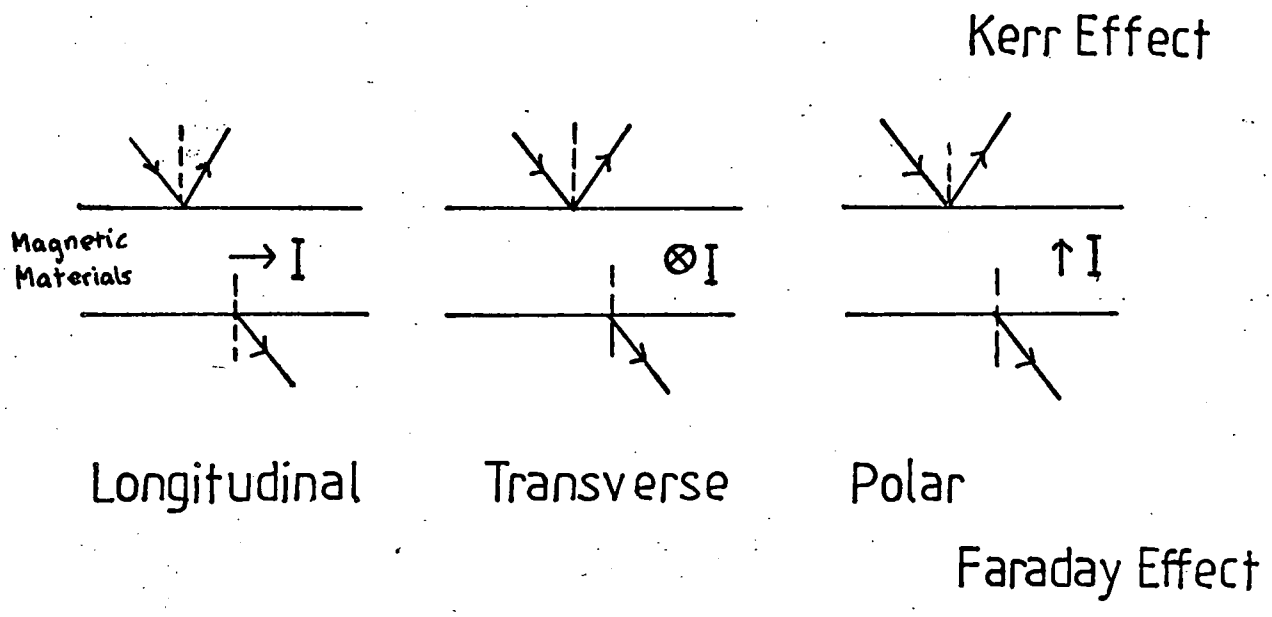

Fig. 5.1 Kerr and Faraday magnetooptical effects.

The final image will, therefore, consist of varying degrees of light intensity across the field of view depending upon the plane of polarization with respect to the analyser. Figure 5.2 shows a schematic arrangement suggested by ENOCH (1975) Enoch used two arrangements. The first was the arrangement of figure 5.2 using the Faraday effect where the magnetization of the specimen is parallel to the direction of propagation of the radiation. The second is illustrated schematically in figure 5.3. This arrangement is used for specimens in which the magnetization direction is perpendicular to the direction of propagation of the radiation (i.e. the magnetization lies in the plane of the slice). The specimen used by Enoch was Yttrium Iron Garnett. (YIG) which has a small uniaxial birefringence due to magnetostriction. (Dillon et al (1969)). Plane polarized light can be regarded as being comprised of left circularly polarized (L.C.P) and right circularly polarized (R.C.P) light superimposed. See Figures 5.4 and 5.5. Birefringence (or double refraction) occurs when a crystal has two refractive indices (one each for the so-called ordinary and extraordinary rays). When the plane of polarization of the light rotates an explanation can be given in terms of the superimposed rays (L.C.P. or R.C.P) having mutually different velocities inside the crystal, the ordinary ray obeying Snell's Law. When this happens the superposition of the electric ($\underline{E}$) vectors gives elliptically polarized light. Plane polarized light passing through a domain wall will usually emerge elliptically polarized. Goranson and Adams (1933) describe an arrangement of polarizer, quarter-wave plate and wave-retarder to obtain plane polarized transmitted light when plane polarized light is incident on the crystal. The results produced by the apparatus shown in Figures 5.2 and 5.3 produce essentially the same results. Because of the variation in orientation of

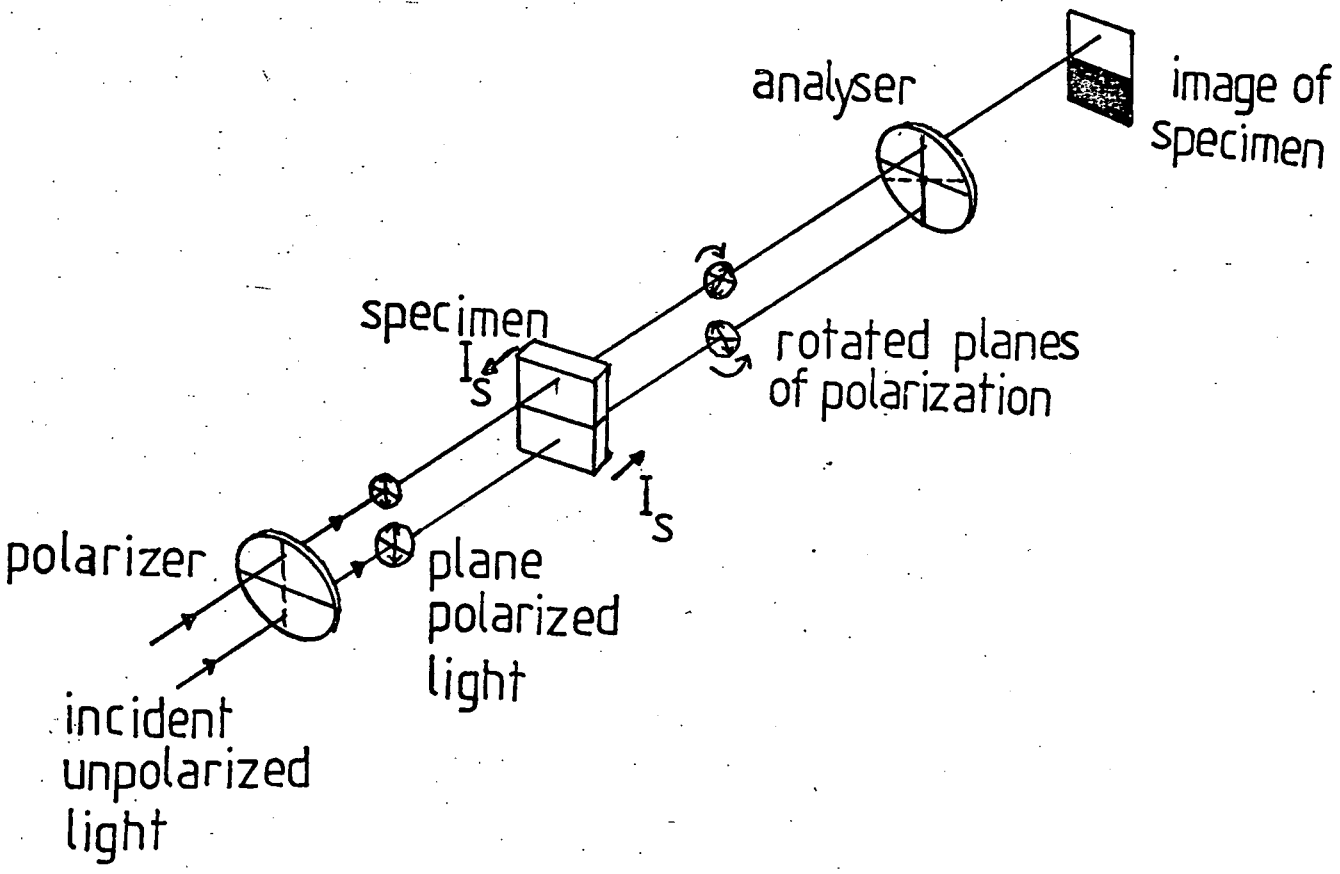

Fig. 5.2 Schematic representation of Faraday Effect apparatus

Magnetization parallel to light direction.

(Enoch (1975))

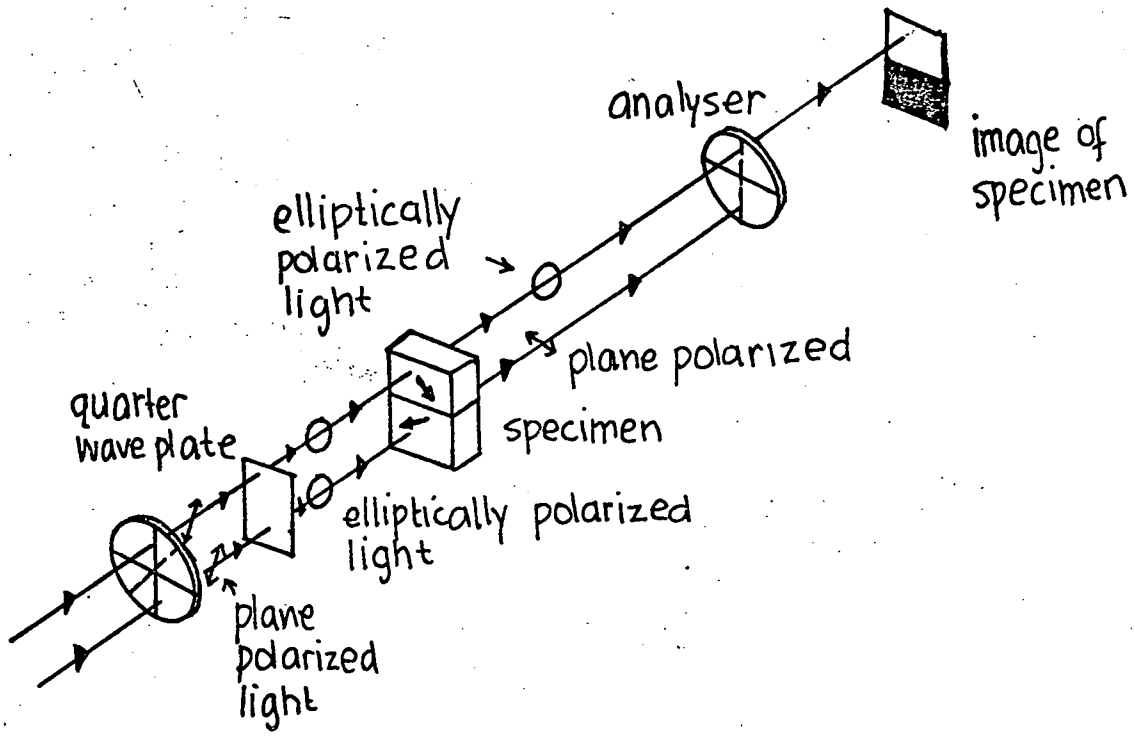

Fig. 5.3 Schematic representation of birefringence method of observing domains. (Magnetization is normal to light direction). (ENOCH (1975))

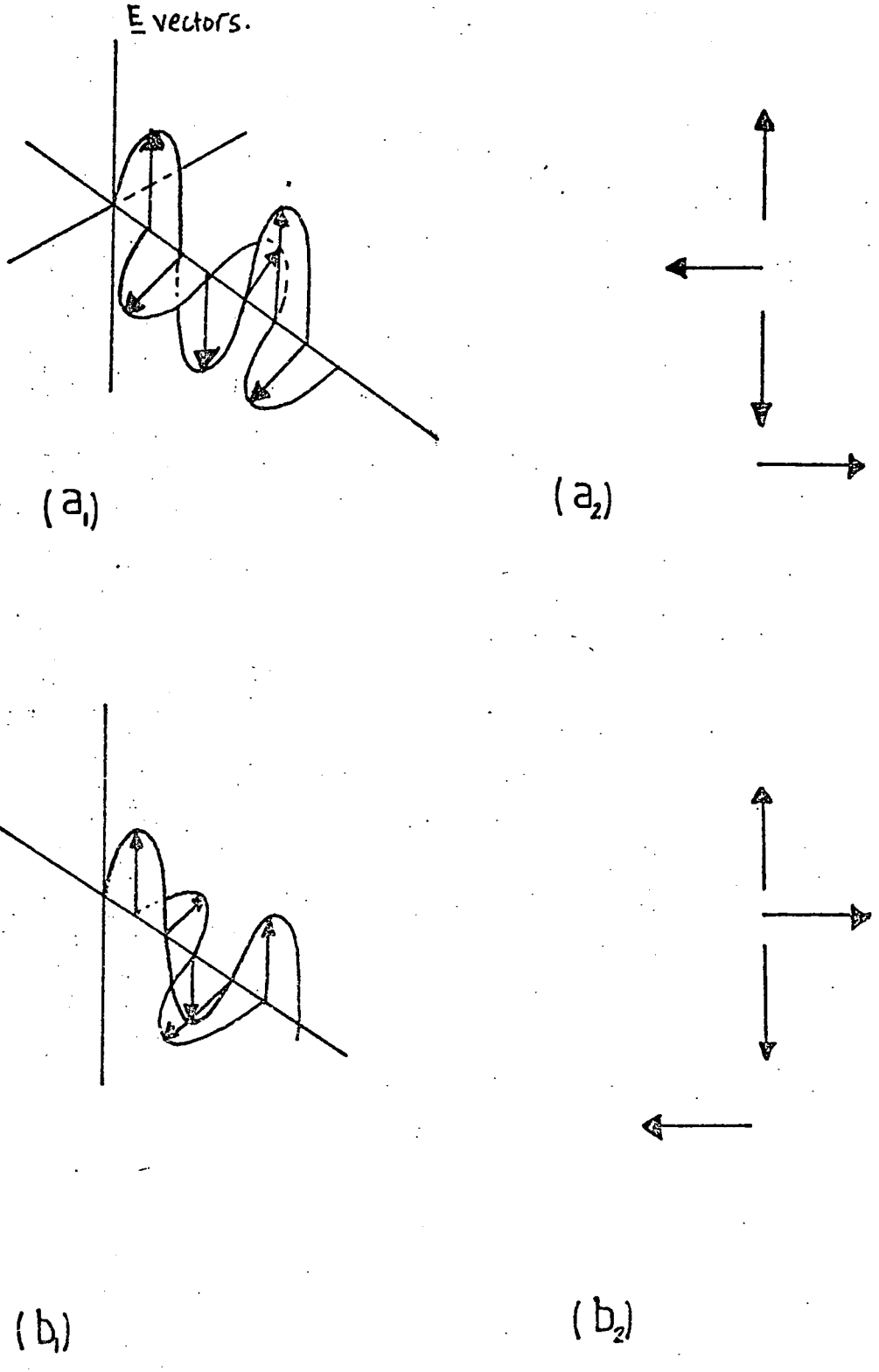

Fig. 5.4 Adopting an arbitrary convention a_1 shows left circularly polarized light, a_2 shows rotation of E vector. Similarly b_1 and b_2 show right circularly polarized light using the same convention.

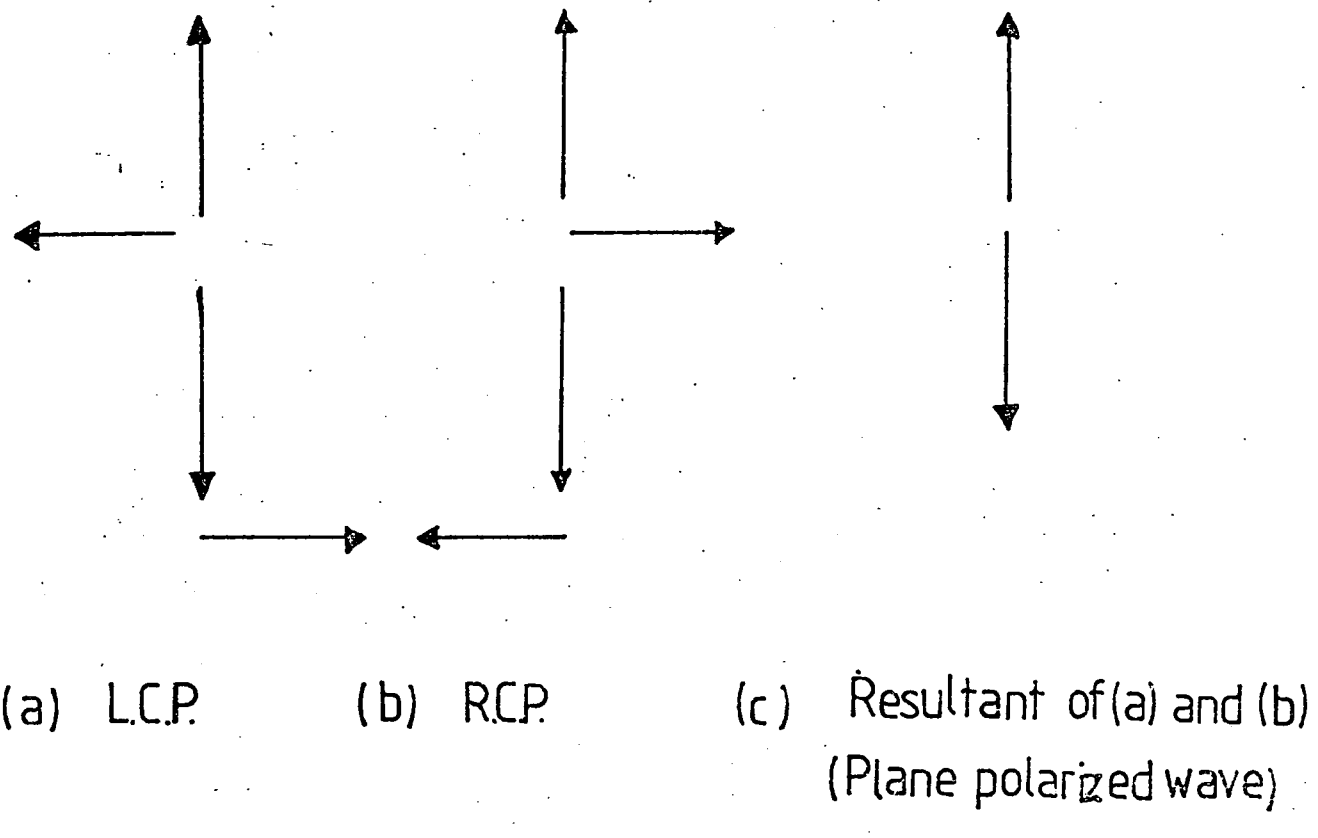

Fig. 5.5 Combination of Left and Right circularly polarized waves to produce plane polarization.

magnetization in the specimen, the image produced will consist of bright and dark regions, depending upon the rotation of the plane of polarization of the radiation.

The Faraday rotation is given by:

$$\theta = \frac{\omega}{2C}(n^+ - n^-) = \frac{\pi}{\lambda}(n^+ - n^-) \qquad (5.1)$$

where n^+ and n^- are the refractive indices for right and left hand circularly polarized light.

λ = wavelength of the radiation used

$$\text{Also } \theta = \theta_m + \theta_E \qquad (5.2)$$

where θ_m and θ_E are rotations associated with a magnetic dipole transition and an electric dipole transition respectively. Derivations for θ_m and θ_E are given by WAUGHNESS (1954) and CROSSLEY (1969) respectively. An account of application of magneto-optic effects in magnetic materials is given by PEARSON (1973) and Table 5.1 giving experimental values of Faraday rotation for unit length is taken from this paper.

5.2.3 The Kerr Effect

If a beam of plane polarized light is reflected from a metal surface one of two effects can occur.

(i) The reflected ray is elliptically polarized.

(ii) The reflected ray is plane polarized.

(ii) occurs when the plane of polarization of the radiation lies in or perpendicular to the plane of incidence.

If, however, the reflecting surface is magnetized then the reflected beam will be elliptically polarized irrespective of the orientation of the plane of polarization of the incident beam. This phenomenon is the Kerr effect, i.e. the plane of polarization is rotated according to the rate of magnetization of the reflecting surface. As mentioned in section 5.2.1, the effect is classified into three types. (Figure 5.1)

(i) Longitudinal effect - in this case the magnetization lies in the plane of incidence and in the plane of the reflecting surface.

(ii) Transverse effect - the magnetization is perpendicular to the plane of incidence and in the plane of the reflecting surface.

(iii) Polar effect - if the crystal surface is considered to be an x y plane then the magnetization in the case of the polar effect is along the z axis.

The greatest rotation of the plane of polarization occurs in the polar effect. Also, with this effect there is a rotation at normal incidence. The rotation with the longitudinal effect is about a factor of 5 less than that of the polar effect. In the transverse effect no

	Material	Faraday rotation /(degree cm^{-1})
Iron	Fe	3×10^5
Cobalt	Co	3×10^5
Manganese bismuth	MnBi	5×10^5
Chromium tribromide	$CrBr_3$	10^5
Europium oxide	EuO	10^4
Manganese ferrite	$MnFe_2O_4$	10^3
Yttrium iron garnet	$Y_3Fe_5O_{12}$	10^3
Terbium iron garnet	$Tb_3Fe_5O_{12}$	2×10^3
Iron borate	$FeBo_3$	10^3
Iron trifluoride	FeF_3	10^2

Table 5.1 Experimental values of Faraday rotation per unit length.
(PEARSON (1973)).

rotation of the plane of polarization occurs. What happens is that the reflection coefficient for light polarized in the plane of incidence changes leaving the reflection coefficient perpendicular to the plane of incidence.

Williams et al (1951) were first to use a reflection magnetooptical effect to investigate ferromagnetic domains in a cobalt crystal. Fowler and Fryer (1954, 1955, 1956 and Fowler et al (1956) used the longitudinal Kerr effect to view ferromagnetic domains. Because the rotation obtained using the longitudinal Kerr effect is very small, the use of crossed Nicol or Glan Thomson prisms results in a pattern of very poor definition and low intensity. Also, surface imperfections such as scratches etc. cause local fluctuations in intensity thereby introducing a considerable amount of noise into the pattern. For a discussion on surface imperfection induced noise and techniques for its elimination see TREVES (1967). Figure 5.6 shows schematically the arrangement for viewing domains using the longitudinal Kerr effect (PRUTTON (1959)). Fowler and Fryer attempted to overcome the difficulty of surface imperfection induced noise by combining a positive transparency photograph of the surface with a negative photograph of the surface containing domains. In this way, viewing the pair of photographs with transmitted light the effect of surface imperfections cancelled out revealing a more clear domain structure. The method is, however, cumbersome and an easier way of increasing contrast is to bloom the surface of the specimen. The process was suggested by Kranz (1956) and Kranz and Dreschel (1958) who assumed that light plane polarized perpendicular to the plane of incidence was reflected giving a component R with unchanged plane of polarization due to metallic reflection and a component of amplitude K which is polarized in the plane of incidence.

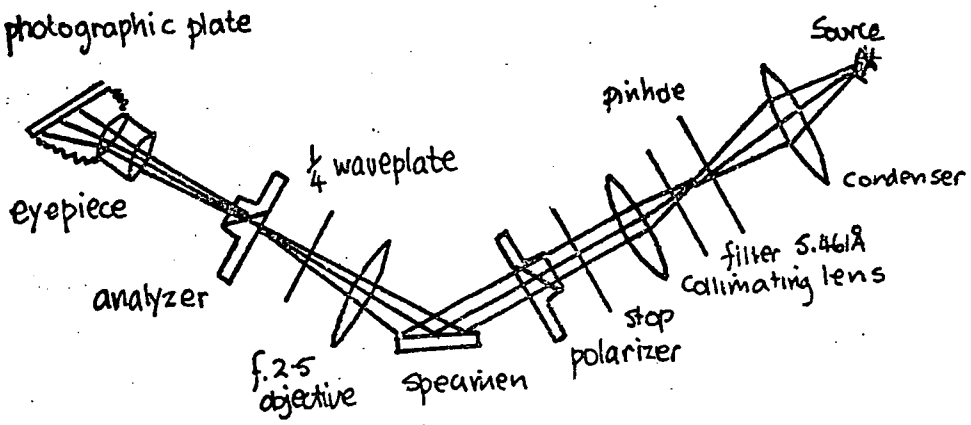

Fig. 5.6 Schematic representation of system for the longitudinal Kerr effect.

(PRUTTON (1959))

For zero phase difference between K and R the Kerr rotation is given by the angle between R and the vector sum of K and R. Because the vector sum of K and R does not always give plane polarized reflected waves, crossing of the polarizer and analyser will not give complete extinction. This was overcome (PRUTTON) by inserting a quarter wave plate before the analyser thus making the reflected beam plane polarized. The zinc sulphide bloomed layer increases the rotation by as much as a factor of 3 by reducing the normally reflected component R (See Figure 5.9). See also PRUTTON (1959) for an account of the method used to deposit the dielectric onto the sample surface. Silicon monoxide (refractive index $\sim$ 1.9) and zinc sulphide (refractive index $\sim$ 2.3) were used and the best contrast was found to occur for the dielectric with the higher refractive index while no discernable pattern was observed without blooming.

Mapps (1978) used an optical system (Figure 5.8) which was a modified version of that used by Fowler and Fryer (1952). The main difference between the apparatus shown in Figure 5.8 and that used by Fryer and Fowler was the use of thin sheet polarizers (P_1 and P_2) rather than Nicol or Glan Thomson prisms as polarizer and analyser. If calcite prisms were used in the optical path in positions before L3 and after L4 then any strain in these lenses would result in the glass exhibiting a birefringence thereby effectively reducing the Kerr rotation. Prisms introduced in positions P_1 and P_2 would not result in this effect but would require parallel light. Prisms were, therefore, not used. The thin sheet polarizers P_1 and P_2 effectively reduced effects due to strain and only the polarization effects introduced by the domain magnetization pattern on the specimen are picked up by the imaging system. (In this case MAPPS used a television camera for teaching purposes.)

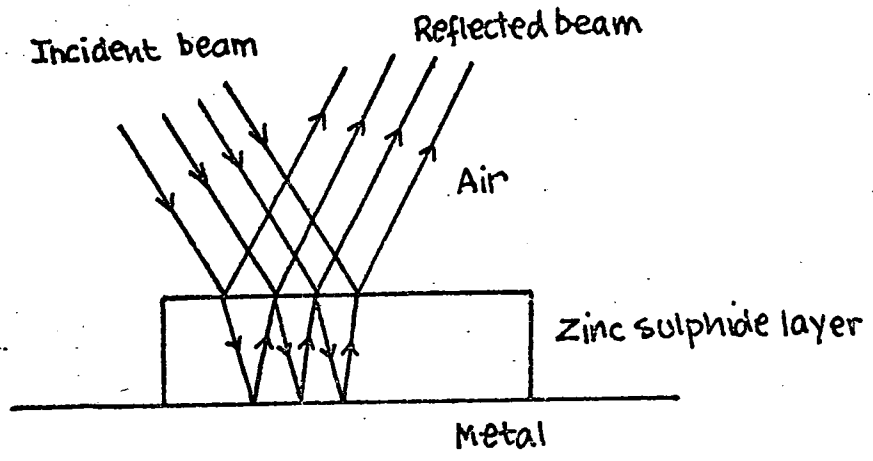

Fig. 5.7 Zinc sulphide antireflection layer. (AFTER DRESCHEL(1958)) Each reflection introduces an extra contribution to the total Kerr rotation.

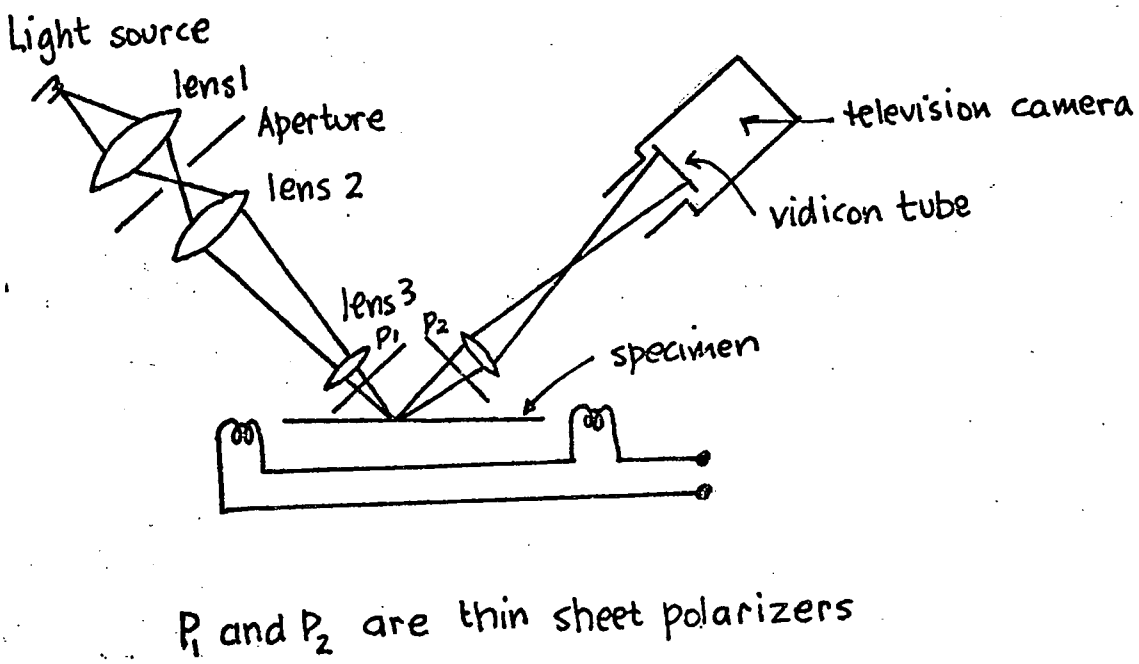

Fig. 5.8 Optical system for the longitudinal Kerr effect (AFTER FOWLER and FRYER (1952) as modified by MAPPS (1978).

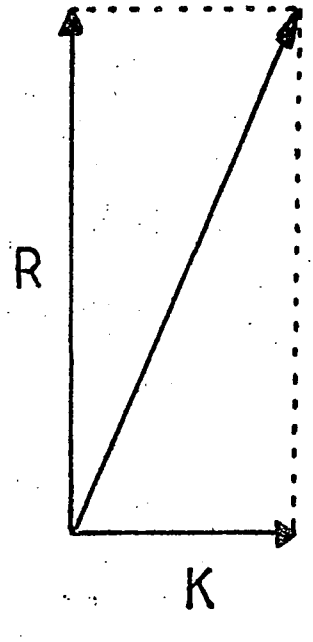

(a) Normal metallic reflection

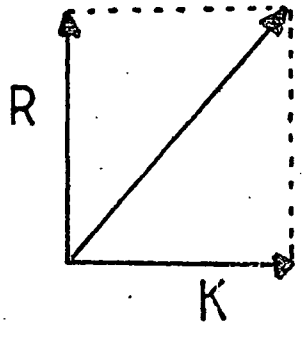

(b) Reflection from bloomed metal surface

Fig. 5.9 Increase in rotation produced by Kerr component K after reduction of normal component by blooming.

The Kerr effect is dependent both on frequency of the light source and on the angle of incidence. Treves (1961)looked at the limitations of the application of Kerr effect techniques in domain studies. He suggested that ellipticity due to metallic reflections was the most important limitation. As previously mentioned, when the reflected light is elliptically polarized this increases the amount of light transmitted by the analyser. Treves found (see Figures 5.10(a) and 5.10(b)) that ellipticity and the Kerr rotation were a maximum for an angle of incidence of $\sim 60^0$. Now for good microscope resolution a large aperture is required. Hence a divergent beam is desirable after reflection from the sample. This, unfortunately, results in an homogeneous array of elliptical polarizations in the reflected ray. (due to the angle between the plane of incidence and the plane of polarization being different for different parts of the incident converging, plane polarized beam). Hence a compromise was suggested (for maximum contrast) between ellipticity and rotation. Treves settled for a beam divergence of $\sim 10^0$ maximizing contrast for an angle of incidence of $\sim 20^0$. Apparatus to obtain these conditions was designed and used by Fowler, Fryer and Treves (1960) to considerable effect. (See CAREY AND ISAAC (1966)).

Many other apparatus designs have been put forward to use the Kerr effect; notably Green and Prutton (1962).

Lee, Callaby and Lynch (1958) measured domain wall movement using a scanning plane polarized light probe.

Dey, Bowman and Booth (1968) suggest an apparatus for viewing domains in Kerr effect microscopy using a laser source. While a laser source produces high monochromaticity there are several effects which introduce noise and confusion into the final image when a laser is used. (as well as the problem of visual observation.) Diffraction effects due to

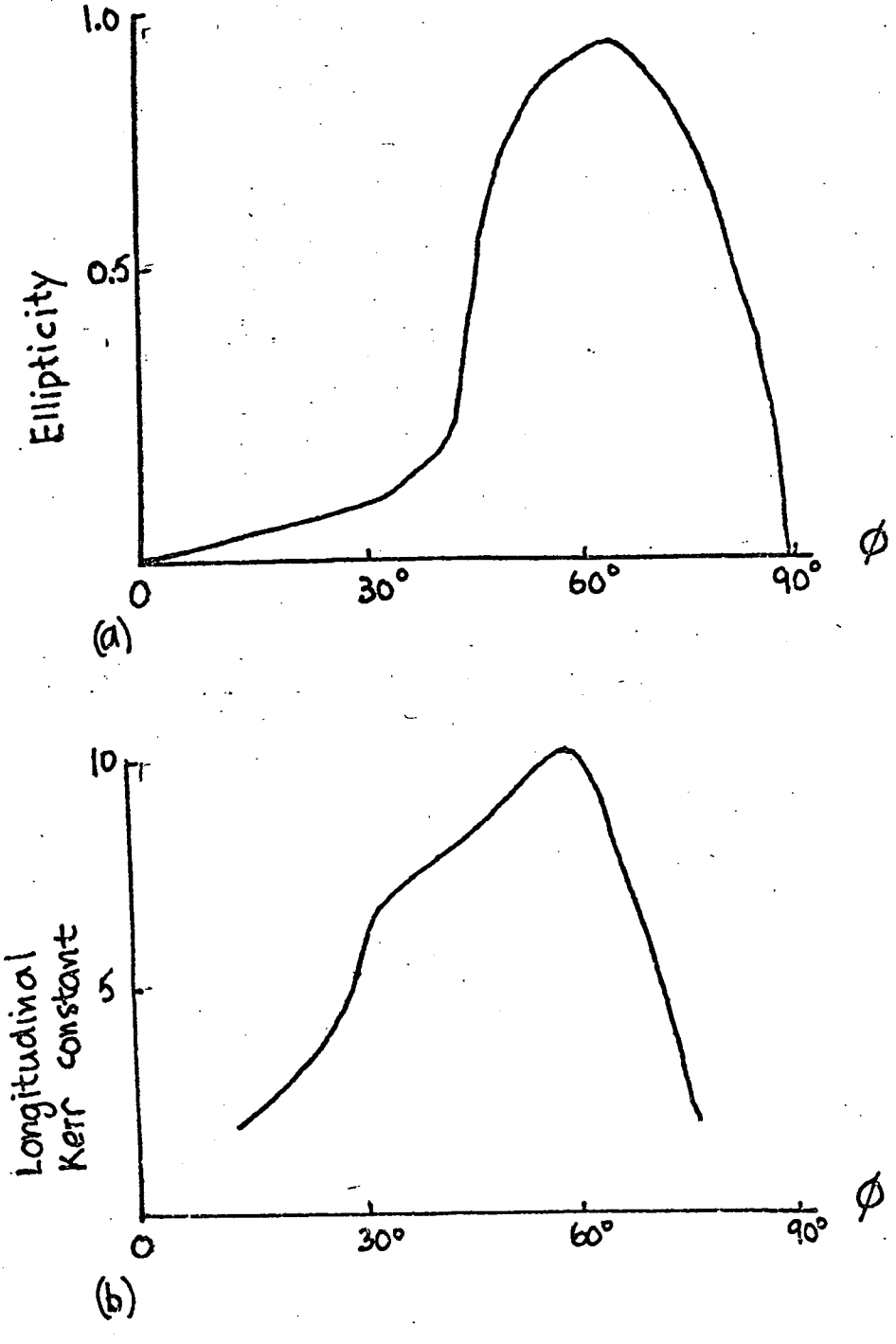

Fig.5.10 (a) Ellipticity versus angle of incidence.

(b) Rotation versus angle of incidence.

(CAREY and ISAAC (after TREVES))

dust or scratches and general imperfections in the optical system produce noise in the final image. These effects can be partly reduced by using a suitable lens system to focus the beams on a very fine aperture. The beam then passes through the aperture while blocking out some of the noise due to the diffraction effects. (There will now be, however, a diverging beam after the aperture.) Other effects occur due to the coherence of the source, e.g. edge ringing and speckling. The technique reported by Day et. al. was designed to improve domain pictures by removing speckling from the pattern. Speckling is caused when a diffused reflecting or transmitting screen is used and is thought to be a three dimensional diffraction spatial effect caused by interference of rays leaving the diffuser with random phases and amplitude. Figure 5.11 shows the experimental arrangement used by Day et al. to reduce speckling. Essentially laser light passes through a diffusing screen D placed in the focal plane of a lens L_1. A collinator lens L_2 forms an image of a stop P_1 and the specimen is placed in the plane of this image P_3 which is virtually coincident with the focal plane of L_2. With $g = f_2$ a Fourier transform pair is realizeable and the final image is the spectrum of a phase modulated wave. By rotating the diffusing screen it is possible to effect a uniform illumination with which to observe the magnetic domains. (see Dey et al.)

The Kerr effect on an unbloomed crystal is usually too small to produce an observeable pattern. With suitable crystal preparation so that contrast is enhanced, the effect produces useful patterns. Because the technique, unlike the colloid technique (discussed earlier in this chapter and in Chapter 6) there are no particles involved which possess inertia. The effect can, therefore, be used where the

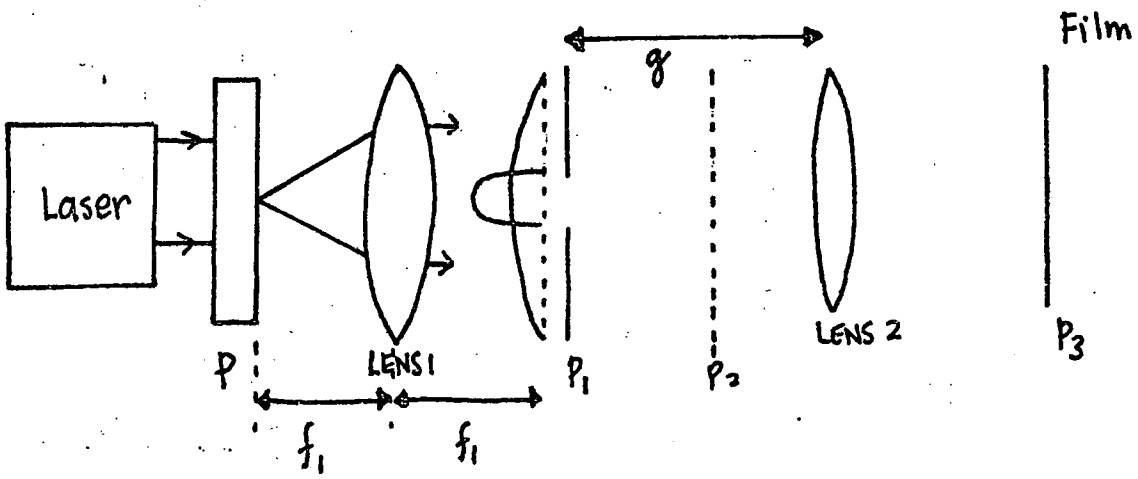

P= diffusing screen

Fig. 5.11 Experimental arrangement for removing speckled appearance of image produced by a laser source.
(DEY et al (1968))

magnetization is changing with time (such as in the observation of domain wall movement, as previously mentioned.) Also, whereas the Bitter colloid technique shows domain boundaries the Kerr effect illustrates domains.

5.2.3.1. Suggestion for Kerr Effect Rig for use at low temperatures

At low temperatures the colloid technique using a suspension of ferromagnetic particles becomes inconvenient bearing in mind the freezing point of the colloid. The dry colloid technique (Chapter 6) offers a solution to the problem but each experimental run must, by necessity, take rather a long time to set up. If the colloid is being evaporated onto the sample then the ambient pressure is critical. It must also be inert and free from moisture (which would condense onto the sample surface at low temperatures.) Hence a vacuum system of some sort is essential and if the pressure inside the dry colloid rig is to be suitably adjusted for each run then a lot of time will be involved.

The Kerr magnetooptic effect offers a solution to the problems of time and inconvenience when working with ferromagnetic materials with low Curie temperatures (the method is not restricted to low temperature).

Figure 5.12 shows an exploded view of the chamber into which the sample is put. Figures 5.13, 5.14 and 5.15 show the construction details while Figure 5.16 shows schematically a suggestion for its use. The construction details are not totally arbitrary but are given after taking into consideration standard sizes for "O" rings, diode thermometers and liquid helium transport lines. So that small angles of incidence can be used it is suggested that a fibre optic be used together with an intense light source such as a mercury vapour lamp (making suitable

arrangements avoiding overheating to components such as the thin sheet polarizers.) The polarizers used as analyzer and polarizer could easily be mounted on the end of the fibre optic and on the objective of the microscope (such that the analyzer is allowed to rotate). Because of the different optical paths within the fibre there will be some ellipticity on reflection which will reduce (or rather effectively reduce) the Kerr rotation. An optimum angle of incidence should be chosen after consideratio given to the sample material.

An arrangement such as that suggested would lead to many advantages over the colloid technique. The colloid apparatus described in Chapter 6 needed cleaning after each run as did the sample. With a magnetooptical rig there would be no requirement to clean either the rig or the sample after each run. Indeed, once the vacuum is established and the sample is cooled below its Curie temperature the temperature can be varied as desired by the inclusion of small non-inductively wound heating coils which it is possible to include near the sample in the chamber. Also, the chamber itself is of dimensions conveniently small enough to allow the rig to be inserted into the space between the poles of a magnet.

Hence such an apparatus would provide a means of viewing domain structures as a function of temperature and applied field. The observations could be made quickly once the optimum conditions had been established. Problems such as definition and contrast could be tackled bearing in mind the nature of the sample and the optical system being used.

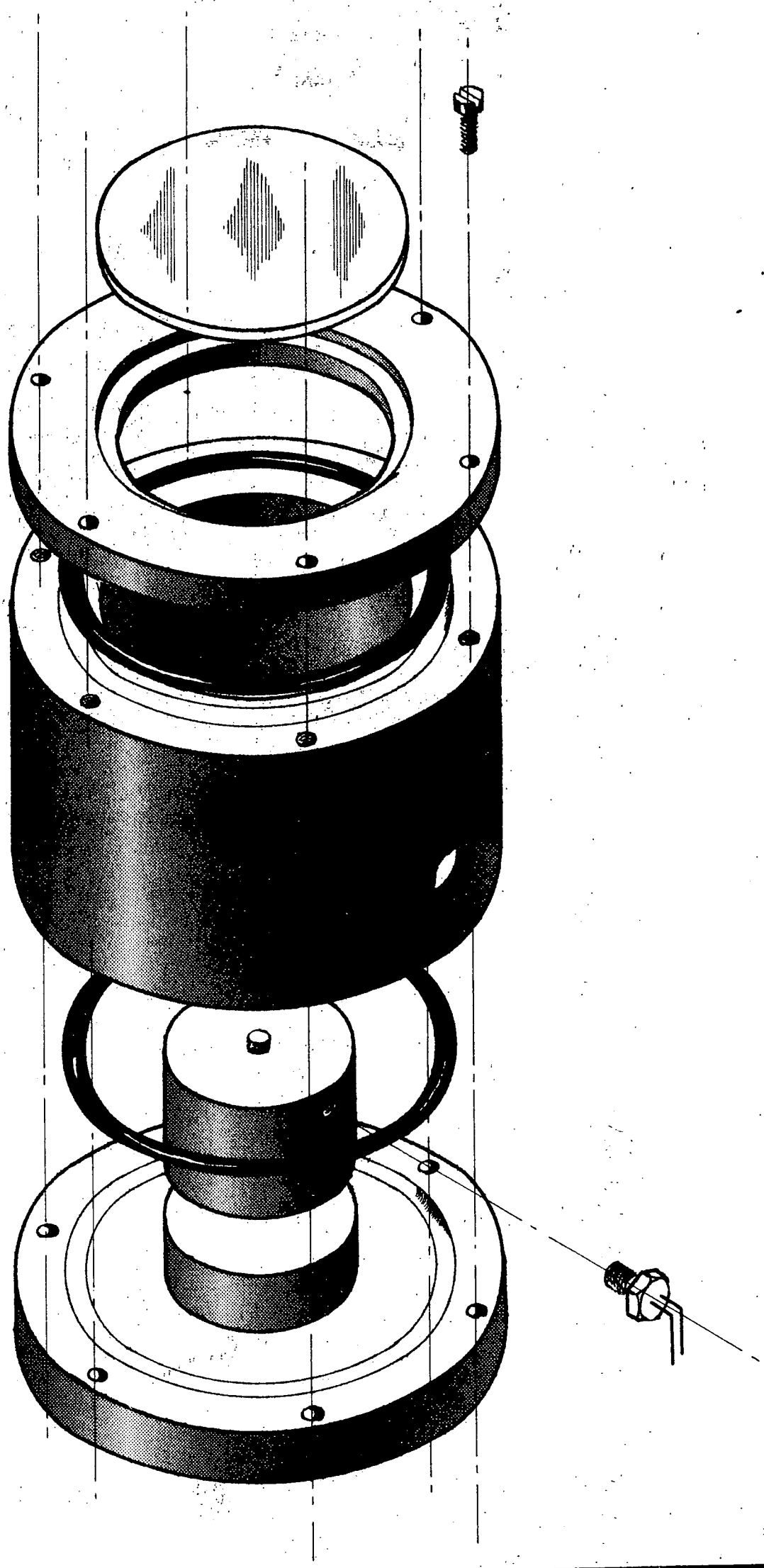

Figure 5.12.

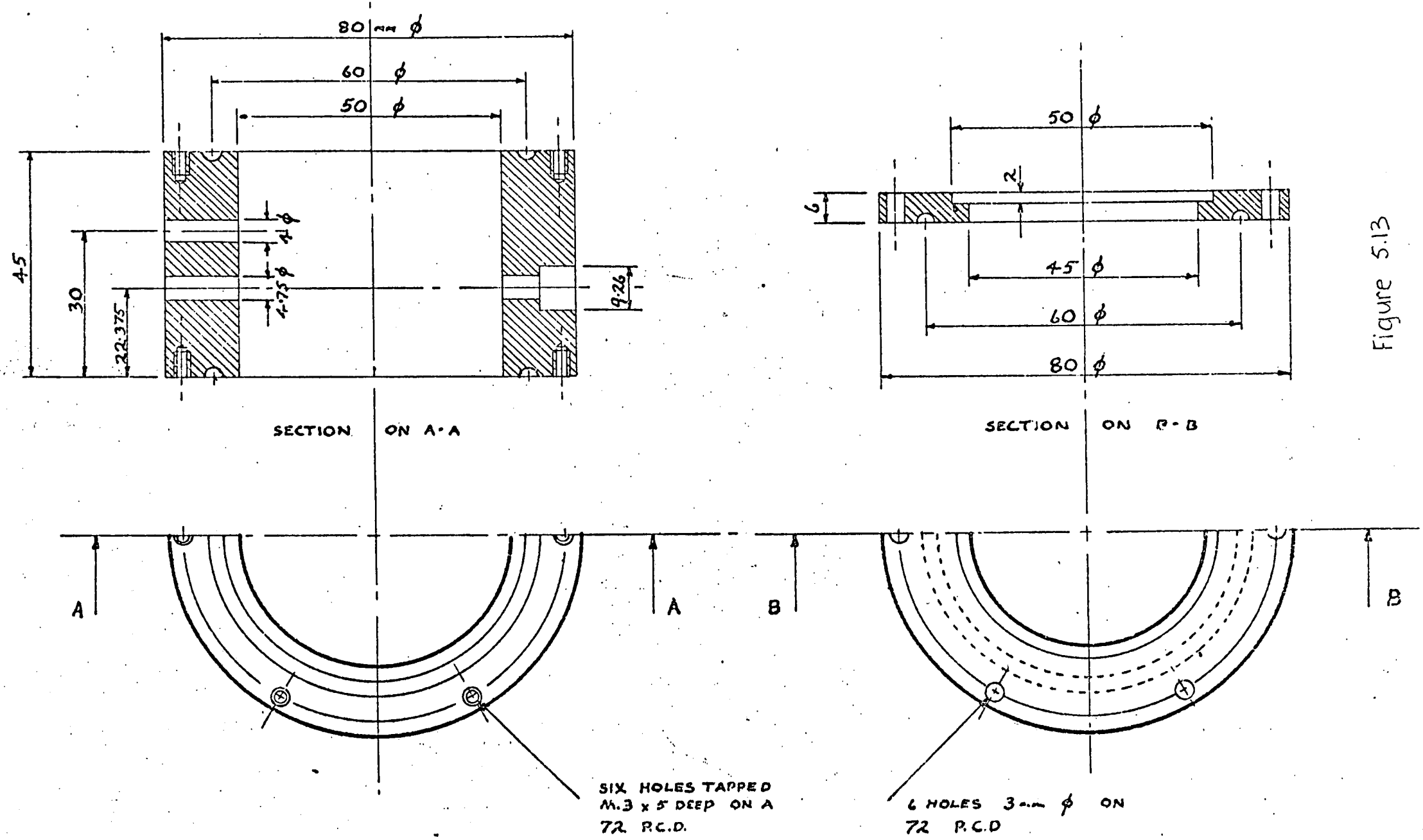

Figure 5.13

PART NO	NAME OF PART	MATERIAL	NO OFF
1	MAIN BODY	BRASS	1
2	TOP CAP	"	"

CHAMBER FOR KERR EFFECT RIG

Figure 5.14.

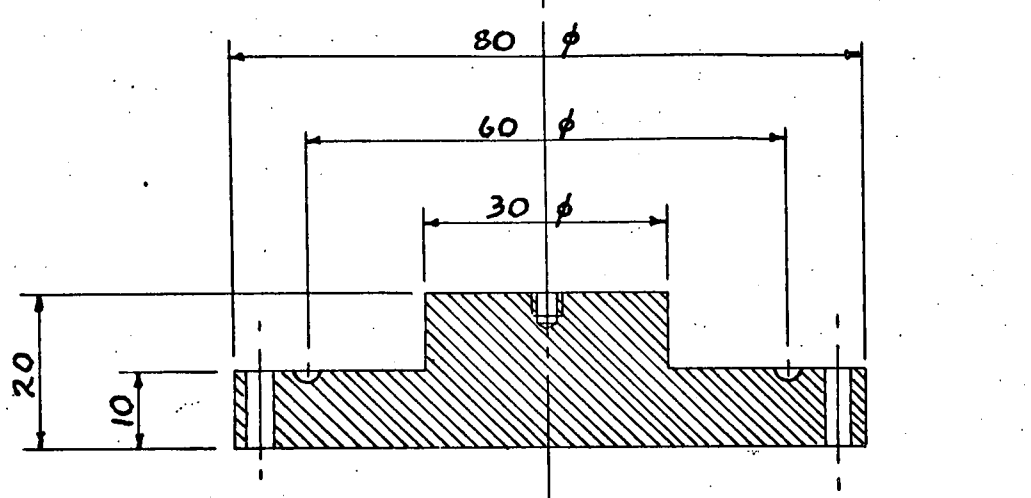

SECTION ON A-A

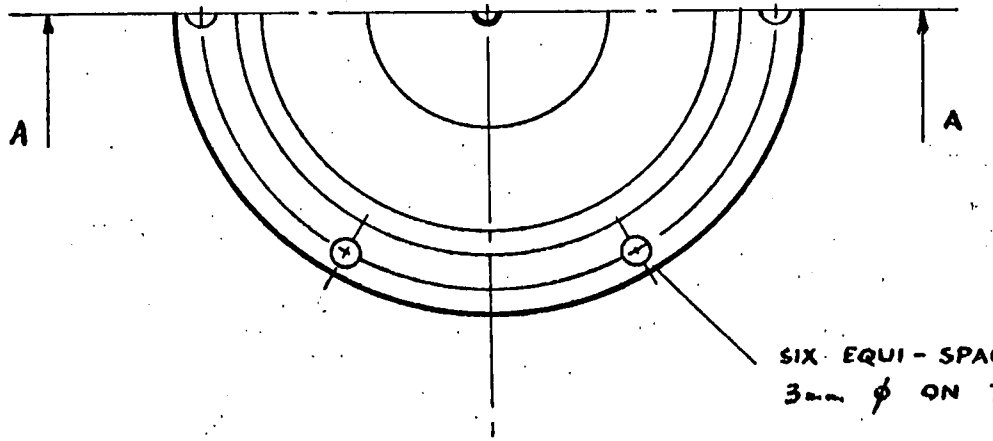

SIX EQUI-SPACED HOLES
3mm ϕ ON 72 P.C.D.

M.3 x 3mm

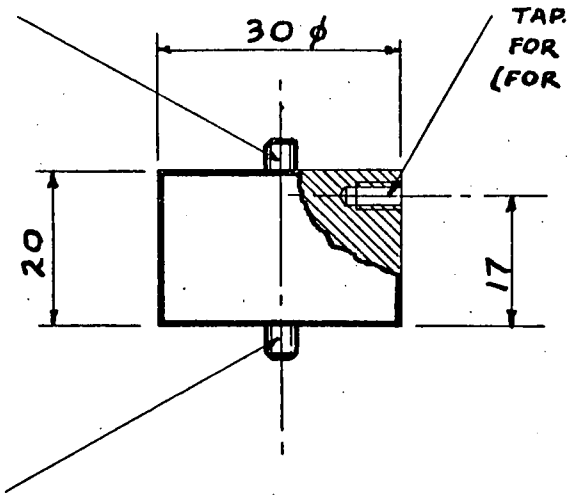

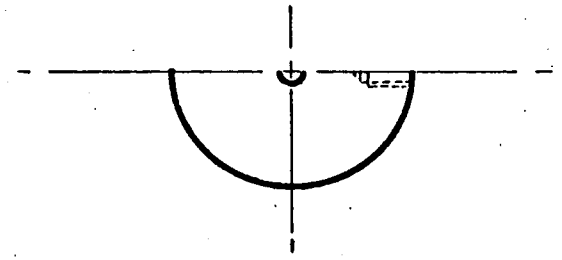

Figure 5.14

PART NO	NAME OF PART	MATERIAL	NO. OFF
3	BASE	TUFNOL	1
8	SAMPLE TABLE	BRASS	-

CHAMBER FOR KERR EFFECT RIG

DRW. NO 2

Figure 5.15

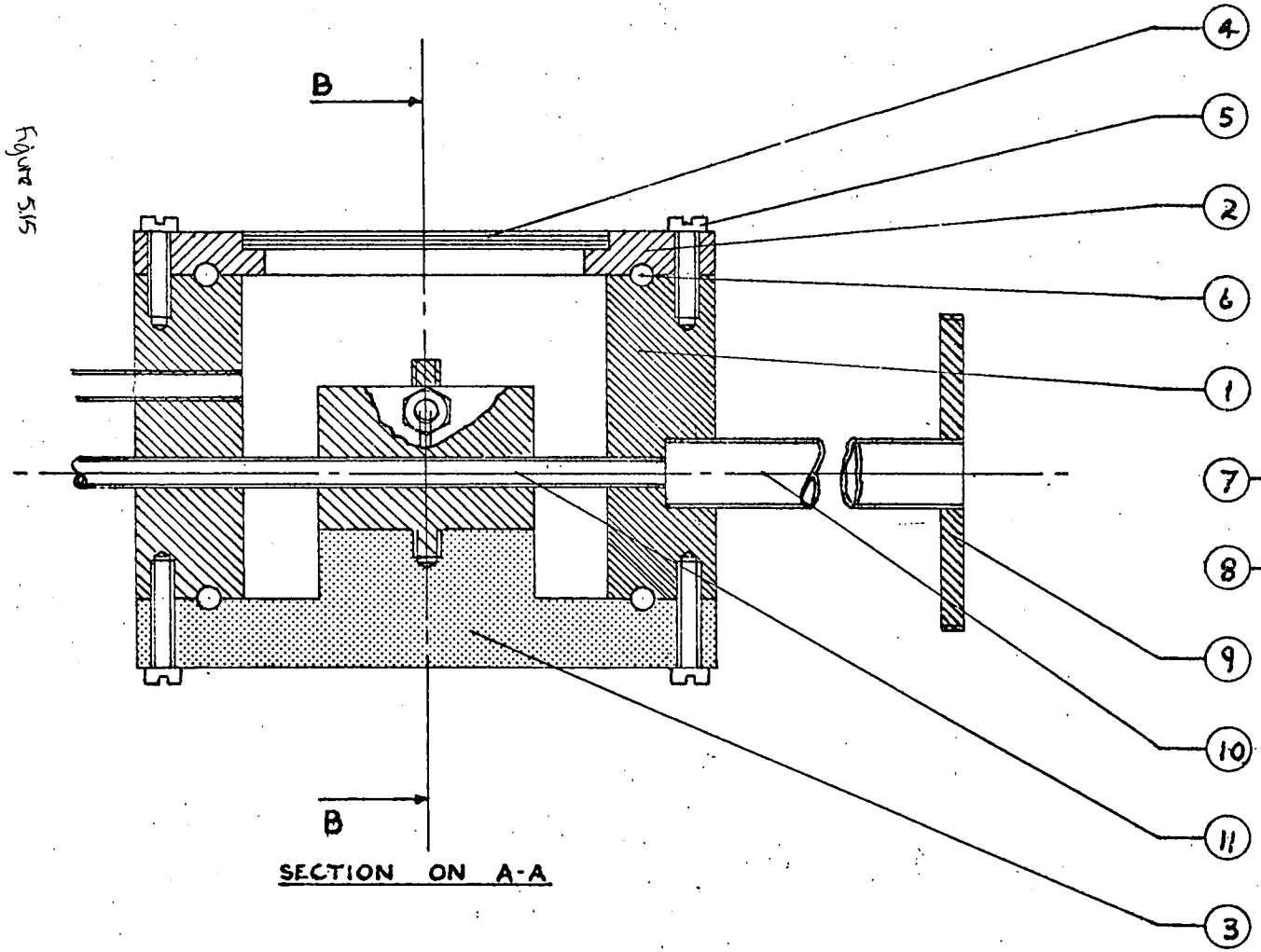

SECTION ON A-A

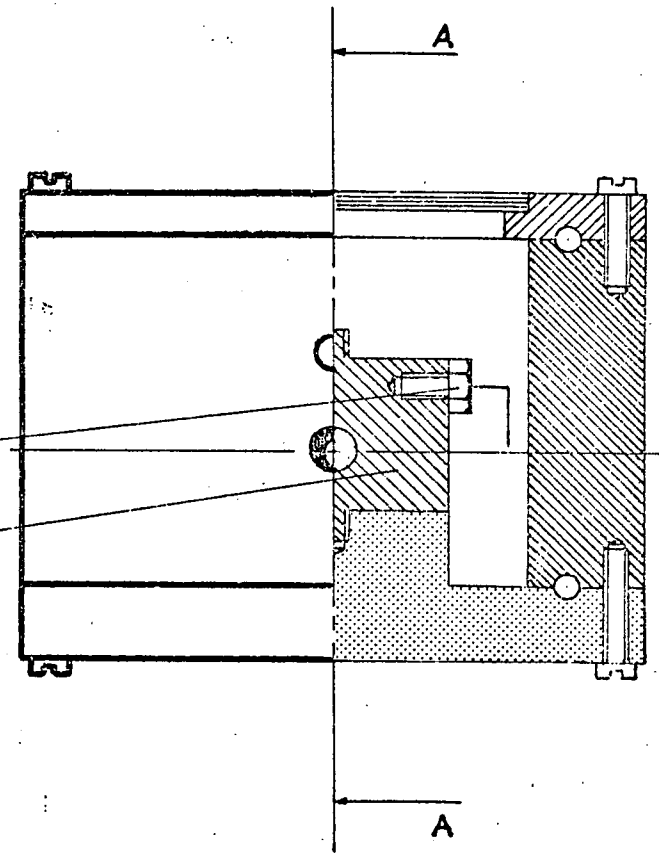

HALF SECTION ON B-B

Figure 5.15

PART NO.	NAME OF PART	MATERIAL	NO. OFF	DRW NO	PART NO	NAME OF PART	MATERIAL	NO OFF	DRW NO.
1	MAIN BODY	BRASS	1	1	7	DIODE	-	1	-
2	TOP CAP	"	"	1	8	SAMPLE TABLE	BRASS	1	2
3	BASE UNIT	TUFNOL	"	2	9	FLANGE	"	"	.
4	WINDOW	QUARTZ	"	-	10	VACUUM WALLED PIPE	"	"	-
5	SCREWS	BRASS	12	-	11	" " "	"	"	.
6	'O' RING	NEOPRENE	2	-					

CHAMBER FOR KERR EFFECT RIG

ASSEMBLY DRAWING

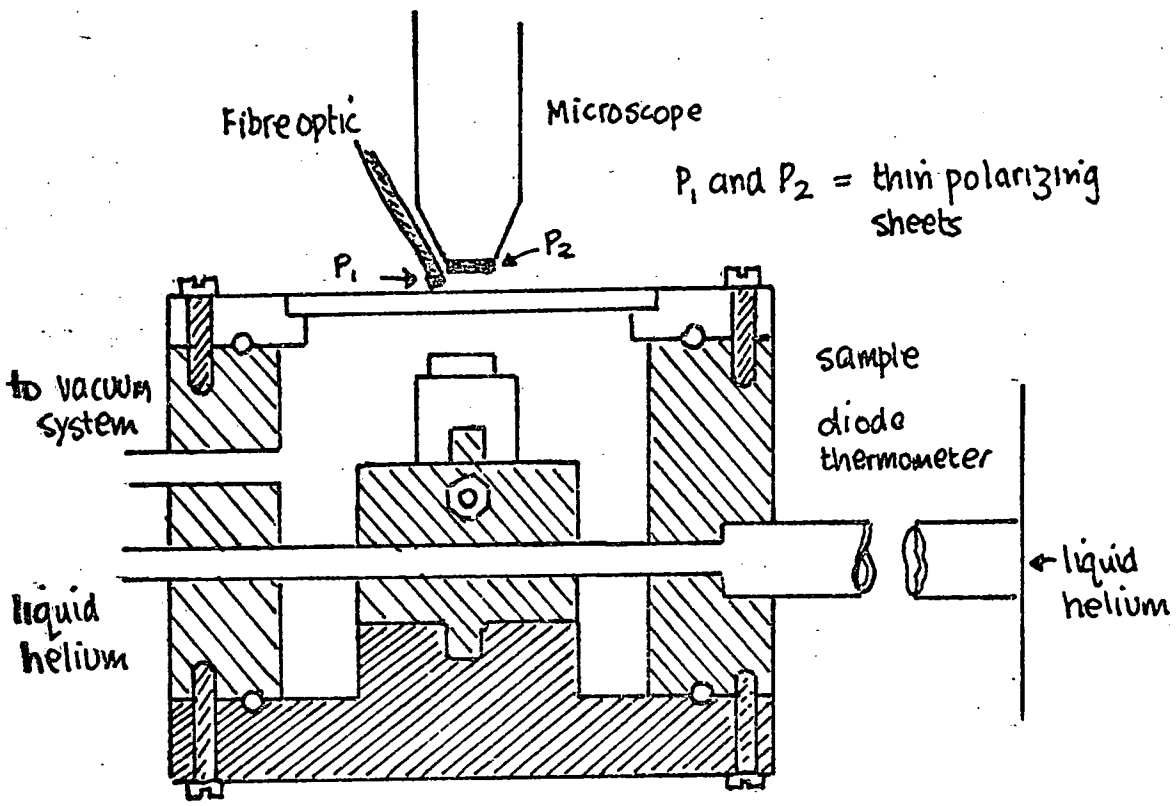

Fig. 5.16 Schematic representation of suggested use of Kerr effect.

5.2.4 The Polar Kerr effect

Figure 16(a) shows the arrangement used by Williams Foster and Wood (1951) to examine the basal plane domain structure of cobalt. The arrangement consisted of a permanently crossed polarizer and analyzer arrangement plus a quarter-wave plate and ellipticity compensator.

5.2.5 The transverse Kerr Effect

This effect, with a suitable arrangement of the sample, produces results very like those produced by the longitudinal effect. The transverse effect arises as a change in the reflectivity of the surface for light polarized in the plane of incidence (the reflectivity for normal incidence remaining undamaged.) Dove (1963) reported the observation of magnetic domains using the transverse Kerr effect. Figure 5.17 shows the basic arrangement for such observations. Dove obtained contrasts of the same order as that obtained using the longitudinal effect by using a phase adjustment. Figure 5.18 shows the apparatus used.

5.3 ELECTRON MICROSCOPY (LORENTZ MICROSCOPY)

Because the transmission electron microscope (T.E.M.) relies on the Lorentz force ($F = Bev$ where v = velocity of electron and the other symbols are the usual symbols for the quantities they represent). The technique is called Lorentz microscopy.

Various microscope techniques have been used and CAREY and ISAAC (1966)(Ch.6) give an excellent detailed account of these techniques.

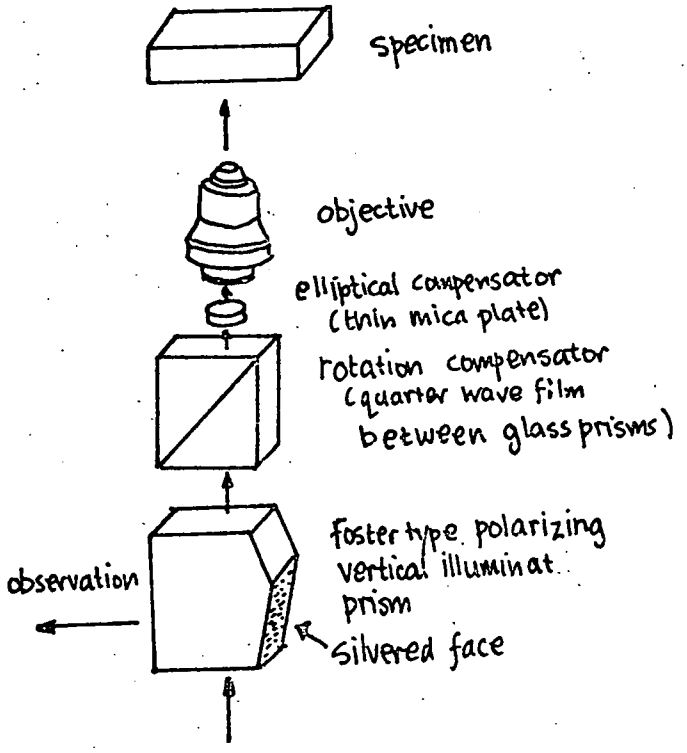

Fig. 5 16 (a) Schematic diagram of microscope for polar effect.
(After Williams, Foster and Wood)

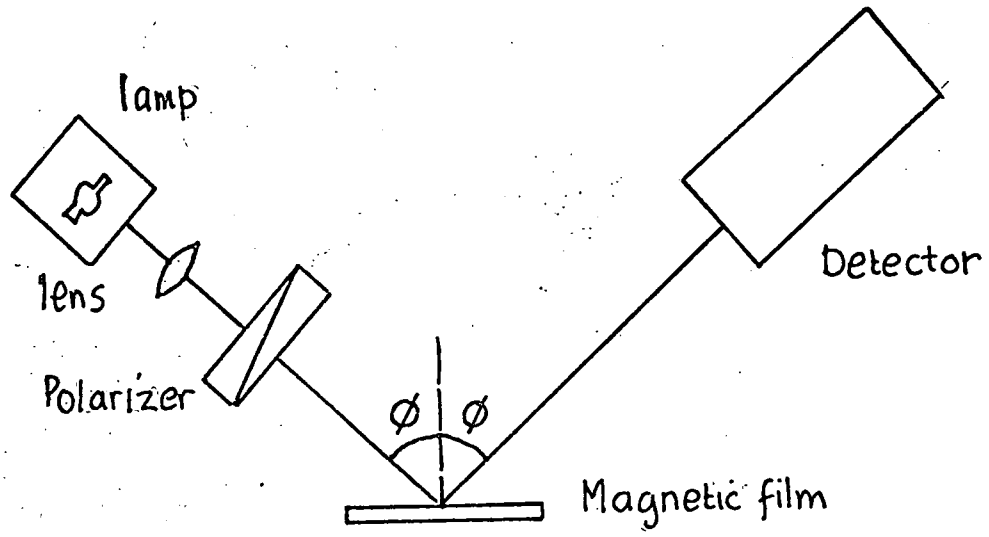

Fig. 5.17 Basic arrangement for observing domains using the transverse Kerr effect.
(DOVE (1963)).

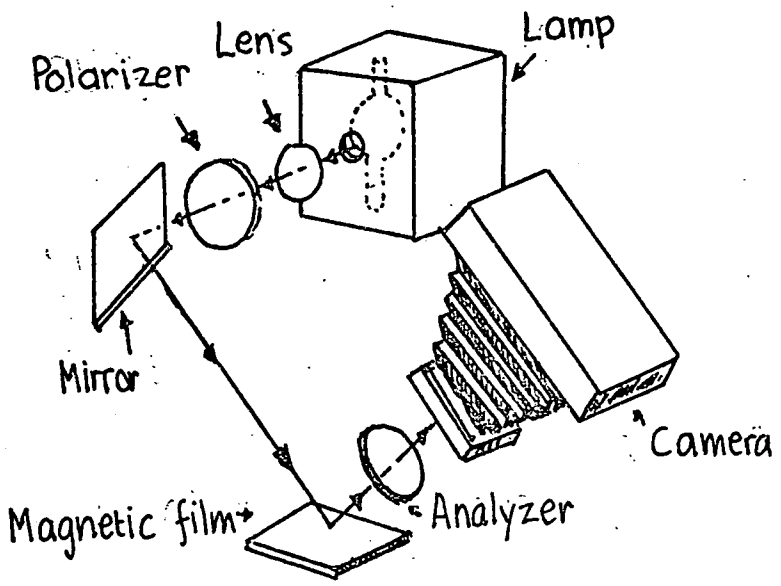

Fig. 5.18 Apparatus for domain photography using the transverse Kerr effect (as reported by DOVE (1963))

Experiments based on electron beam techniques have been extremely varied including shadow techniques and mirror microscopy. Shadow techniques employ the fact that leakage fields near the surface scatter an electron beam (usually incident at a grazing angle) onto a photographic plate. In the electron mirror microscope the specimen is made slightly negative with respect to the electron source. The specimen will, therefore, reflect the electron beam and any surface irregularities on the specimen will modify the local electric field and thereby alter the electron beam as it is reflected. The beam is then passed through a suitable magnetic imaging system in order to produce a magnified image of the surface.

The use of transmission electron microscopy demands the careful preparation of the specimen which must be in the form of a thin film or foil. This means, of course, that the structures observed do not necessarily represent those of the bulk material. The properties of bulk materials can, however, be investigated using scanning electron microscopy techniques which have the added advantage of not introducing problems in terms of the effect of the magnetic field of the objective lens on the domain structure of the sample.

5.4 PROBE TECHNIQUE

There are various types of magnetic probe. Any property of a material which changes with a change in the magnetic field around it can be exploited to measure the intensity of that field. In general probe techniques do not actually form images of domain structures but only facilitate the mapping of these structures as the surface of the specimen is scanned by the probe.

5.4.1 The search coil (is a simple and well known device.)

When it is subjected to a changing magnetic field (whether the field changes or the coil moves is immaterial) then an e.m.f. is induced in the coil. A suitable meter in line with the search coil will produce a deflection which can be calibrated absolutely or relatively.

5.4.2 Magnetoresistance probe

The change in electrical resistance of a specimen subjected to a magnetic field can be used as a means of measuring that field.

5.4.3 Permalloy probe

When a magnetic material is moved in a non-uniform magnetic field it experiences a change in its magnetization. Substances with high permeability such as permalloy can, therefore, be used to sample very small fields. They can be used on very small samples of material in order to measure local fluctuations in the field. In order to render the specimens magnetic field "changing" with respect to the probe, the probe is made to vibrate. (KACZÉR (1955))

5.4.4 Hall probe

When a conductor or semiconductor carrying a current I is subjected to a uniform flux density B perpendicular to the current flow (or at least having a component perpendicular to the current flow) then, because of the Lorentz force on the charge carrier, a voltage known as

the Hall voltage (after its discoverer) appears transversely across the conductor. Figure 5.19 illustrates this. As well as the transverse Hall voltage the deviation of the charge carriers will cause a small change in resistance. This transverse magnetoresistance can be detected as a small current change when the magnetic flux is changed. (See 5.4.2) The effect is related to the Hall effect.

The Hall effect can therefore be used to measure magnetic flux densities. The effect is more pronounced in semiconductors than in metals.

The probe techniques described are not now in current use to show domain structures. They do, however, and particularly the Hall probe technique, represent useful ways of measuring flux densities in reasonably large regions of space such as those between the poles of magnets which are to be used to provide applied fields.

5.5 X-RAY DIFFRACTION

The method of X-ray topography is made up of a variety of X-ray diffraction techniques. For a comprehensive review of X-ray topography and application of X-ray techniques to domain study, see TANNER (1976).

X-ray diffraction is concerned with local variations in the intensity or direction of an X-ray beam which has been diffracted from a crystal according to Braggs Law.

$$\lambda = 2d \sin \theta \qquad (5.3)$$

where d = lattice spacing

θ = Bragg angle.

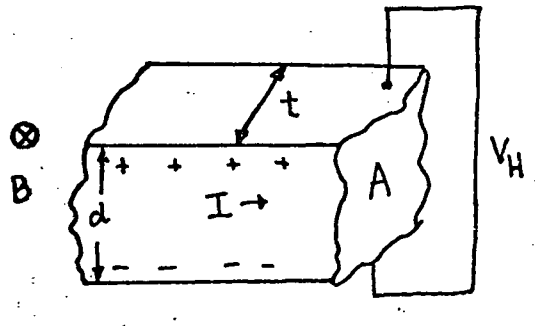

I = conventional current.

The force on the electrons due to the transverse field $(\frac{VH}{d})$ must be equal to the Lorentz force keeping the electrons at the lower face of the conductor.

$F_L = Bev$

$$\therefore \quad Bev = Ee = \frac{V_H e}{d}$$

$$\therefore V_H = Bvd$$

But $I = Nevd$ (N = number of electrons per unit volume, A = Area of cross section of conductor)

$$\therefore V_H = \frac{BI}{Net}$$

or $V_H \propto B$

Fig. 5.19 The Hall Effect

There is no direct interaction between the X-rays and the lattice. The diffraction occurs because of magnetostructive deformation of the lattice either side of domain walls. In the same way, crystal defects can be studied using variations in the diffracted beam. A distinct advantage of the technique is that it is essentially non-destructive and does not subject a sample to radiation damage. Further reviews can be found in TANNER and BOWEN (1980).

5.6 NEUTRON DIFFRACTION

By virtue of the fact that neutrons exhibit a wave nature, they undergo diffraction by a crystal lattice analagous to the Bragg diffraction of X-rays. Diffraction occurs when the wavelength of the neutrons (given by $\lambda = h/mv$ where λ = the de Broglie wavelength, h = Planck's constant, m = mass of the neutron and v is the velocity) is comparable to the interatomic spacing in crystals.

When incident neutrons interact with matter they can do so in two ways.

(i) interaction with an atomic nucleus.

(ii) interaction with atomic magnetic moments.

In (i), the intensity of the scattered beams is considerably less than that for X-rays. However, the amplitude of the scattering for neutrons is approximately the same for all atoms whereas that of X-ray

diffraction (due to interactions with electrons) depends upon atomic number. Also, because the scattering amplitude in neutron diffraction varies in an irregular way with atomic number, neutron diffraction makes it possible to distinguish between different elements within a sample.

In (ii), the neutrons are scattered by atoms possessing a net magnetic dipole moment. Although the neutron is electrically neutral it does possess a spin dipole moment. Because the nucleus can be considered to be a single point, the neutron nuclear scattering is isotropic with scattering angle θ. This is not so with neutron magnetic scattering and magnetic scattering modifies the total diffraction pattern due to (i) in a way which depends upon the kind of magnetic order present.

The magnetic contributions can be set apart from the nuclear scattering contributions by considering the characteristic ways in which they vary with the angles of incidence and diffraction. Figure 5.20 shows the variation in scattering as the angle of incidence changes.

The diffraction patterns obtained using neutron diffraction techniques on a paramagnetic material are different from those obtained using a specimen in a magnetically ordered state. In paramagnetic materials (including ferromagnetic and antiferromagnetic materials above their respective Curie and Néel points) the moments are randomly orientated. This gives a diffuse background due to entirely incoherent reflections of the neutron beam. A calculation is then made to obtain the scattering due to other effects and when this is subtracted from the background the magnetic scattering is obtained.

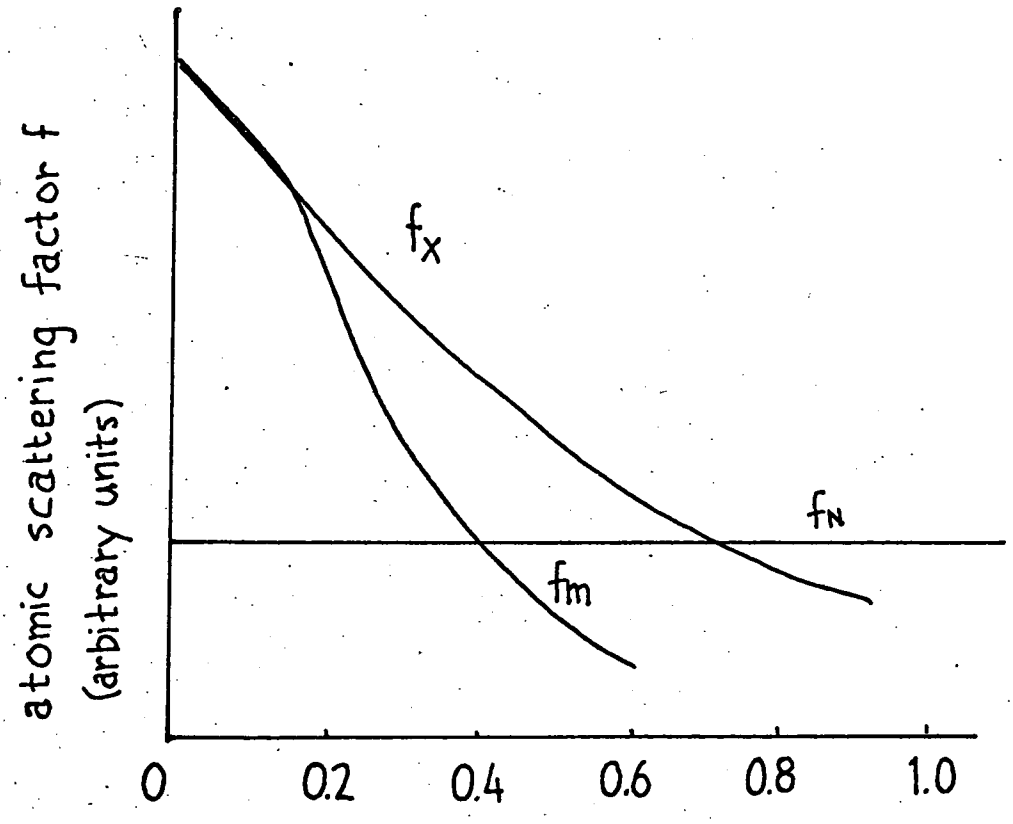

Fig. 5.20 Atomic scattering factors as a function of $\frac{\sin\theta}{\lambda}$

f_x = X-ray scattering factor.

f_N = neutron nuclear scattering factor

f_m = neutron magnetic scattering factor

f is defined as $\frac{\text{amplitude of wave scattered by atom}}{\text{amplitude of wave scattered by a free electron.}}$

When the moments are ordered, there is coherent reflection giving rise to lines in the diffraction pattern. In both cases above, coherent nuclear scattering still occurs. Hence, for the magnetically ordered case, there will be lines in the diffraction pattern due to the coherent nuclear scattering and also lines superimposed on this pattern due to the coherent magnetic scattering. The difference between these factors permits the magnetic scattering to be separated from the nuclear scattering. Consider, for example, an antiferromagnet. In an antiferromagnet the magnetic moments along a crystallographic direction alternate in direction from atom to atom. Hence the magnetic moment will see a crystallographic repeat distance twice that of the repeat distance for nuclear scattering. Hence the magnetic unit cell is larger than the chemical crystallographic cell. This will result in the lines due to magnetic scattering having different positions on the diffraction patterns than those due to nuclear scattering. For ferromagnetic order, superlattice reflections are not observed, but the relative intensities of the diffraction lines change on going from the paramagnetic to ferromagnetic phase. For a discussion on theory of neutron diffraction see MORRISH (1965).

Neutron beams used for diffraction purposes are usually obtained from nuclear fission reactors. The most abundantly available neutrons have a de-Broglie wavelength of about 1Å (For T = 293K λ = 1.49Å) which is the correct order of magnitude for diffraction to occur at the crystal lattice. The beam can be collimated. A monochromatic beam can be obtained using a single crystal e.g. LiF.and irradiating it with the neutron beam. Figure 5.21 shows, very simply, the principle involved in obtaining a monochromatic beam. When the beam makes an angle θ with

the crystal the diffracted beam will have a wavelength according to the equation

$$n\lambda = 2d \sin\theta$$

The wavelength selected will depend upon the lattice constant d.

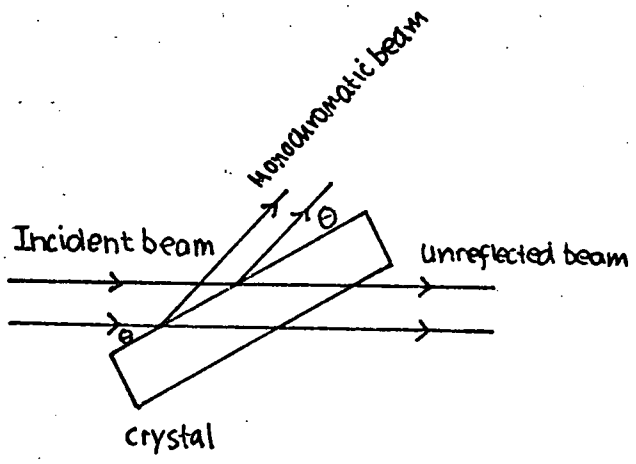

Fig. 5.21 Obtaining a monochromatic beam of neutrons

CHAPTER SIX

THE COLLOID TECHNIQUE

CHAPTER 6

THE COLLOID TECHNIQUE

6.1 THE COLLOID TECHNIQUE

The colloid technique was first suggested by BITTER (1931) and by VON HAMOS and THIESSEN (1931) independently. The basic principle of this technique is essentially the same as that of sprinkling iron filings around a bar magnet in order to examine the flux patterns. The method involves sprinkling a collection of fine magnetic particles over the specimen under examination. Any surface discontinuities, such as scratches or intersections with domain walls, results in stray fields being produced at the surface (Figure 6.1). This results in the aggregation of the fine particles at the points where the stray fields are strongest.

In 1932, Bitter used a suspension of ferric oxide in alcohol which he placed on the specimen. This technique proved more successful than his earlier attempts but did not result in the formation of an actual domain pattern. The reason for this is that the particle size was too large.

The technique requires a highly polished, plane, strain free surface. Mechanically polished specimens contain a strained layer which produces a pattern which is not representative of the domain structure pertaining under the conditions of observation. When there is a lot of surface stress, so called maze patterns result. As the technique is a very popular one, it has been refined by various workers. Because the procedure merely serves to produce an image of the field at the surface and as such may not represent fully the patterns due to the internal

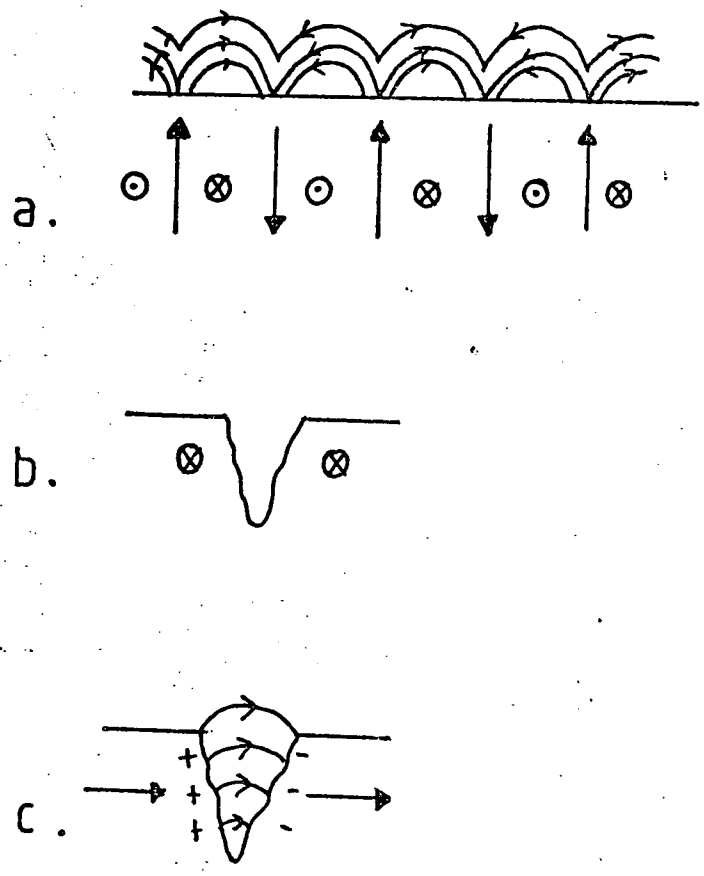

Fig. 6.1 The stray fields arising

a. at the intersection of domain walls at the specimen surface.

b. at crack where the magnetization is parallel to the crack.

c. at right angles to the crack.

domains, refinements were required in terms of surface preparation. Electrolytic and chemical polishing techniques have proved to be very useful when applied to strain free samples. Elmore (1937, 1938) polished the strained layers from cobalt and iron surfaces and produced patterns which did represent domain configurations. Craik (1956) and Garrood (1962) have produced particles of 100 Å diameter using this, so called, wet colloid technique.

Among the disadvantages of this wet colloid technique is the fact that staining of the surface occurs when the colloid is left on the surface for any length of time. Garrood overcame this by isolating the surface from the colloid by means of a transparent film. Another disadvantage is the restriction imposed on the temperature range of application by the freezing point of the colloid. The technique is inapplicable to those ferromagnetic materials with Curie temperatures lower than the freezing point of the colloid. The colloid technique in general represents a simple and very versatile method of domain observation and there are many variations on the technique. In order to overcome the problem of the colloid freezing at low temperatures dry colloid methods are used. Again, the process is that of depositing a fine powder of magnetic particles on the surface in order to delineate the surface flux distribution. There are many specific geometries existing within the range of apparatus assemblies and in applying the method the design of the apparatus must include considerations such as:

a) temperature control of the sample (i.e. the sample must be cooled below its Curie temperature and very often the sample must be heated in order to vary its temperature within a specific range of interest.)

b) method of deposition of the particles

c) application of magnetic fields both for domain contrast and domain wall movement.

d) the monitoring of the sample temperature.

e) the method by which the domains are to be viewed.

One such arrangement is to be described in detail here as it was this arrangement which was used to obtain data for this thesis.

First it will be relevant to discuss the conditions and mechanism of pattern formation.

6.2 THE MECHANISM OF PATTERN FORMATION

When magnetic particles are used to form domain patterns they are subjected to two magnetic fields. These two fields influence the distribution of the particles.

(i) the field due to their own magnetic moment.

(ii) those stray fields around the surface of the crystal.

6.2.1 Upper Limit for Particle Diameters.

Consider (i) The fields of each particle tends to make the particles form aggregates in order to make the flux self enclosed. (Figure 6.2)
When this happens the magnetic moment of the aggregate is too low for it to take part in pattern formation.

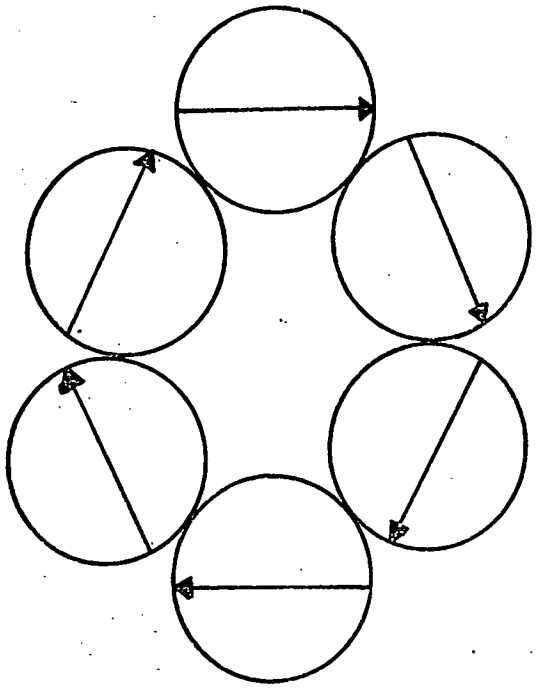

Fig. 6.2 Aggregate of magnetic particles minimizing external flux.

For a single spherical domain particle the magnetic moment is given by

$$\mu = \frac{\pi d^3 Is}{6}$$

where d = diameter of particle

Is = magnetization

The field between adjacent particles is given by

$$H \approx 2\mu/d^3$$

and the condition for particle aggregation is satisfied when

$$\mu H > 3KT$$

$$\therefore \frac{\pi d^3 Is}{6} \cdot \frac{2\pi d^3 Is}{6d^3} > 3KT$$

$$\therefore d^3 > \frac{(27 \times 2KT)}{\pi^2 Is^2}$$

or

$$d > 3\left[\frac{(2KT)}{(\pi^2 Is^2)}\right]^{1/3} \qquad (6.1)$$

From equation 6.1 it can be seen that if the particles in the colloid exceed a diameter of $3(2KT/\pi^2 Is^2)^{1/3}$ then they will form aggregates accompanied by a reduction in magnetic moment of the whole.

Hence the condition for an upper limit of particle size for the formation of domain patterns is

$$d < 3\left[\frac{(2KT)}{(\pi^2 Is^2)}\right]^{1/3} \qquad (6.2)$$

6.2.2 Lower Limit for Particle Diameters

$$\mu H > 3KT$$

$$\frac{\pi d^3 IsH}{6} > 3KT$$

where H is the magnitude of the field at the specimen surface.

KITTEL (1949) estimated the magnitude of this field H_w at a distance above 180^o domain walls.

$$H_w = \frac{2I_w \delta_w}{r} \qquad 1 \frac{2}{+ \mu_w^*}$$

I_w = spontaneous magnetization of specimen

δ_w = domain wall thickness

$$\mu_w^* = \frac{1 + 2\pi I_w^2}{K_w}$$

where K_w = magnetocrystalline anisotropy of the specimen.

From this Bergmann deduced that the value for the lower limit of particle diameter which would result in a domain pattern is given by

$$d_w = 3\left[\frac{KT(1 + \mu_w^*)}{2\pi I_s I_w \delta_w}\right]^{1/2} \qquad (6.3)$$

Hence for the formation of a pattern the particle diameter must lie between

$$3\left(\frac{2KT}{\pi^2 I_s^2}\right)^{1/3} \quad \text{and} \quad 3\left[\frac{KT(1+\mu_w^*)}{2\pi I_s I_w \delta_w}\right]^{1/2}$$

Calculations were performed for iron and nickel using the appropriate values of Is, Iw and Kw (ie K_4) where Iw refers to the spontaneous magnetization of the sample (terbium) with temperature.
Kw represents the magnetocrystalline anisotropy constant K_4 for terbium.

Table 6.1 gives the data for iron.

Figure 6.3 gives the graphs of upper and lower particle size for domain patterns on terbium using iron vapour.

The curves in Figure 6.3 show maximum and minimum particle diameter versus temperature. Where the curves overlap enclose the region where particle diameter is suitable for domain pattern formation.

Table 6.2 gives the data for nickel particles.

Figure 6.4 shows curves for maximum and minimum particle diameter versus temperature for nickel particles deposited on terbium.

6.3 DRY COLLOID APPARATUS USED FOR THIS THESIS

Figure 6.5 shows the dry colloid apparatus due to SMITH, CORNER and TANNER (1980). This apparatus was the apparatus used to obtain domain patterns on a terbium single crystal. The apparatus design involving the cold finger arrangement allowed the construction of a very slim brass chamber which could be fitted between the pole pieces

Temperature (K)	Magnetization I_s emu cc^{-1}	Maximum size particle diameter $d_w = 3\left(\frac{2KT}{\pi^2 I_s^2}\right)^{1/2}$ (cm)	$K_4 \times 10^6$ erg/cc	Magnetization of specimen I_w emu/cc	$\mu_\omega^* = 1 + \left(\frac{2\pi I_w^2}{K_w}\right)$	δ_w = domain width (cm)	Minimum size particle diameter $d = 3\left[\frac{KT(1+\mu_\omega^*)}{2\pi I_s I_w \delta_w}\right]^{1/2}$ (cm)
4.2	1752	10×10^{-8}	2.96	2640	15.8	1.5×10^{-6}	4.5×10^{-8}
25	1752	18×10^{-8}	2.80	2620	16.4	1.75×10^{-6}	10.3×10^{-8}
50	1752	23×10^{-8}	1.6	2560	26.7	2.06×10^{-6}	17.2×10^{-8}
60	1750	24×10^{-8}	1.26	2540	33.2	2.3×10^{-6}	19.9×10^{-8}
77	1752	26×10^{-8}	1.2	2480	33.2	2.36×10^{-6}	22.5×10^{-8}
100	1750	29×10^{-8}	0.53	2400	69.3	3.5×10^{-6}	30.7×10^{-8}
150	1740	33×10^{-8}	0.13	2130	220.3	0.7×10^{-3}	50.3×10^{-8}
210	1720	38×10^{-8}	6.6×10^{-3}	1510	2.2×10^3	3.2×10^{-5}	104.8×10^{-8}
290	1707	42×10^{-8}	-	0	-	-	

Table 6.1 Data for deposition of iron colloid particles on terbium.

dotted curve = minimum particle size versus temperature.

continuous curve = maximum particle size versus temperature.

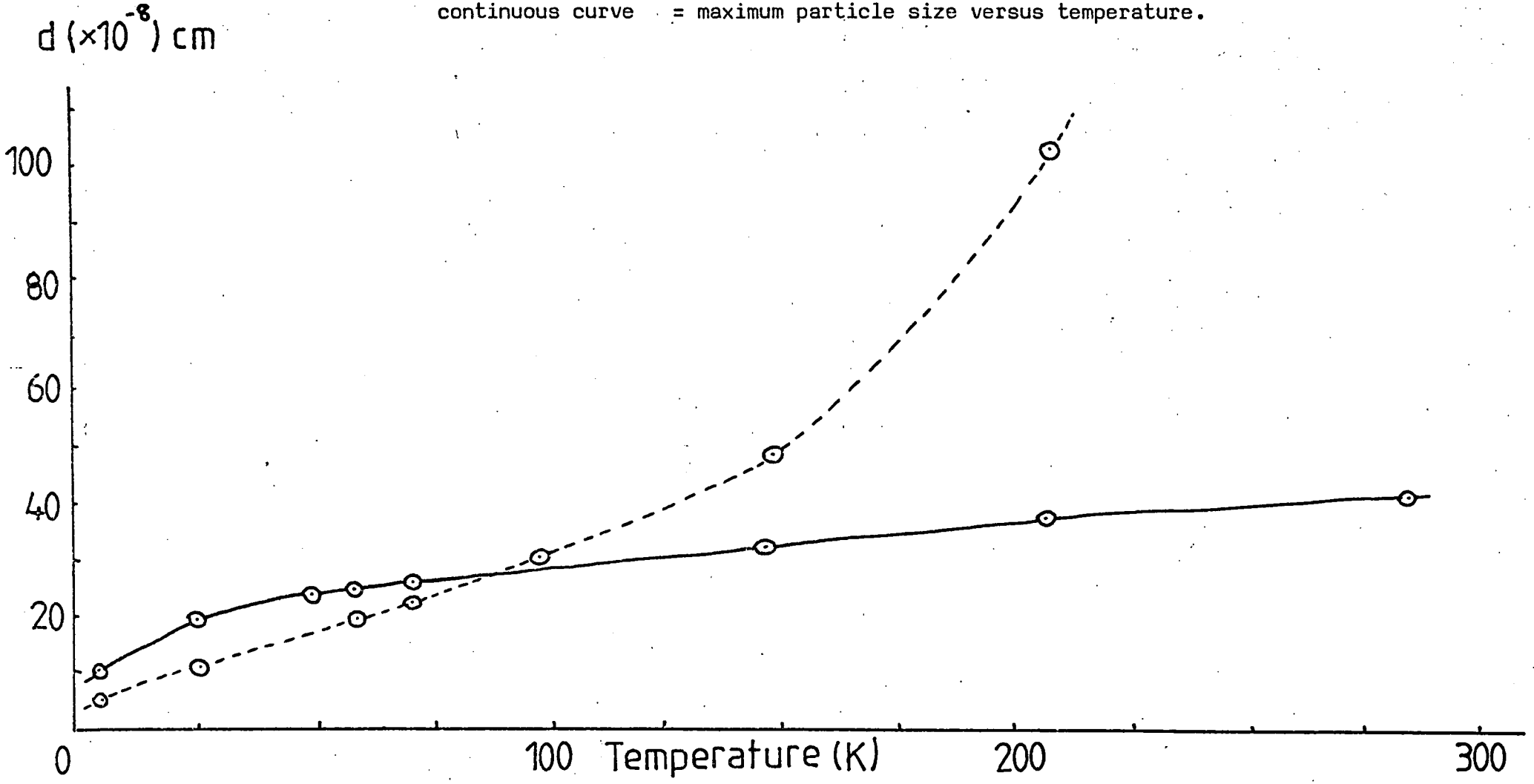

Fig. 6.3 Curves for iron colloid particles deposited on terbium.

Temperature (K)	Magnetisation I_s emu/cc	Maximum size particle diameter $d_w = 3\left(\frac{2kT}{\pi^2 I_s^2}\right)^{1/3}$ (cm)	$K_4 \times 10^6$ erg/cc	Magnetisation of specimen I_w emu cc^{-1}	$\mu_w = 1 + \left(\frac{2\pi I_w^2}{K_w}\right)$	δ_w = domain width (cm)	Minimum size particle diameter $d = 3\left[\frac{kT(1+\mu_w^*)}{2\pi I_s I_w \delta_w}\right]^{1/2}$
4.2	510	23×10^{-8}	2.96	2640	15.8	1.5×10^{-6}	8.3×10^{-8}
25	510	41.7×10^{-8}	2.20	2620	16.4	1.7×10^{-6}	19.5×10^{-8}
50	510	52.5×10^{-8}	1.6	2560	26.7	2.06×10^{-6}	31.9×10^{-8}
60	510	55.8×10^{-8}	1.26	2540	33.2	2.3×10^{-6}	36.9×10^{-8}
62.5	510	56.6×10^{-8}	-	-	-	-	-
77	509	60.7×10^{-8}	1.2	2480	33.2	2.37×10^{-6}	41.7×10^{-8}
100	508	66.4×10^{-8}	0.53	2400	69.3	3.57×10^{-6}	56.5×10^{-8}
125	506	71.7×10^{-8}	-	-	-	-	-
150	504	76.4×10^{-8}	0.13	2130	220.3	7.2×10^{-6}	92×10^{-8}
188	502	82.5×10^{-8}	-	-	-	-	-
210	500	85.9×10^{-8}	6.6×10^{-3}	1510	2.2×10^{3}	3.2×10^{-6}	194.5×10^{-8}
251	493	92.0×10^{-8}	-	-	-	-	-
314	475	101.7×10^{-8}	-	-	-	-	-

Table 6.2 Data for deposition of nickel colloid particles on terbium.

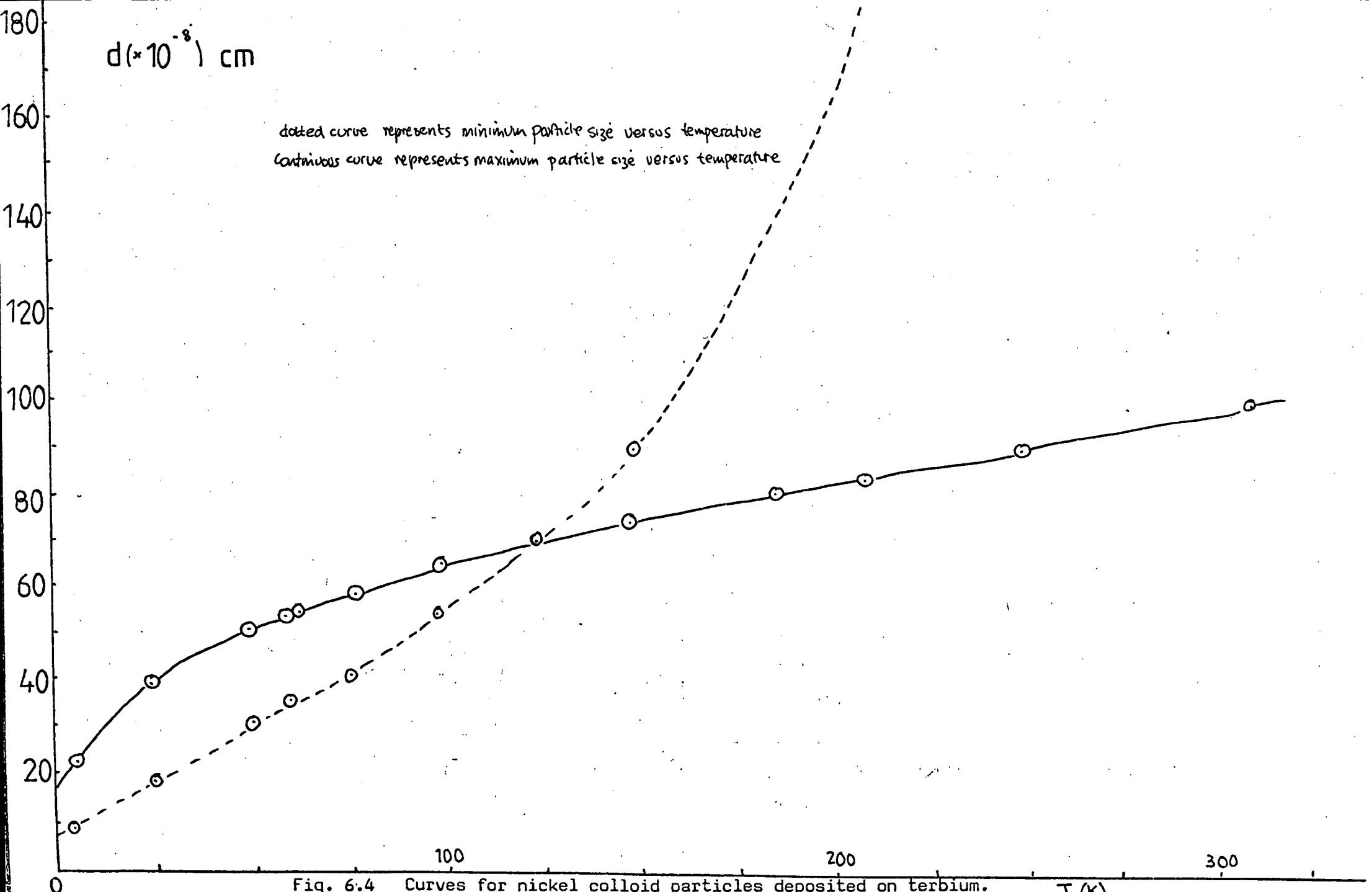

Fig. 6.4 Curves for nickel colloid particles deposited on terbium.

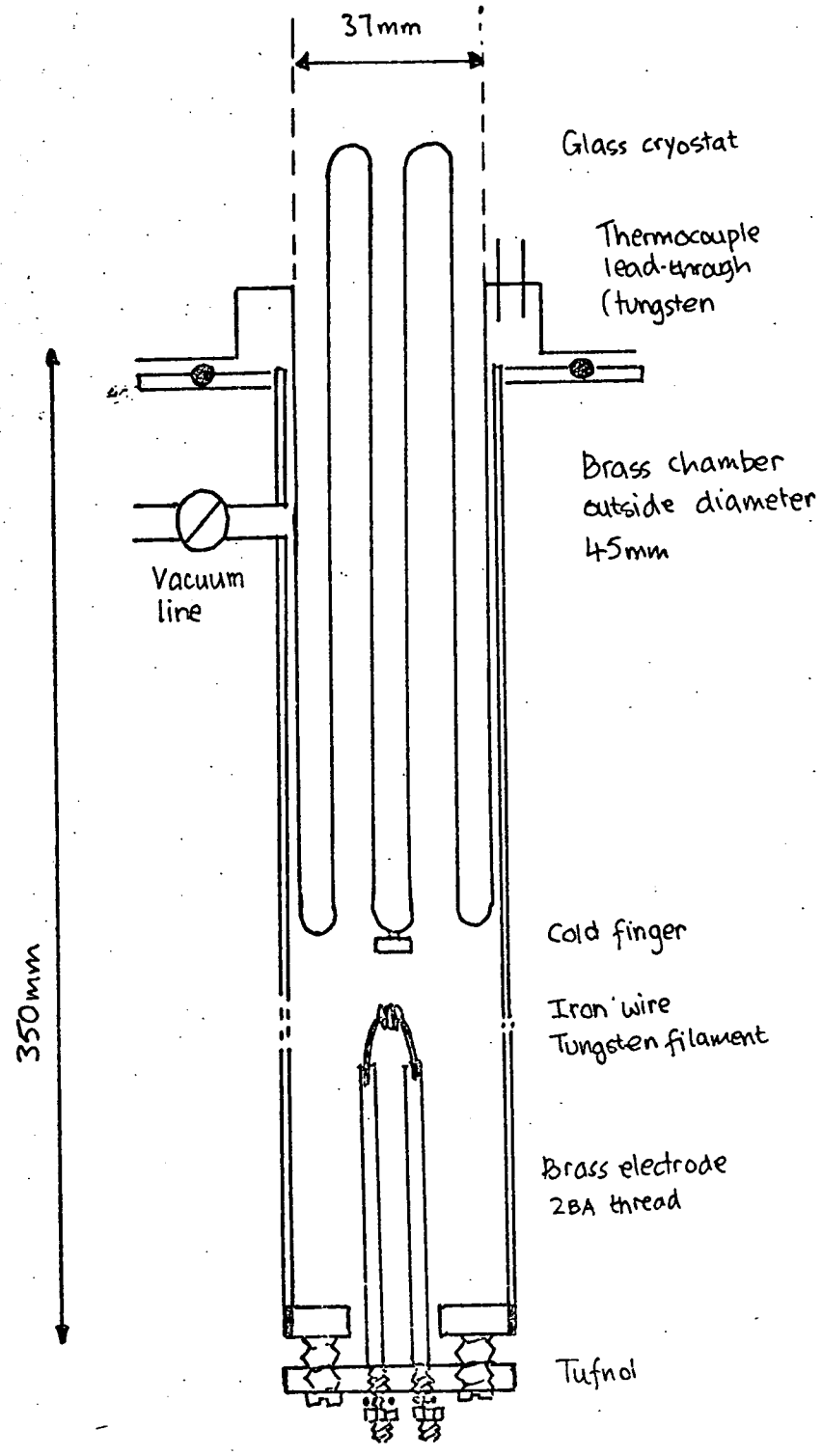

Fig. 6.5 Dry colloid apparatus (SMITH CORNER and TANNER (1980))

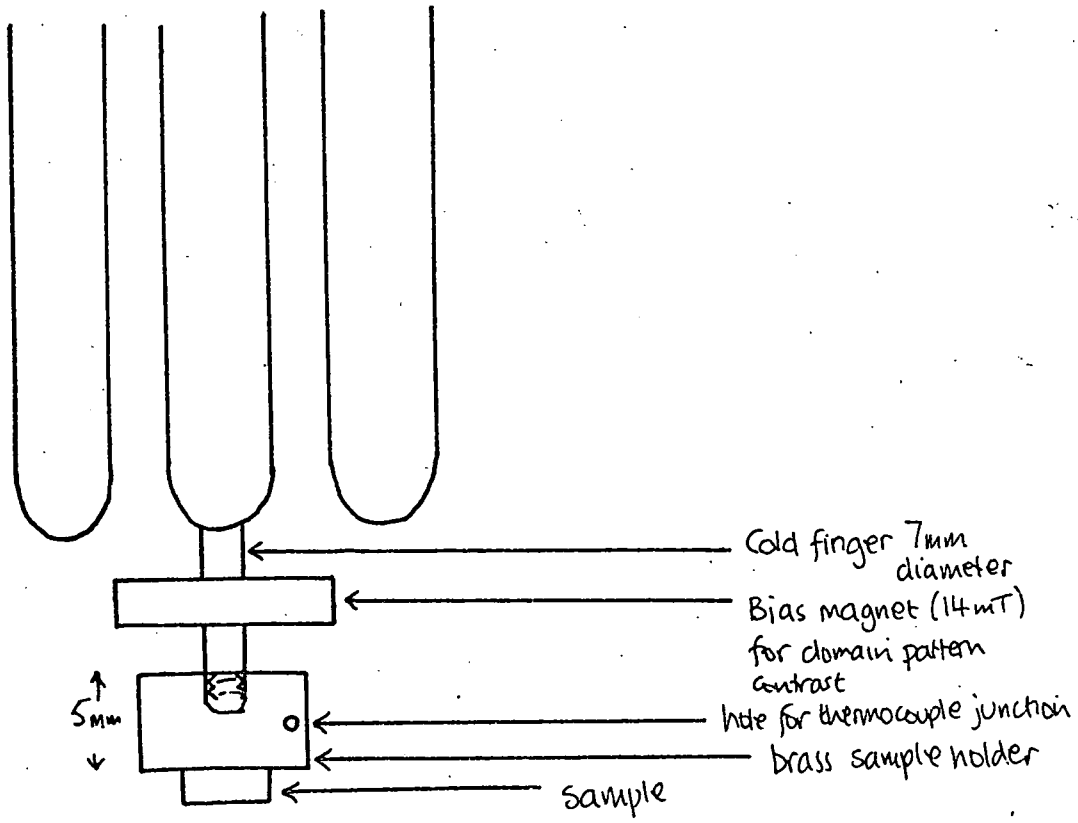

Fig. 6.6 Cold finger with bias magnet and sample holder assembly.

of a magnet, if so required, thus allowing the application of a large external field.

The specimen itself was mounted with Durafix on a brass sample holder in which a hole was drilled to take the hot junction of a copper constantan thermocouple. The temperature was read using a NORONIX NTM 3 temperature meter. During a typical run, iron wire of 0.027 cm diameter and 99.99% purity was evaporated onto the surface of the sample which was mounted upside down onto the cold finger. Previous apparatus, notably due to Herring and Jakuboviks (1973) and Saad (1977) had the samples underneath the evaporating system. This arrangement required temperature stability for a period of time to allow the colloid to settle. The apparatus due to Herring and Jakuboviks is shown in Figure 6.7. The best source for the evaporation was a V shaped tungsten wire of 0.1 cm diameter and 99.97% purity. This was push fitted into holes drilled into the two brass electrodes which were fitted into the chamber. To facilitate cleaning of the chamber and to allow the fitting of a new filament for each run, the electrode assembly was fitted to a tufnol base which was screwed onto the base of the chamber (a rubber O ring between the two). The iron wire was first cleaned (by scraping off the outer layers using pliers) and then wrapped around the tungsten filament as shown in Figure 6.5. The glass cryostat and cold finger assembly was then placed into the chamber and the evaporation sequence started by evacuating the chamber. Using a rotary backing pump and a diffusion pump with a liquid nitrogen trap, the chamber pressure was taken to $\sim 10^{-6}$ torr. Liquid nitrogen was also poured into the double walled glass cryostat in order to cool the sample.

The evaporation temperature was reached by taking the sample to the lowest temperature attainable using the rig and then allowing the temperature to rise to that required. The design of the rig would allow the inclusion of non-inductively wound heating coils at the side of the sample in order to control the temperature, but this was not done as the method previously described did not prove too inconvenient.

The evaporation was carried out using helium as the transport gas. The optimum pressure was found to be 1.5 torr. The introduction of this gas into the rig had two adverse effects. Firstly, if the gas was introduced after the sample had been cooled, the gas warmed up the rig. Secondly, irrespective of whether the gas was introduced prior to or after cooling, the conduction properties (convection and conduction) of the helium meant that the lowest temperature attainable was less than that attainable in the absence of the gas. This was overcome (when temperatures of less than about 120k were desired) by using a polystyrene (liquid hydrogen filled) dewar to surround the rig chamber. Low temperature work involved a few problems. Firstly, when the evaporation of the iron was carried out (by passing a large current through the tungsten filament) the transport properties of the gas was very efficient. This led to the problem of depositing too much iron onto the crystal surface. To overcome this a wire mesh was introduced mid way between the sample and the filament (after SMITH et al). This reduced the amount of iron deposited onto the sample. The mesh arrangement consisted of 0.5 x 0.5 mm copper mesh mounted on a plastic tube which gave a snug fit inside the chamber. Secondly, when the current was passed through the filament the gas warmed up locally and the deposition temperature started to rise. As the deposition duration was 15 seconds this meant that the temperature rose by a few degrees

as the deposition was carried out. Hence for a particular domain pattern the temperature was taken as an average over a small range of temperatures. Thirdly, when the steady state conditions had been reached the reading on the temperature meter fluctuated considerably. It was decided that this was due to the cold nitrogen vapour wafting over the contacts which connected the thermocouple to the outside circuitry. As these contacts were in the proximity of the cryostat liquid nitrogen trap there was little which could be done to prevent the nitrogen vapour from reaching these contacts. After achieving some stability by covering the contacts with small polystyrene blocks, it was decided to replace the thermocouple by a diode. This had the added advantage of robustness as the copper constantan thermocouple junction was prone to snapping owing to the number of times it was moved in and out of the hole in the sample holder (the thermocouple was kept in place by a plasticine plug). The diode chosen was a Lake Shore DT500K silicon diode. Because the junction resistance of a pn diode varies with temperature the junction voltage of a pn diode through which a constant current flows will vary with temperature in a similar way to the resistance temperature variation. Hence the forward voltage V_F of the diode could be used to indicate temperature. The relationship between V_F and T varies with the type of diode used. For a review on temperature dependence of diodes see NOTO and HEUBENER (1978). Figure 6.8 shows the V_F/T curve for the DT500K diode (Lake Shore Cryogenics Bulletin LB11-72-1) as given by Noto and Heubener.

So that the temperature indicated by the diode represented the sample temperature, the diode was mounted as close to the sample as possible. This meant constructing a new sample holder. A brass sample holder was constructed, on the side of which was a tapering groove into which the

diode could be slotted. Covering the top of the diode with a layer of grease improved the thermal contact. Figure 6.9 shows the diode and the sample holder. After each deposition the chamber and contents were cleaned thoroughly to avoid contamination of the sample. A new filament was used each time.

6.3.1 Calibration of the diode

The diode was calibrated by checking the voltage across the junction at two temperatures and drawing a straight line between these two points. The forward voltage of the diode bore a linear relationship with temperature over the range of temperatures of interest (as shown in Figure 6.8). For this reason only two calibration points were required and these were chosen to be liquid nitrogen temperature (77K) and room temperature. Room temperature was obtained using a sensitive mercury in glass thermometer and frequent checks were made on the calibration curve. The constant current source used for the preliminary series of depositions was constructed as per Figure 6.10. This constant current source was used in conjuntion with an Avo digital multimeter to provide the necessary metering for the diode thermometry. Later a MERIC constant current source was used which provided a current of 100 μA . A digital panel voltmeter was used. Figure 6.11 shows the diode calibration curve using the Meric source.

6.3.2 Conditions for evaporation

To successfully obtain a deposition of iron vapour onto the sample, which would illustrate the domain patterns, requires optimisation of several

parameters. Transport gas pressure is important as is the magnitude and duration of the heater current. Initial depositions were carried out using a discarded silicon-iron sample. The power source providing the heating current was a mains rectified d.c. source designed to deliver up to 120A at 5v controlled by a Variac transformer. After many attempts using different currents for varying time durations, good contrast domain patterns were obtained by delivering 50A for 15 seconds to the tungsten filament. The length of iron wire evaporated was usually 7 cm, although 10 cm lengths were used on a few occasions. It was found that a height of about 20 cm was most suitable for the tungsten filament (i.e. the height referred to is distance from the brass electrodes to the top of the filament V with the filament in place. (See Figure 6.12). The helium transport gas pressure was 1.5 torr.

Just above the sample, a ferrite magnet of field strength 14 mT was fitted to the cold finger. This magnet provided a vertical bias field which aided contrast. It was found that using the bias magnet, domain patterns were obtained at all temperatures of interest, whereas, without the bias magnet, domain patterns were only obtained at low temperatures according to the calculations in Section 6.2.1 and 6.2.2. (See Figures 6.3 and 6.4).

The domain patterns obtained and the experimental conditions are discussed in Chapter 7.

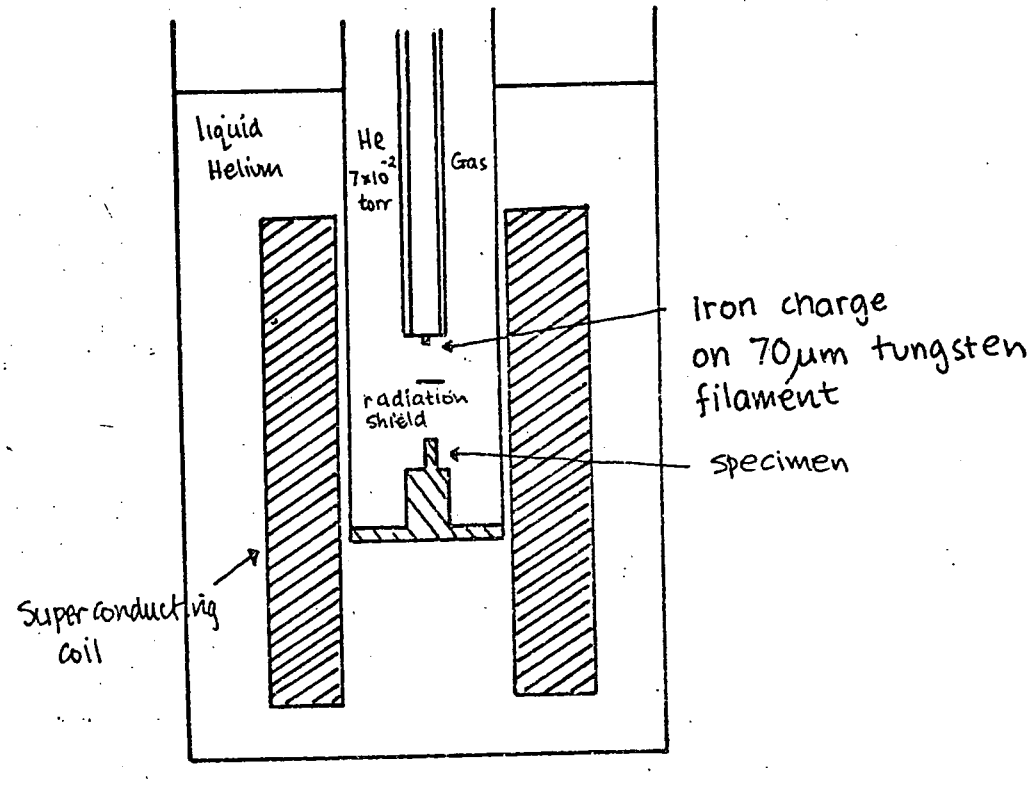

Fig. 6.7 Schematic diagram of the evaporation unit used by Herring and Jakubovics (1973).

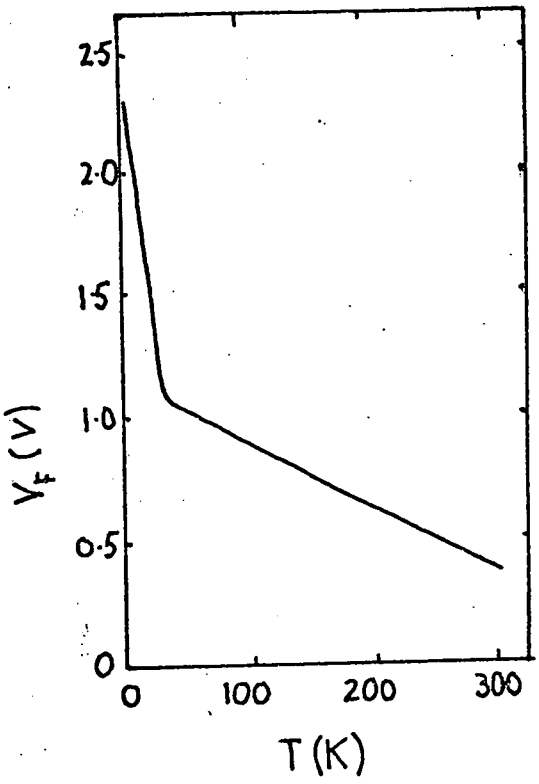

Fig. 6.8 Temperature dependence of forward voltage V_F, in Lake Shore DT 500K silicon diode. (NOTO and Huebener (1978)).

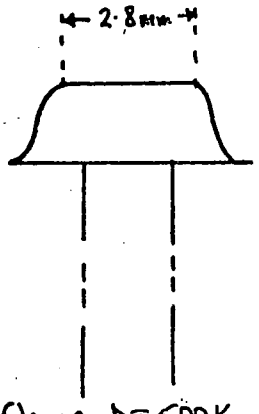

a. Lake Shore DT500K diode

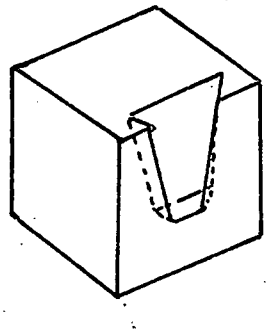

b.

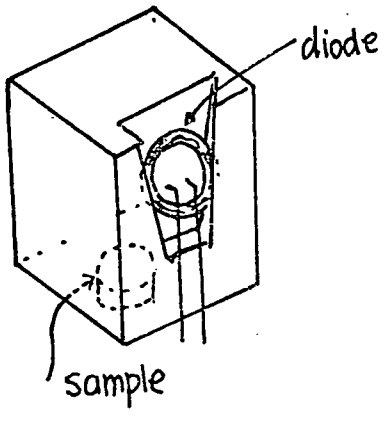

c.

Fig. 6.9 Diode and sample holder.

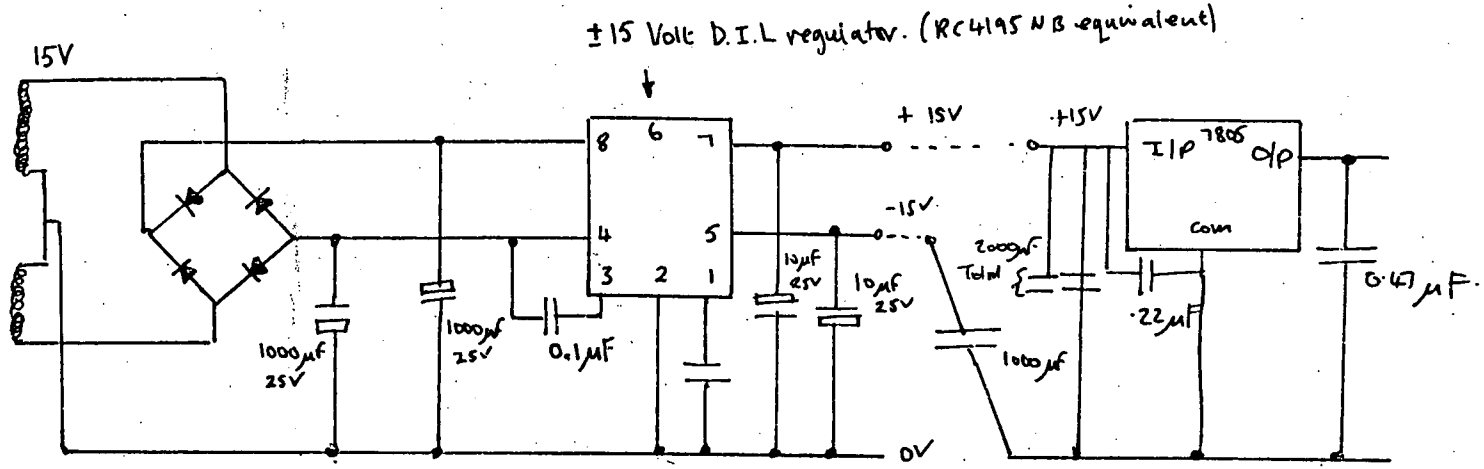

Fig. 6.10 Constant current source used for preliminary depositions to optimize deposition conditions.

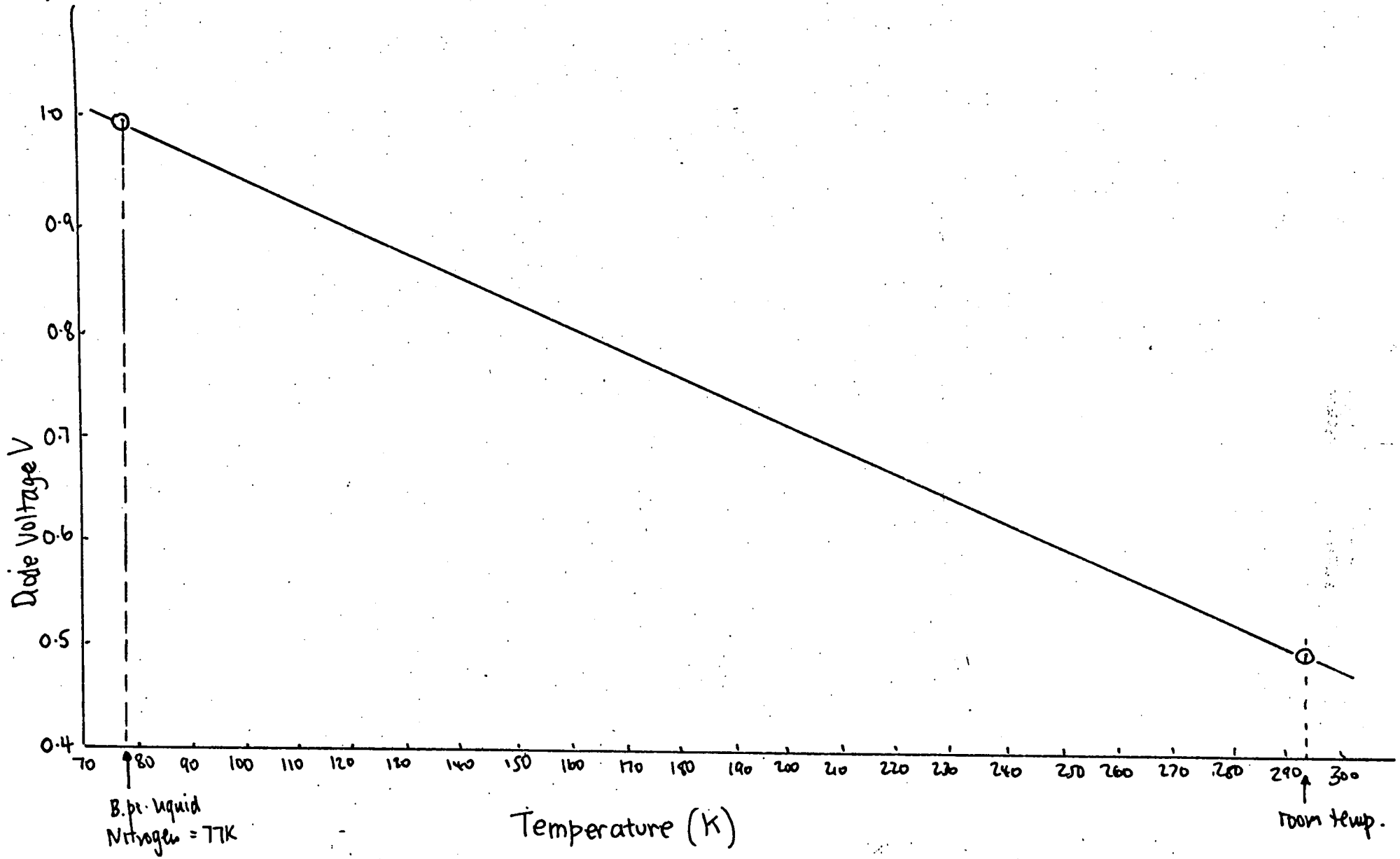

Figure 6.11 Calibration of Lake shore diode (DT500K.) (silicon).

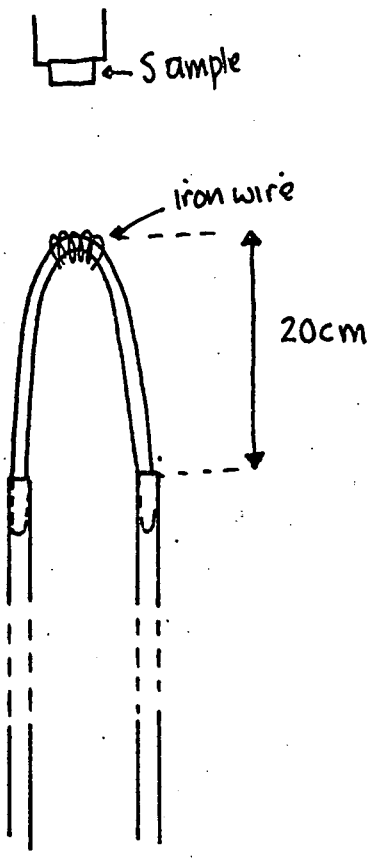

Fig. 6.12 Filament height

CHAPTER SEVEN

MAGNETIC DOMAIN STRUCTURES IN TERBIUM SINGLE CRYSTALS

CHAPTER 7

MAGNETIC DOMAIN STRUCTURES IN TERBIUM SINGLE CRYSTALS

7.1 INTRODUCTION

The sample used for domain structure studies was a single crystal of 99.99% pure terbium grown by electron beam float zone melting in ultra high vacuum. The sample was cut by electro-spark erosion in order to avoid stressing. Figure 7.1 shows the sample dimensions and c- axis orientations. The sample was in the form of a circular disc 1.5 mm thick and 5 mm in diameter. The orientation was such that the c- axis made an angle of 14^{o} with the specimen surface and a b-axis made an angle of 7^{o} with the surface.

Domain structures were studied as a function of temperature using the dry colloid apparatus described in Chapter Six. Typical photographs are shown in Figures 7.2 and 7.3. These photographs show domain patterns at temperatures of 180K and 100K respectively. The high magnetocrystalline anisotropy in terbium confines the magnetization to the b- axis and Figures 7.2 and 7.3 are typical of results on polished unstrained specimens.

The crystal polish used at first consisted of 50% glacial acetic acid with 50% nitric acid and the polishing was followed by a methanol wash. While this process produced a highly polished surface, tarnishing occurred rapidly after the residual polish had been washed from the surface and the surface had dried. This problem of tarnishing was overcome by polishing with 25:25:50 acetic acid, nitric acid, methanol, followed by a methanol

wash. It proved expedient to keep the sample in methanol after the wash, until it was to be inserted into the dry colloid chamber. (i.e. the sample did not tarnish in air when it was kept wet with methanol). The sample was mounted on the brass holder with durofix and the fact that methanol is a solvent for durofix did not cause any problems because, although the time between polishing the sample and inserting it into the chamber was large enough to cause tarnishing of the dry sample, the actual time the sample was wet with methanol was not long enough for the durofix to dissolve.

7.2 DOMAIN PHOTOGRAPHS

The photographs of the domain patterns were taken with a Praktica camera used in conjunction with a Vickers M17 microscope. The general method used was to scan the crystal surface photographing any area showing a domain pattern. Figures 7.4 to 7.12 show contact prints of scans showing domain patterns at various temperatures.

Table 7.1 shows the conditions for each deposition. Several graticule photographs have been included to give the contact prints scale. The graticule was a 1mm mark graduated at 0.01 intervals.

The domain spacings obtained experimentally are discussed in section 7.4.

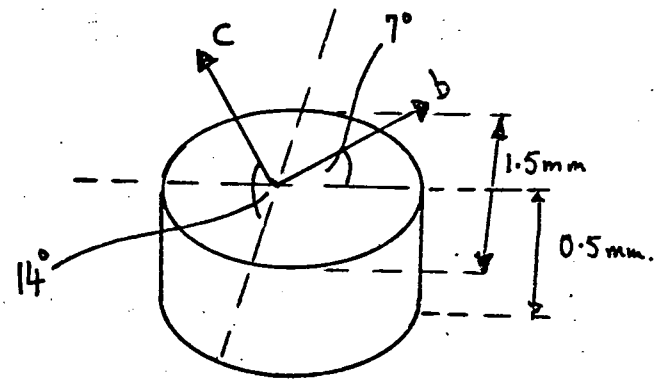

Fig. 7.1 Terbium sample used to study domain structures.

Fig 7.2

Domains in terbium at 180K

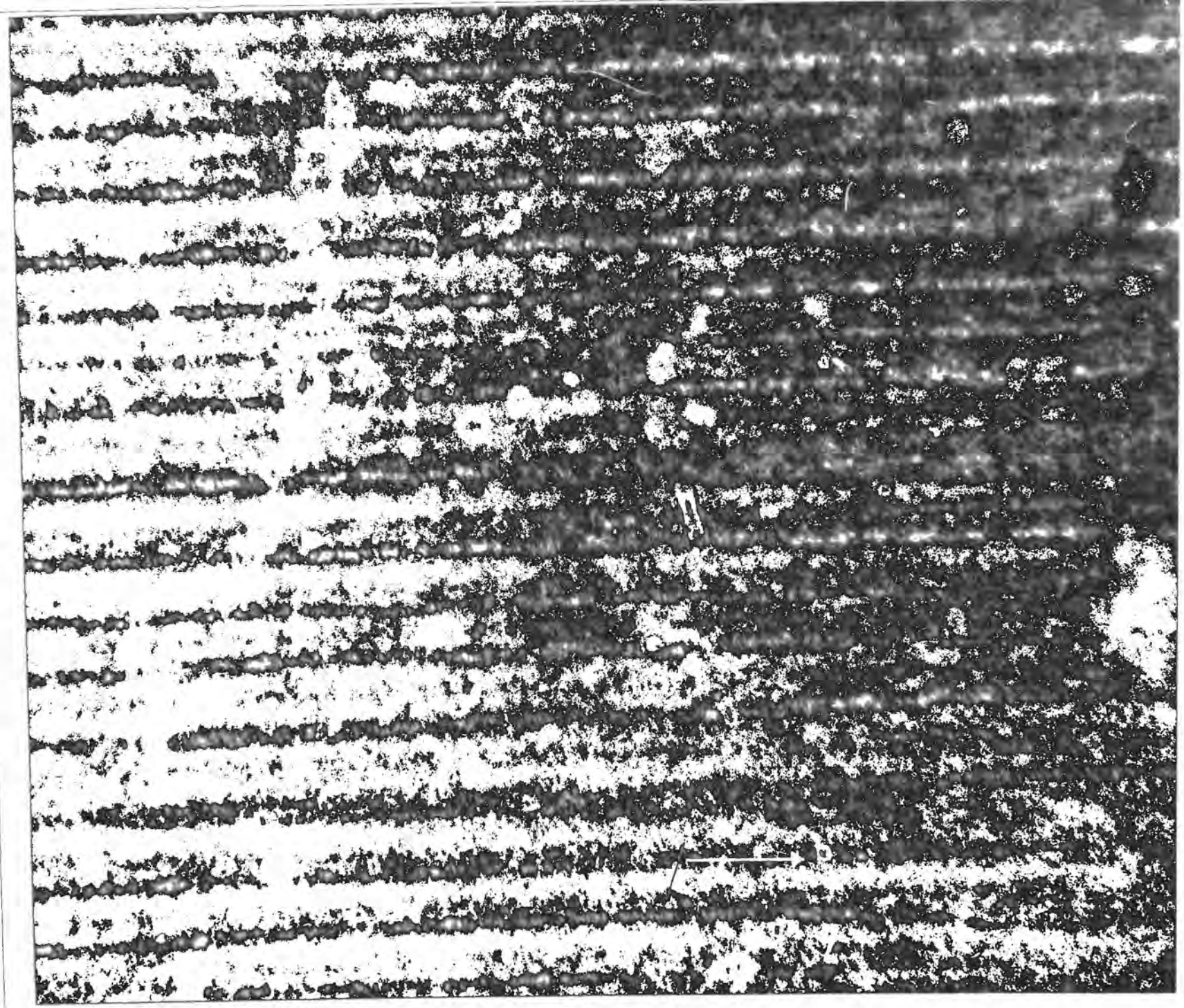

Fig 7.3 Domains in terbium at 100×

Figure	Temperature	Condition of deposition (all at 50A for 15 sec)		
	K $\pm$ 2	pressure	Filament height	Length of iron wire.
7.4	95K	1.5 Torr	20 mm	7 cm
7.5	100K	1.5 Torr	20 mm	7 cm
7.6	118K	1.5 Torr	20 mm	10 cm
7.7	150K	1.5 Torr	20 mm	7 cm
7.8	180K	1.5 Torr	20 mm	8 cm
7.9	"	"	"	"
7.10	199K	1.5 Torr	20 mm	7 cm
7.11	215K	1.5 Torr	20 mm	7 cm
7.12	224-228K	1.5 Torr	20 mm	9 cm

Table 7.1

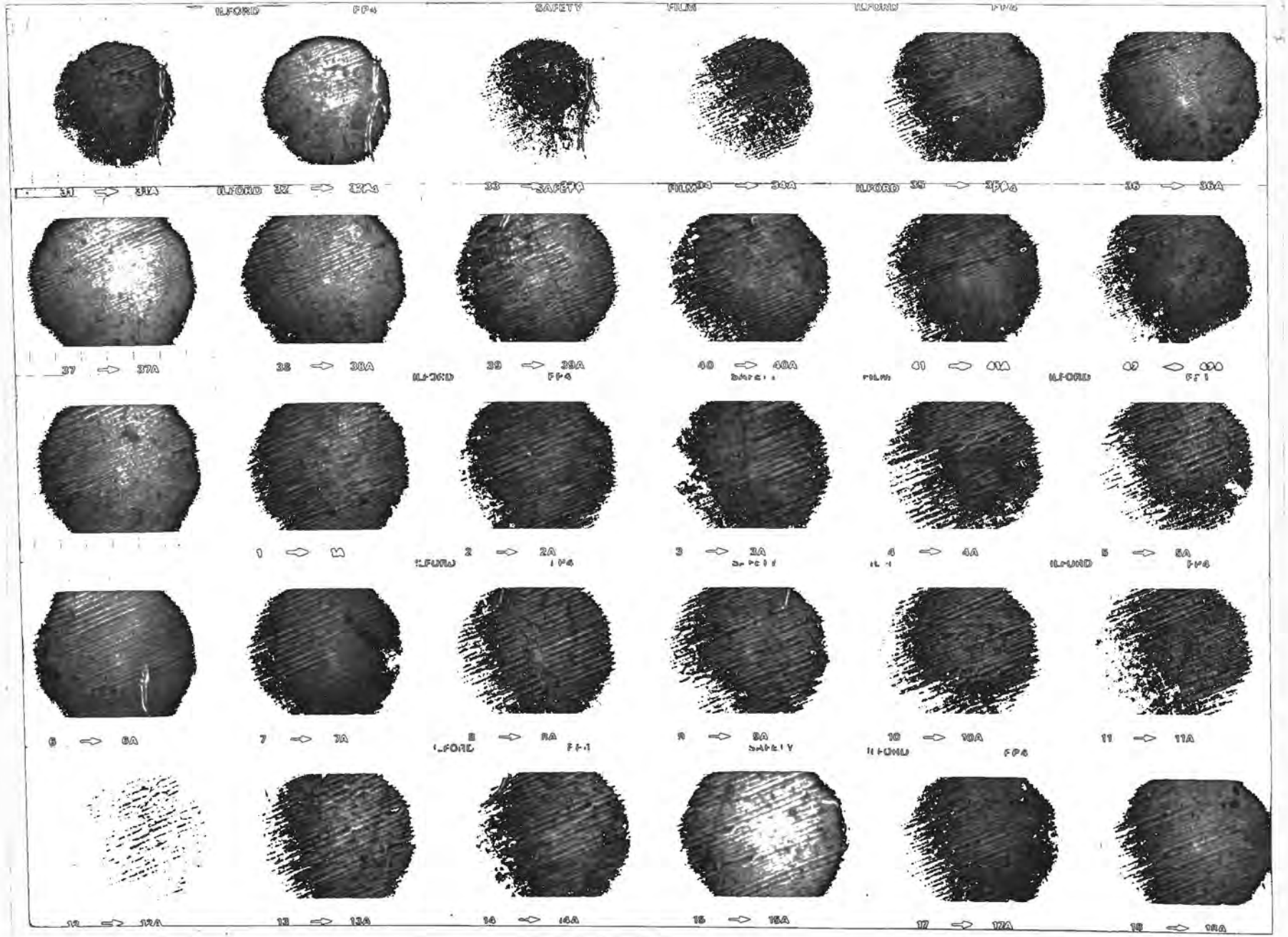

Figure 7.4

Magnetic domains in terbium at 95K

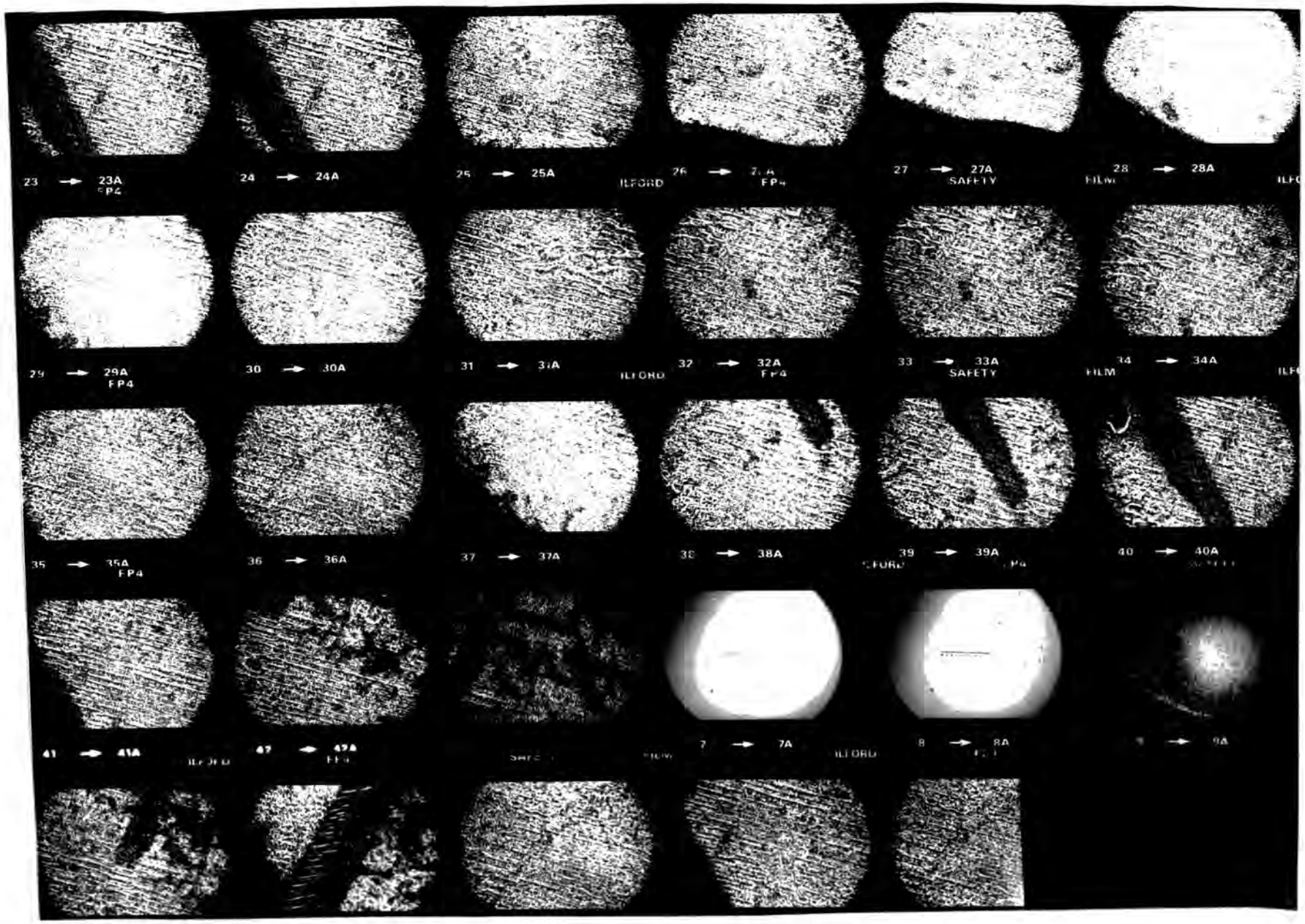

Figure 7.5
Magnetic domains in terbium at 100K

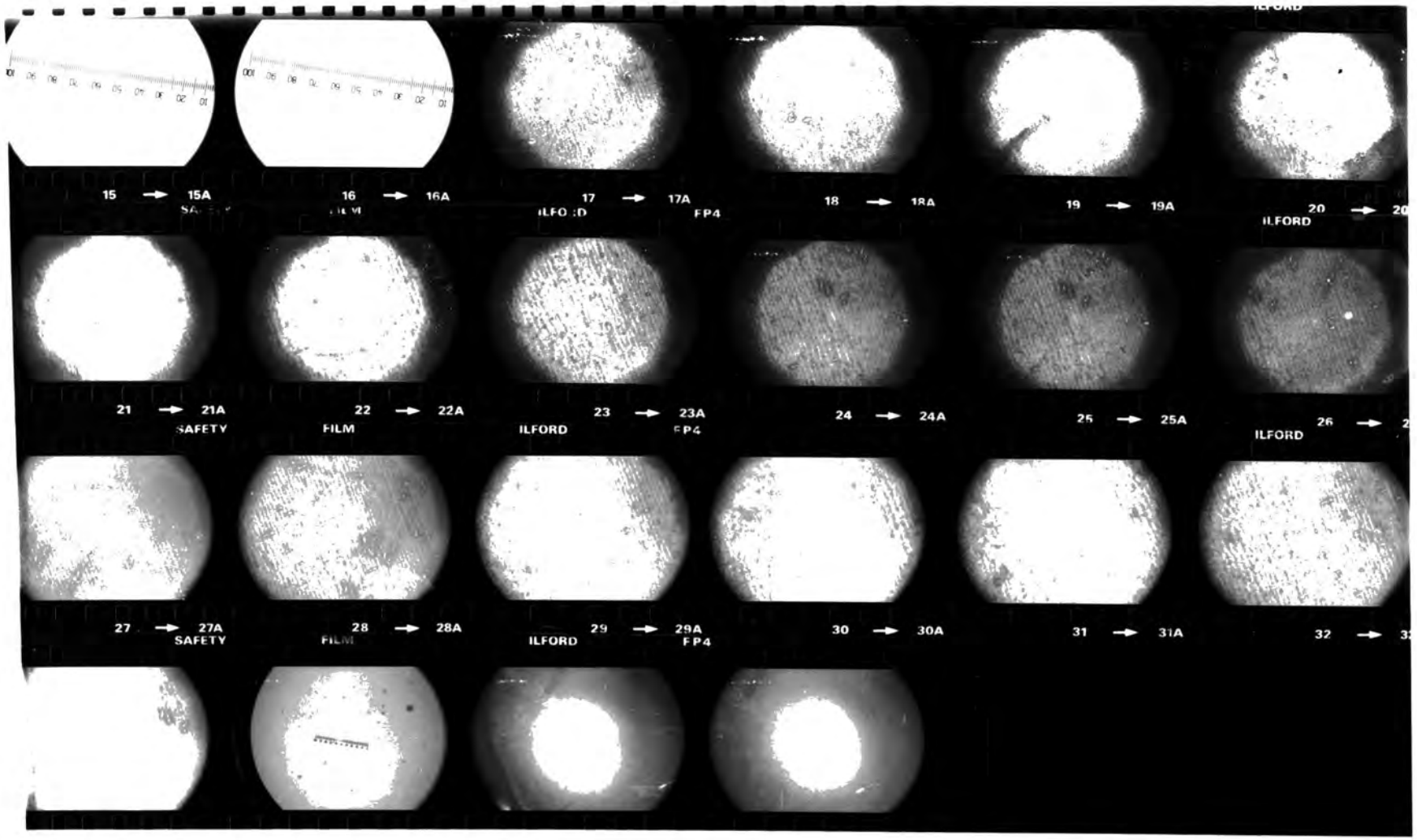

Fig 7.6 Domains in terbium at 118K.

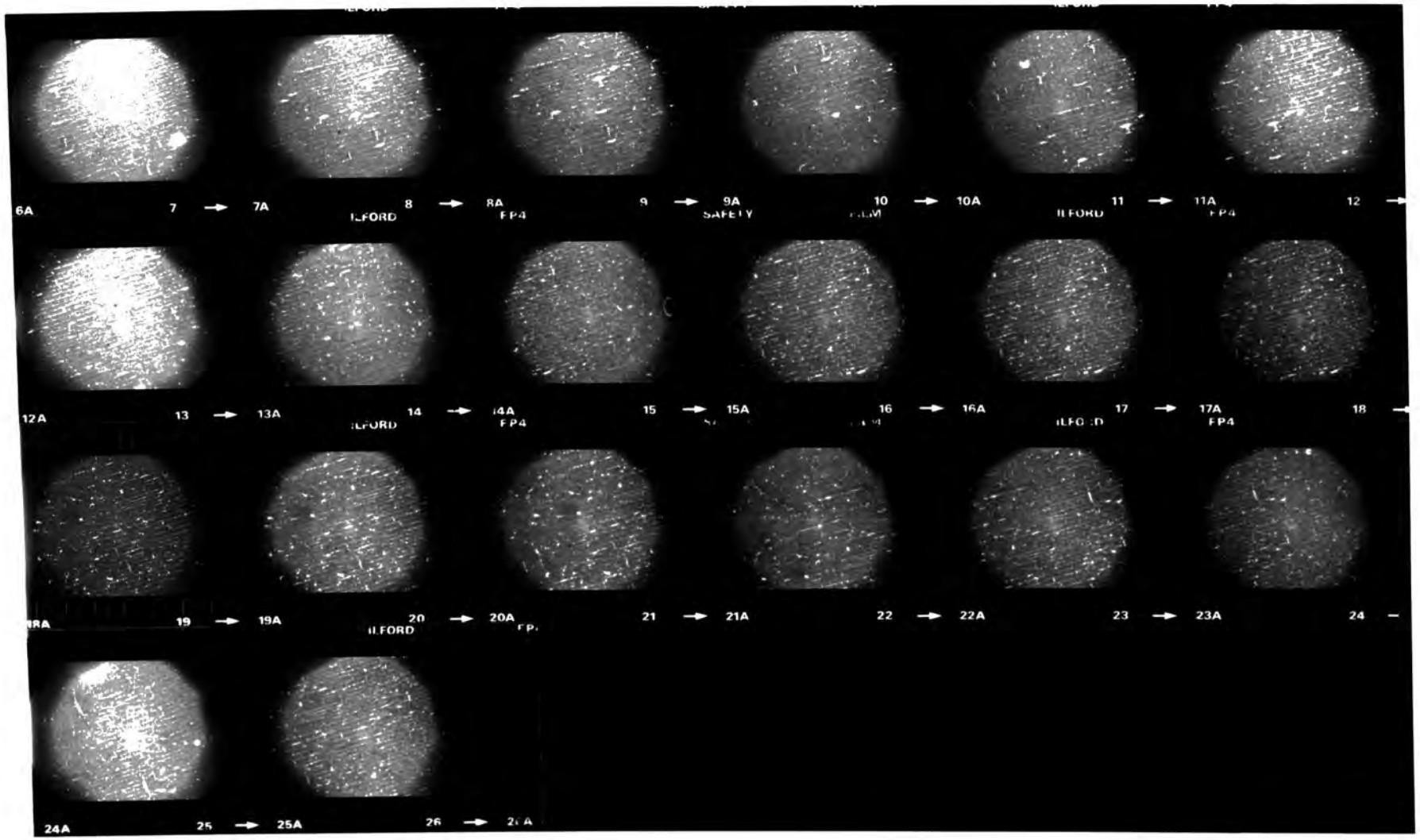

Fig 7.7 Domains in terbium at 150K

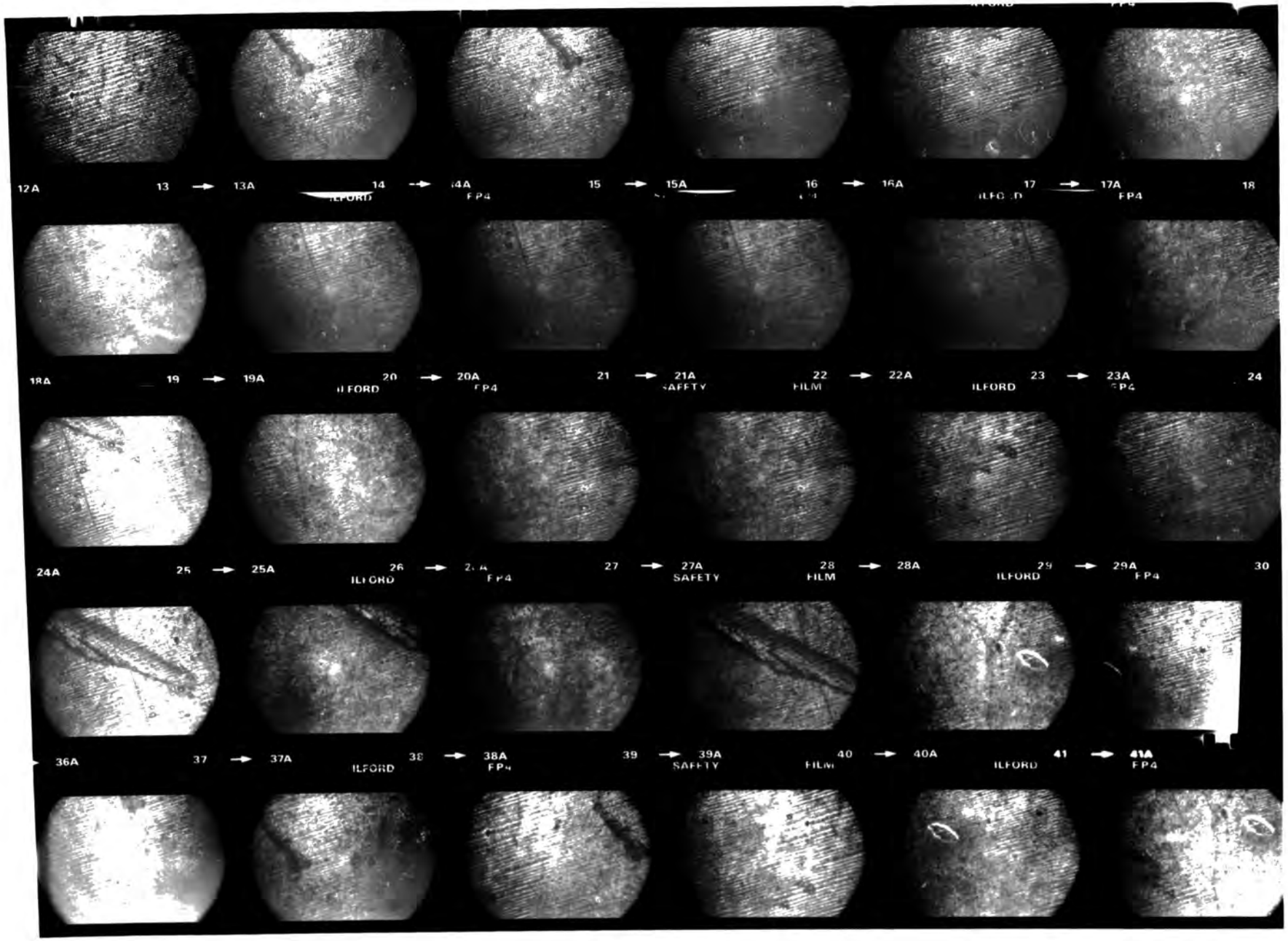

Fig. 7.8
Domains in terbium at 180K

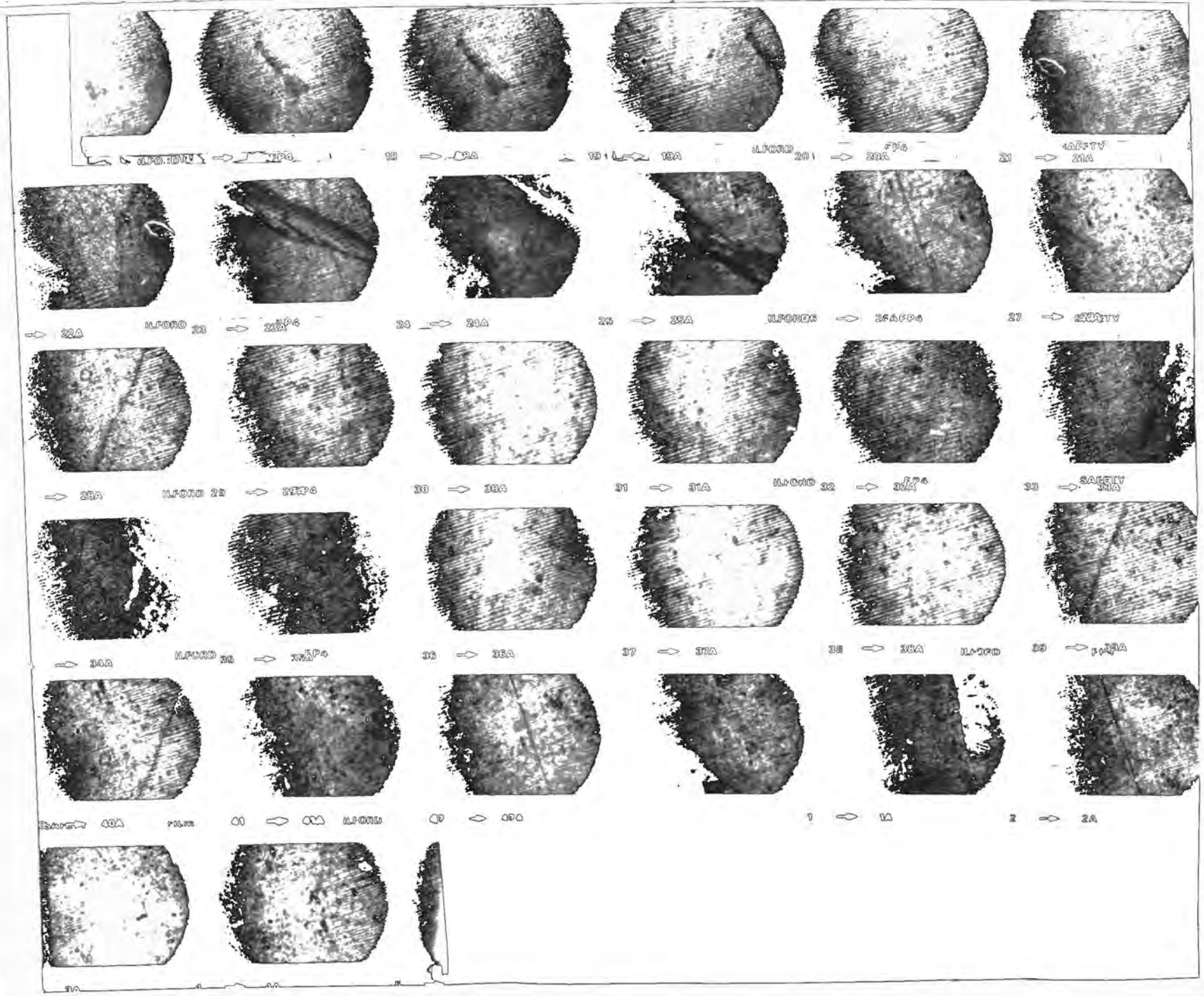

Fig 7.9
Domains in terbium
at 180K

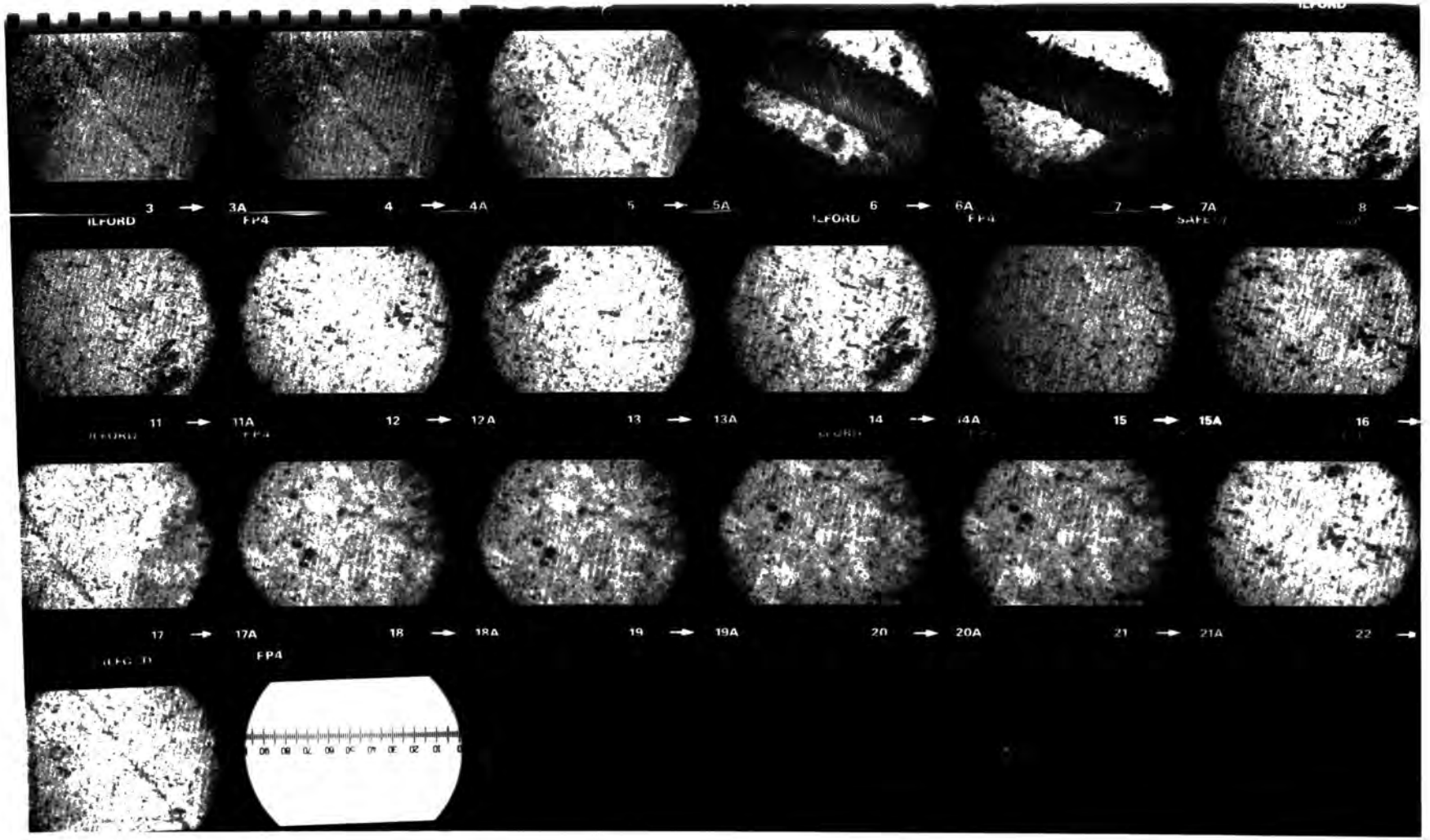

Fig 7.10 Domains in terbium at 199K

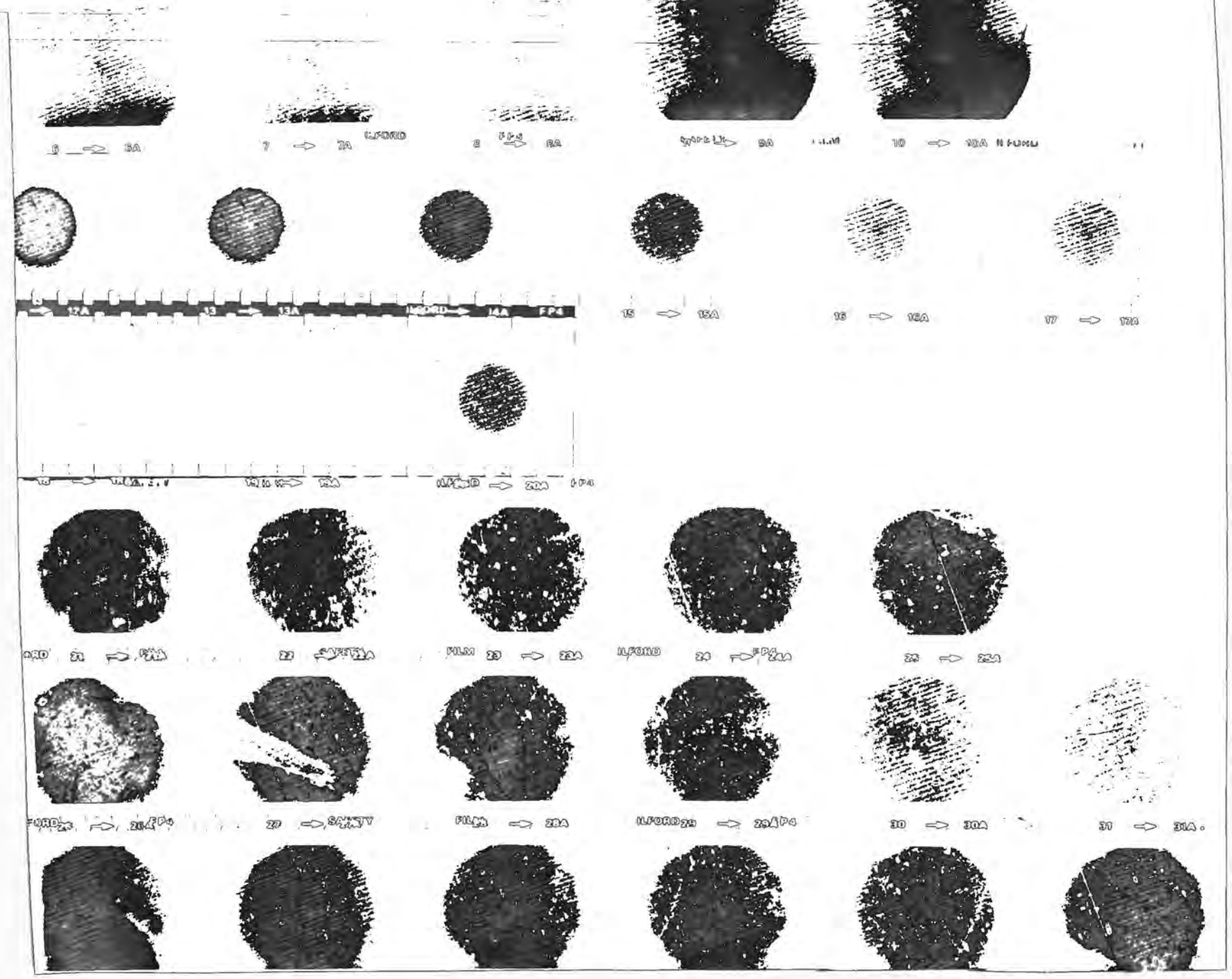

Fig 7.11
Domains in terbium at 215K.

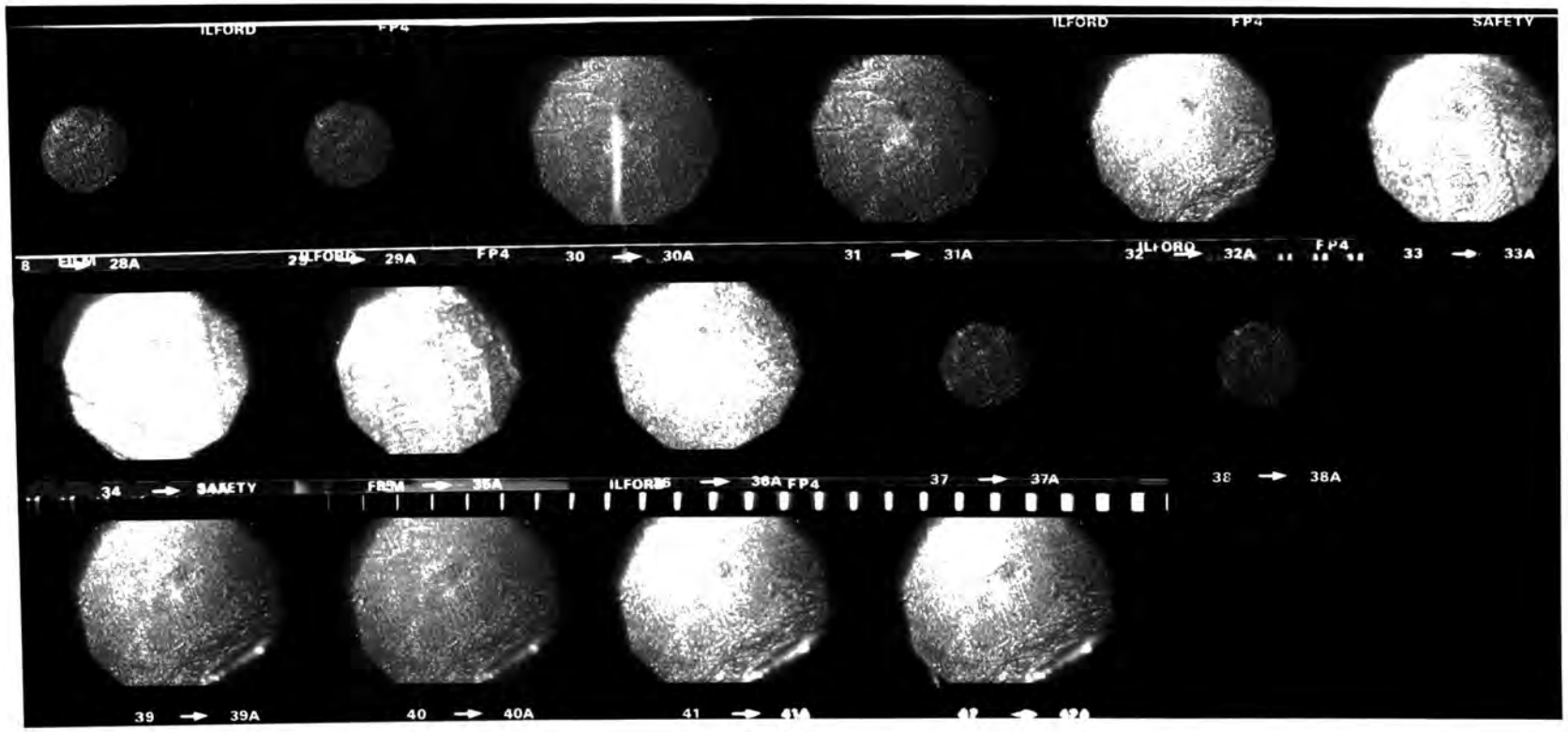

Fig 7.12 Domains in terbium at 224- 228 K.

7.3 SLAB DOMAIN MODEL FOR TERBIUM

In order to explain the domain structures which they observed in a cubic single crystal of terbium, Corner and Al-Bassam (1971) devised a model based on 60°, 120° and 180° Bloch walls. (Figure 7.13). The magnetostatic energy due to free poles on the $\{11\bar{2}0\}$ surfaces (a planes) was given as

$$Em = 1.7 \left(\frac{\sqrt{3}}{2} I_s^2 \right)^2 \; 2 \, Dyz \qquad (7.1)$$

The magnetostatic energy on $\{10\bar{1}0\}$ surfaces (b planes) was given as

$$Em = 1.7 \left(\frac{I_s}{2} \right)^2 \; 2 \, Dxz \qquad (7.2)$$

Laüe diffraction patterns indicated that the sample used in the present observations was orientated with a b-plane enclosing an angle of 7° with the crystal surface (Figure 7.1).

On the assumption that the observed structures consist of 180° walls between domains magnetized parallel and antiparallel to the b direction almost in the surface, an equivalent equation 7.2 can be written as

$$Em = 1.7 \left(\frac{I_s}{2} \sin 7 \right)^2 \; 2Dxz$$

$$= 0.85 \, I_s^2 \sin^2 7 \; Dxz \qquad (7.3)$$

This ignores any term due to free poles on the curved surfaces of the specimen. Such an assumption is valid if the specimen thickness is small

compared to the diameter.

The wall energy is $E_w = \frac{xyz}{D}(\gamma_{180})$

for 180^0 Bloch walls.

The total wall energy is the sum of the magnetostatic energy and the wall energy.

$$E_T = E_w + E_m$$

$$E_T = 0.85\, I_s^2 \sin^2 7\, Dxz + \frac{xyz}{D}\gamma_{180}$$

The equilibrium condition will be a minimum in the energy with respect to Z.

Explicitly,

$$\frac{d}{dD}\left(\frac{E_T}{dz}\right) = 0.85\, I_s^2 \sin^2 7\, Dx + \frac{xy\,\gamma_{180}}{D} = 0$$

which gives $$D_o = \left(\frac{y\gamma_{180}}{0.85}\right)^{1/2} \cdot \frac{1}{I_s \sin 7} \qquad (7.4)$$

where D_o is an equilibrium domain width.

Thus,

$$D_o = \frac{3.45}{\sqrt{2}}\left(\frac{\gamma_{180}}{I_s^2}\right)^{1/2} \qquad (7.5)$$

Now $\gamma_{180} = \frac{\gamma_0}{2}$ where $\gamma_0 = 8(AK_4)^{\frac{1}{2}}$

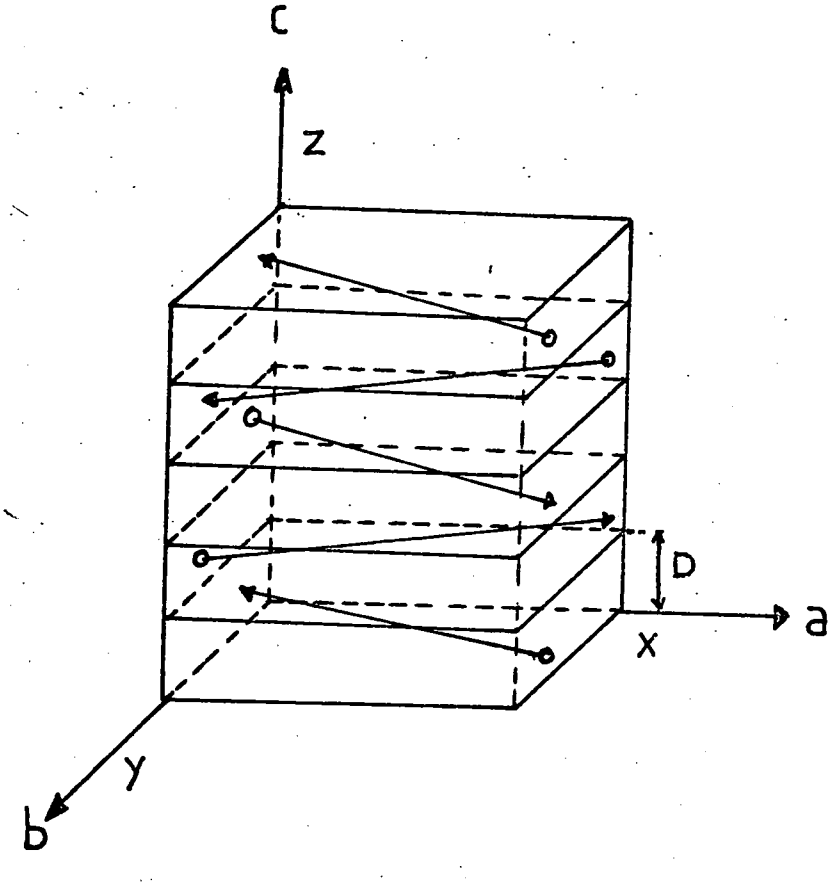

Fig. 7.13 Layer domain structure of terbium cube

(CORNER and AL-BASSAM (1971))

where K_4 is the basal plane anisotropy constant

A is the exchange integral which is given by

$$A = \frac{2K\,Tc}{a_o}$$

and K is Boltzmann's constant

Tc is the Curie temperature (taken as 222K)

a_o is the lattice parameter = 3.6×10^{-8} cm

This gives a value for A = 1.7×10^{-6} erg cm^{-1}

Therefore

$$Do = \frac{3.45}{\sqrt{2}} \left(4 \frac{(AK_4)^{1/2}}{I_s^2}\right)^{1/2}$$

or

$$Do = \frac{3.45\sqrt{2}}{I_s} A^{1/4} K_4^{1/4} \qquad (7.6)$$

In order to allow for end effects it is preferable to write

$$D_o = \gamma \frac{K_4^{1/4}}{I_s} \qquad (7.7)$$

The value of the fitting parameter γ is 0.176 if the end corrections are ignored and equation 7.5 is used.

Table 7.2 gives values of K_4 from Bly (1967) (Figure 7.17). It also gives Is values from Hegland et al. (1963) (See Figure 7.16) and Is values from neutron diffraction data (Dietrich and Als-Nielsen (1967)).

Equation 7.7 is used to obtain curves of domain width versus temperature using the two sets of Is values. The curves are shown in Figures 7.18 and 7.19.

7.4 DOMAIN SPACINGS FROM EXPERIMENTAL OBSERVATIONS

The photographs of magnetic domains in terbium shown in Figures 7.20 to 7.28 and Figure 7.30 are at various magnifications (the variations being introduced at the enlarging stage). Appropriate scales have been added to these figures. The domain spacing at any particular temperature varied (sometimes quite drastically) across the crystal surface. (It was for this reason the surface was scanned by the microscope and several photographs taken.) Figure 7.20 shows four photographs which illustrate this variation at 118K. The photographs shown represent only a few of the many photographs taken of domain patterns on this particular sample. All of the domain patterns shown by these photographs were obtained in the presence of an applied vertical field of 14 mT. This field, as previously mentioned, aided contrast but could, concievably, account for some of the anomalous effects which appear on some of the prints.

Table 7.3 shows domain spacings (d) at various temperatures. Because the domain widths varied so much at a particular temperature, the values of d given represent a realistic estimation, considering the feasibility of some of the widths shown on the photographs. The error bar given for d is taken to be $\pm$ 2μm long. While some of the variations exceeded this, those variations were, perhaps, due to stress in the crystal (See section 7.5). ($\pm$ 1 μm is accepted at 100K as very little variation in d appeared).

The temperature error bar is accepted as being $\pm$ 2K. As mentioned in Chapter Six, when the current was passed through the tungsten filament in order to evaporate the iron wire wrapped around the filament, the transport gas heated up and the diode sensor detected a change in the chamber's ambient temperature (or at least the temperature of the brass sample holder, and hence the sample), of a few degrees K. This could mean one of two things. Either the colloid was deposited on the sample surface over the whole duration of the deposition (15 seconds), in which case the temperature conditions changed as the pattern formed, or else the initial deposition of colloid occurred quickly at the beginning of the 15 seconds and later additions of colloid adhered to this initial configuration. In the latter case the temperature of deposition is, therefore, the temperature at the start of the 15 seconds. Intuitively it is felt that if the colloid delineated the domain walls at the start of the deposition, then any slight variation in temperature would do little to shift this pattern. It is likely, therefore, that the temperature conditions at the beginning of the deposition process are those which can be used in terms of domain spacing estimation.

Temperature (K)	$K_4^{\frac{1}{4}}$ erg/cc)$^{\frac{1}{4}}$ (Bly)	Is (Hegland et al (1963) (emu/cc)	Is Neutron diffraction data (Dietrich + Ali Nielsen (1967) (Arbitrary units)	Do (μm)	Do (Neutron diffraction) data Arbitrary units.
55	34.2	2550	4.28	23.61	1.41
77	31.3	2500	4.25	22.05	1.30
96	29	2410	4.15	21.2	1.23
113	25.2	2325	4.05	19.1	1.10
135	21.6	2225	3.85	17.1	0.99
150	17.2	2125	3.65	14.25	0.83
175	13.6	1925	3.20	12.45	0.75
197	12.8	1675	2.40	13.46	0.94
210	9.0	1475	1.60	10.75	0.99

Table 7.2

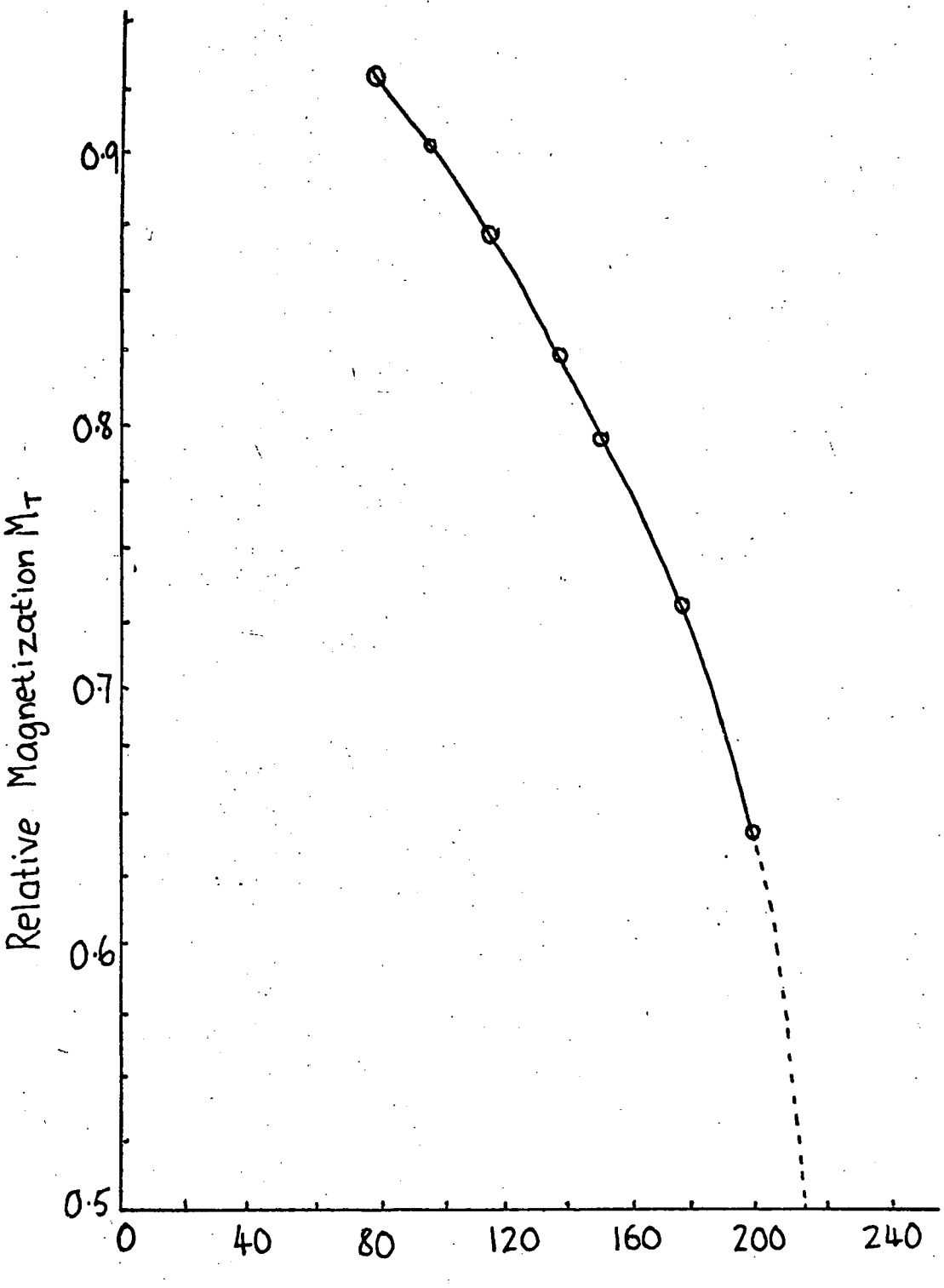

Fig. 7.14 Relative magnetization of terbium versus temperature (WELFORD)(1974)

Figure 7.15. Spontaneous Magnetization versus Temperature (Terbium)
(Dietrich and Als-Nielsen (1967))

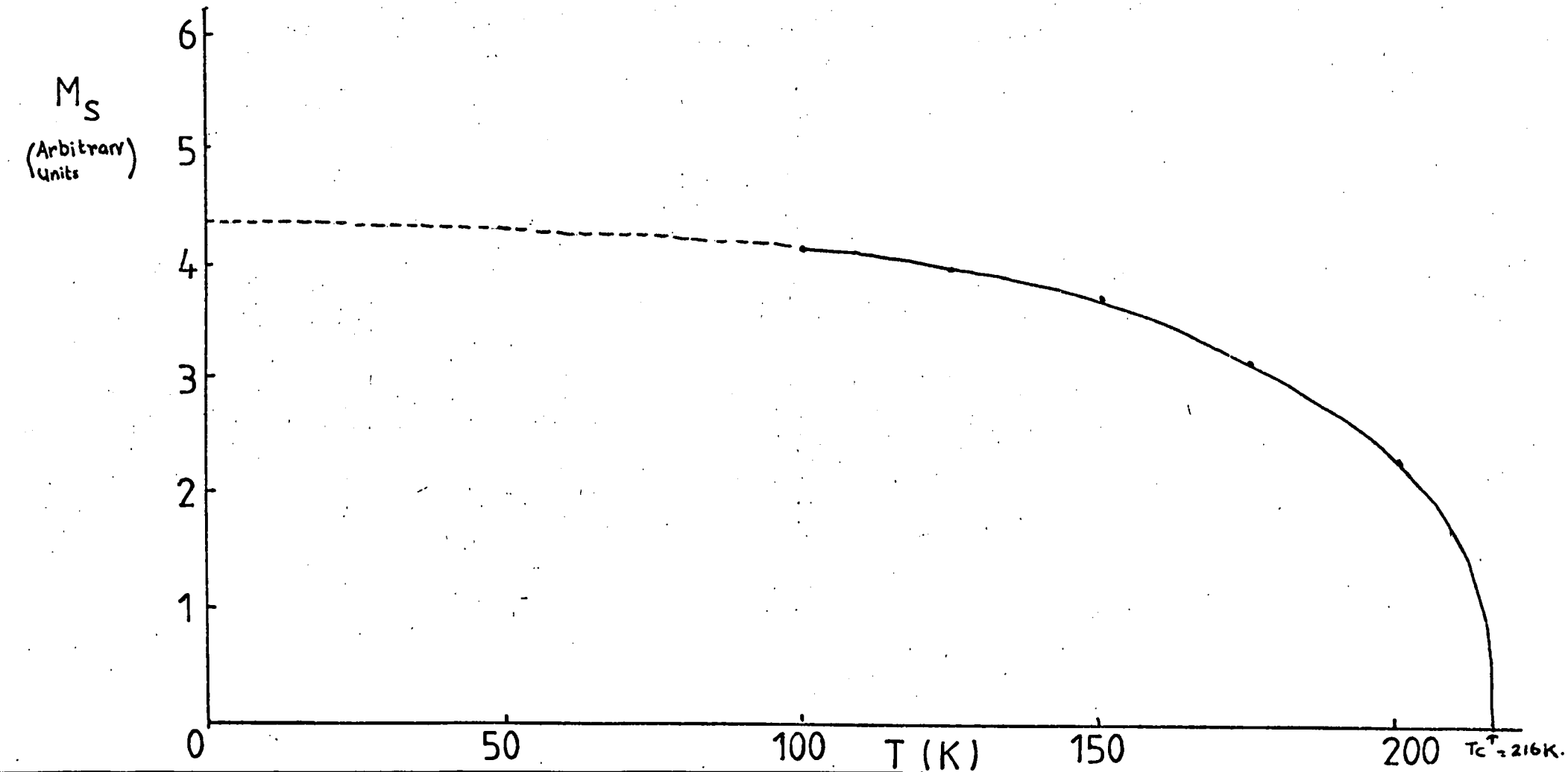

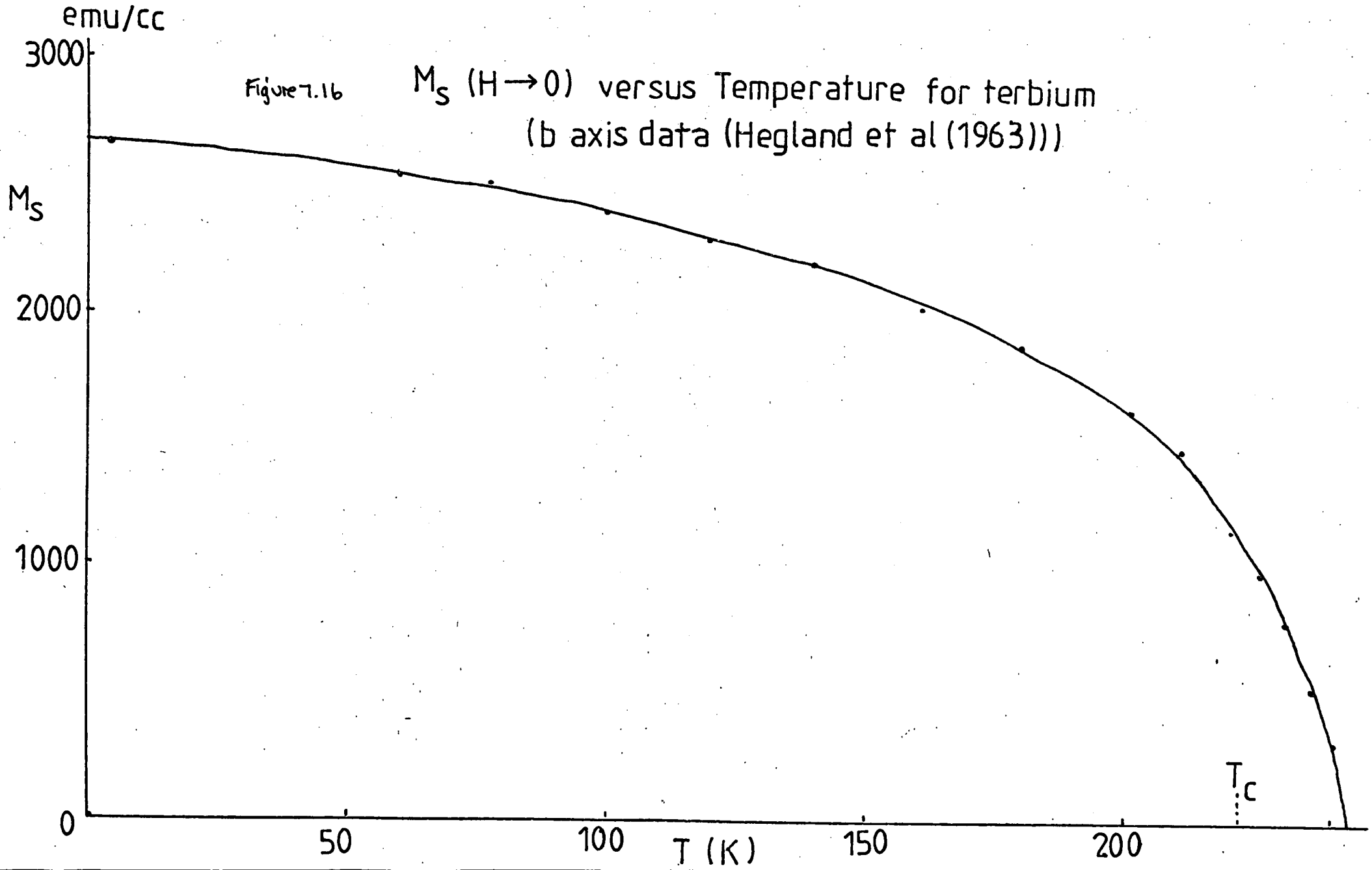

Figure 7.16 M_S (H → 0) versus Temperature for terbium (b axis data (Hegland et al (1963)))

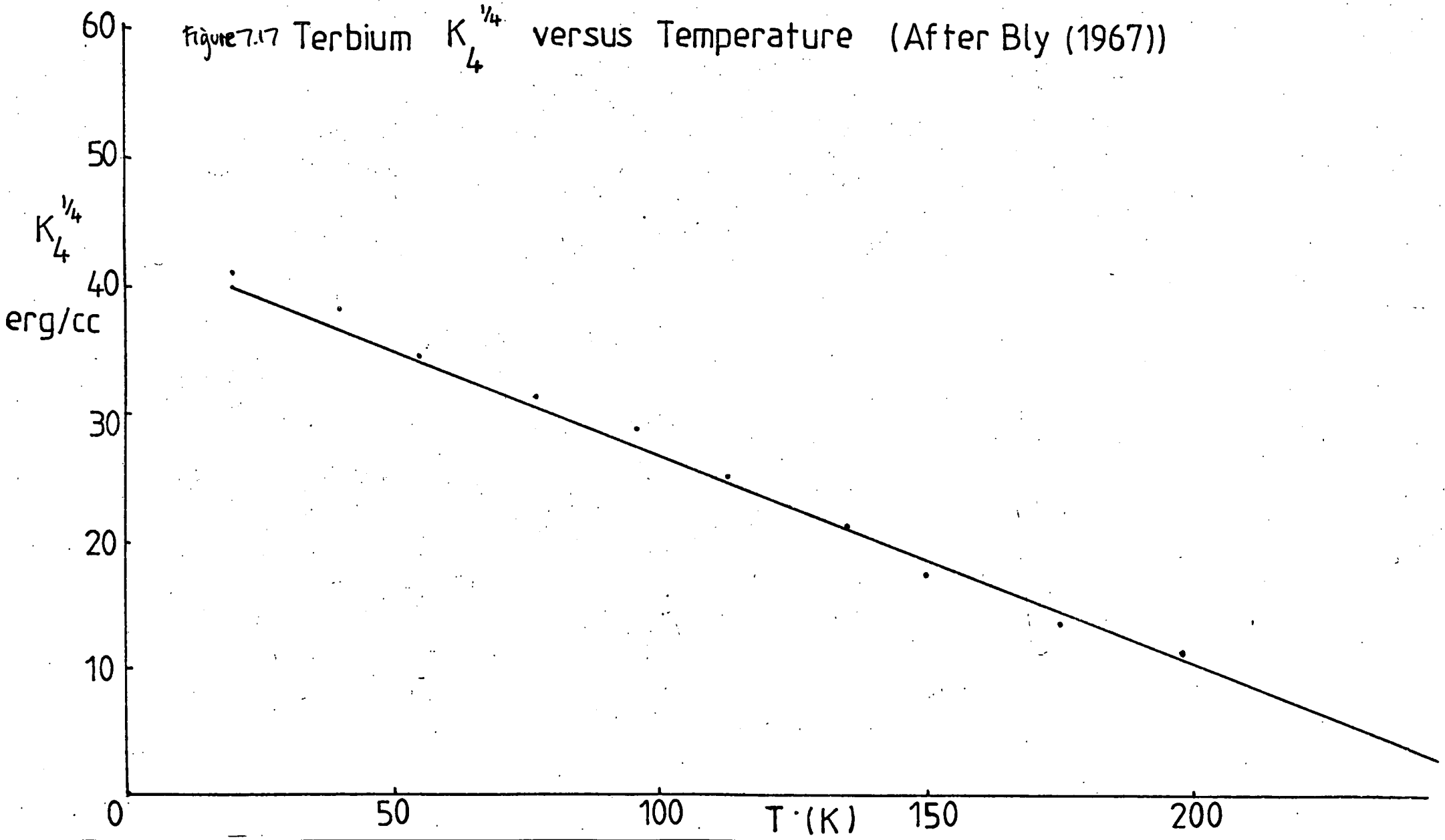

Figure 7.17 Terbium $K_4^{1/4}$ versus Temperature (After Bly (1967))

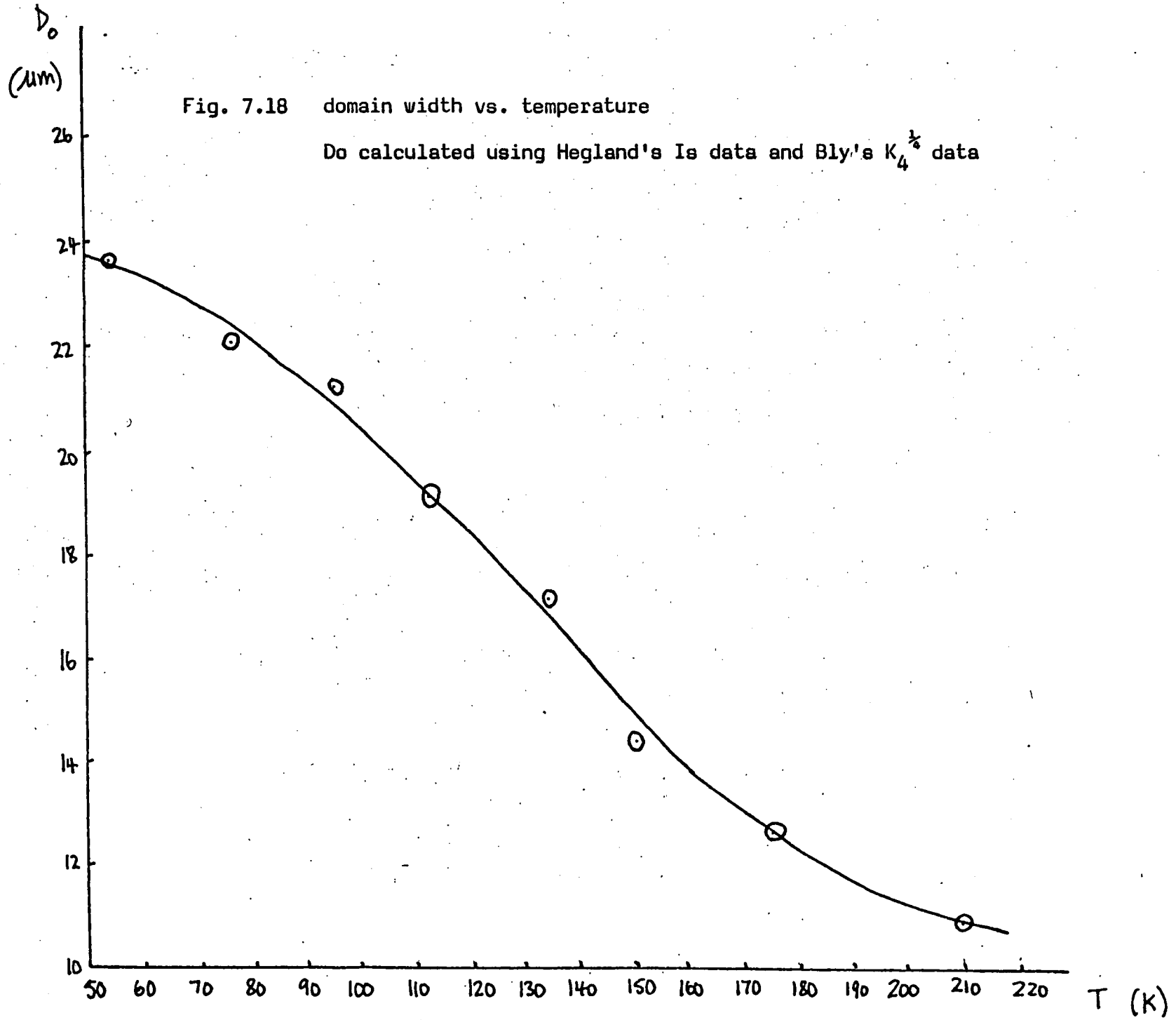

Fig. 7.18 domain width vs. temperature

Do calculated using Hegland's Is data and Bly's $K_4^{\frac{1}{6}}$ data

Fig. 7.19 Ms arbitrary units neutron diffraction data Dietrich + Als-Nielsen

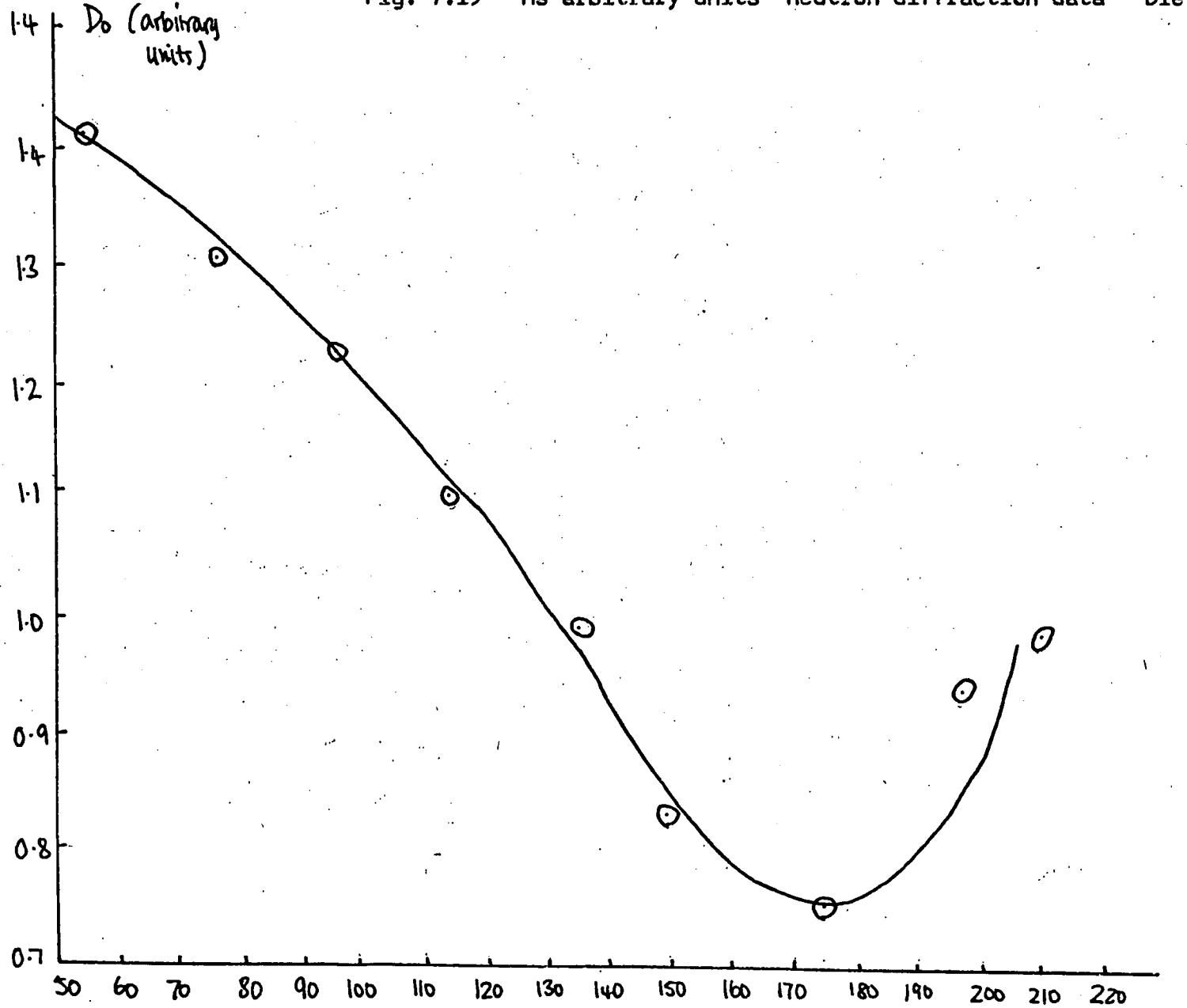

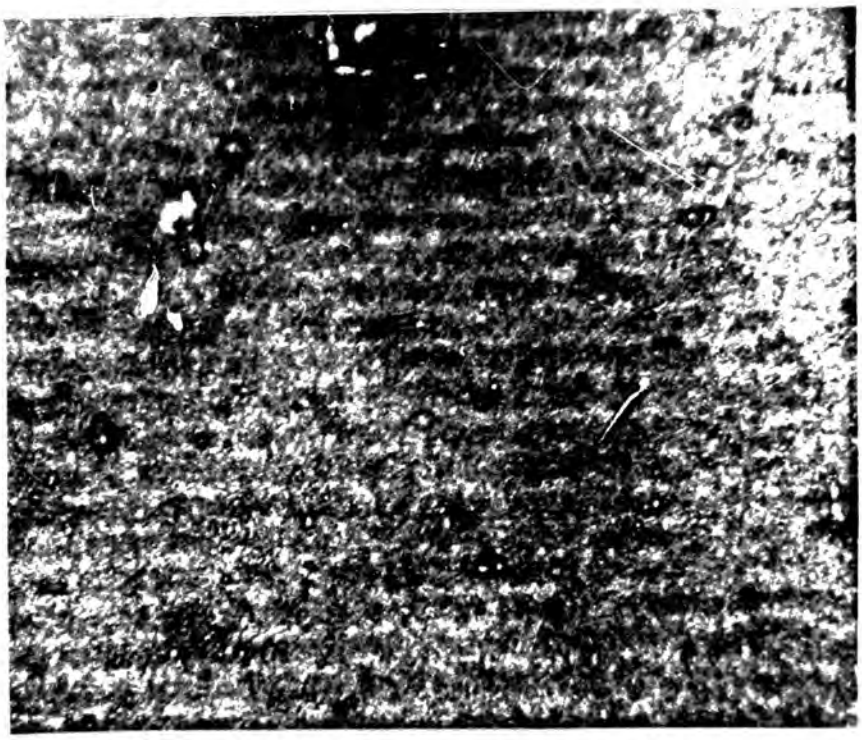

(a)

(b)

Fig. 7.20 Magnetic domains in terbium at 118K

(c.)

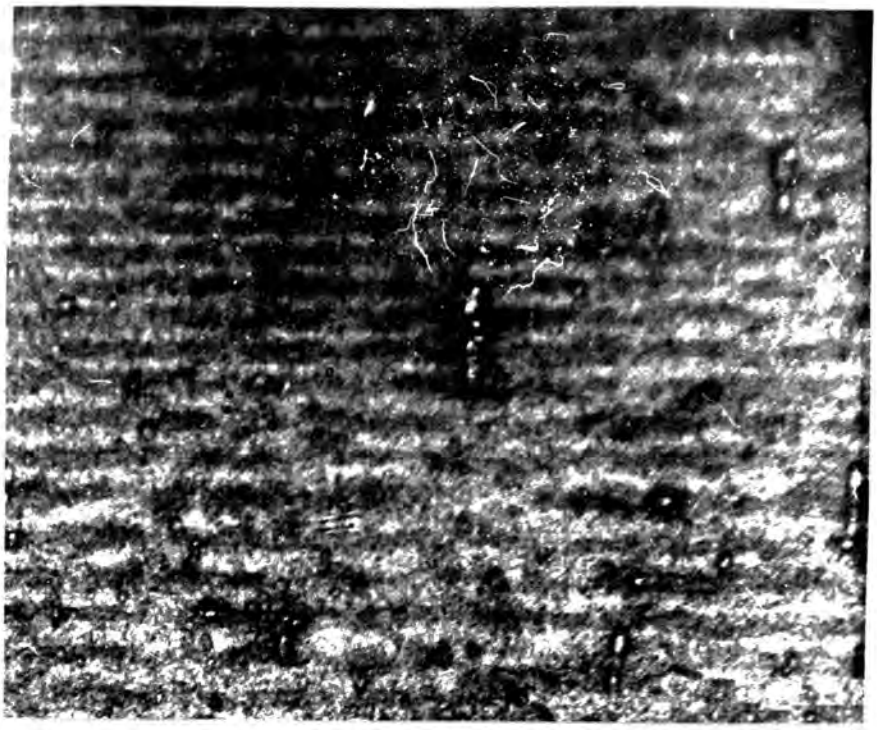

(d.)

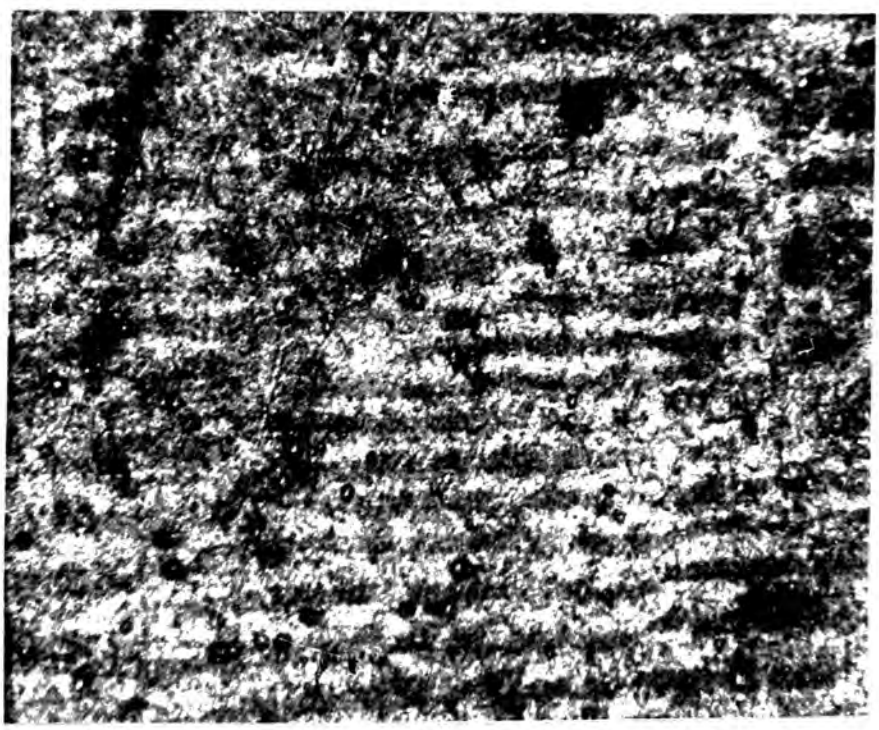

Fig. 7.20 (continued)

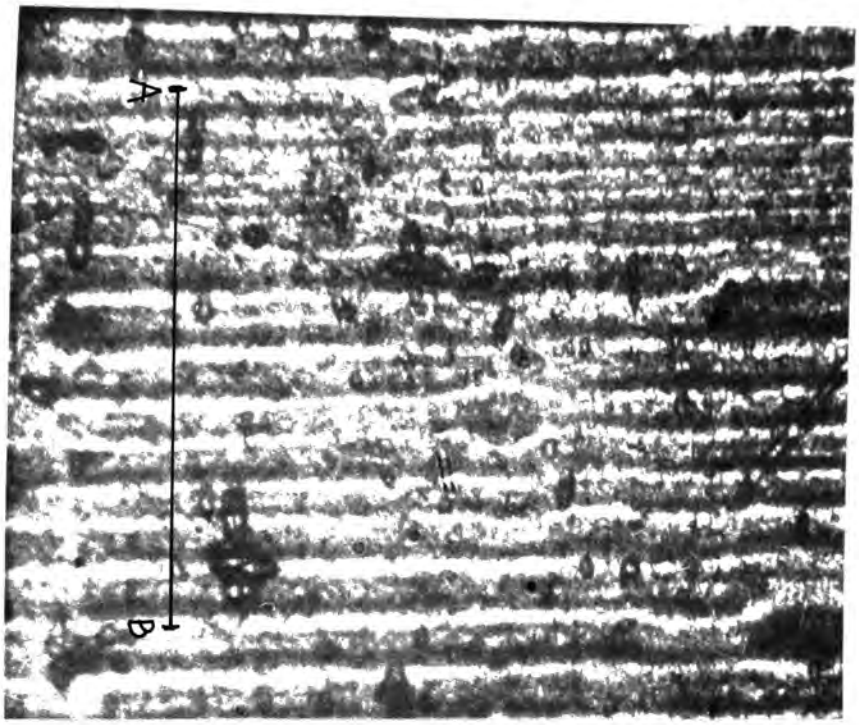

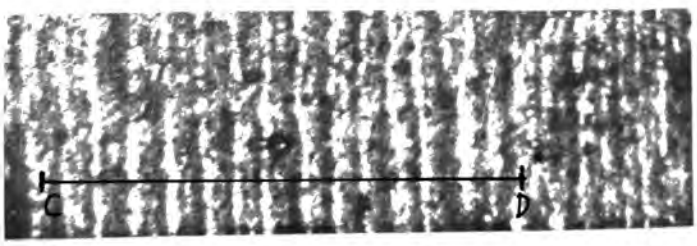

Fig. 7.21 Domains in terbium at 95K
The line AB is taken as spanning 15 domain spacings and is 319μm long. (d = 21.3μm)
The line CD spans 15 domain spacings and is 292μm long. (d = 19.4μm)

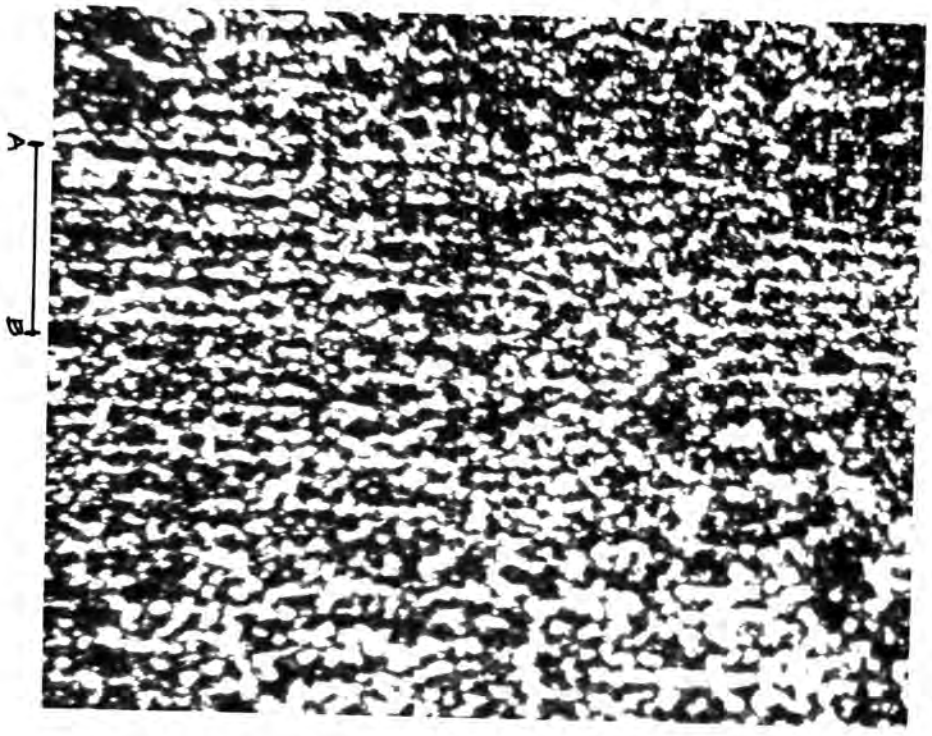

100 μm

Fig. 7.22 Domains in terbium at 100K

The line AB is taken to represent 5 domain spacings (taking the prominent dark lines to represent the positions of the walls) AB is 102 μm long.

80 μm

Fig 7.23 Domains in terbium at 150K

60μm

Fig 7.24 Domains in terbium at 180K

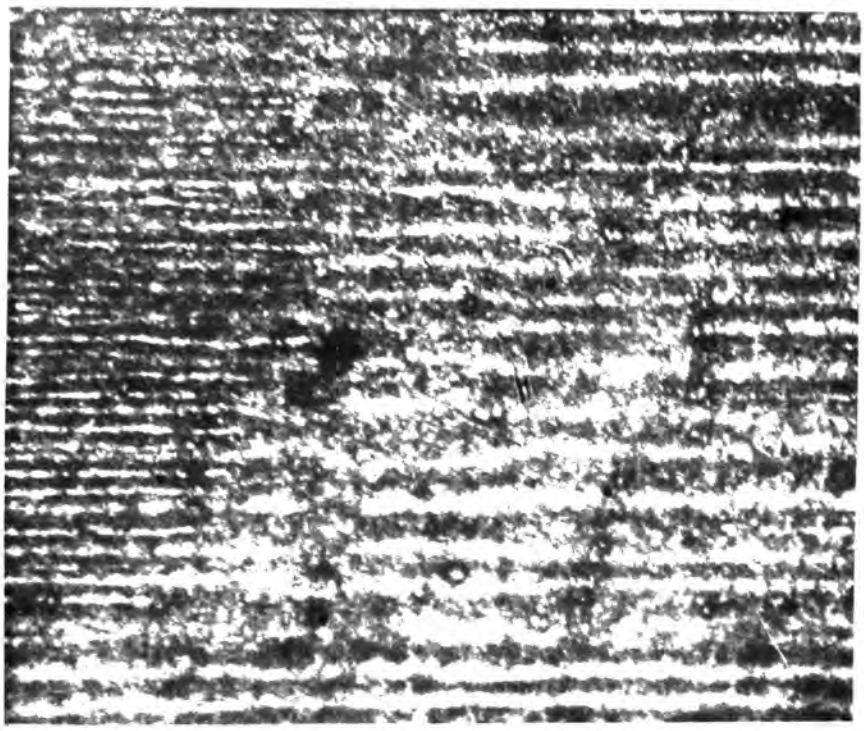

Fig. 7.25 Domains in terbium at 180K
The photograph shows the striking difference between domain spacing as measured at different parts of the surface.

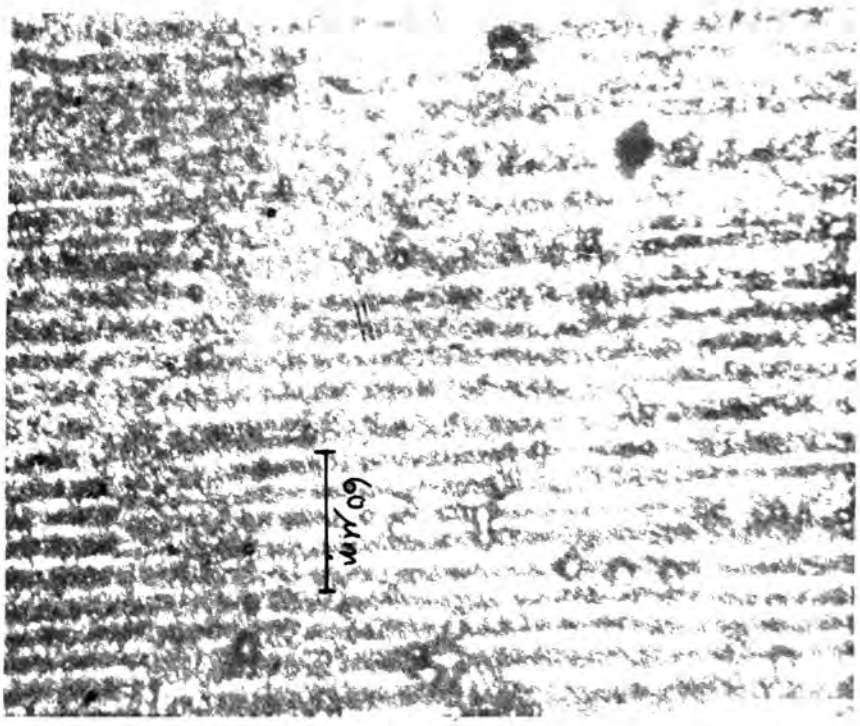

60μm

Fig. 7.26 Domains in terbium at 199K.

Fig. 7.27 Domains (Tb) at 215K

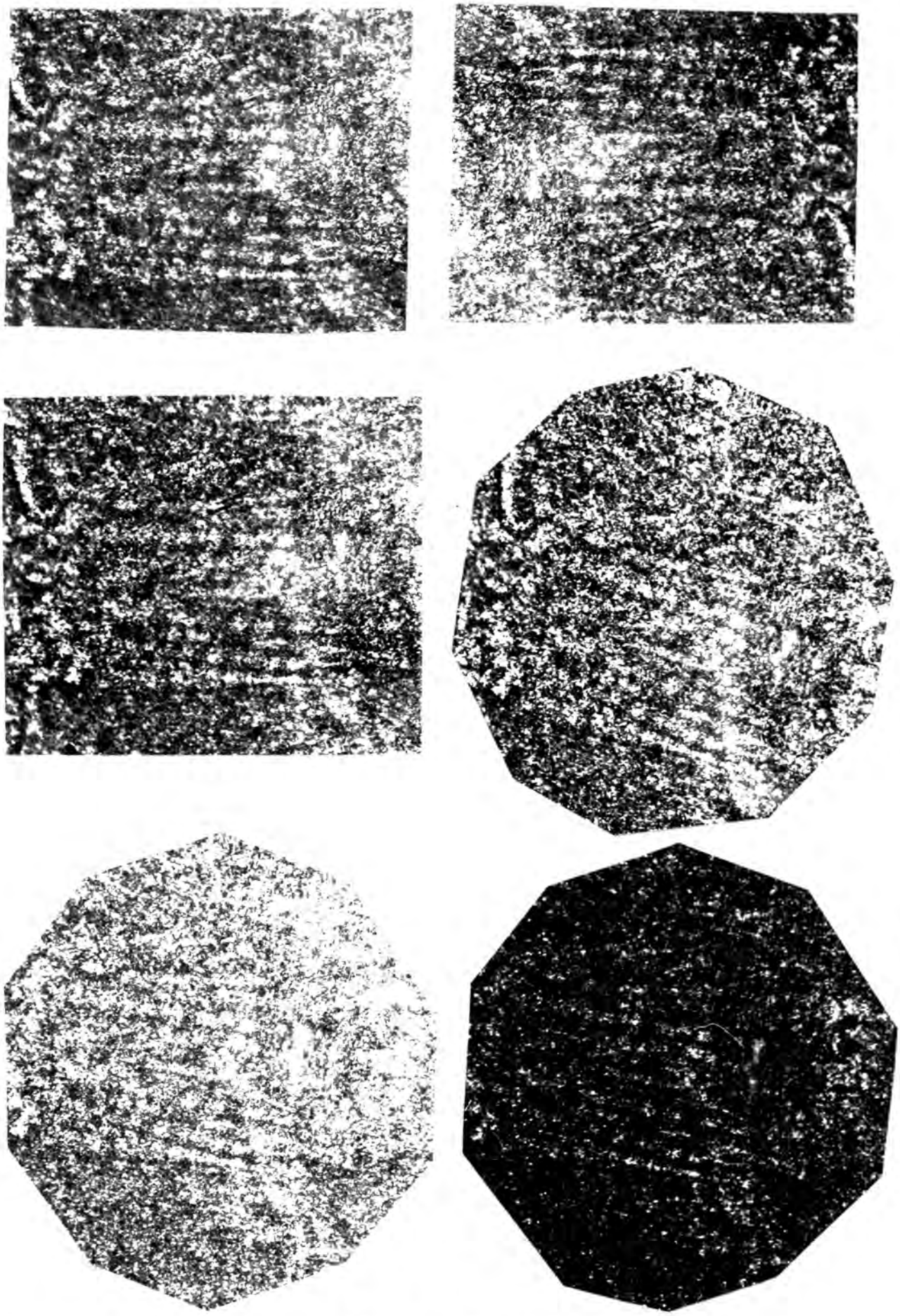

Fig. 7.28 Domains in terbium at temperature in the range 224 – 228 K

Temperature (K)	Domain spacing (μm) $\pm$ 2 ($\pm$ 1 at 180K)
95 $\pm$ 2	21.3
100 $\pm$ 2	20.4
118 $\pm$ 2	19
150 $\pm$ 4	16.6
180 $\pm$ 2	12.4
199 $\pm$ 2	12
215 $\pm$ 2	16

Table 7.3 Domain spacing as a function of temperature (Terbium)

Figure 7.29. The points are experimental observations
(see table 7.3.)
The curve is that of figure 7.18

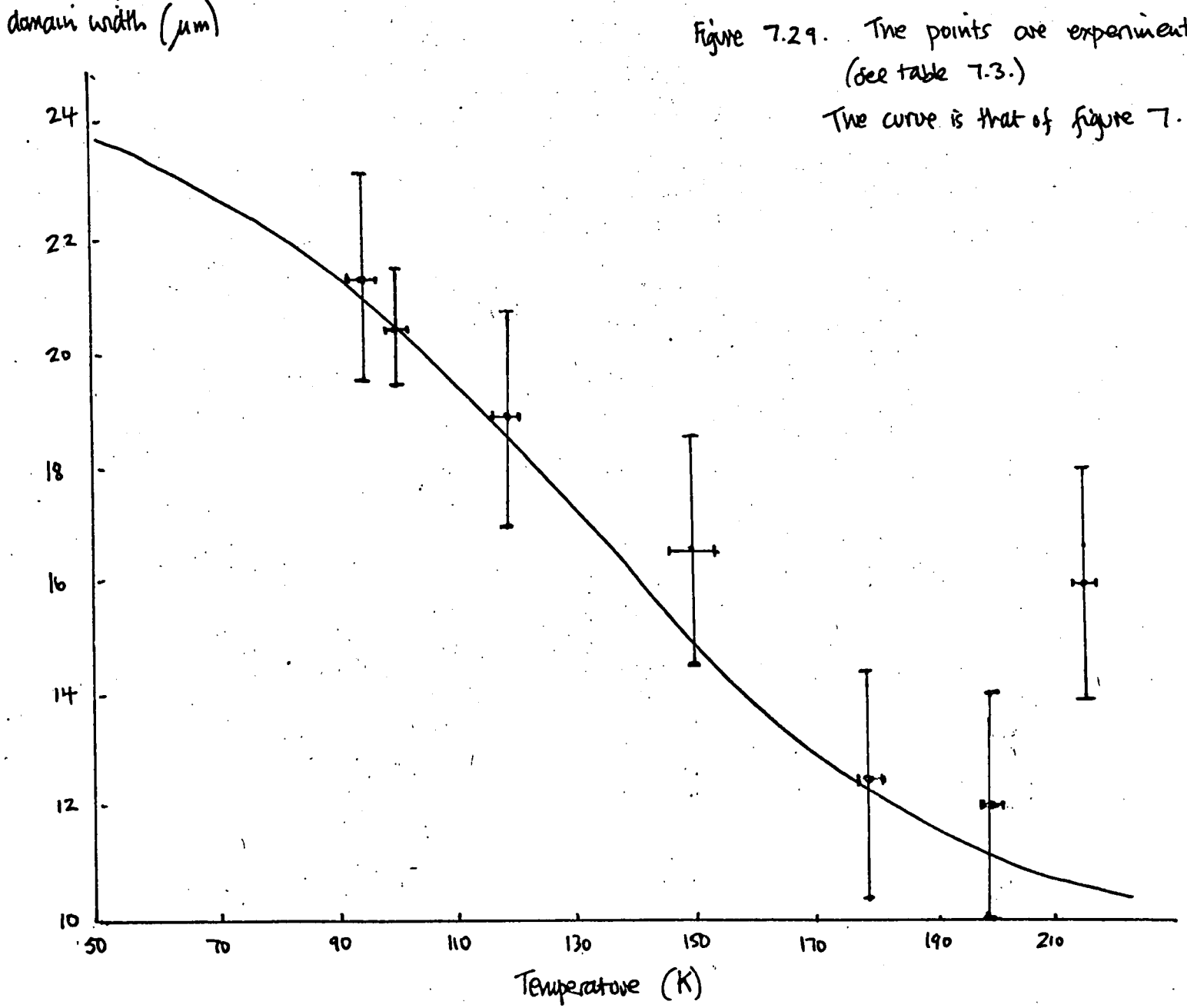

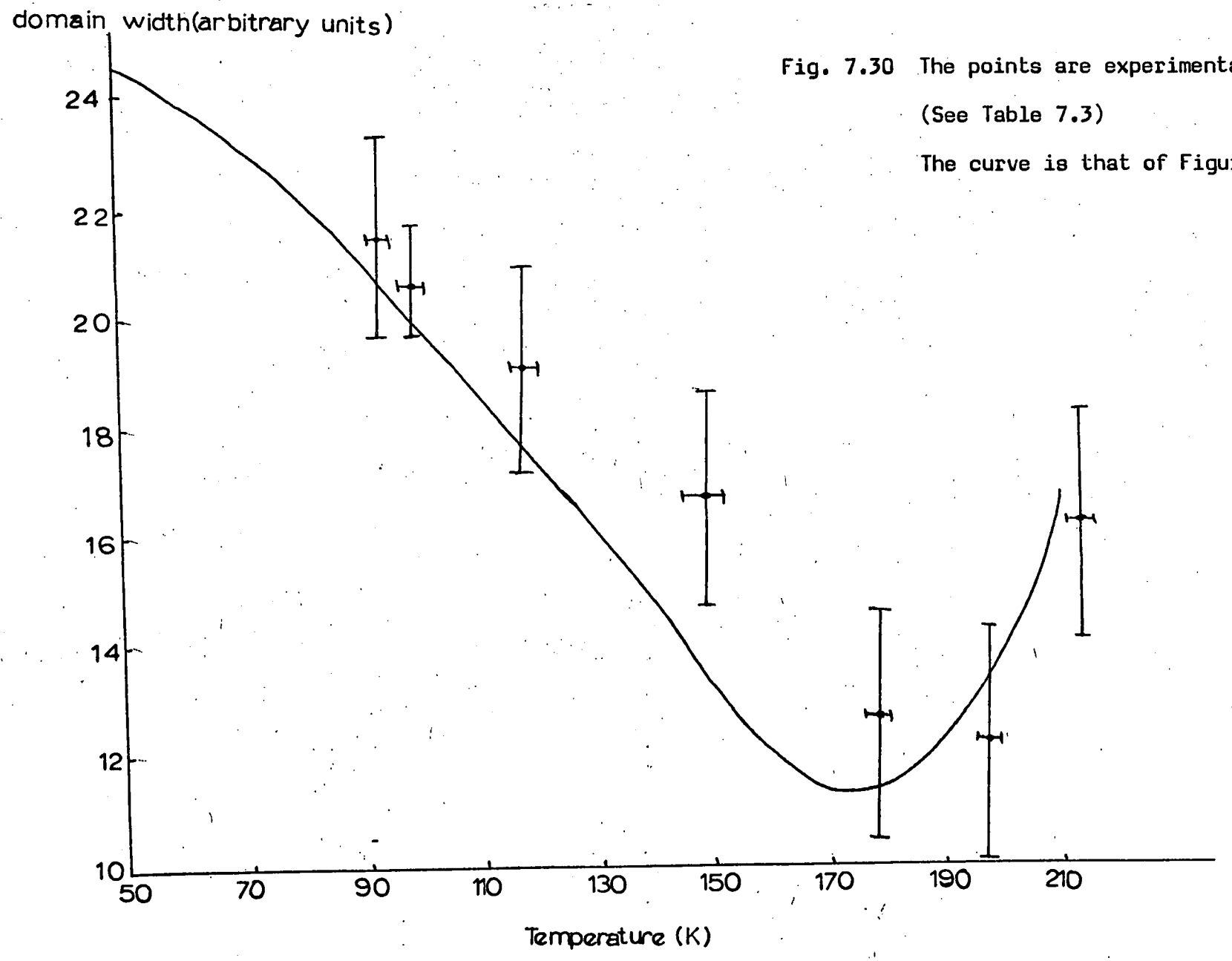

Fig. 7.30 The points are experimental observations

(See Table 7.3)

The curve is that of Figure 7.19

7.5 DISCUSSION

As previously mentioned (7.4) the domain spacing varied markedly across the crystal surface at any particular temperature. It is quite possible that sample thickness variations could account for some of the variations in d. It is, however, highly likely that stress in the crystal gave rise to magnetostriction which caused local variations in domain width. Figure 7.25 shows domains at 180K. The photograph shows two distinct domain widths, the smaller probably being due to stress effects. These effects, however small, are very difficult to avoid. Mounting the sample on and removing it from the holder inevitably causes stress. The chemical polishing process, while less harsh than a mechanical polish, involved rotating the crystal face down onto a polishing cloth under the pressure exerted by its own weight plus that of the sample holder. No estimation of magnetostriction in the sample has been made and the error bar associated with d has been made, as previously mentioned, in terms of the feasibility of the measured values of d.

The domain widths proved, on occasions, very difficult to measure due perhaps to the colloid particles being too large. In Chapter Six the calculations for optimum colloid particle diameter for pattern formation were done for zero bias field. Under these conditions, as previously mentioned, pattern formation occurred only a low temperatures. For pattern formation at higher temperatures the application of the bias field was essential. This field (14mT) could, quite conceivably, have the additional effect of allowing pattern formation with large colloid particles. These particles, being in effect single domains, could form aggregates thus increasing the graininess of the domain walls outlined by the colloid.

Figure 7.22 shows a domain pattern which is particularly difficult to assess in terms of domain width. This is due to the colloid graininess.

Figures 7.27 and 7.31(d) show a very interesting substructive (at 215K). (Colloid graininess obviously is not a problem here). No definite explanation can be given for this substructure other than to suggest magntostrictive effects, or else the presence of domain walls other than the simple 180^{0} walls previously discussed. There may be 60^{0} or 120^{0} walls present in addition to the main 180^{0} walls which could result in the substructure pattern shown. Faint lines of colloid also appear in the bright areas taken to be the main surface domain areas.

Figure 7.28 shows a set of photographs showing magnetic domains for a temperature range of 224 to 228 K. Although there is some controversy about the Curie temperature of terbium 228K seems to be high. While bearing in mind the previous discussion on the temperature range of deposition it must be pointed out that there is no reason to mistrust the reliability and accuracy of the diode sensor or the associated temperature measuring apparatus. Again stress effects could result in varying values for Tc.

Another interesting effect arises as a result of using a vertical bias field. B.K.Tanner (1981) points out that for zero vertical bias, leakage field calculations for various distances above the specimen show a maximum at the walls. With a bias field however, similar calculations show maximum above domain centres close to the specimen surface. Figure 7.32 shows this. This distribution of leakage field

(a)

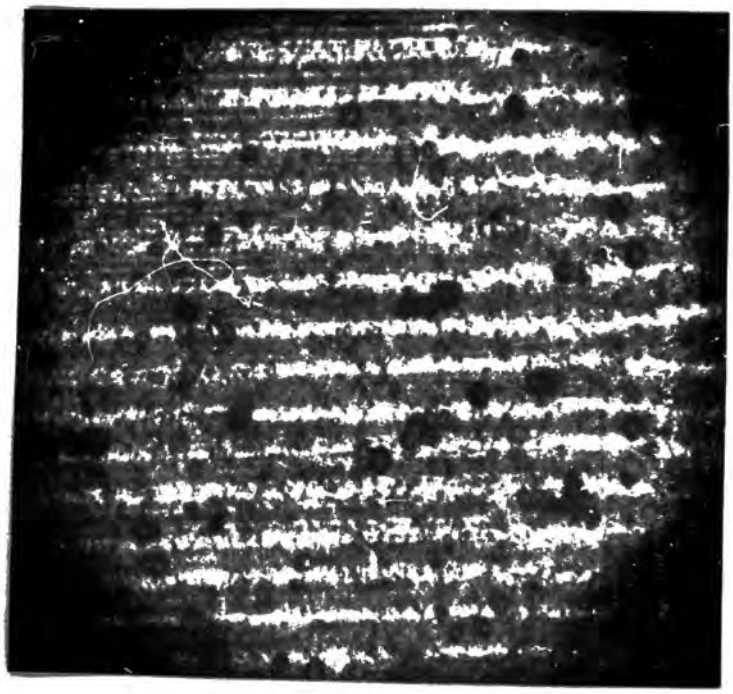

(b)

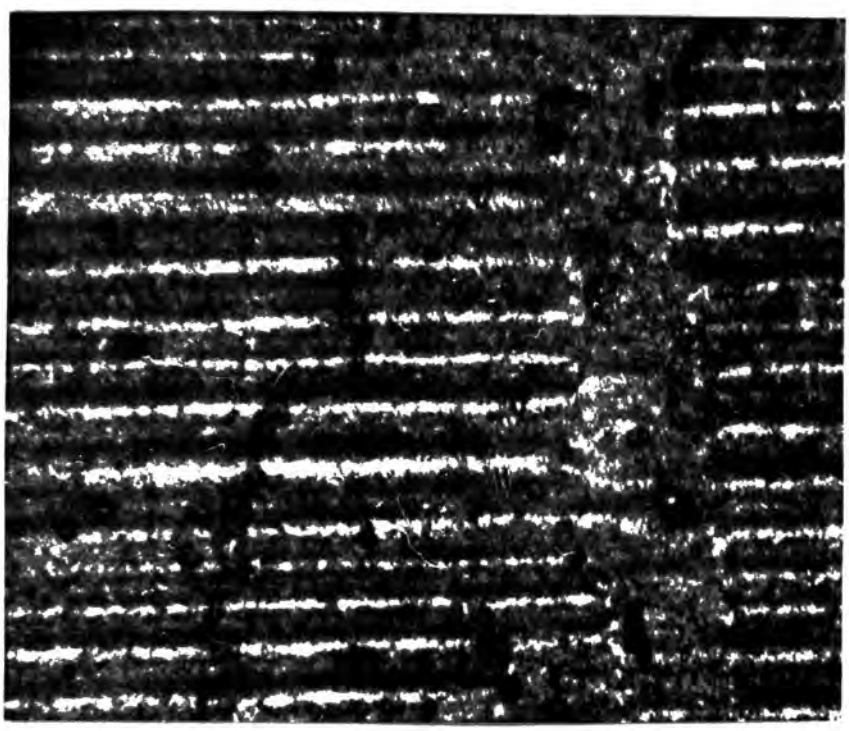

Fig. 7.31 (a) Domains in terbium at 215K
Photograph shows a fine substructure

(b) Domains in terbium at 95K
Photograph shows light and dark contrast of domains due to vertical bias field (as discussed in text).

(shown in figure 7.32 (a)) results in a change in the domain contrast. Instead of the bright dark contrast in the absence of the bias field, a bright dark, grey, dark, bright contrast is obtained. Figure 7.31 (b) shows this effect in terbium at 95K with a vertical bias field of 14 mT.

Figure 7.19 shows the curve of domain width versus temperature. The domain widths were calculated using the Is values obtained from neutron diffraction data, and using equation 7.7. Figure 7.7 shows this curve redrawn and superimposed are the experimental data points obtained using the dry colloid apparatus. As can be seen, the data agrees very well with the theoretical curve and the data certainly indicates the trend for d to increase as T_c is approached. According to the theoretical model adopted d approaches infinity at T_c. It would appear, therefore, that the experimental determination of domain widths at various temperatures has provided data which agrees well with the Corner - Al -Bassam slab domain model as applied to a sample where 180^0 walls are present.

7.6 SUGGESTIONS FOR FURTHER WORK

The results obtained for domain spacing versus temperature agree reasonably well with the results predicted by the Corner - Al-Bassam slab domain model (for 180^0 walls). The effects of stress have not been estimated at all in this thesis and it is suggested that consideration of stress would have yielded results which explained (or at least partly explained) the wide variation in d across the surface of the crystal at a given temperature. Also, the investigation of domain structures without a vertical bias field could explain the fine substructure observed

at 215K. It is not clear whether the substructure is due to stress effects or whether there are walls other than simple 180^{o} walls present. Problems in obtaining domain patterns at 215K would exist without the vertical bias field but different colloid materials could be used at low temperature without a bias field and at high temperatures with a bias field. This work could establish whether or not colloid contrast is linked with fine structure. Also, the use of finer colloid particles with and without bias field would enable a better contrast to be achieved and remove some of the problems involved in measuring domain spacing on the photographs.

One of the biggest problems encountered in the present observations was the problem of the tedious technique used for the observations. The technique was discussed in detail in Chapter Six but suffice it to say that the technique required a great deal of time in order to prepare the sample and prepare the apparatus for a run. There is also the problem of cooling the sample, setting optimum conditions for a deposition and then warming the sample before removing it and taking it to the microscope. One possibility for the convenient observation of domain structures is the Kerr magneto-optic effect (as mentioned in Chapter 5). While this technique, like the colloid technique, observes surface magnetization and does not represent the bulk material, it does offer a convenient way of observing wall movement (which the colloid technique does not). Because no particles are involved a suitable imaging system would allow the observation of domain wall movement. A suitable Kerr effect apparatus would allow the sample to be placed in a chamber (See Chapter 5) and the temperature on an applied field could be varied without the necessity to remove the sample. An added advantage would be that repeated polishing (and hence stressing) of the crystal would not be required.) There remains, however, the problem

of resolution with the Kerr effect as applied to rare earth metals. Perhaps use of such an apparatus with other samples would provide answers which could be applied to solving some of the problems encountered by the use of the dry colloid technique.

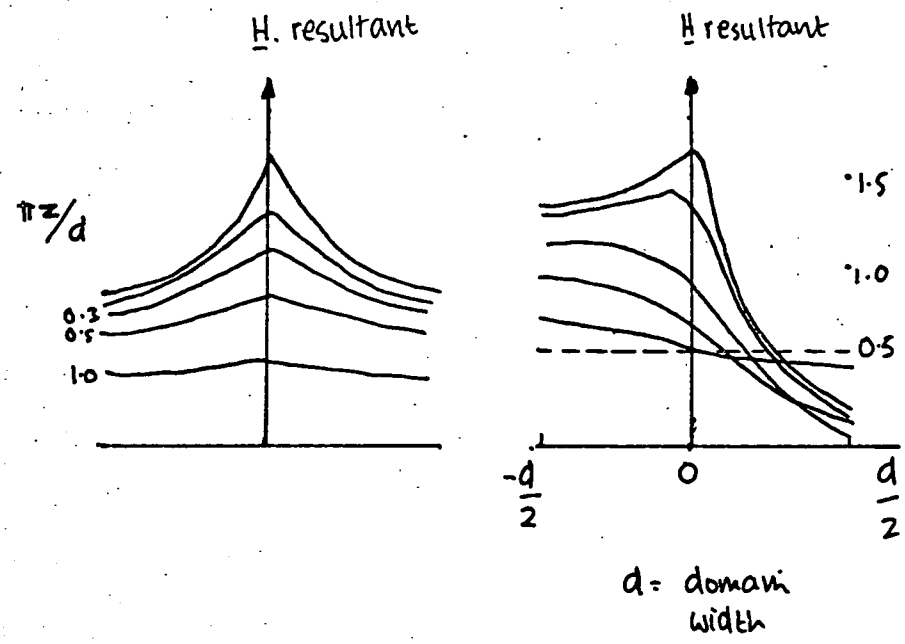

Fig. 7.32 Calculations of leakage field at various distances above a rare earth garnet crystal.

(a) zero vertical bias.

(b) with vertical bias (2 mT)

(B. K. TANNER (1981))

REFERENCES

Akulov N.S(1929) Z Physik 57, (1931) 69,78

Akulov N.S(1936) Z Physik 100,197

Akulov N.S. (1928) Z Physik 52,389

Barkhausen H. (1919) Z Phys. 20,401

Bates L.F. & Neale F.E. (1949) Physica 15,220

Bates L.F. & Wilson G.W. (1951) Proc. Phys. Soc. A64,691

Becker R & Doring W.D. (1939) Ferromagnetismus (Springer, Berlin)

Birss R.R. & Keeler G.J. (1974) Phys. Stat. Sol. B64,357-366

Birss R.R., Keeler G.J., Pearson P & Potton R.J. (1978)
J. Phys. E. 11,928

Bitter F. (1931) Phys. Rev. 38,1903

Bitter F. (1931) Phys. Rev. 41,1903

Bloch F. (1932) Z. Physik 74,295

Bly P.H. (1967) PHD Thesis Durham

Bly P.H., Corner W.D., Taylor K.N.R. & Darby M.I. (1968)
Magnetic Anisotropy of Rare Earth Metals J.Appl.Phys.
39,1336-1338

Bowman & Booth (1969) (See Dey, Bowman and Booth)

Bozorth R.M. (1954) Phys. Rev. 96,311

Callen E. & Callen H.B. (1965) Phys. Rev. 139,A455-A471

Callen E.R. & Callen H.B. (1963), Phys. Rev. 129,578

Callen H.B. & Callen E.R. (1966) J. Phys. Chem. Solids 27,1271-1285

Carey R. & Isaac E.D. (1966) Magnetic Domains and their Observation
(English Universities Press)

Carr (1960) J. Appl. Phys. 31,69

Clark (1980) PHD Thesis Durham (After Palmer (1980))

REFERENCES

Clark A.E. (1980) (A) Magnostrictive Rare Earth FE2 Compounds (Contribution to Ferromagnetic Materials ED. E.P. Wohlfarth (North-Holland))

Clark A.E. De Savage B.F. & Bozorth R. (1965) Phys. Rev. 138,A216 (1963) Phys. Letters 5,100)

Clark G.F. (1980) PHD Thesis Durham University.

Clark G.F. Private Communication

Coqblin B. (1977) The Electronic Structure of Rare Metals and Alloys. (Academic Press)

Corner W.D. & Bassam T.S. (1971) J. Phys. C. Solid St. Phys. 1971 Vol.4.

Craik & Tebble (1965) Ferromag. and Ferromag. Doms (North-Holland)

Craik (1956) Proc. Phys. Soc. B69, 647.

Crangle J. (1971) The Magnetic Properties of Solids (Arnold)

Crossley W.A., Cooper R.W., Page J.C. & Van Stapele R.P. (1969) Faraday Rotation in Rare Earth Iron Garnet Phys. Rev. 181, 896-904

Darnell F.J. (1963) Phys. Rev. 132,128

Darby, M.I and Isaac, ED I.E.E.E. Trans. Magnetics MAG -10, 259-304 (1974)

De Gennes P.G. (1962) J. Phys. Radium 23, 510

Dey S. K., Bowman M.J. & Boothe A.D. (1969) Journal of Scientific Instruments (Journal of Phys. E) Sents 2 Vol.2

Dietrich O.W. & Als-Nielsen J. (1967) Phys. Rev. 162,315

Dillon J.F., Remeika J.R. & Staton C.R. (1969) J. Appl. Phys. 40,1510-1511

Dirac P.A.M. (1926) Proc. Roy. Soc. 112A,661

REFERENCES

Dove (1963) J. Appl. Phys., 34, 2067.

Dreschel W. and Kranz J. (1958) Z.Phys. 150,632

Elmore W.O. (1937) Phys. Rev. 51,982 (1938) 53,757, (1938) 54,309

Enoch R.D. (1975) Contemp. Phys. Vol. 16,NO.6, 561 - 573

Feron J.L. (1969) Thesis Grenoble (Phd)

Fowler C.A. & Fryer E.M. (1952) Phys. Rev. 86,426

Fowler C.A. & Fryer E.M. (1954) Phys. Rev. 94,52 (1955)
IBID100,746, (1956) FBID 104,552

Fowler C.A., Fryer E.M. & Stevens J.R. (1956) Phys. Rev. 104,645

Fowler C.A., Fryer E.M. & Treves D. (1960) Observation of Domains
in Iron Whiskers under High Fields. J. Appl. Phys. 31,2267

Fowler C.A., Fryer E.M. and Treves D.J. (1960) J. Appl. Phys. 31,2267

Frank A. (1932) Phys. Rev. 39,119

Garrood (1962) J.R. Proc. Phys. Soc. 79, 1252

Goodenough (1956) Phys. Rev. 102,356

Goranson R.W. & Adams L.H. (1933) J. Franklin Inst. 216,475-504

Green A. & Prutton M. (1962) Magneto-optic Detection of Ferromagnetic
Domains using Vertical Illumination J. Sci. Instrum.40,490

Hegland D.E., Legvold S. & Spedding F.H. (1963) Phys. Rev. 131,158

Heisenberg W. (1926) Z. Physik. 38,441

Heisenberg W. (1928) Z. Physik 49,619

Heitler & London (1927) Zeits F. Physik 44,455

Herring & Jakubovics (1973) Metal Phys. Vol3, 1

Huber E.E., Smith D.O. & Goodenough J.B. (1958) J. Appl. Phys. 29,294

Jones D.W., Farrant S.P. & Jordan R.J. & D. Fort. Inst. Phys. Conf. Ser
No 37. (1978).

REFERENCES

Jones G.H. (1976) Science Progress 63,219

Kaczer J. (1955) A New Method for Investigating the Domain Structure of Ferromagnetics Amer. J. Phys., 5,239

Kasuya T. (1956) Prog. Theor. Phys. 16,45

Kasuya T. (1966) Magnetism Vol. 11B (Eds. Rado G.T. & Suhl H.) (Academic Press New York) P.215

Keffer F. (1955) Phys. Rev. 100,1692

Killel C. (1949) Rev. Mod. Phys. 21,541

Kittel C. (1968) Solid state Physics 22, 1.

Koehler W.C. (1965) J. Appl. Phys. 36,1018

Koehler W.C. (1967) In Transaction of the American Crystallographic Association (H.G. Smith Ed.) Polycrystal Book Service Pittsburgh Vol. 3,P53

Koehler W.C., Child H.R., Wollan E.D. & Cable J.W. (1963) J. Appl. Phys. Suppl. 34,1335

Kosimaki D.C., Oschneidner K.A. & Panousis N.T. (1974) J. Cryst. Growth 22,225

Kozlowski G. & Zietek W (1966) Acata Physica Polonica 29, 261.

Kranz J. & Drechsel W. (1958) Z. Physik. 100,632

Kranz J. (1956) Naturwissenschaften, 43,370

Landau L. & Lifshitz E. (1935) Phys. Z. Sowjet 8,153

Lee E.W. (1955) Rep. Prog. Phys. 18,184

Lee E.W., Callaby D.R. & Lynch A.C. (1958) The use of the Kerr Effect for Studying the Magnetization of a Reflecting Surface Proc. Phys. Soc. 72,233

REFERENCES

Lifshitz E. (1944) J. Phys. USSR. 8,337

Lilley B.A. (1950) Phil. Mag. 41,792

MacKormack B.I. Private Communication

Mahajani (1929) G.S. Phil.Trans. 228,63

Mapps D.J. (1978) Magnetic Domain Demonstrations using the Kerr Mag.-Optic Effect.

Martin D.H. (1967) Magnetism in Solids (Iliffe Books)

Mason W.P. (1954) Phys. Rev. 96,302

Morrish A.H. (1965) The Physical Principles of Magnetism (Wiley)

Middlehoek (1963) J. Appl. Phys. 34,1054

Néel (1955) Contemp. Rend. 241,533

Néel L. (1944) J. Phys. Radium 5,265

Noto, Koshichi & Heubener (1978) R.P. Japan J. Appl. Phys. Vol.17 No.4

Osborn (1945) Phys. Rev. 67,351

Pearson R.F. (1973) Application of Magneto-Optic Effects in Magnetic Materials Contemp. Phys. Vol.14 No.3, 201-211

Prutton M. (1959) The Observation of Domain Structure in Magnetic Thin Films by means of the Kew Mag.-Optic Effect Phil. Mag. Ser. 8 Vol. 4 P.127

Rhyne J.J. & Clark A.E. (1967) J. Appl. Phys. 38,1379

Rhyne J.J. & Mc Guire R. (1972) IEEE Trans. on Magnetics 8,165

Rhyne J.J. & Legvold S. (1965) Phys. Rev. 138,A507

Rhyne J.J. & Legvold S. (1965) S. Phys. Rev. 140,A2143

Roberts B.W. & Bean C.D. (1954) Phys. Rev. 96,1494

Roeland L.W., Cock G.J., Mueller E.A., Moleman A.C., Mc Ewan K.A., Jordan R.G. & Jones D.W. (1975) J. Phys. F5,L233

Ruderman M.A. & Kittel C. (1954) Phys. Rev. 96,

REFERENCES

Saad F. (1977) PHD Thesis Durham.

Sato H. & Chandresekar B.S. (1957) Phys. Chem. Solids 1,228

Scott G.G. & Coleman R.V. (1957) J. Appl. Phys. 28,1512

Slater J.C. (1936) Phys. Rev. 49,537, (1936) 49,931 (1937) 52,198

Revs. Mod. Phys. 25,199 (1953)

Smith R.L., Corner W.D. & Tanner B.K. (1980) J. Phys. E: Sci. Instrum., Vol 13.

Stephan W. (1955) Exper. Tech. Der. Phys. 3,1

Stevens, K.W.H. Proc. Phys. Soc. A 65, 209-215 (1952)

Stoner E.C. (1950) Rep. Prog. Phys. 13,114

Stoner E.C. (1938) Proc. Roy. Soc. A-165,372 (1939) A-169,339 (1938)

Phil. Mag. 25,899

Stoner E.C. (1946) Phil. Mag. 38,816 & Phil. Mag. 36,803

Tanner B.K. (1976) X-Ray Diffraction Topography Pergamon A.76

Tanner B.K. (1979) Contemp. Phys. 20

Tanner B.K. (1981) Prog. Sci. Vol 67. No 267.

Tanner B.K. and Bowen D.K. (Eds) Characterization of Crystal Growth Defects by X ray methods Plenum N.Y. (1980)

Taylor K.N.R. & Darby M.I. (1972) Phys. of Rare Earth Solids

(Chapman and Hall)

Taylor K.N.R. (1970) Contemp. Phys. Vol 11 No. 5 PP 423-454

Temple J.A.G., Fairbairn. W.M. and Pickett G.R. (1977) J. Phys. F 7, 1003

Topp, N.C. The Chemistry of the Rare Earth metals (1965)

Treves (1961) Limitation of the Magneto Optic Kerr Technique in the

Study of Microscopic Magnetic Domain Structures

J. Appl. Phys. 32,258

Treves D. (1967) J. Appl. Phys. 38 1192-6

Tyler F. (1931) Phil Mag. II 596

Van Vleck J.H. (1932) Electric and Magnetic susceptibilites

REFERENCES

Van Vleck J.H. (1956) AIEE Conf. Mag.Mat., Boston

Van Vleck J.H. (1959) J. Phys. Radium. 20,124

Von Hamos L. & Thiessen P.A. (1931) Z. Physik 71,442

Waughness R.K. (1954) Phys. Rev. 95,339

Welford (1974) PHD Thesis Durham.

Welford J. (1974) PHD Thesis Durham.

Williams H. J. & Goertz M. (1952) J. Appl. Phys. 23,356

Williams H. J. & Shockley W. (1949) Phys. Rev. 75,178

Williams H. J., Bozorth R.M. & Shockley W. (1949) Phys. Rev. 75,155

Williams J., Foster F.G., Wood E.A. (1951) Observation of Magnetic Domains using the Kerr Effect Phy. Rev. 82 119

Wohlfarth E.P. (ED.) (North Holland (1980) Ferromagnetic Materials.

Yamamoto M. & Iwata T. (1953) Sci. Rep. R.I.T.U. A5,433

Yang, J.J.H. (1971) "The Origin and Application of Magnetic Anisotropy" Ph.D Thesis. University of California. U.S.A.

Yosida K. (1957) Phys. Rev. 106,893

Zener C. (1954) Phy. Rev. 96,1335

BIBLIOGRAPHY

Abraham, M. and Becker R. — Classical Theory of Electricity and Magnetism. Blackie & Sons.

Anderson. J.C. — Magnetism and magnetic materials Chapman and Hall (1968)

Bates. L.F — Modern Magnetism. Camb. Univ. Press (1961)

Bleaney B.I. and Bleaney B. — Electricity and Magnetism 3rd Ed. Oxford University Press (1976)

Brailsford F. — The Physical Principles of Magnetism. Van Nostrand (1966)

Brown W.F. — Magnetostatic Principles in Ferromagnetism. North-Holland Publishing Company.

Carey R. and Isaac E.D. — Magnetic Domains and Techniques for their observation. English University Press (1966)

Chikazumi S. — Physics of Magnetism. Wiley (1964)

Coqblin B. — The Electronic Structure of Rare-Earth Metals and Alloys. Academic Press (1977)

Corner W.D. and Tanner B.K. — (Eds) Rare Earth and Actinides (1977) I.O.P. Conf. series number 37.

Craik D.J. and Tebble R.S. — Ferromagnetism and Ferromagnetic Domains. North-Holland (1965)

Craik D. J. and Tebble R.S. — Magnetic Materials. Wiley (1969)

Crangle J. — The Magnetic Properties of Solids. Arnold (1977.)

BIBLIOGRAPHY

Elliot R.J. (Ed.) Magnetic Properties of Rare-Earth Metals. Plenum 1972.

Lee E.W. Magnetism. Pelican.

Martin D.H. Magnetism in Solids. Iliffe 1967.

Mattis D.C. The Theory of Magnetism. Harper and Row 1965.

Morrish A.H. The Physical Principles of Magnetism. Wiley (1965)

Sinha K.P. and Kumar N. Interactions in Magnetically ordered Solids. Oxford University Press (1980)

Smit J. Magnetic Properties of Materials. McGraw Hill (1971)

Stewart K.H. Ferromagnetic Domains. Cambridge University Press (1954)

Tebble R.A. Magnetic Domains. Methuen (1969)

Thompson J.E. The Magnetic Properties of Materials. Newnes (1968)

Topp N.C. The Chemistry of the Rare Earth Metals Elsevier (1965)

Van Vleck The Theory of Magnetic Susceptibilities. Oxford Clarendon Press (1932)

Wohlfarth E.P. (Ed.) Ferromagnetic Materials Volume 1. North-Holland (1980)

Zulstra H. Experimental Methods in Magnetism Volume IX parts 1 and 2. North-Holland (1967)

BIBLIOGRAPHY

Bozorth R.M. — Ferromagnetism. Van Nostrand (1951)

Craik D.J. — Structure and Properties of Magnetic Materials. Pion (1971)

Cullity B.D. — Introduction to Magnetic Materials. Addison Wesley (1972)

Kittel C. — Introduction to Solid State Physics. Wiley (1976)

Rado G.T. and Sull H. — Magnetism Volumes II and III Academic Press (1963)

Williams D.G.T. — The Magnetic Properties of Matter. Longmans (1966)